Capacity Prediction of Repaired and Unrepaired Bridge Beams with Deteriorated Ends

FINAL REPORT – SEPTEMBER 2025

Department of Civil & Construction Engineering
College of Engineering and Applied Sciences

Western Michigan University

1. Report No. SPR-1745	2. Government Accession No. N/A	3. Recipient's Catalog No. N/A
4. Title and Subtitle Capacity Prediction of Repaired and Unrepaired Bridge Beams with Deteriorated Ends		**5. Report Date** 09/30/2025
		6. Performing Organization Code N/A
7. Author(s) Upul Attanayake, Ph.D., P.E., Sanjoy Bhowmik, M.Eng., Kevin Saleh, B.Sc., Yufeng Hu, Ph.D., P.E., and Neal Berke, Ph.D.		**8. Performing Org. Report No.** N/A
9. Performing Organization Name and Address Western Michigan University College of Engineering and Applied Sciences 1903 West Michigan Avenue Kalamazoo, Michigan 49008-5316		**10. Work Unit No.** N/A
		11. Contract or Grant No. Contract 2022-0434 Z1
12. Sponsoring Agency Name and Address Michigan Department of Transportation Research Administration 8885 Ricks Road P.O. Box 30049 Lansing, Michigan 48909		**13. Type of Report & Period Covered** Final Report 10/01/2022 – 09/30/2025
		14. Sponsoring Agency Code N/A

15. Supplementary Notes
Conducted in cooperation with the U.S. Department of Transportation, Federal Highway Administration. MDOT research reports are available at www.michigan.gov/mdotresearch.

16. Abstract
The Michigan Department of Transportation (MDOT) identified significant deterioration at the ends of steel and prestressed concrete (PSC) beams, requiring systematic evaluation and improved decision-making protocols for Requests for Action (RFAs). This comprehensive study examined 431 steel beam ends and 267 PSC bridges to develop capacity-based assessment methods and repair guidelines. For steel beam ends, the analysis revealed a strong preference for bolted repairs over welded repairs due to field welding challenges and concerns about fatigue. Section loss limits of 20% for webs and 10% for flanges were established as RFA thresholds. Finite element analysis of W30×108 beams with corrosion-induced holes resulted in capacity reduction factors ranging from 0.39 to 0.74, depending on hole geometry and the presence of stiffeners. Fatigue analysis revealed a significant reduction in fatigue life due to bolt holes with high surface roughness and pre-existing cracks. For PSC beam ends, a Strut-and-Tie Method was implemented to model complex load transfer mechanisms, establishing 15% capacity reduction as the critical RFA threshold. Specific deterioration limits showed that spalls with ≥15% strand exposure or ≥40% section loss without strand exposure warrant immediate action. Accelerated corrosion testing of repair methods identified that combining latex-modified concrete patches with zinc-rich epoxy primer and elastomeric surface coatings provided optimal performance. Field evaluations demonstrated superior long-term durability of reinforced overcasts with FRP U-wraps and protective coatings when compared to unreinforced patches. Updated inspection guidelines, calculation tools, and comprehensive repair selection criteria were developed to enhance bridge safety while optimizing maintenance resource allocation through rational correlations between visual inspection data and structural performance.

17. Key Words	18. Distribution Statement
Beam ends, Concrete, Deteriorated, Fatigue, Prestressed, Rating, Steel	No restrictions. This document is available to the public through the Michigan Department of Transportation.

19. Security Classif. (of this report)	20. Security Classif. (of this page)	21. No. of Pages	22. Price
Unclassified	Unclassified	216 (w/o appendices)	N/A

Capacity Prediction of Repaired and Unrepaired Bridge Beams with Deteriorated Ends

Final Report
(2022 - 2025)

Project Manager: Donald W. Tempinson, P.E.

Submitted to:

MDOT
Michigan Department of Transportation

Submitted by:

Upul Attanayake, Ph.D., P.E.
Professor and Director
Center for Structural Durability
(269) 276 – 3217
upul.attanayake@wmich.edu

Sanjoy Bhowmik, M.Eng.
Graduate Research Assistant
Center for Structural Durability
(269) 276 – 3210
sanjoykumar.bhowmik@wmich.edu

Kevin Saleh, B.Sc.
Graduate Research Assistant
Center for Structural Durability
(269) 276 – 3210
kevinmakubuli.saleh@wmich.edu

Yufeng Hu, Ph.D., P.E.
Master Faculty Specialist
Department of Civil & Construction Engineering
(269) 276 – 3210
yufeng.hu@wmich.edu

Neal Berke, Ph.D.
Vice President of Research
Tourney Consulting Group, LLC
(269) 384 – 9980
nberke@tourneyconsulting.com

Western Michigan University
Department of Civil & Construction Engineering
College of Engineering and Applied Sciences
Kalamazoo, MI 49008-5316
Fax: (269) 276 – 3211

DISCLAIMER

"This publication is disseminated in the interest of information exchange. The Michigan Department of Transportation (hereinafter referred to as MDOT) expressly disclaims any liability, of any kind, or for any reason, that might otherwise arise out of any use of this publication or the information or data provided in the publication. MDOT further disclaims any responsibility for typographical errors or accuracy of the information provided or contained within this information. MDOT makes no warranties or representations whatsoever regarding the quality, content, completeness, suitability, adequacy, sequence, accuracy or timeliness of the information and data provided, or that the contents represent standards, specifications, or regulations."

"This material is based upon work supported by the Federal Highway Administration under SPR OR23-001. Any opinions, findings and conclusions or recommendations expressed in this publication are those of the author(s) and do not necessarily reflect the views of the Federal Highway Administration."

If you require assistance accessing this information or require it in an alternative format, contact the Michigan Department of Transportation's (MDOT) Americans with Disabilities Act (ADA) coordinator at Michigan.gov/MDOT-ADA.

ACKNOWLEDGEMENTS

This project is funded by the Michigan Department of Transportation (MDOT). The authors would like to acknowledge the support and effort of Mr. Donald Tempinson in initiating and managing this research to a successful conclusion. The authors also wish to recognize the contributions of the Research Advisory Panel (RAP) members to the advancement of this study. The authors appreciate the contribution of graduate students Harsha Amunugama and Hamahang Sherzai for the successful completion of this study. Special thanks are due to Larry Wachowski, Mike Wachowski, and several others of Tourney Consulting Group (TCG) for their contribution to the project. Dr. Danush Wijekularathna's contribution to this study as the statistical consultant is greatly appreciated.

EXECUTIVE SUMMARY

INTRODUCTION

The Michigan Department of Transportation (MDOT) uses the Agency-Developed Element (ADE) 826 to document the condition of a beam end only when deterioration or repair meets the definitions in Condition State (CS) Table 9 of the Michigan Bridge Element Inspection Manual (MiBEIM 2017). The quantity is reported per beam end when the deterioration or repair is within 5 ft of the bearing. Bridge inspection engineers and consultants submit requests for action (RFAs) due to safety concerns associated with steel and PSC beam end conditions. Region bridge engineers review RFAs and submit them to the Bridge RFA Coordination Committee (BRFACC) for deliberation. The RFAs and subsequent decisions are made based on the currently available inspection guidelines and the experience of inspection engineers, region bridge engineers, and BRFACC members. Having focused guidelines and tools for bridge inspection engineers, region bridge engineers, and other members of the BRFACC can streamline the RFA submission and evaluation process. Additionally, the availability of beam end maintenance and repair guidelines, including repair details and their impact on load capacity, is vital to overcoming programming and resource allocation challenges while ensuring public safety and avoiding potentially unnecessary restrictions on the motoring public. This project was initiated to address this broad scope, and the findings are briefly discussed in this executive summary.

STEEL BEAM ENDS

Preference for Bolted Repairs over Welded Repairs

Thirty-two (32) scoping reports, inspector comments, bridge plans, and other associated documents were reviewed to collect condition data on 431 beam ends. Welded repairs are typically recommended for sections with cracks, buckled webs, buckled flanges, or a combination of these defects. Repairs recommended at 98% of the 431 beam ends were bolted repairs. The data indicate a strong preference for bolted repairs due to the challenges associated with field welding requirements, fatigue concerns, and the difficulty in finding qualified welders.

Section Loss Limits for Repair Recommendations

The review of the literature and the survey of highway agencies indicated inconsistency in the guidelines used for submitting RFAs for steel beam ends. For example, 1/8-inch section loss, 30% section loss, and 10% section loss are used by various agencies to submit RFAs. Considering the statistics presented in Chapter 2, it is recommended to use a 20% web section loss as the limit for

determining the need for repairs on webs up to 0.625 inches thick, unless unique conditions at the specific beam end dictate otherwise. Similarly, it is recommended to use a 10% flange section loss as the limit for determining the need for repairs on flanges up to 1.25 inches thick when a beam end has both web and flange section losses.

Capacity Prediction of Beam Ends with Holes

Sixty-two percent (62%) of beam end deteriorations are associated with the web area, particularly affecting the bearing and shear zones near beam supports. The capacity of beam ends with holes resulting from corrosion was studied. The impact of holes on beam end capacity was evaluated using the most commonly used beam section in Michigan bridges—the W30×108. Both unstiffened and stiffened beam ends with various hole configurations documented during bridge inspections were used in this study. The analysis considered holes within the overhang, holes extending from the overhang to the bearing, holes located over the bearing, and holes starting at the middle of the bearing and extending toward the span. Both eigenvalue buckling analysis and post-buckling analysis using the Riks method were employed to determine failure loads, incorporating web out-of-plane deformations (imperfections) of 50%, 75%, and 100% of the web thickness to reflect field conditions.

For unstiffened W30×108 beam ends, web crippling controls the failure mode with a nominal resistance of 231 kips. The finite element analysis showed excellent correlation with AASHTO (2020) analytical solutions, with failure loads within 3% of the nominal resistance. For stiffened beam ends, bearing resistance controls with a nominal resistance of 260 kips, while axial resistance provides a capacity of 470 kips. When holes are located within the bottom 4 inches of the web height with web crippling controlling, the remaining capacity of the beam end with 100% imperfection can be calculated using the following load factors:

If $HL/N \leq 0.80$: $\varphi = 0.50$ (retains 50% of original capacity)

If $HL/N > 0.80$: $\varphi = 0.38$ (retains 38% of original capacity)

Where HL is the hole length and N is the bearing length.

For stiffened beam ends, the location of holes relative to the bearing stiffener is critical:

- When holes are located on both sides of the bearing stiffener: $\varphi = 0.39$ (retains 39% of original capacity)
- For all other hole configurations: $\varphi = 0.74$ (retains 74% of original capacity)

The MDOT load rating spreadsheet was updated to incorporate the effects of holes at beam ends, including:

- Addition of beam overhang parameter
- Input fields for hole length and stiffener configuration
- Automatic calculation of average remaining web thickness
- Implementation of capacity reduction factors based on hole geometry and web out-of-plane deformation magnitudes (i.e., imperfections).

The following recommendations are derived for practice:

- *Inspection*: Measure thickness loss within the deteriorated region on a grid and report the average value as the thickness loss. Report the thickness loss within the bottom 4 inches of the web height near beam ends separately for load rating. Report the dimensions of the holes resulting from corrosion, typically the length and height, and their location with respect to the beam end and the top of the bottom flange.
- *Load Rating*: Apply the recommended load factors when evaluating beam ends with documented section loss, considering both hole length and stiffener presence.
- *Maintenance Planning*: Beam ends with hole length-to-bearing length ratios exceeding 0.80 should receive priority for rehabilitation due to significant capacity reductions.
- *Design Considerations*: The presence of end diaphragms with bent plates provides minimal improvement in capacity for beams with deterioration, suggesting that resources may be better allocated to direct web repair or stiffener installation.
- *Further Research*: Additional investigation is recommended for holes exceeding 14% of web height and for the long-term effects of progressive deterioration on beam end capacity.

Longevity and Fatigue Prediction of Bolted Steel Repairs at Beam Ends

Scoping inspections documented fatigue cracking at beam ends with bolted repairs. These bolted repairs were implemented to address section loss at beam ends, which increases surface roughness and the potential for fatigue crack development. The fatigue life of steel beam ends with bolted repairs was evaluated using finite element analysis (FEA) and the fe-safe fatigue analysis software. A W30×108 steel beam with a 50 ft span and 6 ft beam spacing was selected. The Brown-Miller strain-based fatigue-life algorithm was used to represent the material behavior.

The investigation examined multiple analysis cases, including as-designed beams, beams with bolt holes, beams with pre-existing cracks of varying sizes ($0.15t_w$ and t_w), and beams with bolted repairs and pre-existing cracks. Surface finish effects were incorporated through surface finish factors (K_t) of 1.0, 1.3, and 1.5, representing polished surfaces, 1000 μ-in. surface roughness, and approximately 2000 μ-in. surface roughness, respectively.

The presence of bolt holes and a crack size of 0.15tw significantly reduces the fatigue life compared to the as-designed beam conditions of this particular structure. The critical locations identified through analysis corresponded well with crack patterns documented during field inspections. These findings underscore the importance of early crack detection and repair in maintaining structural integrity.

The study provides fatigue life calculation tables for all 28 Michigan legal truck configurations and AASHTO fatigue trucks. Using Miner's rule with actual traffic data, engineers can estimate the remaining fatigue life of similar details. The comprehensive procedure developed in this study can be applied to other structural details not covered in the AASHTO LRFD specifications, providing engineers with valuable tools for assessing the fatigue life of steel bridge members.

Impact of Pack Rust on Beam Capacity

The comprehensive review of literature and practice revealed that the impact of pack rust on beam capacity is the least studied topic. This is primarily due to the challenge of quantifying the section loss by measuring component deformation, which depends on the section thickness, boundary conditions (bolt or weld patterns), the amount of corrosion products, the type of corrosion, and the relationship between the amount of corrosion and the section loss. The current practice is to clean the corroded details and use the remaining thickness for capacity calculation.

PSC I-BEAM ENDS

RFA and Scoping Inspection Guidelines

MDOT currently uses various templates and guidelines to document PSC I-beam end distress and deterioration during inspections. A comprehensive review of nineteen scoping inspection reports, Bridge Safety Inspection Reports (BSIRs) of 267 bridges, several RFA reports, and related documents from the MiBRIDGE database revealed that existing inspection guidelines are insufficient for collecting the minimum required data to assess beam end capacity and make informed decisions regarding maintenance, repair, or load posting.

To address these shortcomings, inspection guidelines and templates specifically designed for PSC I-beam ends were developed. The guidelines include a systematic approach to beam end discretization and detailed documentation procedures for delamination, spalls, and cracking. These guidelines were developed with consideration for the future implementation of drone and computer vision technologies to enhance traditional visual inspection methods.

The templates provide standardized data collection formats that include span identification, pier information, beam numbers, dimensional measurements, and spaces for recommended repairs and additional observations. This systematic approach ensures consistent documentation across different inspection teams, facilitating more accurate condition assessments and maintenance planning.

RFA Decision Matrix

MDOT required improved decision-making tools for evaluating PSC beam end deterioration to enhance the identification of bridges requiring RFAs. Current RFA guidelines rely on general condition ratings and visual inspection that lack clear correlations with structural performance, creating challenges in determining when deteriorated beam ends require immediate attention versus continued monitoring.

This project addressed the need for a rational, capacity-based assessment method by developing a comprehensive beam end deterioration classification system using the Strut-and-Tie Method (STM). The study focused on evaluating the PSC I-beam end capacity, particularly addressing factors such as exposed prestressing strands, bearing area loss, and structural cracking that significantly impact structural performance but are inadequately addressed by current inspection protocols using ADE 826.

The research analyzed disturbed regions (D-regions) at beam ends, considering four primary failure modes: longitudinal tie failure, bearing face failure, strut-to-node interface failure, and transverse tie failure. Capacity calculations were validated using experimental data from 16 PSC I-beam specimens.

The Strut-and-Tie Method was successfully implemented to model complex load transfer mechanisms at PSC beam ends, providing a superior representation of failure modes compared to conventional flexural design assumptions. A comprehensive set of Mathcad calculation sheets

was developed and delivered to MDOT for calculating capacities of as-designed, deteriorated, and repaired beam ends.

Sensitivity analysis revealed that beam end shear capacity is primarily controlled by longitudinal tie failure and is directly proportional to the percentage of exposed prestressing strands. Beam section loss without strand exposure has minimal impact on capacity.

A 15% capacity reduction was established as the critical threshold for RFA decisions based on structural safety considerations. Specific deterioration limits were developed, indicating that narrow-flange beams, such as AASHTO Type III, can tolerate up to 35% loss of the bottom flange section before reaching critical strand exposure levels. In contrast, wider-flange beams reach thresholds at lower section loss percentages. For bearing area loss, a width of concrete spall up to 39% is acceptable at the bottom flange over the bearing, provided no strands are exposed. For spalls on only one side of the bottom flange, the recommended limit is 20% of the flange width.

The developed capacity-based deterioration classification system should be integrated with the current condition state definitions, which rely solely on section loss measurements. The implementation of this classification system is expected to enhance bridge safety while optimizing maintenance resource allocation by establishing rational correlations between visual inspection data and structural performance.

Performance of Beam End Preservation and Repair Methods

MDOT has observed that traditional concrete patching methods for PSC beam ends provide only short-term solutions and may contribute to accelerated concealed corrosion. In response, MDOT developed Special Provision for Maintenance Repair of Prestressed Concrete Beam for Contract Identification 25031-214869, 20SM712(A175), which requires cleaning of exposed steel reinforcement and application of zinc-rich epoxy primer to enhance durability. However, the performance of this preservation approach had not been evaluated prior to this study.

An experimental study was conducted to assess the effectiveness of various preservation and repair techniques for deteriorated PSC beam ends through accelerated corrosion testing. A modified, lower-cost version of the Bureau of Standards M-82 Protocol for Topical and Patch Repairs was employed to evaluate ten concrete slab specimens (1 ft × 1 ft × 5.5 in.) with embedded reinforcing steel. The study examined four different preservation and repair methods, including latex modified

concrete (LMC), zinc-rich epoxy primer for steel, a silane penetrating sealer, and a breathable concrete surface coating with crack bridging abilities.

The results indicate that patch repair with LMC provides protection only to the reinforcing steel within the repaired area and offers no protection to adjacent steel elements. A similar limitation was observed when a silane penetrating sealer was applied over regular concrete repairs, suggesting limited effectiveness in preventing corrosion beyond the immediate repair zone.

The application of zinc-rich epoxy primer demonstrated reduced corrosion activity in the surrounding reinforcement in most test cases. The combination of zinc-rich epoxy primer with concrete surface treatments (either silane penetrating sealer or elastomeric coating) showed improved performance compared to other methods. Among surface treatments, the elastomeric coating provided slightly better corrosion control relative to the silane penetrating sealer. The concrete repair with zinc-rich epoxy primer for steel and concrete surface coating yielded the most consistent and effective corrosion mitigation across all test scenarios and is recommended for PSC I-beam ends. Additional testing with a larger number of specimens is recommended to validate these preliminary findings, as this study was limited in scope.

PSC I-beam End Repair and Capacity Improvement

MDOT recognizes that deteriorated PSC beam ends require systematic repair approaches to restore structural capacity and extend service life. The repair methods examined during this study range from basic crack sealing and concrete patching to more comprehensive solutions such as full-depth reinforced concrete overcasts and fiber-reinforced polymer (FRP) strengthening systems. Field performance reviews revealed that beam end repairs, which combined reinforced overcasts with FRP wraps and concrete surface coatings, demonstrated the best long-term durability. In contrast, unreinforced overcasts and repairs without protective coatings consistently demonstrated poor performance, with common issues including early-age cracking, coating failure, and delamination within 2 to 11 years of installation. The use of breathable concrete surface coatings with crack-bridging properties, combined with FRP strips, significantly enhances repair performance. For beam ends with span-to-depth (a/d) ratios closer to one, FRP U-wraps provide minimal improvement in structural capacity.

The study utilized STM to quantify capacity improvements achieved through overcast repairs. Capacity calculations revealed that exposing additional strands during repair preparation (chipping and cleaning) reduces beam end capacity. Three alternative Full-Depth Reinforced Concrete Overcast (FDRCO) repair details were developed and analyzed: *Alternative 1* (typical MDOT detail), *Alternative 2* (with hooked longitudinal reinforcement), and *Alternative 3* (incorporating strand splicing with 90-degree bents). *Alternative 3* FDRCO details, which incorporate strand splicing and 90-degree bents, can restore and potentially exceed the original design capacity. An alternative repair detail with welded wire fabric and adhesive anchoring is suggested for situations where maintaining the original beam geometry and vertical clearance is critical. It is recommended to experimentally evaluate the performance of *Alternative 2* and *Alternative 3* details before implementing them on in-service bridges.

TABLE OF CONTENTS

LIST OF TABLES

LIST OF FIGURES

1 INTRODUCTION

1.1 OVERVIEW

The Michigan Department of Transportation (MDOT) uses the Agency-Developed Element (ADE) 826 to document the condition of a beam end only when deterioration or repair meets the definitions in Condition State (CS) Table 9 of the Michigan Bridge Element Inspection Manual (MiBEIM 2017). The quantity is reported per beam end when the deterioration, or repair, is within 5 ft of the bearing. As shown in Figure 1-1, CS Table 9 defines four condition states for beam end deterioration solely based on section loss, even though many other conditions and details also impact the beam end capacity. However, the inspectors can use the CS Table 3 for steel beams, shown in Figure 1-2, to assess the impact of deteriorations (e.g., corrosion), distresses (e.g., cracking), conditions (e.g., distortion, damage, missing bolts), and details (e.g., connections) on the beam end capacity. Further, as shown in Figure 1-3 and Figure 1-4, the manual includes a collection of steel beam photographs describing condition states. The manual only provides pictures or graphics describing steel beam end deteriorations, conditions, and details to support bridge inspectors' decisions, and lacks guidance for assessing prestressed concrete (PSC) beam ends. The available manuals and guidelines lack information and data, particularly on PSC beam ends, to relate the condition state to beam end capacity.

CS TABLE 9 – BEAM END (Deterioration, Contact, Temp Support)

	Condition State 1	Condition State 2	Condition State 3	Condition State 4
Defects	**GOOD**	**FAIR**	**POOR**	**SEVERE**
Beam End Deterioration (826)	Section loss to element has been repaired.	Section loss exists and has not been repaired. Structural analysis is not yet warranted.	Measurable section loss that warrants detailed inspection to determine remaining section.	The condition warrants a structural review to determine the effect on strength or serviceability of the element. A request for action (RFA) should be submitted requesting a structural evaluation and/or repairs.
Beam End Contact (844)	Beam ends have been modified to address contact.	Beam ends are in contact. No visible distress observed.	Beam ends are in contact, distress is observed.	
Beam End Temporarily Supported (845 SH, 846 FH)	Temporary support(s) in place and functioning as designed.	Minor section loss on temporary support.	Moderate section loss on temporary support.	

Figure 1-1. Beam end condition state definitions (Source: MiBEIM 2017).

CS TABLE 3 - STEEL

	Condition State 1	Condition State 2	Condition State 3	Condition State 4
Defects	**GOOD**	**FAIR**	**POOR**	**SEVERE**
Corrosion (1000)	None.	Freckled Rust. Corrosion of the steel has initiated.	Section loss is evident or pack rust is present but does not warrant structural review.	The condition warrants a structural review to determine the effect on strength or serviceability of the element or bridge; OR a structural review has been completed and the defects impact strength or serviceability of the element or bridge.
Cracking/Fatigue (1010)	None.	Cracks that have self-arrested or have been arrested with effective arrest holes, doubling plates or similar.	Identified cracks exist that are not arrested and do not require structural review.	
Connections (1020)	Connection is in place and functioning as intended.	Loose fasteners or pack rust without distortion is present but the connection is in place and functioning as intended.	Missing bolts, rivets, broken welds, fasteners or pack rust with distortion but do not warrant a structural review.	
Distortion (1900)	None.	Distortion not requiring mitigation or mitigated distortion.	Distortion that requires mitigation but does not require structural review.	
Settlement – Substructure Elements (4000)	None.	Exists within tolerable limits or arrested with effective actions taken to mitigate.	Exceeds tolerable limits but does not warrant structural review.	
Scour – Substructure Elements (6000)	None.	Exists within tolerable limits or arrested with effective countermeasures.	Exceeds tolerable limits but is less than the limits determined by scour evaluation, and does not warrant structural review.	
Damage (7000)	Not applicable.	The element has minor damage caused by vehicular or vessel impact.	The element has moderate damage caused by vehicular or vessel impact.	The element has severe damage caused by vehicular or vessel impact.

Figure 1-2. Steel beam condition state definitions (Source: MiBEIM 2017).

Figure 1-3. Photographs showing CS for corroded beams and connections with missing bolts (Source: MiBEIM 2017).

Figure 1-4. Photographs showing CS of cracked or damaged beams (Source: MiBEIM 2017).

Bridge inspection engineers and consultants submit requests for action (RFAs) due to safety concerns associated with steel and PSC beam end conditions. Region bridge engineers review RFAs and submit them to the Bridge RFA Coordination Committee (BRFACC) for deliberation. RFAs and subsequent decisions are made based on the currently available inspection guidelines, an Excel spreadsheet with limited features for capacity calculation, and the experience of inspection engineers, region bridge engineers, and BRFACC members. Providing focused guidelines and tools for bridge inspection engineers, region bridge engineers, and other members of the BRFACC can streamline the RFA submission and evaluation process. Additionally, the availability of beam end maintenance and repair guidelines, including repair details and their impact on load capacity, is vital to overcoming programming and resource allocation challenges while ensuring public safety and avoiding potentially unnecessary restrictions on the motoring public. These tools and guidelines also help the Load Rating Unit (LRU) load rate deteriorated and repaired beam ends.

1.2 OBJECTIVES AND TASKS

The project objectives are to:

1. Address specific areas of concern for deteriorated steel beam ends, including the capacity prediction of beam ends with holes, impact on beam capacity due to pack rust between members of built-up sections, longevity and fatigue prediction of bolted steel repairs, and recommendations for the use of bolted versus welded steel repairs.
2. Characterize and document the types and extent of beam end deterioration in in-service concrete beams.
3. Provide a generalized method for quantifying the capacity of concrete beams with deteriorated beam ends featuring various levels of deterioration for load rating and bridge design.
4. Identify several repair techniques for each concrete beam type and extend the capacity prediction method to repaired beams to aid in determining the appropriate type and extent of the repair.

The following tasks were completed to accomplish the above-stated objectives:

1. Document and learn from existing research, including any data from previous lab tests of beam ends, best practices nationwide for beam end repair and capacity prediction, and current MDOT practices for beam end repair.
2. Collect information on existing bridges with damaged and repaired beam ends.
3. Address the specific areas of concern for deteriorated steel beam ends.
4. Classify the types and levels of deterioration on concrete beam ends.
5. Model various types and levels of deterioration on concrete beam ends.
6. Develop a generalized method for quantifying the capacity of concrete beams with deteriorated ends for various types and levels of deterioration.
7. Classify the types of repairs for the varying types of deterioration of concrete beam ends.
8. Model selected concrete beam end repair options.
9. Identify repair options and extend the capacity prediction method to these repaired beams.
10. Develop conclusions and recommendations, including design details for repairs, inspection guidelines for when an updated load rating is warranted, and procedures for load rating deteriorated beam ends.
11. Produce a final report and other deliverables.

1.3 REPORT ORGANIZATION

This report is organized into 10 chapters. It does not have a dedicated chapter for state-of-the-art literature and practice review. Since this project encompassed a broad range of objectives across multiple topics, relevant information from the review of state-of-the-art literature and practice is integrated into each chapter as needed. A survey of state highway agencies was conducted for this project. The survey questionnaire and summary of responses are documented in Appendices A and B. The survey results are integrated into various chapters as needed.

Chapter 1 includes the introduction and outlines the research project objectives, tasks, and the report organization.

Chapter 2 presents MDOT bridge inventory analysis results, the condition of deteriorated beam ends, repair recommendations, limitations of current guidelines for repair recommendations, and the performance of repaired beam ends.

Chapter 3 presents guidelines and procedures for documenting RFA and scoping inspections of PSC I-beams in a format that is helpful for capacity calculation and load rating.

Chapter 4 presents a comprehensive matrix to support the RFA decisions. The matrix was developed following a comprehensive parametric analysis that considered the impact of various beam end conditions and details on beam end capacities. The Strut-and-Tie Method (STM) was employed for modeling both as-designed and deteriorated beam ends, as well as for capacity calculation.

Chapter 5 presents the performance of beam end preservation and repair methods.

Chapter 6 presents details of beam end repair and capacity improvement methods. The STM was used for modeling repaired beam ends and calculating capacities.

Chapter 7 describes the impact of holes on the end capacity of steel beams. This chapter provides recommendations for the capacity calculation of beam ends with holes (complete section loss).

Chapter 8 describes the longevity and fatigue prediction of bolted steel repairs.

Chapter 9 includes a summary, conclusions, and recommendations.

Chapter 10 presents the cited references.

2 MDOT BRIDGE INVENTORY ANALYSIS

2.1 OVERVIEW

To accomplish project objectives, it was required to collect information on bridges with deteriorated beam ends as well as those with previously repaired beam ends. The MiBRIDGE database includes inventory data, element data, bridge plans, information about Requests for Action (RFAs), subsequent activities completed to address the conditions required for an RFA, scoping reports, and other relevant documents.

A condition state (CS) is assigned to a beam end based on the level of deterioration within 5 ft of the bearing and the criteria defined in CS Table 9 of the Michigan Bridge Element Inspection Manual (MiBEIM 2017). Table 2-1 shows the content of the CS Table 9 in MiBEIM (2017). According to the criteria provided in the table, CS1 is assigned to the beam ends that were repaired and are in good condition. CS4 is assigned, and an RFA is submitted when a beam end "condition warrants a structural review to determine the effect on [the] strength or serviceability of the element." The current guidelines rely on the heuristic knowledge of inspectors to determine the need for an RFA. Thus, this project was initiated to develop a robust set of guidelines, based on the quantitative assessment of deteriorated beam end capacity, to determine the need for RFAs. Other deliverables of this project include calculation tools for assessing the capacity of deteriorated and repaired beam ends, as well as details and procedures for beam end repairs. These deliverables are expected to enhance bridge safety, promote uniformity in bridge inspection, maintenance, and repair practices, reduce bridge closures or load restrictions, improve durability and service life, and achieve cost savings.

To review and document conditions requiring RFAs, findings from scoping inspections, recommended repairs, and different types of beam end repairs and details, it was necessary to identify bridges with beam ends in CS1. It was necessary to identify the bridges with beam ends in CS 2 to CS4 to document different beam end conditions, classify them based on the degree of deterioration, determine the causes of deterioration, evaluate the impact on beam end capacity, and assess the performance of repairs.

Table 2-1. Beam End Condition State (CS Table 9, MiBEIM 2017)

Defects	Condition State 1	Condition State 2	Condition State 3	Condition State 4
	GOOD	**FAIR**	**POOR**	**SEVERE**
Beam End Deterioration (826)	Section loss to element has been repaired.	Section loss exists and has not been repaired. Structural analysis is not yet warranted.	Measurable section loss that warrants detailed inspection to determine remaining section.	The condition warrants a structural review to determine the effect on strength or serviceability of the element. A request for action (RFA) should be submitted requesting a structural evaluation and/or repair.

2.2 AVAILABLE DATA AND ANALYSIS CHALLENGES

MDOT shared two spreadsheets with *Bridge Inventory* and *Bridge Element Inventory* data on January 04, 2023. On January 24, 2023, the 2022 National Bridge Inventory (NBI) data were also downloaded from https://infobridge.fhwa.dot.gov/ and referred to as the *2022 NBI data* in this report.

According to the Michigan Structure Inventory and Appraisal Coding Guide (MDOT 2022), item 43A is used to define ten different types of structures based on the types of main span materials, as shown in Table 2-2. The scope of this study is limited to the main span materials represented by the codes 3, 4, 5, and 6.

Table 2-2. Bridge Main Span Material (MDOT 2022)

Code	Materials
1	Concrete
2	Concrete continuous
3	**Steel simple or cantilever**
4	**Steel continuous**
5	**Prestressed***
6	**Prestressed concrete continuous***
7	Timber
8	Masonry
9	Aluminum, W.I or C.I.
0	Other
*Post-tensioned concrete is coded as prestressed concrete.	

The bridges with the types of main span materials 3, 4, 5, and 6 owned by MDOT were selected from the NBI and shared datasets. The numbers in each dataset were different for the following reasons:

1. MDOT inventory has more structures relative to FHWA (NBI data) because MDOT also stores non-NBI structures, which are not required to be submitted to FHWA. Additionally,

the FHWA submittal occurs once a year in March, resulting in a lag in their data relative to the MDOT live database.

2. Pedestrian bridges in NBI were not in the shared datasets.
3. The structures missing from the load rating table were not included in the shared datasets. Structures with only general rating items, without an in-depth load rating, are excluded from the MDOT load rating table.
4. Other reasons:
    i. Recently reconstructed structures with different main span material types.
    ii. Recently reconstructed structures that have not been reported to FHWA.
    iii. Recently constructed new structures added to the MDOT inventory.
    iv. Recently removed structures from the MDOT inventory.
    v. Culverts listed in the NBI data are not included in the MDOT datasets.
    vi. Recently changed jurisdictions.
    vii. The presence of non-NBI bridges.
    viii. Exclusion of unique structures, such as the Blue Water Bridge Authority owned and maintained structures, from the shared datasets.

Finally, the *Bridge Inventory* dataset included a total of 5906 NBI and non-NBI bridges owned by MDOT, with the types of main span materials 3, 4, 5, and 6. The *Element Inventory* listed a total of 3526 bridges after removing 161 duplicate records. Since the element level data collection started recently, 2380 bridges listed in the *Bridge Inventory* dataset were not listed in the *Element Inventory* dataset. As expected, all the bridges in the *Element Inventory* dataset were in the *Bridge Inventory* dataset. The Agency Developed Element (ADE) 826 is used to record beam end conditions. Column (c) of Table 2-3 shows the number of bridges with beam end deterioration. Beam end deterioration was predominantly reported in a total of 992 bridges, representing the types of main span materials 3, 4, and 5. The steel simple structure, the type of main span material 3, has the highest percentage of beam end deterioration (27%). The prestressed concrete, the type of main span material 5, has the second highest percentage of beam end deterioration (19%).

Table 2-3. MDOT Own Bridges with Beam End Deterioration

Structure Type, Main (a)	MDOT Own Bridges		
	NBI and non-NBI (b)	With End Deterioration (ADE 826)	
		Number of Bridges (c)	Percentage (%) (d)
0	0	0	NA
1	1428	2	0.14
2	181	2	1.10
3	**2468**	**644**	**26.90**
4	**416**	**62**	**14.90**
5	**1389**	**266**	**19.15**
6	**10**	**1**	**10.00**
7	11	0	0.00
8	0	0	NA
9	3	0	0.00
Total	5906	997	16.88

The *Element Inventory* dataset was further analyzed to evaluate the distribution of bridges in each MDOT region with repaired and deteriorated beam ends (Table 2-4). According to the criteria listed in Table 2-1, CS1 is assigned to repaired beam ends in good condition. However, the review of inspector comments and available documents in the MiBRIDGE database for a selected number of bridges with CS1 data showed that the CS1 was also assigned for beam ends in good condition without repairs. Due to this inconsistency in data recording, collecting information on beam end repairs through the MiBRIDGE database was not practical.

Table 2-4. Beam End Condition State of Structures with Main Span Materials 3 to 6

Region	No. of Bridges in CS1 with Beam End Deterioration					No. of Bridges in CS2 with Beam End Deterioration					No. of Bridges in CS3 with Beam End Deterioration					No. of Bridges in CS4 with Beam End Deterioration				
	Structure Type Main					Structure Type Main					Structure Type Main					Structure Type Main				
	3	4	5	6	Total (3-6)	3	4	5	6	Total (3-6)	3	4	5	6	Total (3-6)	3	4	5	6	Total (3-6)
Bay	82	4	9	0	**95**	33	2	25	0	**60**	47	0	16	0	**63**	0	0	2	0	**2**
Grand	62	0	6	0	**68**	36	0	30	0	**66**	3	0	5	0	**8**	0	0	0	0	**0**
Metro	54	18	8	0	**80**	4	1	14	0	**19**	7	0	3	0	**10**	1	0	0	0	**1**
North	3	0	0	0	**3**	8	1	10	0	**19**	14	1	0	0	**15**	4	0	0	0	**4**
Southwest	59	1	2	0	**62**	99	6	47	0	**152**	7	1	35	0	**43**	0	0	0	0	**0**
Superior	0	0	0	0	**0**	4	0	0	0	**4**	2	0	1	0	**3**	1	0	0	0	**1**
University	98	3	26	0	**126**	246	26	95	0	**367**	26	1	22	0	**49**	7	1	2	0	**10**
Big Bridge	1	2	2	0	**5**	1	2	4	1	**8**	2	1	0	1	**4**	0	1	0	0	**1**
Total =	**358**	**28**	**53**	**0**	**439**	**431**	**38**	**225**	**1**	**695**	**108**	**4**	**82**	**1**	**195**	**13**	**2**	**4**	**0**	**19**

After discussing the challenges of finding the required information with the project consultants and MDOT RAP, a request for the data and resources listed in Appendix C was submitted. MDOT provided a compiled list of bridge inspector comments in August 2023 and two datasets related to steel and PSC I-beam bridges in November and December 2023, respectively. The steel beam

bridge dataset included 31 scoping reports, 67 shop drawings, 636 original plans, and 13,949 images representing 926 bridges. The PSC I-beam bridge dataset included 19 scoping reports, 214 project letting documents, 38 shop drawings, 338 original plans, and 12,841 images representing 846 bridges. With the additional scoping reports received from the regions, content from a total of 55 scoping reports, comprising 36 for steel bridges and 19 for PSC I-beam bridges, was utilized for this project.

Processing a large volume of inspector comments representing 926 steel structures and 846 PSC structures to identify specific information was a challenge—the sheer volume of information required efficient data analysis tools and methodologies. Extracting relevant data demanded a comprehensive approach. Additionally, ensuring the accuracy of information was crucial, as errors could affect subsequent analysis. This required robust data processing capabilities and advanced algorithms to streamline the identification process and enhance the overall efficiency of the analysis. Inspector comments and the text in other documents were analyzed using natural language processing (NLP) with Python scripting in addition to manually reviewing a large volume of documents and images in various formats. Relevant data from the compiled text were extracted using the process shown in Figure 2-1.

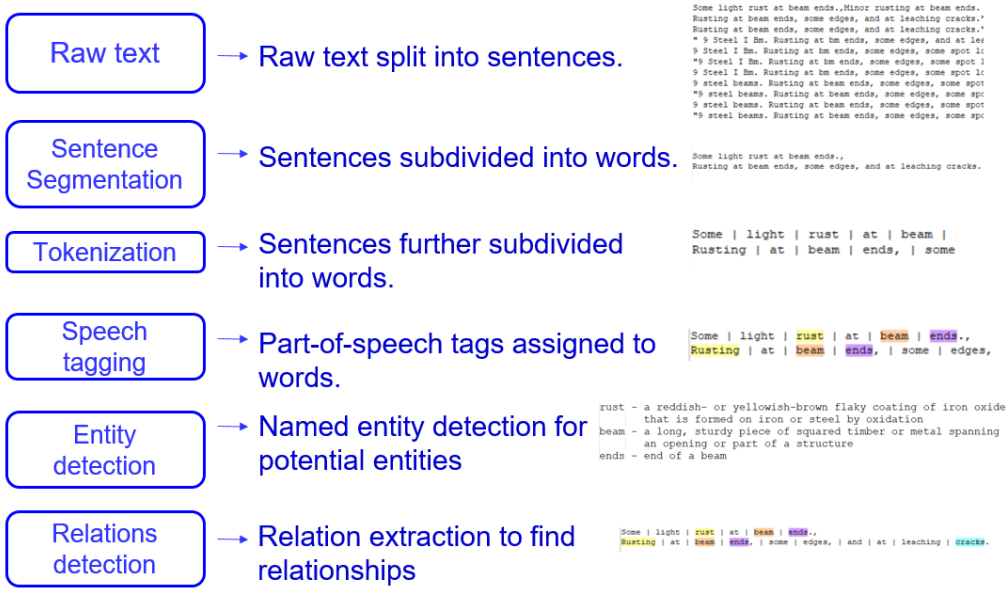

Figure 2-1. The process for extracting data from inspector comments.

2.3 STEEL BEAM END CONDITION AND REPAIR

Thirty-two of thirty-six scoping reports were reviewed to collect condition data on 431 beam ends. One of the scoping reports was for a single span bridge with beam ends embedded into the backwall. Another scoping report only included section loss data within the span. Two reports did not include section loss data, which excluded them from the review. Scoping reports present data related to beam ends with loss of section, holes, cracks, as well as buckled sections, beam end contacts, existing repairs, and the recommended repairs. Certain scoping reports document the rationale for recommending specific repair types and the section loss thresholds used for recommending bolted repairs. Welded repairs are typically recommended for sections with cracks, buckled webs, buckled flanges, or a combination of these defects, as shown in Figure 2-2 to Figure 2-4. Repairs were recommended for 197 of 431 beam ends, 193 (98%) and 4 (2%) beam ends were recommended for bolted and welded repairs, respectively. The data indicate a very high preference for bolted repairs.

The review of the literature and the survey of highway agencies indicated a high preference for bolted repairs due to the challenges associated with field welding requirements, fatigue concerns, and the difficulty of finding qualified welders. Only the Texas DOT stated an extensive use of welded repairs for steel beam repairs. However, several responses indicated excellent performance with welded repairs when (i) the reverse side of the plate is seal-welded to prevent moisture ingress and (ii) full-penetration welds are used. A copy of the highway agency survey questionnaire and a compiled list of responses are provided in Appendices A and B.

Figure 2-2. Welded repair recommended for the beam end because of ¼ to ½-in. web and flange buckling.

Figure 2-3. Welded repair recommended for the beam end because of ¼ to ½-in. web and flange buckling with a 3-in. long crack in the web closer to the bottom flange.

Figure 2-4. Welded repair recommended because of a 4.5-in. long crack and 34% section loss.

Although a 20% section loss is commonly used in the reviewed scoping reports as the threshold for recommending bolted repairs, several scoping reports included bolted repair recommendations for beam ends with section losses significantly lower than the 20% threshold. The review of the literature and the survey of highway agencies indicated inconsistency in the guidelines used for submitting RFAs. For example, 1/8-inch section loss, 30% section loss, and 10% section loss are used by various agencies to submit RFAs. The MnDOT Bridge Inspection Field Manual (BIFM2016) provides Condition State (CS) definitions based on the section loss, as shown in Figure 2-5.

#881: Steel Section Loss (1 Each)

This element applies to bridges with primary steel members with section loss due to corrosion. This typically refers to steel superstructure members but could also apply to steel substructure members (such as pilings) that serve as primary supports. Section loss is typically expressed as a percentage of the total cross-section area of the member (the percentages listed below are intended to be general guidelines).

- The presence of flaking rust or pack rust indicates that at least some section loss is present.
- This element should not be used for culvert structures.

Structural Member	Defect Element Condition States			
	1 Good	2 Fair	3 Poor	4 Severe
Flanges or tension members	Less than 2% section loss of the flange cross-section area.	2% to 5% section loss of the flange cross-section area.	5% to 10% section loss of the flange cross-section area.	More than 10% section loss of the effective flange cross-section.
Webs or compression members	Less than 2% section loss (average over the full height of the web). No through corrosion.	2% to 5% section loss (average over the full height of the web). No through corrosion.	5% to 10% section loss (average over the full height of the web). Isolated through corrosion.	More than 10% section loss (average over full height of the web). Significant through corrosion.
Stiffeners, Lacing, or Batten Plates	Moderate section loss.	Extensive section loss. Isolated through corrosion.	Severe section loss. Significant through corrosion.	NA

Figure 2-5. Condition State (CS) definitions used by MnDOT for steel section loss.

According to the limits set by MnDOT, a section loss exceeding 10% requires further investigation to determine the necessary repairs. This mismatch in the limits used for deciding RFAs is primarily due to the process used for calculating section losses. For example, MnDOT uses the web section loss calculated as the average over the full height of the web. The other practices include,

- Taking measurements over the entire section loss area and reporting the maximum loss.
- Taking measurements over the entire section loss area on a grid and reporting as the average.
- Taking measurements randomly at several discrete points over the entire section loss area and reporting as the average.

The analysis of data related to beam ends shows that 62% section losses are reported at the web, and only 23% of the beam ends include flange and web section losses, as shown in Table 2-5. Please note that the totals listed in Table 2-5 and other tables do not match because the section losses reported in the scoping reports included dimensions of the section loss area only for 365 beam ends. As shown in Table 2-6, 33% of the web section losses are limited to a maximum height of 4 inches, and 69% are limited to 8 inches. As shown in Table 2-7, 77% of web section losses are limited to a length of 20 inches from the beam end. The length of flange section losses is mostly limited to 50 inches (Table 2-8). Therefore, bolted repairs are mostly needed to cover a small area of the beam. Bolted repairs with properly sealed interfaces have demonstrated enhanced durability.

Table 2-5. Section Loss Locations at Beam Ends

Location	Number	Percentage (%)
Flange	63	15
Web	267	62
Web and flange	101	23
Total	431	

Table 2-6. Height of Web Section Loss

Height (in.)	Number	Percentage (%)
[0, 4]	122	33
(4, 6]	94	26
(6, 8]	38	10
(8, 10]	29	8
(10, 15]	21	6
(15, 20]	17	5
(20, 25]	26	7
(25, 30]	13	4
(30, 35)	5	1
Total	**365**	

Table 2-7. Length of Web Section Loss

Length (in.)	Number	Percentage (%)
(0, 5]	90	25
(5, 10]	80	22
(10, 20]	111	30
(20, 30]	46	13
(30, 50]	29	8
(50, 190]	9	2
Total	**365**	

Table 2-8. Length of Flange Section Loss

Length (in.)	Number	Percentage (%)
(0, 5]	21	13
(5, 10]	25	15
(10, 20]	31	19
(20, 30]	35	21
(30, 50]	28	17
(50, 70]	10	6
(70, 100]	9	6
(100, 240]	4	2
Total	**163**	

Steel sections associated with these 431 beam ends were selected. The web and flange section loss percentages of each section were calculated assuming a section loss of 1/8 inch. The web section loss percentages range from 7% to 35%. However, the 7% and 35% losses are limited to only two cases each. The section loss of 70% of beam ends ranges from 20% to 24%. The section loss of more than 90% of beam ends ranges from 20% to 27%. Considering these statistics, it is recommended to use a 20% web section loss as the limit for determining the need for repairs on webs up to 0.625 inches thick, unless unique conditions at the specific beam end dictate otherwise.

Since most of the section losses are limited to a small area on the web closer to the bearing, it is recommended to take the average of measurements within that area to calculate the section loss. The section loss percentage of the flanges was calculated using 1/8-inch as the limit. It is recommended to use a 10% flange section loss as the limit for determining the need for repairs on flanges up to 1.25 inches thick when a beam end has both web and flange section losses.

As stated previously, repairs were recommended for 197 of 431 beam ends. Bolted and welded repairs were recommended for 193 (98%) and 4 (2%) beam ends, respectively. As shown in Table 2-9, bolted repairs were recommended for 150 beam ends because of the web section loss. One hundred and nineteen (79%) of those beam ends had at least 1/8-inch web section loss. Therefore, bolted repairs were recommended for 21% of beam ends with web section loss for unknown reasons. As shown in Table 2-10, bolted repairs were recommended for 43 beam ends because of the flange section loss. Thirty-six (84%) of those beam ends had at least a 1/8-inch flange section loss. Therefore, bolted repairs were recommended for 16% of beam ends with flange section loss for unknown reasons. This data shows that the number of beam ends recommended for bolted repairs with section loss less than 1/8 inch could have been reduced if clear guidance for determining the need for repairs had been provided. It is recommended to use 20% web section loss and 10% flange section loss (in the presence of web section loss) as the minimum limit requiring beam end repairs, unless unique conditions at the specific beam end dictate otherwise. These limits should be applied to beam sections with web and flange thicknesses not exceeding 0.625 inches and 1.25 inches, respectively. Include the unique conditions requiring beam end repairs in the scoping reports.

Table 2-9. Beam Ends with Bolted Repair Recommendations Based on Web Section Loss

	Beam End with Bolted Repair Recommendations	
	Number	Percentage (%)
Above threshold	119	79
Below threshold	31	21
Total	150	

Table 2-10. Beam Ends with Bolted Repair Recommendations Based on Flange Section Loss

	Beam End with Bolted Repair Recommendations	
	Number	Percentage (%)
Above threshold	36	84
Below threshold	7	16
Total	43	

2.4 PSC BEAM END CONDITION AND REPAIR

Eight bridges with overcast repairs and four bridges with Carbon Fiber Reinforced Polymer (CFRP) wrapping were selected for inspection. The findings are documented in Appendix D. The girder end conditions noted in the respective RFAs and scoping reports were summarized and used to develop the inspection guidelines presented in Chapter 3, the capacity calculation for developing the Request for Action (RFA) Decision Matrix presented in Chapter 4, and the repair details presented in Chapter 6. Additional information from relevant bridge plans, literature, and surveys of state highway agencies was used to complete the tasks and develop the deliverables.

3 RFA AND SCOPING INSPECTION GUIDELINES FOR PSC I-BEAM ENDS

3.1 OVERVIEW

In this study, nineteen (19) scoping inspection reports, Bridge Safety Inspection Report (BSIR) reports of 267 bridges, several RFA reports, and other related documents in the MiBRIDGE database were reviewed, documenting the types, locations, and severity of PSC I-beam end distress and deterioration. A detailed discussion of beam end conditions is provided in Sections 4.5.1 and 4.5.2. Beam end maintenance and repair practices are discussed in Section 6.1. For element-level inspection, MDOT uses the Agency Developed Element (ADE) 826 to document beam end conditions and assign condition state ratings. Inspectors utilized various templates and guidelines to document types, locations, and severity of beam end distress and deterioration during RFA and scoping inspections. Two such examples are shown in Figure 3-1 and Figure 3-2. Figure 3-1 shows the guidelines and format for documenting the locations and dimensions of delamination, spall, spall-to-steel, vertical and horizontal cracks, map cracking, and concrete patches. Figure 3-2 shows guidelines for documenting spalls, shear cracks, and exposed strands. Figure 3-3 shows a tabular format used for documenting the data collected using the guidelines given in Figure 3-2. As shown in Figure 3-3, the data table includes the span, pier, beam number, dimensions of the spalls, and the number of exposed strands. The last column of the table includes recommended repairs and additional observations as notes. However, the available scoping inspection guidelines are not sufficiently detailed to collect the minimum required data for assessing beam end capacity and making decisions on maintenance, repair, or load posting.

To address the shortcomings in the current RFA and scoping inspection guidelines, the following sections present (i) discretization of a beam end into specific zones and (ii) guidelines and templates for documenting delamination, spall, and cracking at PSC I-beam ends. Please note that these guidelines were developed with consideration for the potential implementation of drones and computer vision technologies in the near future to alleviate the challenges associated with typical visual inspections.

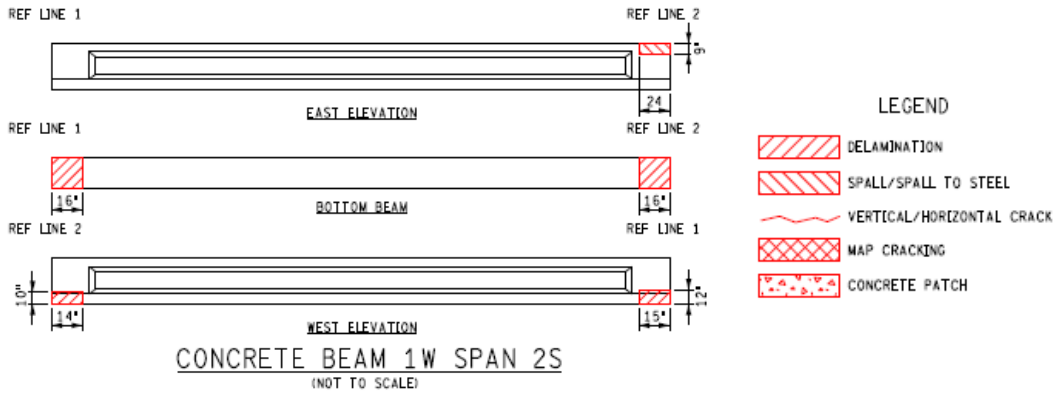

Figure 3-1. PSC I-beam end condition reporting guidelines (Source: MiBRIDGE SN1718).

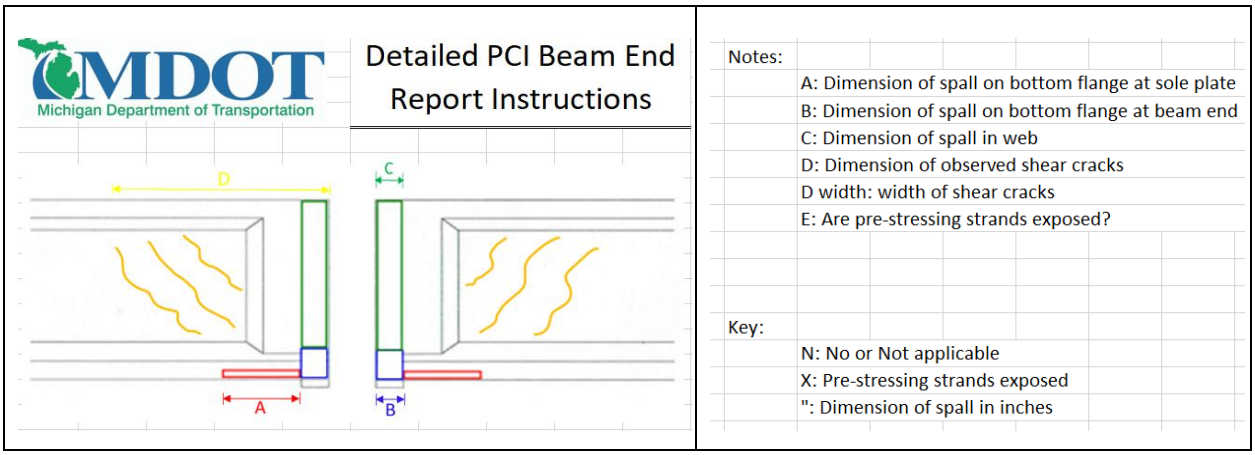

Figure 3-2. PSC I-beam end condition reporting guidelines (Source: MiBRIDGE SN4779).

MDOT Michigan Department of Transportation	Detailed PCI Beam End Report						Bridge ID: STR 4779, 41027-S06
							Date: 08-21-2023
							Inspector(s): CAR / JH
	Span: 1				Pier: 1		
Beam #	A	B	C	D	D width	E	Notes
1w	10	12					
2w	12	16				2/1	Bolster Block Repair (BBR) - Bearing Undermined
3w	6	10				2	BBR
4w	12	10					BBR - Bearing Undermined
5w	12	10				1	BBR - Bearing Undermined 30%
6w	16	5					BBR - Bearing Undermined 50%
7w	14	14				2	BBR - Bearing Undermined 50%
8w	16	20				1	BBR
9w	10	16				1	BBR - Bearing Undermined 40%
10w	10	8				1	BBR - Bearing Undermined 50%
11w	12						BBR - Bearing Undermined
12w	12	6	6			2	incipient spall on bottom flange @ midspan

Figure 3-3. A summary of beam end inspection data collected using the guidelines given in Error! Reference s ource not found. **(Source: MiBRIDGE SN4779).**

3.2 BEAM END ZONES

A PSC I-beam end is divided into several zones, as shown in Figure 3-4.

- Figure 3-4(a) and (b): beam cross-section with three vertical zones (left of the web - LW, along the web - W, and right of the web - RW).
- Figure 3-4(b and c): five zones along the beam height (bottom flange – BF_1, bottom flange to web transition – BF_2, web – WB, top flange to web transition – TF_2, and top flange – TF_1).
- Figure 3-4(c): three zones along the length (overhang portion of the beam – Z_1, section above the bearing footprint – Z_2, and the section from the edge of the bearing towards the span up to 5 ft of bearing – Z_3.

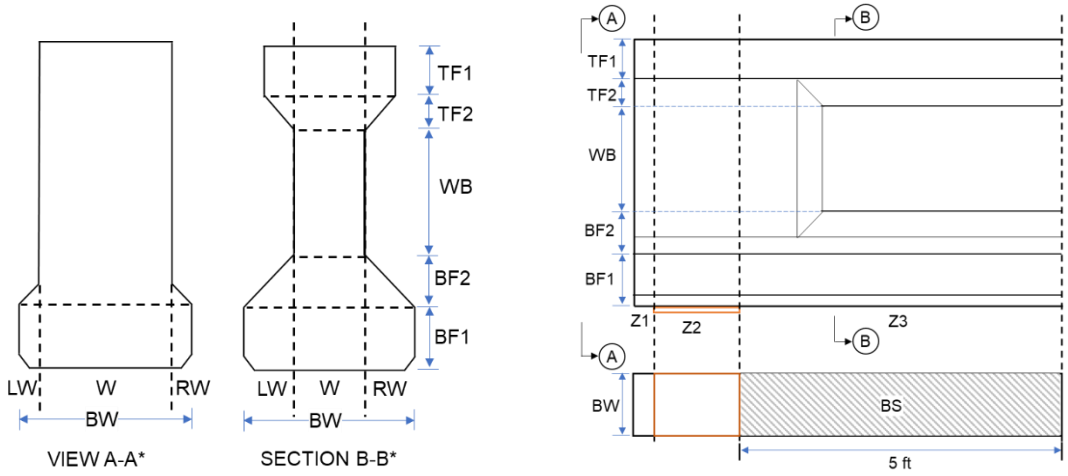

(a) Cross-section with endblock

(b) Cross-section without endblock

(c) Elevation and bottom surface views

Figure 3-4. Definitions of PSC I-beam end zones

LW = Cross-section on the left of the web
W = Cross-section of the web
RW = Cross-section on the right of the web
TF_1 = Top flange (rectangular section)
TF_2 = Section between the web and TF_1
WB = Web
BF_1 = Bottom flange (rectangular section)
BF_2 = Section between the web and BF_1
BS = Beam soffit (from the edge of bearing towards the span up to 5 ft)
BW = Bottom flange width
Z_1 = Zone 1, overhang portion at the beam end
Z_2 = Zone 2, beam section over the bearing plate
Z_3 = Zone 3, beam section from the edge of bearing towards the span up to 5 ft of bearing.

* Prestressing strand and reinforcement are not shown.

3.3 INSPECTION GUIDELINES AND TEMPLATES

3.3.1 Spall/Delamination

3.3.1.1 Spall/Delamination at the Soffit

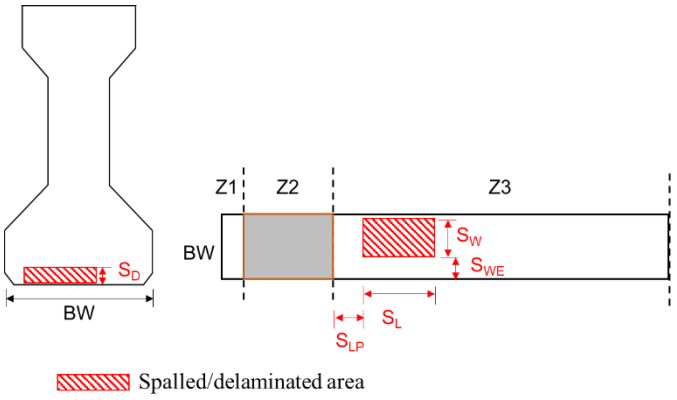

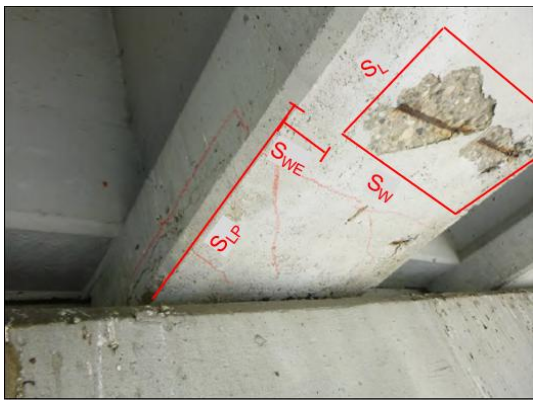

Legend:

S_D = spall/delamination depth
S_L = spall/delamination length along the beam
S_{LP} = distance from bearing to the spall/delamination (consider the shortest distance measured from bearing)
S_W = spall/delamination width
S_{WE} = distance from the beam edge to the spall/delamination
N_{PS} = number of prestressing strands exposed
N_S = number of non-prestressing steel bars exposed
N_{ST} = number of stirrups exposed

Table 3-1. Inspection Template for Beam Soffit – Spall/Delamination

Beam Soffit – Spall/Delamination									
Beam End	**Type**	**S_D (in.)**	**S_L (in.)**	**S_{LP} (in.)**	**S_W (in.)**	**S_{WE} (in.)**	**N_{PS} (no.)**	**N_S (no.)**	**N_{ST} (no.)**
Sp1W_P1W_B1S	Spall								
	Del.								
Sp2W_P1W_B1S	Spall								
	Del.								
	Spall								
	Del.								
	Spall								
	Del.								
B = Beam; Del. = Delamination; P = Pier; S=South; Sp = Span; W= West									

Note: The following labels are suggested when a beam end is over an abutment:
AE – East abutment; AW – West abutment; AN – North abutment; AS – South abutment

3.3.1.2 *Spall/Delamination at the Bottom Flange and Web*

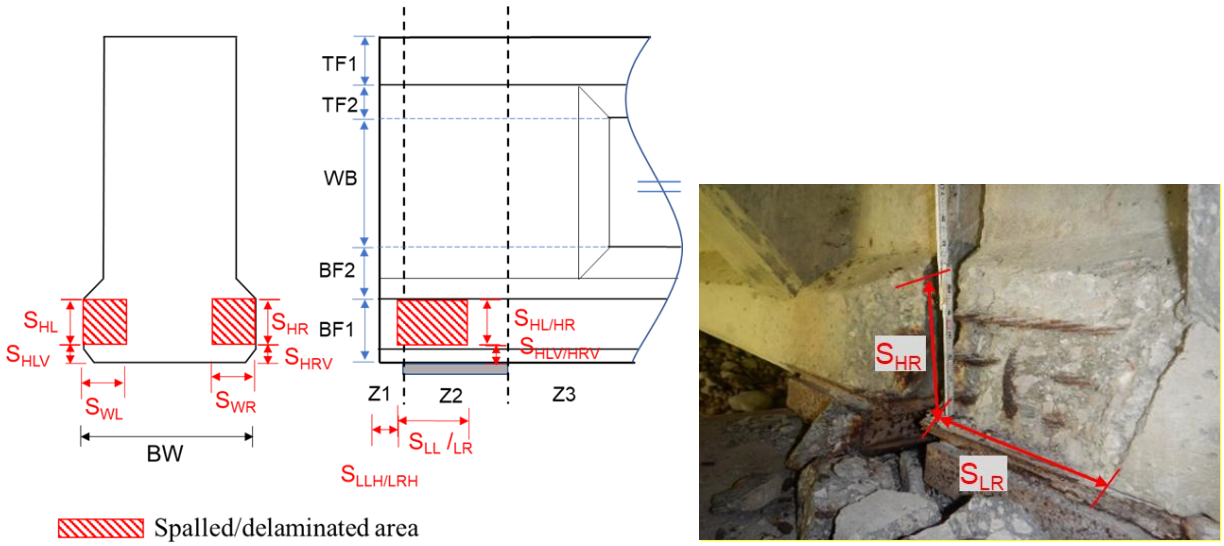

Legend:

S_{HL} = height of spall/delamination on the left side
S_{HR} = height of spall/delamination on the right side
S_{HLV} = vertical distance from the beam soffit to the spall/delamination on the left side
S_{HRV} = vertical distance from the beam soffit to the spall/delamination on the right side
S_{LL} = length of spall/delamination on the left side
S_{LR} = length of spall/delamination on the right side
S_{WL} = depth of spall/delamination on the left side
S_{WR} = depth of spall/delamination width/depth on the right side
S_{LLH} = horizontal distance from the beam end to the spall/delamination on the left side
S_{LRH} = horizontal distance from the beam end to the spall/delamination on the right side
N_{PSL} = number of prestressing strands exposed on the left side
N_{SL} = number of non-prestressing steel bars exposed on the left side
N_{STL} = number of stirrups exposed on the left side
N_{PSR} = number of prestressing strands exposed on the right side
N_{SR} = number of non-prestressing steel bars exposed on the right side
N_{STR} = number of stirrups exposed on the right side

Table 3-2. Inspection Template for Beam Bottom Flange and Web (Left Side) – Spall/Delamination

Beam Bottom Flange and Web – Spall/Delamination									
Beam End	**Left Side of the Web**								
	Type	**S_{HL} (in.)**	**S_{HLV} (in.)**	**S_{LL} (in.)**	**S_{WL} (in.)**	**S_{LLH} (in.)**	**N_{PSL} (no.)**	**N_{SL} (no.)**	**N_{STL} (no.)**
Sp1W_P1W_B1S	Spall								
	Del.								
Sp1W_P1W_B2S	Spall								
	Del.								
	Spall								
	Del.								
B = Beam; Del. = Delamination; P = Pier; S=South; Sp = Span; W= West									

Table 3-3. Inspection Template for Beam Bottom Flange and Web (Right Side) – Spall/Delamination

Beam Bottom Flange and Web – Spall/Delamination									
Beam End	**Right Side of the Web**								
	Type	**S_{HR} (in.)**	**S_{HRV} (in.)**	**S_{LR} (in.)**	**S_{WR} (in.)**	**S_{LRH} (in.)**	**N_{PSR} (no.)**	**N_{SR} (no.)**	**N_{STR} (no.)**
Sp1W_P1W_B1S	Spall								
	Del.								
Sp1W_P1W_B2S	Spall								
	Del.								
	Spall								
	Del.								
	Spall								
	Del.								
B = Beam; Del. = Delamination; P = Pier; S=South; Sp = Span; W= West									

3.3.2 Beam End Cracking

3.3.2.1 Cracks at the Bottom Flange and Web

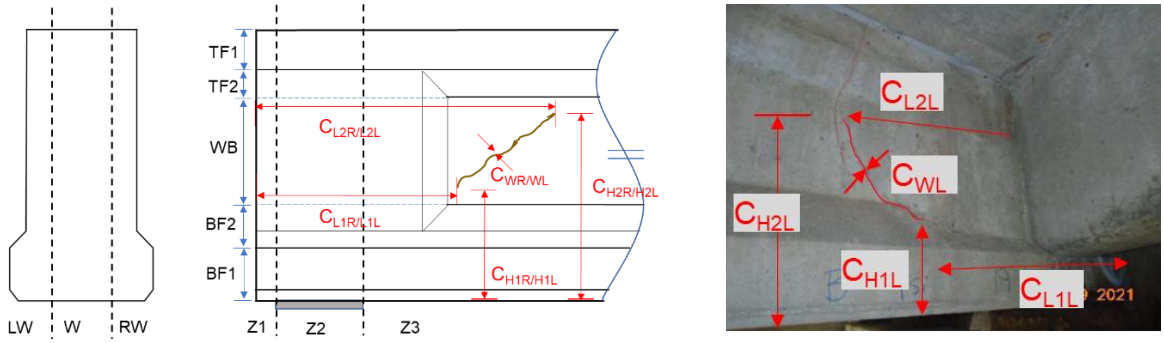

Legend:

C_{L1R} = crack starting location from the beam end on the right side
C_{L2R} = crack ending location from the beam end on the right side
C_{L1L} = crack starting location from the beam end on the left side
C_{L2L} = crack ending location from the beam end on the left side
C_{H1R} = crack starting location from the beam soffit on the right side
C_{H2R} = crack ending location from the beam soffit on the right side
C_{H1L} = crack starting location from the beam soffit on the left side
C_{H2L} = crack ending location from the beam soffit on the left side
C_{WR} = crack width on the right side
C_{WL} = crack width on the left side

Table 3-4. Inspection Template for Beam Bottom Flange and Web – Cracks

Beam Bottom Flange and Web – Cracks											
Beam End	**Type**	**Left Side of the Web**					**Right Side of the Web**				
		C_{WL} (in.)	C_{L1L} (in.)	C_{L2L} (in.)	C_{H1L} (in.)	C_{H2L} (in.)	C_{WR} (in.)	C_{L1R} (in.)	C_{L2R} (in.)	C_{H1R} (in.)	C_{H2R} (in.)
Sp1W_P1W_B1S	Longitudinal										
	Transverse										
	Shear										
Sp1W_P1W_B2S	Longitudinal										
	Transverse										
	Shear										
	Longitudinal										
	Transverse										
	Shear										
B = Beam; P = Pier; S=South; Sp = Span; W= West											

3.3.2.2 Cracks at the Soffit

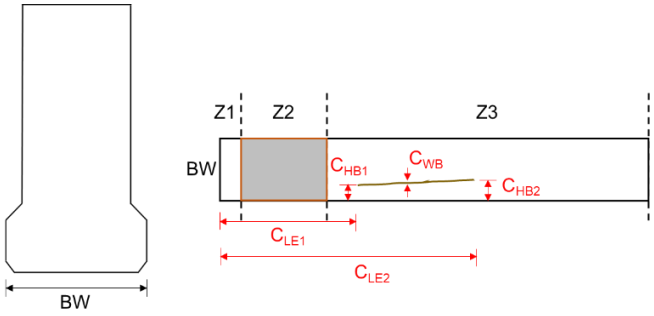

Legend:

C_{LE1} = crack starting location from the beam end
C_{LE2} = crack ending location from the beam end
C_{HB1} = crack starting location from the beam edge
C_{HB2} = crack ending location from the beam edge
C_{WB} = crack width

Table 3-5. Inspection Template for Beam Soffit – Cracks

Beam End	**Type**	**C_{LE1} (in.)**	**C_{LE2} (in.)**	**C_{HB1} (in.)**	**C_{HB2} (in.)**	**C_{WB} (in.)**
Sp1W_P1W_B1S	Longitudinal					
Sp2W_P1W_B1S	Transverse					
	Diagonal					
B = Beam; P = Pier; S=South; Sp = Span; W= West						

4 REQUEST FOR ACTION (RFA) DECISION MATRIX

4.1 OVERVIEW

Bridge inspection engineers and consultants submit requests for action (RFAs) due to safety concerns associated with the conditions of steel and prestressed concrete (PSC) beams. Region bridge engineers review RFAs and submit them to the Bridge RFA Coordination Committee (BRFACC) for deliberation. The MiSIM (2019) Table 5.13.13 lists various conditions to be considered when evaluating the need for RFAs (Table 4-1). For example, the current guidelines for deciding the need for an RFA for PSC beams include the following:

- In-depth inspection required
- Element quantities in Condition State (CS) 4
- 25% or greater reduced bearing surface
- Exposed prestressing strands
- Structural cracking
- Required strengthening or reduced inspection frequency resulting from load rating.

Table 4-1. Concrete and Steel Beam Conditions Requiring the Submission of RFAs (MiSIM 2019, Table 5.13.13)

Request for Action	Beam/Girder Material	
	Concrete	Steel
In-depth Inspection Required	X	X
Element Quantities in Condition State 4	X	X
10% or Greater Section Loss or Buckling		X
25% or Greater Reduced Bearing Surface	X	
Exposed Prestressing Reinforcement	X	
Beam End Contact	X	X
Moderate Section Loss on Temporary Support	X	X
Structural Cracking in Primary Members	X	X
Cracking in Welded Connections		X
Required Strengthening or Reduced Inspection Frequency Resulting from Load Rating	X	X
Observed Damage Meeting Type 2 or 3 Criteria	X	X
Instable Bridge Sign Connection	X	X
Prestressed Concrete Spalling Resulting in Strand Exposure	X	

An in-depth inspection is required when a detailed assessment of structural deterioration is necessary to ensure safety and develop maintenance decisions. Specifically, this type of inspection becomes mandatory when the superstructure element, identified by National Bridge Inventory (NBI) Item 59, receives a condition rating of 6 or lower. Table 4-2 presents the NBI condition rating guidelines for concrete superstructure elements, ranging from 9 (new condition) to 0 (failed).

These ratings are used to evaluate the severity of deterioration and determine the urgency of further action.

Table 4-2. BSIR# 9 Superstructure (SI&A Item 59) for Concrete Material (MDOT 2017)

Code	Condition	Description
9	NEW	No deficiencies in any of the structural components will affect long-term performance.
8	GOOD	All protective coatings are sound and functioning but with minor weathering of the coating.
7	GOOD	Hairline cracks in C.I.P. concrete or sealed cracks spaced at more than 3' with no other defects present.
6	FAIR	Cracks in C.I.P. concrete 1/16" wide or less or hairline cracks in P.S. concrete spaced at more than 3'. Minor delamination and spalling with exposed mild steel reinforcement without section loss or rust staining.
5	FAIR	Cracks in C.I.P. concrete 1/16" wide or less or hairline cracks in P.S. concrete spaced at 1' to 3'. Moderate delamination, spalling, or exposed prestressing reinforcement without section loss. Minor efflorescence present.
4	POOR	Cracks in C.I.P. 1/16" wide or greater or hairline cracks in P.S. concrete spaced at less than 1'. Moderate delamination and spalling or exposed prestressing reinforcement without section loss.
3	SERIOUS	Structural cracking or reinforcement section loss may affect load capacity.
2	CRITICAL	The superstructure will not support design loads. Posting, emergency repairs installed, or temporary shoring is required.
1	IMMINENT FAILURE	The bridge is closed to traffic due to the potential for superstructure failure, but corrective action may put it back in service.
0	FAILED	The bridge is closed due to conditions. Coordinate with SI&A Item 41 and notify Bridge Field Services.

Since the NBI inspection does not document the condition of specific bridge elements, the element level inspection was introduced. As shown in Table 4-3, an Agency Developed Element (ADE) 826 is used to document CS of beam ends based on the level of deterioration within 5 ft of the bearing (MiBEIM, 2017). The loss of section at each beam end is the only parameter included in the CS Table 9, even though exposed strands, bearing area loss, structural cracking, etc., have an impact on the beam end capacity. Essentially, the current guidelines lack the clarity and rationale necessary for inspectors to determine a specific CS for beam ends. To alleviate these limitations, a capacity-based beam end deterioration classification system is needed. This new beam end deterioration classification system is expected to enhance correlations between visual inspection data and structural performance, thereby providing a rational process for identifying the need for RFAs.

Table 4-3. CS Table 9 with Beam End Condition State Definitions (MiBEIM 2017)

Defects	Condition State 1 GOOD	Condition State 2 FAIR	Condition State 3 POOR	Condition State 4 SEVERE
Beam End Deterioration (826)	Section loss to element has been repaired	Section loss exists and has not been repaired. Structural analysis is not yet warranted.	Measurable section loss that warrants detailed inspection to determine remaining section	The condition warrants a structural review to determine the effect on strength or serviceability of the element. A request for action (RFA) should be submitted requesting a structural evaluation and/or repairs

The development of this guidance document involved the following key steps:

(1) Selection of a beam end capacity calculation model.

(2) Evaluation of the margin-of-safety as the ratio of experimental capacity and the factored shear resistance.

(3) Evaluation of the factored shear resistance (*capacity*) and the factored shear at the beam end (*demand*) to establish a capacity-to-demand ratio.

(4) Evaluation of the impact of beam end conditions on capacity to establish limits for deciding the need for an RFA.

4.2 BEAM END CAPACITY CALCULATION MODEL

The Strut-and-Tie Method (STM) is used to model and analyze disturbed regions, known as D-regions in structural components, utilizing an idealized truss composed of compression struts and tension ties. A disturbed region with complex load paths that violate the linear strain distributions assumed in flexural design develops due to a load and/or geometric discontinuity (AASHTO LRFD 2020). According to Jang et al. (2022), STM is capable of representing complex load paths and failure modes (e.g., nodal failure and lateral splitting) at PSC I-beam ends more accurately than models that use linear strain and planar section assumptions. Additionally, a 3D model with struts and ties can be used to represent the complex load path within a PSC I-beam cross-section near the bearing to evaluate the adequacy of confining reinforcement for preventing lateral splitting at the bottom flange (Ross et al., 2013; Shahrooz et al., 2017).

PSC I-beams, including bulb-tee and Michigan 1800 sections, exhibit significant geometric discontinuities at the ends, resulting in a complex load transfer mechanism. These regions typically contain harped strands, debonded strands, and a high concentration of straight strands in the bottom flange. Beam end deterioration increases the complexity of the stresses developed at the ends. For these reasons, STM is used in this study to calculate the capacity of beam ends with as-designed details, deteriorations, and repairs. The STM considers longitudinal tie, bearing face,

strut-to-node interface, and transverse tie capacities to establish a beam end capacity. *A set of Mathcad calculation sheets was developed to calculate the capacities of as-designed, deteriorated, and repaired beam ends and delivered to MDOT.* A manual describing the content and use of these Mathcad sheets was developed and submitted to MDOT along with the calculation sheets. A copy of the manual is provided in Appendix E.

Figure 4-1 shows a model with struts and ties for a beam end with straight strands. The development of longitudinal tie and strut forces resulting from the applied load at a span-to-depth ratio of one is illustrated in Figure 4-1(a). As shown in Figure 4-1(b), a CCT (Compression-Compression-Tension) node is developed above the bearing when a tension tie intersects the node from only one direction. A compression strut is formed between the load application point and the centroid of the horizontal bonded strands located above the bearing centerline, as shown in Figure 4-1(a). The critical section for the development of the tie is located at the intersection of the centerline of the tie and the boundary of the strut, as shown in Figure 4-1 (b). The distance from the beam end to the critical section for the development of the tie is l_x. According to the AASHTO LRFD (2020), the transfer length, l_t, is defined as 60 times the strand diameter (d_b).

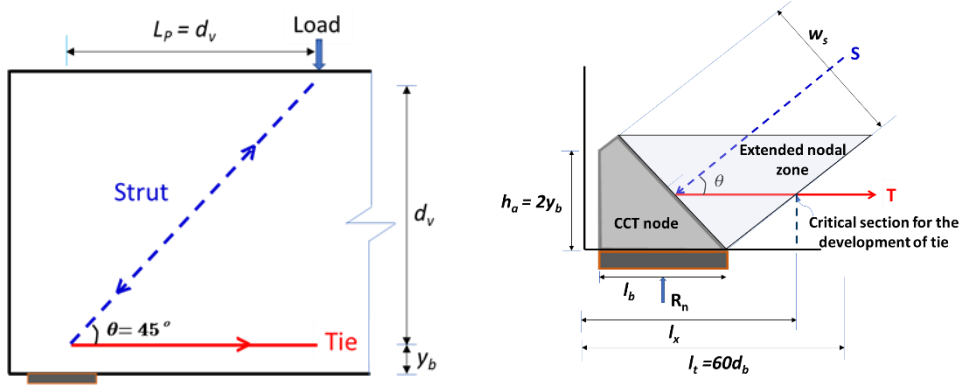

(a) Strut and tie forces (b) CCT node geometry

Figure 4-1. A model with struts and ties for a beam end with straight strands.

The strut-and-tie model for a beam end with harped strands includes two tension ties (T_1 and T_3), three compressive struts (S_1, S_2, and S_3), and an additional node, N_h, that connects S_1, S_2, and T_3. The following conditions govern the location of node N_h.

(i) The angle θ_1 between S_1 and T_3 shall be greater than 25 degrees.

(ii) The angle θ_2 between S_2 and T_1 shall not be greater than 90 degrees.

(iii) The angle θ_3 between S_3 and T_1 is maintained at 45 degrees to be consistent with the configuration used for beams without harped strands.

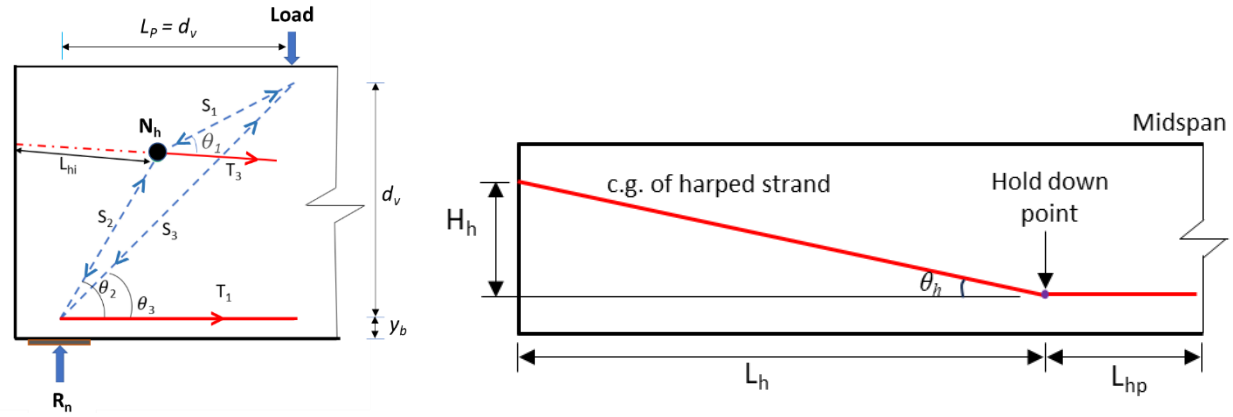

(a) Strut and tie forces (b) Harped strands angle

Figure 4-2. A model with struts and ties for a beam end with harped and straight strands (Jang et al. 2022).

4.2.1 Longitudinal Tie Capacity

The failure of a longitudinal tie is abrupt and resembles a brittle fracture. As shown in Figure 4-3, the failure initiates with the formation of vertical flexural cracks at the bottom of the beam. Crack widths and lengths increase as the applied load increases, allowing the cracks to propagate diagonally toward the upper part of the beam, moving in the direction of the applied load. This progression reflects the transition from flexural to shear behavior. When cracks develop near the beam ends, strand anchorage is compromised, causing the strands to slip and fail. It can also lead to crushing of the compression zone due to rotation induced, in part, by strand slippage. This form of failure is often referred to as "diagonal shear-tension failure" (Shahrooz et al., 2017), "bond-shear failure", or "bond-tension failure" (Ross 2012).

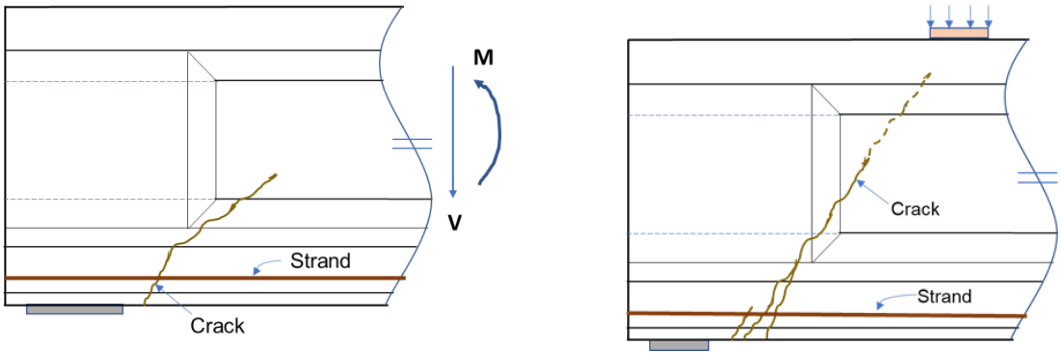

(a) Crack initiation (b) Crack propagation

(c) Failure observed during laboratory testing (Shahrooz et al. 2017)

Figure 4-3. Diagonal shear-tension failure at the beam end.

The longitudinal tie force, T, shown in Figure 4-1(b) for a section with straight strands is calculated using Eq. 4-1.

$$T = A_{ps} \times f_{pe} \times l_x/l_t \qquad \textit{Eq. 4-1}$$

where,

A_{ps} = *total area of bonded prestressing strands in the bottom flange*

f_{pe} = *effective stress in prestressing steel after losses*

l_t = *transfer length*

l_x = *distance from the beam end to the location of the critical section for the development of the tie*

For a section with straight strands, the factored shear resistance at the beam end provided by the longitudinal tie, V_{uLT_S}, is calculated using Eq. 4-2.

$$V_{uLT\_S} = \phi \times T \times \tan\theta = \phi \times V_{nLT\_S} \qquad \textit{Eq. 4-2}$$

where,

V_{nLT_S} = *the nominal shear resistance at the beam end with straight strands provided by the longitudinal tie*

θ = *the angle between the strut and tie*

ϕ = *the resistance factor for tension-controlled members in STM*

= *1.0 (Article 5.5.4.2 of AASHTO LRFD (2020))*

For a section with harped and straight strands, the tie force developed in straight strands, T_1, is calculated using Eq. 4-1. The tie force along the harped strand profile, T_3, is calculated using Eq. 4-3.

$$T_3 = A_{hps} \times f_{pe} \times L_{hi}/l_t \qquad \textit{Eq. 4-3}$$

where,

A_{hps} = *total area of bonded harped strands*

L_{hi} = *distance between beam end and* N_h *measured along the harped strand profile*

The vertical component of T_3, V_{nLVT}, is calculated using Eq. 4-4.

$$V_{nLVT} = A_{hps} \times f_{pe} \times \sin(\theta_h) \qquad \textit{Eq. 4-4}$$

where,

θ_h = *the angle between the centerline of the harped strands and the horizontal line through the hold down point*

The forces S_1 and S_2 are calculated considering horizontal and vertical force equilibrium at N_h.

Considering horizontal force equilibrium at N_h,

$$S_1(L_p - X_i)/L_{S1} - S_2(X_i/L_{S2}) = T_3L_h/(\sqrt{(L_h^2 + H_h^2)}) \qquad \textit{Eq. 4-5}$$

where,

H_h = *vertical distance between the centroid of the harped strands at the beam end and at the hold-down point*

L_h = *distance from the beam end to the harped strands hold-down point*

L_P = *distance from the bearing center to the loading point*

L_{S1} = *length of strut* S_1

L_{S2} = *length of strut* S_2

X_i = *horizontal distance between the bearing centerline and* N_h

Considering vertical force equilibrium at N_h,

$$S_1(d_v - Y_i)/L_{S1} - S_2(Y_i/L_{S2}) = -T_3H_h/(\sqrt{(L_h^2 + H_h^2)}) \qquad \textit{Eq. 4-6}$$

where,

d_v = *effective shear depth of the beam*

Y_i = *vertical distance between the centroid of horizontal strands and* N_h

The force in S_3 is calculated considering horizontal equilibrium at the CCT node.

$$S_3 = (T_1 - S_2 X_i / L_{S2}) / (L_P / L_{S3}) \quad \text{Eq. 4-7}$$

where,

L_{S3} = *length of strut* S_3

The reaction force, R_n, is calculated considering the vertical equilibrium at the CCT node.,

$$R_n = S_2 \times \sin(\theta_2) + S_3 \times \sin(\theta_3) \quad \text{Eq. 4-8}$$

For a section with harped and straight strands, the factored shear resistance at the beam end provided by the longitudinal ties, V_{uLT_H}, is calculated using Eq. 4-9.

$$V_{uLT\_H} = \phi \times (R_n - V_{nLVT}) = \phi \times V_{nLT\_H} \quad \text{Eq. 4-9}$$

where,

V_{nLT_H} = *the nominal shear resistance at the beam end with harped and straight strands provided by the longitudinal tie*

ϕ = *the resistance factor for tension-controlled members in STM*

= *1.0 (Article 5.5.4.2 of AASHTO LRFD (2020))*

4.2.2 Bearing Face Capacity

Bearing face failure is observed as concrete crushing or diagonal shear-compression failure. Figure 4-4 shows beam end crack patterns due to shear-compression failure.

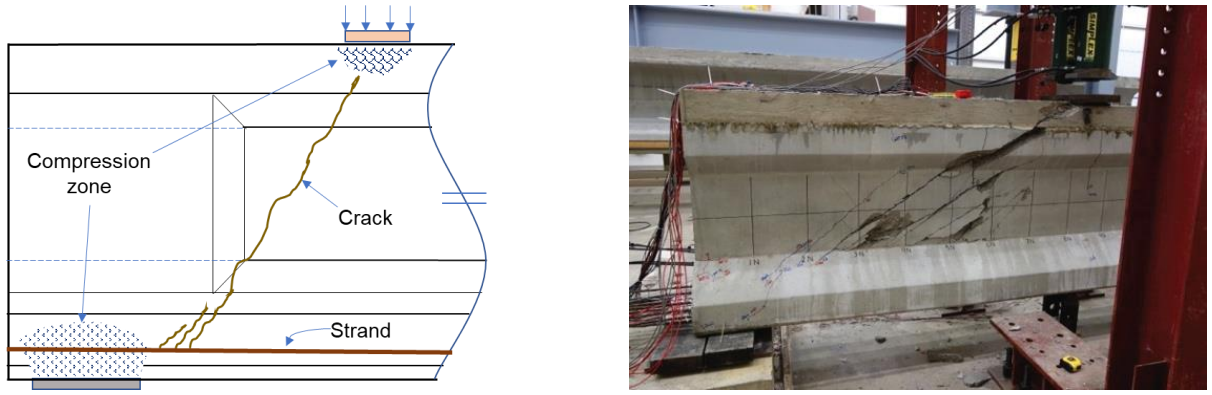

(a) (b)

Figure 4-4. Shear-compression failure of an I-beam: (a) an illustration and (b) a tested beam (Shahrooz et al. 2017).

Even though this failure mode is typically initiated with concrete crushing at the loading point during laboratory studies, this type of failure is not practical under in-service conditions because

the concentrated load used in lab tests does not reflect the in-service loads at the beam top flange. Therefore, the factored bearing face resistance, P_{r1}, is calculated at the CCT node using Eq. 4-10.

$$P_{r1} = \phi_c \times f_{cu1} \times l_b \times w_p \qquad \textit{Eq. 4-10}$$

where,

f_{cu1} = *limiting compressive stress at the bearing face*

$= m \times v \times f_c'$

f_c' = *design concrete compressive strength*

m = *confinement modification factor (Article 5.8.2.5.3a of AASHTO LRFD (2020))*

v = *concrete efficiency factor (Table 5.8.2.5.3a-1 of AASHTO LRFD (2020))*

l_b = *bearing length*

w_p = *bearing width*

ϕ_c = *resistance factor for compression in STM*

= *0.7 (Article 5.5.4.2 of AASHTO LRFD (2020))*

Since the maximum reaction force, R_n, developed at the bearing face is limited by the factored bearing face resistance, P_{r1}, at that location, the factored shear resistance at the beam end controlled by the bearing face failure mode, V_{uBF}, is calculated using Eq. 4-11.

$$V_{uBF} = (V_{uLT\_S} \text{ or } V_{uLT\_H})(P_{r1}/R_n) \qquad \textit{Eq. 4-11}$$

4.2.3 Strut-to-Node Interface Capacity

The strut-to-node interface is shown in Figure 4-5. The strut-to-node interface failure occurs when the concrete at the interface between the strut (compression member) and the node (the convergence point of internal forces) fails to resist the applied compressive stresses. This is also referred to as the "web base crushing" failure. Figure 4-5(b) shows CCT node dimensions, including the strut-to-node interface length. At the CCT node, the width of the strut, w_s, is equal to the length of the strut-to-node interface.

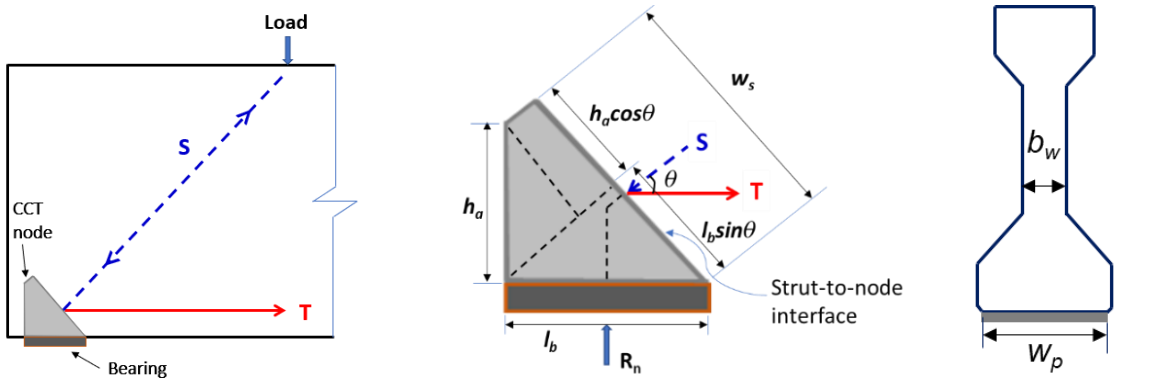

(a) Beam end with a strut, tie, and CCT node (b) CCT node (c) Beam cross-section

Figure 4-5. CCT node formation between the bearing and the strut.

The factored strut-to-node interface resistance, P_{r2}, at the CCT node is calculated using Eq. 4-12.

$$P_{r2} = \phi_c \times f_{cu2} \times w_s \times w_p \qquad \textit{Eq. 4-12}$$

where,

f_{cu2} = *limiting compressive stress at the strut-to-node interface*

$= m \times v \times f_c'$

f_c' = *design concrete compressive strength*

m = *confinement modification factor (Article 5.8.2.5.3a of AASHTO LRFD (2020))*

v = *concrete efficiency factor (Table 5.8.2.5.3a-1 of AASHTO LRFD (2020))*

w_p = *bearing width*

w_s = *length of the strut-to-node interface*

ϕ_c = *resistance factor for compression in STM*

$= 0.7$ *(Article 5.5.4.2 of AASHTO LRFD (2020))*

The length of the strut-to-node interface, w_s, is calculated using Eq. 4-13.

$$w_s = (h_a \times cos\theta) + (l_b \times sin\theta) \qquad \textit{Eq. 4-13}$$

where,

h_a = *height of the back face of the CCT node*

l_b = *bearing length*

θ = *angle between strut and tie*

The recommended height of the back face of the node, h_a, is twice the distance from the beam soffit to the centroid of the tension steel at the bottom flange (Tuchscherer et al. 2011). The typical practice of calculating the effective area of the strut-to-node interface is to multiply the bearing width (w_p) and the length of the strut-to-node interface (w_s). However, this practice could lead to

an overestimation of the interface capacity when h_a is greater than the height of the rectangular section at the beam bottom flange, as shown in Figure 4-6. The figure shows the heights of the bottom flange (h_B), rectangular section (h_R), and trapezoidal section (h_T) of an I-beam section. The same figure shows a CCT node with $h_a > h_B$.

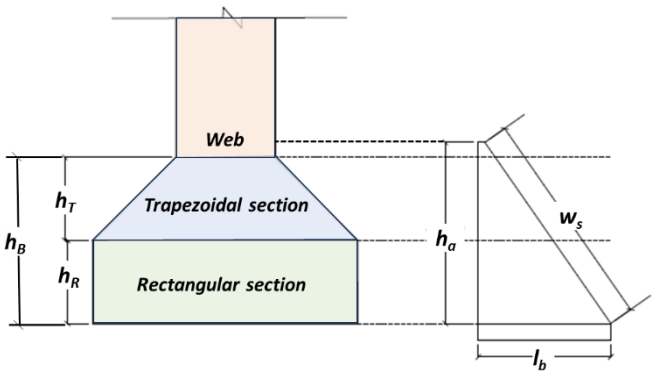

Figure 4-6. Variation of beam cross-section along the height of a CCT node.

Because of the above concern, MI 1800, bulb tee, and AASHTO Type I, II, and III beam details were selected from 14 bridge plans to calculate h_a and compare it with the bottom flange heights of the respective sections. Table 4-4 lists the selected beam sections, bottom flange dimensions, bearing length, back face height of the CCT node, and the strut width at the CCT node interface. As listed in Column (f), 11 out of 15 sections have h_a greater than h_R. In all Type I beams, h_a is greater than h_B. Figure 4-7 shows the CCT node geometry of Type Ib and MI 1800d sections listed in Table 4-4.

Table 4-4. CCT Node Dimensions at a Selected Number of Beam Ends

Beam Section (a)	Bottom Flange Height (in.)			Bearing Length, l_b (in.) (e)	Back Face Height of CCT Node, h_a (in.) (f)	Strut Width at CCT Node, w_s (in.) (g)
	Rectangular Section, h_R (b)	Trapezoidal Section, h_T (c)	Total, hB (d)			
MI 1800a	5.875	5.5	11.375	8.0	**6.4**$^{+}$	10.2
MI 1800b				7.0	5.9	9.1
MI 1800c				12.2	5.9	12.8
MI 1800d				9.0	**10.8**	14.0
BT 60x49	5.5	9	14.5	12.5	**7.2**	13.9
BT 36x49				8.0	5.5	9.5
Type IIIa	7	7.5	14.5	8.0	**7.2**	10.8
Type IIIb				8.0	6.4	10.2
Type IIIc				8.0	**9.1**	12.1
Type IIId				8.0	**7.7**	11.1
Type IIa	6	6	12	8.0	**7.1**	10.7
Type IIb				8.0	**6.5**	10.3
Type Ia	5	5	10	8.0	**10.7**$^{++}$	13.2
Type Ib				8.0	**10.9**	13.3
Type Ic				8.0	**10.7**	13.2

+ bold text, $h_a > h_R$ ++ bold and red text, $h_a > h_B$

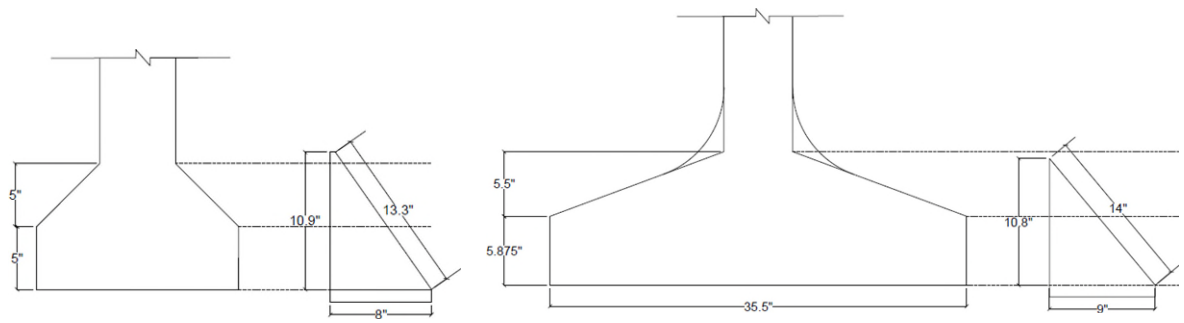

(a) Type Ib (b) MI 1800d

Figure 4-7. CCT node at Type I and MI 1800 beams.

Finite Element (FE) models with a span-to-depth ratio of 1.0 were developed to study the load path at beam ends. As shown in Figure 4-8with dark blue contours, compressive stress concentrations are observed at the web-to-bottom flange interface. The principal stress distribution also displays similar stress concentration at the web-to-bottom flange interface (Figure 4-9). As shown in Figure 4-10, experimental results have shown failure at the web-to-bottom flange interface, which is commonly known as web base crushing.

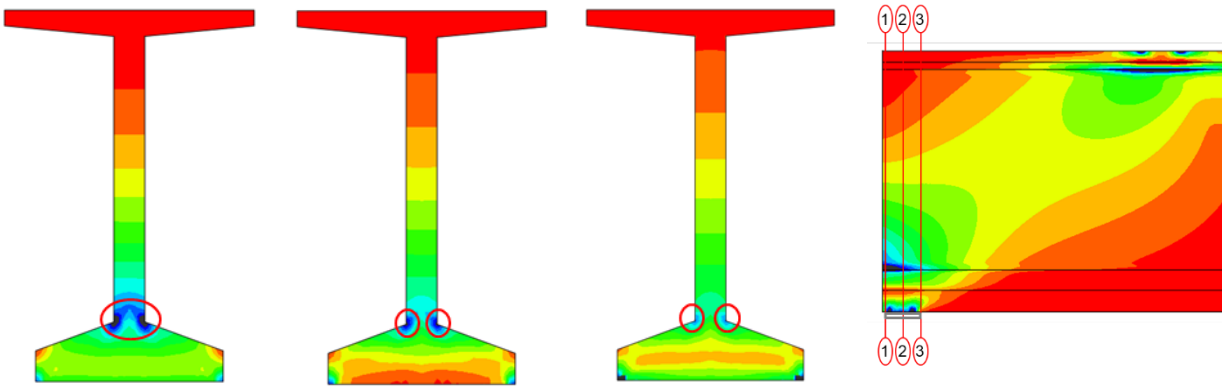

(a) Section 1-1 (b) Section 2-2 (c) Section 3-3 (d) Elevation

Figure 4-8. Principal stress distribution at the end of an MI 1800 beam.

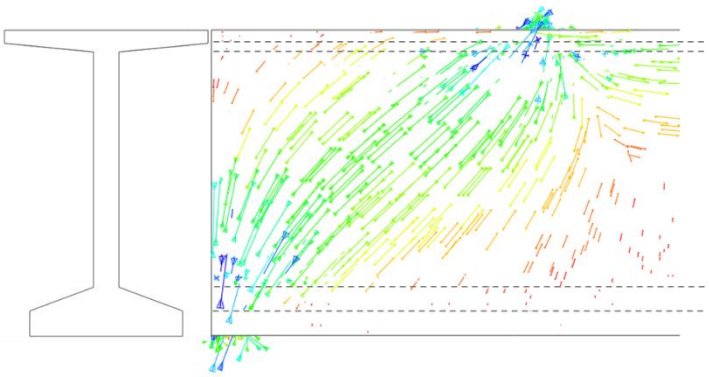

Figure 4-9. Principal stress distribution at the end of an MI 1800 beam.

Figure 4-10. Web base crushing failure of a bulb tee section (Shahrooz et al. 2017).

The effective area at the strut-to-node interface can be calculated by considering the bottom flange geometry at the beam end if the stress is well distributed across the width of the bottom flange. Finite element analysis of an MI 1800 beam shows that the compressive stress is well distributed within the width of the bottom flange (Figure 4-11). Therefore, the width of each cross-section along the length of the strut-to-node interface can be used to accurately calculate the effective area.

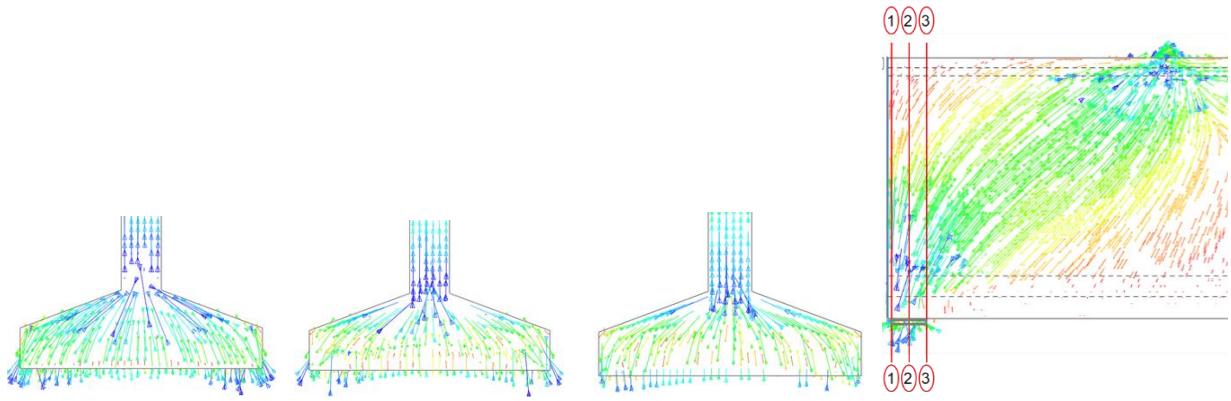

(a) Section 1-1 (b) Section 2-2 (c) Section 3-3 (d) Elevation

Figure 4-11. Principal stress distribution within the end region of an MI 1800 beam.

To demonstrate the capacity overestimation and the impact of using the effective area for the strut-to-node interface, the MI 1800d beam details listed in Table 4-4 are used. As shown in Figure 4-12 and listed in Table 4-4, this beam has a 5.875-in. thick web, 9-in. long and 32.5-in. wide bearing, and a CCT node with 10.8-in. back face and 14-in. long interface. The strut-to-node interface area, calculated using a bearing width of 32.5 in., is 455 in.^{2} (i.e., 32.5 × 14). The strut-to-node interface area, calculated considering the variation of beam bottom flange width along the interface length, is 379.8 in.^{2} (i.e., 32.5 × 7.6 + (32.5 + 9)/2 × 6.4). The use of bearing width for this MI 1800d beam to calculate the strut-to-node interface capacity resulted in a 20% overestimation. For an accurate representation of the strut-to-node interface capacity, this study considers the variation of the beam bottom flange width for the interface capacity calculation.

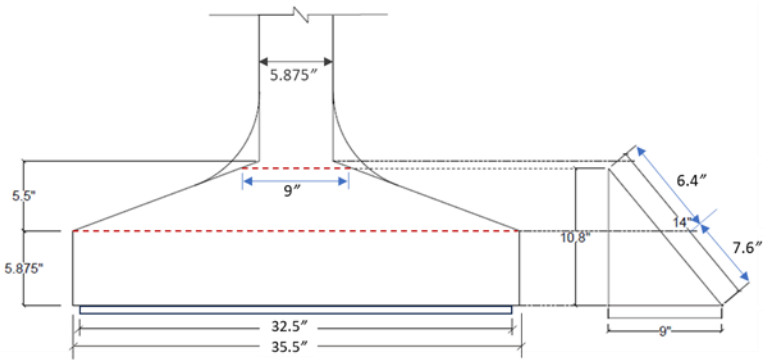

Figure 4-12. CCT node geometry of the MI 1800d beam.

Since the maximum strut force, S, developed at the strut-to-node interface is limited by the factored strut-to-node interface resistance, P_{r2}, at that location, the factored shear resistance at the beam end controlled by the strut-to-node interface failure mode, V_{uSN}, is calculated using Eq. 4-14.

$$V_{uSN} = (V_{uLT\_S} \text{ or } V_{uLT\_H})(P_{r2}/S) \qquad \text{Eq. 4-14}$$

The strut force (S) developed at the strut-to-node interface with only straight strands, S_S, and with both straight and harped strands, S_{SH}, is calculated using Eq. 4-15 and Eq. 4-16.

$$S_S = \sqrt{(T^2 + V_{nLT\_S}{}^2)} \qquad \textit{Eq. 4-15}$$

$$S_{SH} = \sqrt{[(S_2 \cos\theta_2 + S_3 \cos\theta_3)^2 + (S_2 \sin\theta_2 + S_3 \sin\theta_3)^2]} \qquad \textit{Eq. 4-16}$$

4.2.4 Transverse Tie Capacity

The lack of transverse reinforcement to resist lateral tensile forces developed within the bottom flange over the bearing results in lateral splitting cracks (Figure 4-13). Inadequate transverse tie capacity can also lead to longitudinal cracking at the beam soffit. Beams without embedded sole plates or with inadequate confinement reinforcement are particularly susceptible to this failure mode that promotes the slippage of prestressing strands (Ross 2012). This lateral splitting failure eventually leads to bond-shear failure, which in turn promotes longitudinal tie failure.

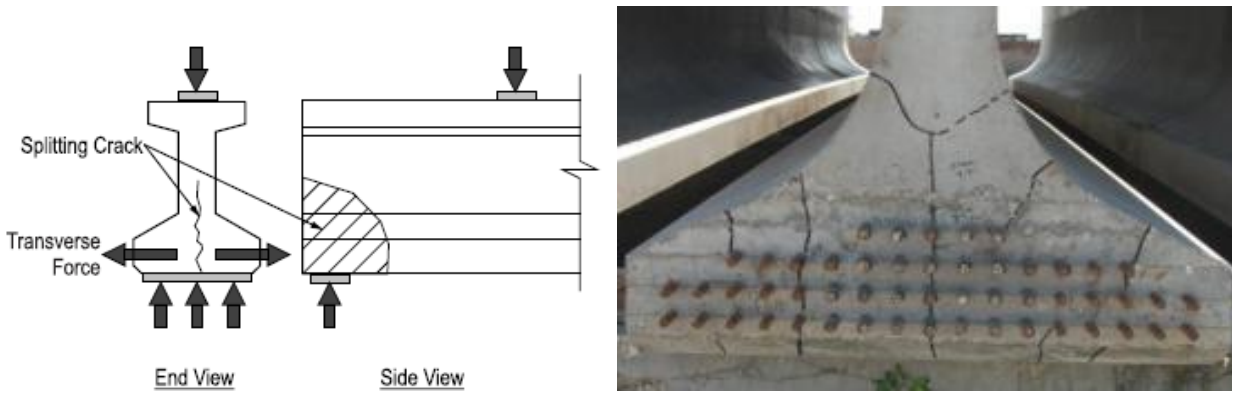

(a) Illustration (b) Lateral splitting cracks

Figure 4-13. Formation of lateral splitting cracks (Ross 2012).

Starting with the 3D STM model presented in Ross et al. (2013), 2D STM models were developed by Ross et al. (2013) and Shahrooz et al. (2017) to calculate the transverse tie forces developed within the bottom flange of I-shaped beams. As shown in Figure 4-14, Shahrooz et al. (2017) described a rational process to determine the load path, including the spacing between the vertical reactions developed at the beam soffit, considering the bearing pressure distribution across the bearing width. This figure illustrates the load path through the web and the bottom flange onto the bearing pad. Shahrooz et al. (2017) developed the 2D STM based on the following assumptions:

1. The STM model is symmetric about the vertical axis of the section.
2. The angle of the inclined struts in 3D STM does not affect the 2D (cross-sectional) STM configuration because the horizontal strands are sufficient to anchor these struts in the longitudinal direction of the beam.

3. All bonded strands resist the generated tie force equally. In addition, each strut is anchored at a node corresponding to the centroid of a strand group, and the corresponding strut force is proportional to the number of bonded strands represented by the node.
4. Girders are not skewed at their ends.

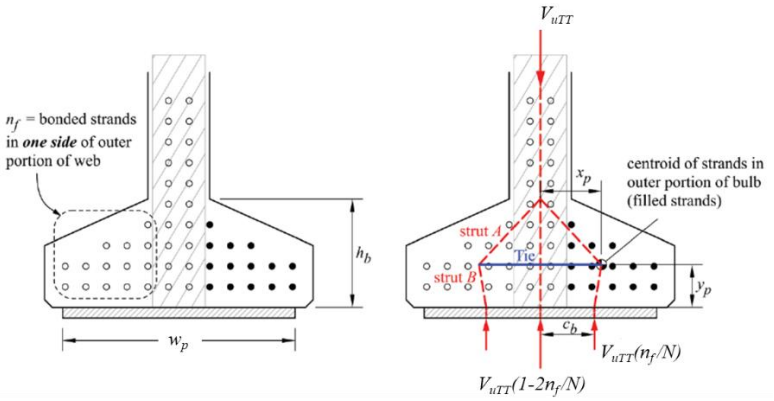

Figure 4-14. STM model for transverse tie capacity calculation (Shahrooz et al. 2017).

In the 2D STM, the distance between the vertical reactions, c_b, is defined assuming a uniform bearing pressure distribution across the bearing width. To validate this assumption, the bearing pressure distribution of an I-beam was evaluated using a finite element (FE) model. In the FE model, the elastomeric bearing pad is modeled using spring elements. The spring stiffness was calculated using the modulus of elasticity of a typical neoprene bearing pad, as presented in Aktan et al. (2008). The reaction force distribution along the bearing width is uniform, as shown in Figure 4-15, and supports the primary assumption used in the 2D STM. Even though the reaction forces along the bearing length slightly increase towards the front edge of the bearing, it has no impact on the assumption used in the 2D STM. In this particular model, the reaction forces along the bearing length changed from 110 to 117 lb (≈ 5%).

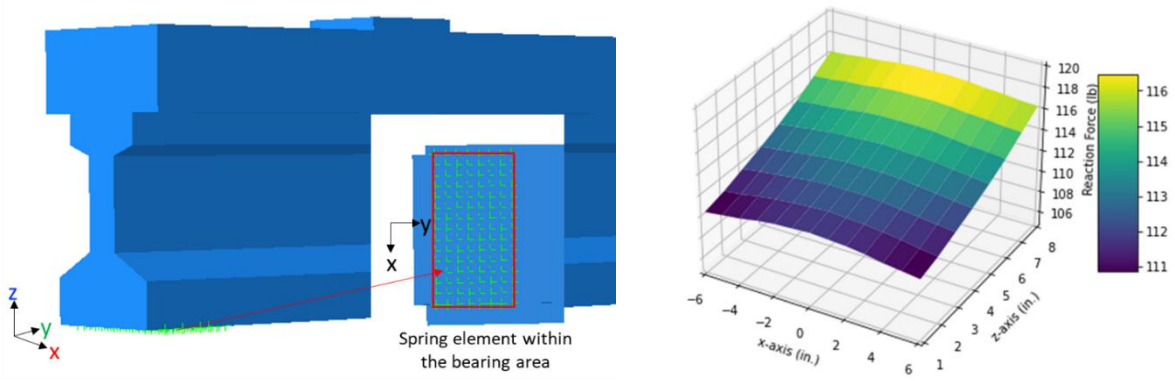

(a) Isometric view of the composite section and a close-up view of the bearing footprint

(b) Reaction force distribution within the bearing footprint

Figure 4-15. Beam geometry and reaction force distribution within the bearing footprint.

Figure 4-14 shows the geometry of the STM used to calculate the transverse tie force at the beam end. The nominal shear resistance at the beam end controlled by the transverse tie failure mode, V_{nTT}, is calculated using Eq. 4-17.

$$V_{nTT} = t_r/[(n_f/N) \times \{x_p/(h_B - y_p) + (x_p - c_b)/y_p\}] \quad \text{Eq. 4-17}$$

where,

c_b = *distance between two vertical reaction force components*

$= (w_p/2)\ (1 - n_f/N)$

N = *total number of straight bonded strands*

n_f = *number of bonded strands on one side of the outer portion of the web*

wp = *width of the bearing*

h_B = *vertical distance between flange bottom surface to web and bottom flange intersection*

t_r = *resistance provided by the confining steel within* L_{ct}

$= f_y(2A_{st})L_{ct}/s$

A_{st} = *cross-sectional area of a single confinement steel*

f_y = *yield strength of confinement steel*

L_{ct} = *beam length with confinement steel resisting the tie force*

$= (h_c/4) + l_b$

h_c = *height of the composite beam section*

l_b = *length of bearing*

s = *spacing of confinement steel over* L_{ct}

x_p = *horizontal distance from the beam centerline to the centroid of* n_f *strands in the outer portion of the bottom flange*

y_p = *vertical distance from the beam soffit to the centroid of* n_f *strands in the outer portion of the bottom flange*

The factored shear resistance at the beam end controlled by the transverse tie failure mode, V_{uTT}, is calculated using Eq. 4-18.

$$V_{uTT} = \phi \times V_{nTT} \quad \text{Eq. 4-18}$$

where,

ϕ = *the resistance factor for tension-controlled members in STM*

= 1.0 (Article 5.5.4.2. of AASHTO LRFD (2020))

4.3 MARGIN OF SAFETY FOR CAPACITY CALCULATION

To utilize the STM with confidence for practical applications, a correlation between theoretical and experimental capacities must be established. Therefore, the experimental data and the associated PSC I and bulb tee beam end details were compiled from the available literature. Table 4-5 presents concrete compressive strength values and beam end details documented in Hawkins and Kuchma (2007), Shahrooz et al. (2017), and Osborn et al. (2012). Hawkins and Kuchma (2007) evaluated the capacities of AASHTO BT-63 beams with three different concrete compressive strengths (10,000, 14,000, and 18,000 psi), different numbers of prestressing strands (ranging from 24 to 42), and harped and debonded strands. Shahrooz et al. (2017) evaluated the capacities of AASHTO BT-54 and Type III beams with concrete compressive strengths ranging from 12,200 to 17,400 psi and varying degrees of debonded strands. Osborn et al. (2012) evaluated AASHTO Type II beams salvaged from bridges that were in service for 42 years.

Table 4-5. Beam Geometry, Material Properties, and Sectional Details

Source (a)	Beam Section Label (b)	Concrete Compressive Strength (psi) (c)	Cross-Section Area (in.^{2}) (d)	Strand Diameter (in.) (e)	Strands at Beam Ends			Bearing Length (in.) (i)
					Total (f)	Harped (g)	Debonded (h)	
Hawkins and Kuchma (2007)	BT-63a	10,000	1133.00	0.600	32	0	0	9
	BT-63b				32	6	0	9
	BT-63c				38	0	0	9
	BT-63d				38	6	0	9
	BT-63e	14,000			42	0	0	9
	BT-63f				42	0	0	9
	BT-63g				42	0	0	9
	BT-63h				42	0	0	9
	BT-63i				42	0	0	9
	BT-63j	18,000			24	0	0	9
	BT-63k				42	0	0	9
	BT-63*l*				42	0	18	9
Shahrooz et al. (2017)	BT-54a	17,400	871.83	0.600	20	0	12	12
	BT-54b	15,200	871.83		20	0	2	12
	Type IIIa	12,600	637.82	0.500	16	0	8	12
	Type IIIb	12,200	637.82		16	0	4	12
	Type IIIc	13,800	637.82		18	0	10	12
	Type IIId	13,200	637.82		18	0	4	12
Osborn et al. (2012)	Type IIa	7100	443.87	0.438	12	0	0	8
	Type IIb		443.87		12	0	0	8

Table 4-6 presents (i) beam end factored resistance calculated using STM and relevant resistance factors from the AASHTO LRFD Article 5.5.4.2, (ii) the actual capacities evaluated through laboratory testing, and (iii) the Margin of Safety (MoS) calculated as a ratio of the experimental

capacity and the factored resistance listed in column (f). Columns (b), (c), (d), and (e) present the beam end factored resistance associated with each failure mode considered during the application of STM - longitudinal tie, bearing face, strut-to-node interface, and transverse tie. A resistance factor of 1.0 is used for tension-controlled failure modes (the longitudinal tie and transverse tie failure). A resistance factor of 0.7 is used for compression-controlled failure modes (the bearing face and strut-to-node interface failure). The minimum value from these four potential failure modes is selected as the beam end factored resistance and listed in column (f). The factored resistance of a majority of BT sections is controlled by the factored resistance of the transverse tie. According to Ross (2012), the embedded sole plates provide additional confinement in I and bulb tee sections, improving the transverse tie resistance by 160% to 171%. However, the study by Ross (2012) recommends increasing the transverse tie resistance calculated using STM by 150% in the presence of a sole plate. Since none of the beams listed in Table 4-6 has sole plates, the factored resistance of the transverse tie is not adjusted. The experimental capacities documented in the respective literature are listed in column (g). The ratio of experimental capacity to factored resistance is calculated and presented in column (h) as the Margin of Safety (MoS). The results show that the actual capacity of beam ends ranges between 100% and 350% of the factored resistance calculated using STM and AASHTO LRFD resistance factors. Similar observations were reported by Osborn et al. (2012), who analyzed the capacity of seven decommissioned girders using STM before experimentally evaluating their capacity. However, their results are not included in this section because the publication does not explicitly specify whether the nominal or factored resistances were used for the comparison.

Table 4-6. Beam End Factored Resistance, Experimental Capacity, and the Margin of Safety

Beam Section Label (a)	Failure Mode and Factored Resistance (kip)				Factored Resistance (kip) (f)	Experimental Capacity (kip) (g)	Margins of Safety (MoS) (h) = (g)/(f)
	Longitudinal Tie (b)	Bearing Face (c)	Strut-to-Node Interface (d)	Transverse Tie (e)			
BT-63a	545	1872	674	**464**	464	530	1.1
BT-63b	418	1872	618	**245**	245	621	2.5
BT-63c	682	1872	**666**	872	666	686	1.0
BT-63d	493	1872	631	**464**	464	794	1.7
BT-63e	**643**	2621	931	677	643	721	1.1
BT-63f	**643**	2621	931	677	643	859	1.3
BT-63g	**643**	2621	931	677	643	678	1.1
BT-63h	**643**	2621	931	677	643	678	1.1
BT-63i	**643**	2621	931	677	643	669	1.0
BT-63j	426	3370	966	**273**	273	408	1.5
BT-63k	682	3370	1197	**677**	677	671	1.0
BT-63*l*	422	3370	1197	**276**	276	563	2.0
BT-54a	**130**	2660	1211	458	130	452	3.5
BT-54b	**305**	2324	1133	1362	305	511	1.7
Type IIIa	**110**	1630	742	901	110	311	2.8
Type IIIb	**171**	1578	761	2698	171	357	2.1
Type IIIc	**110**	1785	813	901	110	321	2.9
Type IIId	**201**	1708	836	4804	201	383	1.9
Type IIa	**81**	501	282	704	81	150	1.8
Type IIb	**81**	501	282	704	81	176	2.2

The longitudinal tie and transverse tie are the dominant failure modes of the BT-63 series. The BT-63a specimen exhibited transverse splitting cracks (Figure 4-16), likely due to the lack of transverse tie capacity. Although several BT-63 beams have lower transverse tie capacities, photographs or experimental data are not available in the relevant literature to confirm the observed failure modes during the laboratory testing of those specimens.

Figure 4-16. Lateral splitting cracks documented at the BT-63a beam end (Hawkins and Kuchma 2007).

The STM results of BT-54a show longitudinal tie failure as the controlling failure mode. The picture of BT-54a, shown in Figure 4-17, indicates a vertical crack at the bottom flange that led to a shear-tension failure associated with the longitudinal tie failure.

Several beam end testing results show inconsistencies between the theoretically identified failure modes and experimental failures. The controlling failure mode of BT-54b is the longitudinal tie failure. However, the picture of BT-54b, shown in Figure 4-18, indicates web base crushing. Similar observations are also documented for Type III beams. The longitudinal tie failure mode limits the STM capacity of all Type III beams. However, during experimental testing, failure was primarily observed at the loading point due to bearing crushing, which led to shear-compression failure (Figure 4-19). Since the large, concentrated loads applied during laboratory testing do not represent the loading conditions experienced by an in-service bridge beam with a deck, these beams could have withstood significantly higher loads before failure under typical highway loads.

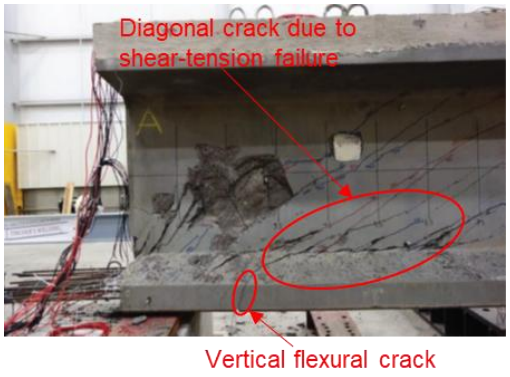

Figure 4-17. Shear-tension failure of BT-54a specimen (Shahrooz et al. 2017).

Figure 4-18. Failure patterns of BT-54b specimen (Shahrooz et al. 2017).

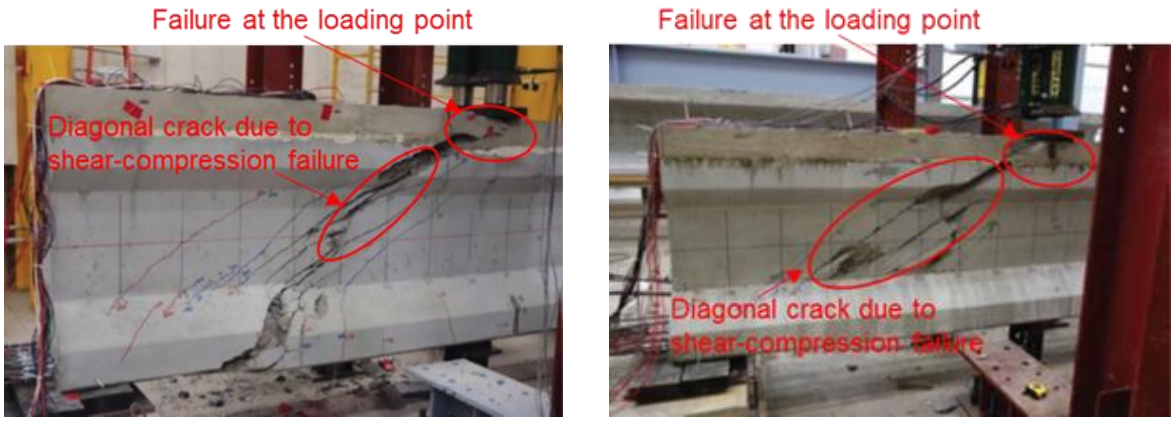

(a) Type IIIa (b) Type IIIb

Figure 4-19. Shear-compression failure at Type III beam ends (Shahrooz et al. 2017).

The MoS ranges between 1.0 and 3.5, depending on section geometry, detailing, and the difference between the actual prestress transfer length and the values used in the STM calculations. The MoS of the BT-63 series ranges from 1.0 to 2.5. The BT-54a stands out with a notably high MoS of 3.5. This section only had 8 bonded strands but exhibited a significantly high experimental capacity. The calculated STM capacity by Shahrooz et al. (2017) is higher than the values presented in this report. This difference is primarily due to the $30d_b$ transfer length used in their analysis based on experimental and finite element analyses. This shorter transfer length, compared to the $60d_b$ calculated as per the AASHTO LRFD guidelines, increases the beam end capacity. In this report, the $60d_b$ transfer length is used to be consistent with other studies and derive conservative results to represent beam end factored resistances. Type III beams exhibit consistently high MoS values, ranging from 1.9 to 2.9. The MoS of Type II beams, despite their age and reduced strand count, ranges from 1.8 to 2.

The AASHTO Type beams exhibit consistently high MoS values ranging from 1.8 to 2.9, indicating that their beam end resistance can exceed theoretical capacities by at least 180%. In contrast, BT-63 beams show a wide range of MoS values. For 50% of the sections included in this comparison, the experimental capacities did not exceed 110% of the theoretical capacities, while 20% showed identical theoretical and experimental capacities. The results show that STM did not underestimate the capacities, and the method can be used confidently for developing RFA guidelines.

4.4 CAPACITY-TO-DEMAND RATIO (CDR)

A pool of 15 PSC beams (from 14 bridges) was selected, representing MI 1800, Bulb Tee (BT), and AASHTO Type beams, to calculate the beam end capacity-to-demand ratio (CDR). Table 4-7 shows a summary of bridge details, beam end details, and the factored shear at the beam end. Table 4-8 presents the factored shear resistance corresponding to each beam end failure mode, the minimum factored shear resistance (highlighted in bold) selected to represent beam end factored shear resistance, and the capacity-to-demand ratio (CDR).

In this section of the report, *the **capacity** represents the factored shear resistance calculated using STM and the AASHTO LRFD resistance factors, whereas the **demand** represents the factored shear at the beam end*. The scope of analysis is limited to the interior beams of the selected bridges. The factored shear was calculated using bridge plan details of the respective bridges. A total of 15 PSC I-shape and bulb tee beams were selected. Eleven of the selected beams had harped strands, and five of them contained debonded strands.

Table 4-7. Bridge and Beam End Details and the Factored Shear

Beam			Strands at Beam End				Bearing Length (in.)	Design Load	Factored Shear (Demand) (kip)
Section (a)	Length (ft) (b)	Spacing (ft) (c)	Diameter (ft) (d)	Total (e)	Harped (f)	Debonded (g)	(h)	(i)	(j)
MI 1800a	132.87	8.05	0.600	42	4	8	8.0	HS25	357
MI 1800b	133.53	6.89	0.600	34	6	2	7.0	HS25	309
MI 1800c	133.53	6.89	0.600	34	6	2	12.2	HS25	322
MI 1800d	110.00	9.67	0.600	32	2	10	9.0	HL-93 Mod.	353
BT 60x49	109.25	7367	0.600	44	0	10	12.5	HL-93 Mod.	335
BT 36x49	85.25	6.90	0.600	32	5	0	8.0	HL-93 Mod.	266
Type IIIa	65.10	6.50	0.500	26	6	0	8.0	HS 20-44	160
Type IIIb	67.83	6.25	0.500	24	4	0	8.0	HS 20-44	167
Type IIIc	64.50	6.21	0.438	36	8	0	8.0	HS 20-44	160
Type IIId	65.83	6.00	0.438	30	4	0	8.0	H15-44	131
Type IIa	57.00	6.08	0.438	24	6	0	8.0	H15-44	106
Type IIb	49.33	6.25	0.438	20	4	0	8.0	H15-44	100
Type Ia*	34.70	6.25	0.500	12	0	0	8.0	HS 20-44	102
Type Ib	35.20	6.00	0.438	14	0	0	8.0	H15-44	78
Type Ic	35.50	6.08	0.438	12	0	0	8.0	H15-44	79
*Except Type Ia, all other Type I, II, and III are constructed with an end block at the beam end.									

Table 4-8. Beam End Factored Shear Resistance, Factored Shear, and the Capacity-to-Demand Ratio (CDR)

Beam Section	Failure Mode and Factored Shear Resistance (kip)				Factored Shear Resistance (kip)	Factored Shear (Demand) (kip)	CDR
	Longitudinal Tie	Bearing Face	Strut-to-Node Interface	Transverse Tie+			
(a)	(b)	(c)	(d)	(e)	(f)	(h)	(i)= g/h
MI 1800a	368	1068	646	344(516)	368	357	1.03
MI 1800b	296	942	576	152**(227)**	227	309	0.74
MI 1800c	430	1561	776	180**(270)**	270	322	0.84
MI 1800d	**303**	1188	732	NA	303	353	0.86
BT 60x49	**562**	1831	969	758	562	335	1.68
BT 36x49	**315**	1315	741	1191	315	266	1.18
Type IIIa	**210**	723	443	1240	210	160	1.31
Type IIIb	**240**	723	425	8079	240	167	1.44
Type IIIc	**274**	723	497	884	274	160	1.71
Type IIId	**240**	723	471	803	240	131	1.83
Type IIa	**161**	592	360	939	161	106	1.52
Type IIb	**138**	592	346	784	138	100	1.38
Type Ia	**168**	526	340	833	168	102	1.65
Type Ib	**143**	526	374	NA	143	78	1.84
Type Ic	**122**	526	371	NA	122	79	1.54

+ Values in the bracket represent (tie capacity x 1.5), the capacity adjusted in the presence of a sole plate. The factored shear resistance controlled by the transverse tie failure mode is not defined (i) when bottom flange strands are located within the web portion and (ii) when $(x_p - c_b)$ is negative.

Out of all four MI 1800 beams, MI 1800b and c have the lowest factored shear resistance controlled by the transverse tie failure mode. As noted in Section 4.3, following the recommendation by Ross (2012), these factored shear resistance values are multiplied by 1.5 and compared with the rest to identify the controlling failure mode and the beam end factored shear resistance.

Even after increasing the factored shear resistance by 1.5 times, this failure mode still governs in two of the four MI 1800 beams, resulting in a CDR of less than 1.0. This is primarily due to a wider bottom flange relative to web thickness in MI 1800 beams and with strands mostly distributed within the outer portions of the bottom flange, as shown in Figure 4-20(a). As shown in Figure 4-14, n_f/N and x_p increase when most of the strands are located within the outer portions of the bottom flange, resulting in a lower shear resistance controlled by the transverse tie failure mode, as illustrated by Eq. 4-17. As an example, the MI 1800b, shown in Figure 4-20(a), has all of the beam end bottom flange strands in the outer portions of the flange, resulting in a 152-kip factored shear resistance. On the contrary, MI 1800d, shown in Figure 4-20(b), has a majority of the bottom flange strands located within the footprint of the web, resulting in a negative value for $(x_p - c_b)$. As a result, the transverse tie failure mode is not a concern for this beam.

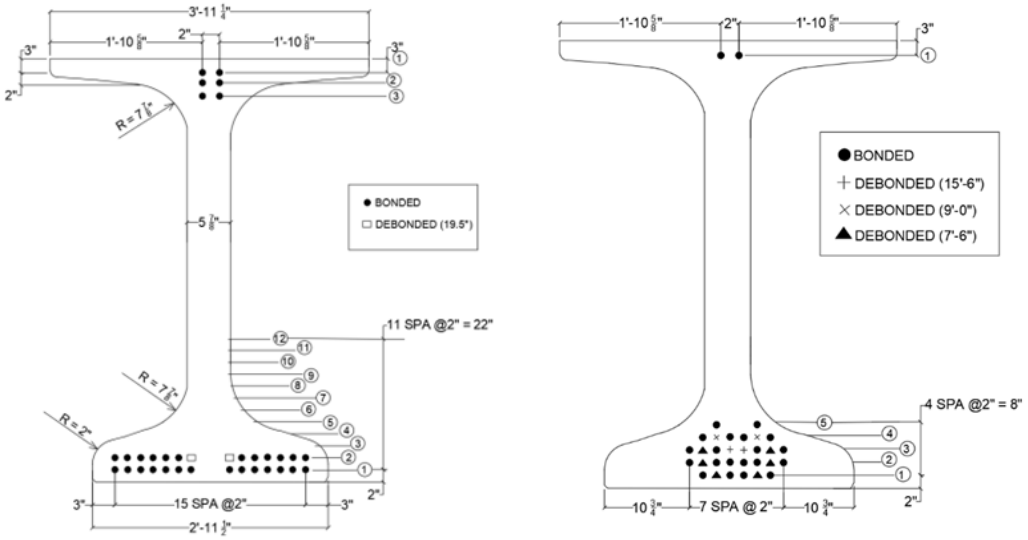

(a) MI 1800b **(b) MI 1800d**

Figure 4-20. Beam end strand pattern of MI 1800

A similar observation is documented in Shahrooz et al. (2017) for deep NU girders with wider bottom flanges, where most of the strands are located in the outer portions. Longitudinal cracking due to the large transverse tie force was observed (Figure 4-21). These cracks typically do not impact the longitudinal tie resistance unless they interact with the strands.

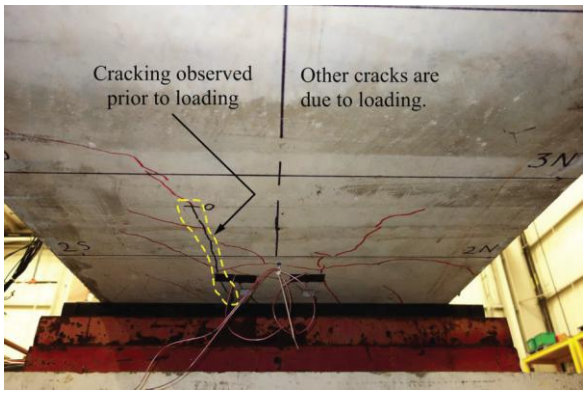

Figure 4-21. Development of longitudinal cracking in a beam with wider bottom flanges and most of the strands located in the outer portions of the flange (Shahrooz et al. 2017).

The MI 1800d beam shows a CDR of 0.86. Its capacity is limited by the factored shear resistance, which is governed by the longitudinal tie failure mode. The factored shear demand of MI 1800a and d is similar, but the number of bonded strands in MI 1800a and d beams is 30 and 20, respectively. Since the number of bonded strands controls the longitudinal tie failure mode, the MI 1800d beam has a lower factored shear resistance compared to the MI 1800a beam.

All the sections except MI 1800 listed in Table 4-8 possess an adequate factored resistance with a CDR greater than 1.0. The BT 60×49 and BT 36×49 have a consistently high CDR of 1.68 and 1.18, respectively. The AASHTO Type III, II, and I display a good overall CDR, ranging from 1.31 to 1.84. Therefore, to develop the RFA guidance, a minimum reserved capacity of 115% is used for all beam types except MI 1800. For MI 1800 beams, it is recommended to calculate the factored shear demand and resistance for the specific beam under consideration to determine the reserved capacity.

4.5 IMPACT OF BEAM END CONDITIONS ON SHEAR CAPACITY

The most common beam end conditions are classified into two groups: (1) spall and/or delamination at the beam soffit in front of the bearing and (2) spall and/or delamination at the bottom flange. The MoS and CDR calculations indicate that the beam end shear capacity is sensitive to various parameters, including the total number of strands, the presence of harped strands, the percentage of debonded strands, the bearing length, and the transfer length. The number of bonded prestressing strands and the remaining bearing area are reduced due to spall and delamination at the beam end. Hence, the sensitivity of beam end shear capacity to beam end condition is evaluated to determine the limits for deteriorated beam ends to support loads safely and to develop guidelines for RFA decisions. As stated previously, a minimum reserved capacity of 115% is used for all beam types, except MI 1800, to establish the thresholds for RFA decisions.

To perform the sensitivity analysis, three representative beam types were selected: MI 1800, Bulb Tee (BT), and AASHTO Type III sections. These beam types cover a range of I-beams and strand configurations commonly used in Michigan bridges. Figure 4-22 illustrates the selected beam-end sections and strand patterns.

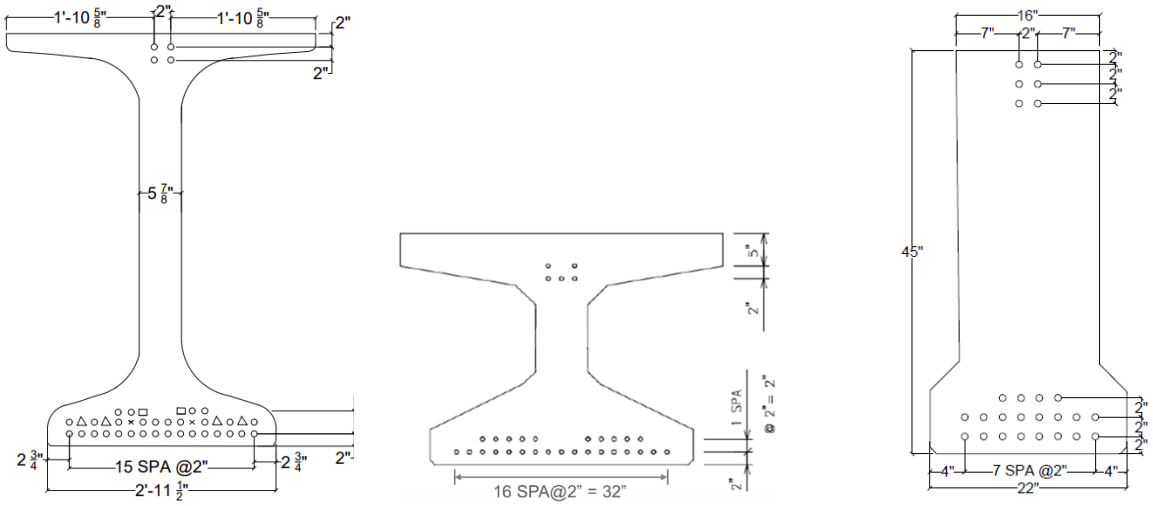

(a) MI 1800 (b) BT 36×49 (c) AASHTO Type III

Figure 4-22. Beam end sections with strand arrangement.

4.5.1 Beam End Shear Capacity with Spalls at the Beam Soffit in Front of the Bearing

Figure 4-23 and Figure 4-24 present spalls at the beam soffit in front of the bearing. Figure 4-23(a) has two beam ends. Beam 1 has a 100% section loss while Beam 2 has approximately a 40% section loss along the beam width direction. The beam end shown in Figure 4-23(b) has a deeper section loss, with approximately a 30% loss across the beam width. Beam ends shown in Figure 4-24 have section losses with exposed strands and stirrups. Inspection guidelines and templates were developed for documenting such conditions during scoping and RFA inspections (Figure 4-25). The ratio of the width of the spall (S_W) and the width of the beam soffit (BW) defines the percentage of section loss at the soffit.

(a) (b)

Figure 4-23. Section loss at the beam soffit without exposing strands or reinforcement.

(a) (b)

Figure 4-24. Section loss at the beam soffit with exposed strands and stirrups.

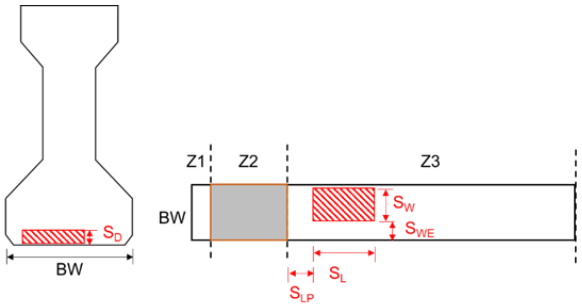

BW: bottom flange width
S_D: spall/delamination depth
S_L: spall /delamination length along the beam
S_{LP}: distance from sole plate to the spall /delamination
S_W: spall /delamination width
S_{WE}: distance from beam edge to the spall /delamination
Z_1: zone 1, overhang portion at the beam end
Z_2: zone 2, beam section over the bearing plate
Z_3: zone 3, beam section from the edge of bearing towards the span up to 5-ft of bearing

Figure 4-25. Beam end discretization and variables for documenting section loss and/or delamination at the beam soffit.

Figure 4-26 presents the impact of beam soffit section loss and strand loss on beam end shear capacity. These three graphs present the following information:

(i) The vertical axis represents the capacity reduction as a percentage.

(ii) The top horizontal axis represents the section loss as a percentage of the width of the beam soffit.

(iii) The bottom horizontal axis represents the exposed stands as a percentage of the total number of straight strands in the bottom flange and the lower portion of the web.

(iv) The capacity loss percentage is approximately proportional to the percentage of exposed strands (i.e., ineffective strands due to spall, delamination, cracking, or a combination thereof).

(v) Shallow section loss at the beam soffit without exposed strands has no impact on the beam end capacity. As shown in Figure 4-27, a 6-in. wide shallow spall resulted in a 17% section loss without exposing strands. This section loss did not result in a capacity loss as indicated by point A in Figure 4-26(a). Even having a 100% section loss without exposed prestressing strands does not reduce the beam end shear capacity. However, if a similar section loss, as shown in Figure 4-28, exposes 14% of the strands (four bonded strands in

the bottom flange), the beam end shear capacity decreases by 12%, as represented by point B in Figure 4-26(a). A similar capacity reduction is represented by point C, representing the combined effect of section and strand loss. For a 15% capacity reduction, approximately 17% of the strands must be exposed, along with a 23% section loss.

(vi) For a capacity reduction of 15%, both MI 1800 and bulb tee (BT 36×49) beams require about 17% exposed strands and 23% section loss (Figure 4-26(b) and (c)). However, beams with narrow bottom flanges, such as the AASHTO Type III, require more than 35% section loss to expose 17% of strands to have a 15% capacity reduction.

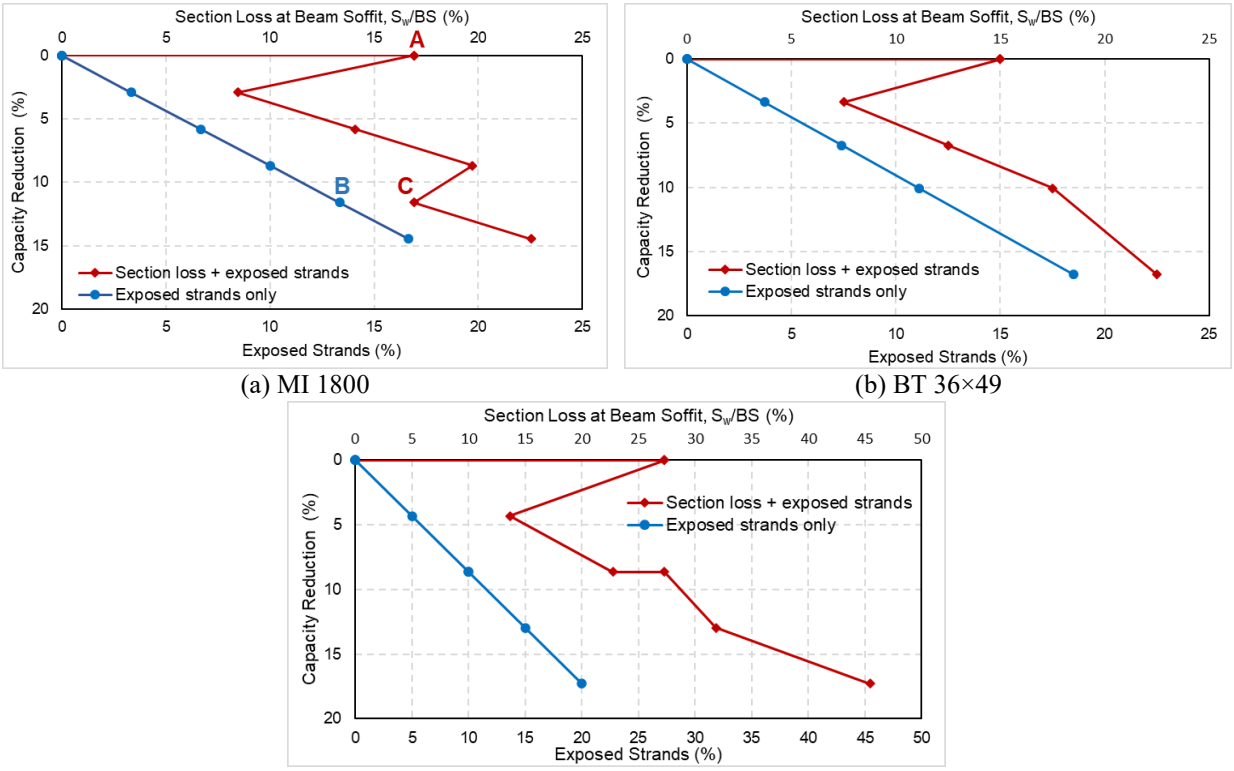

(a) MI 1800

(b) BT 36×49

(c) Type III

Figure 4-26. Capacity reduction due to the loss of a section at the beam soffit.

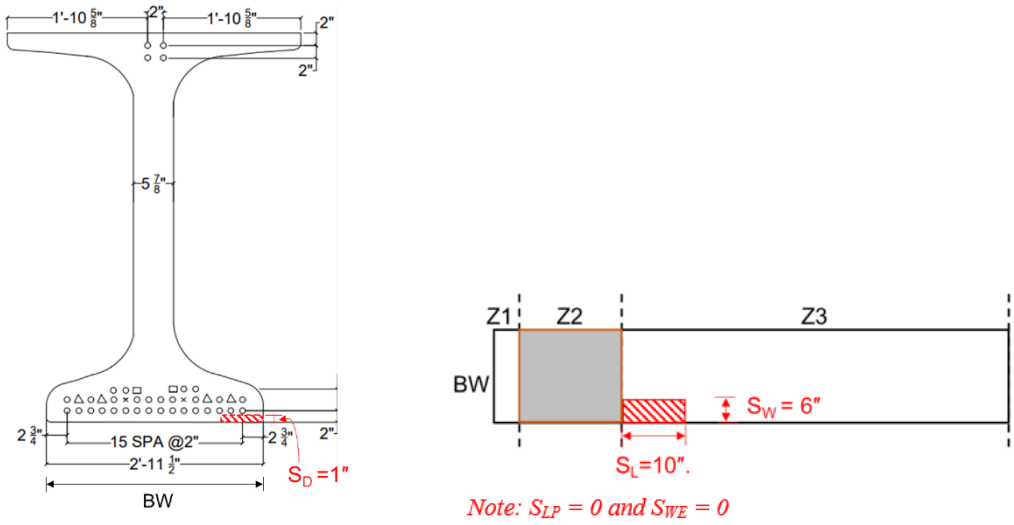

(a) Cross-section (b) Beam soffit

Figure 4-27. Beam soffit section loss corresponding to point A in Figure 4-26(a).

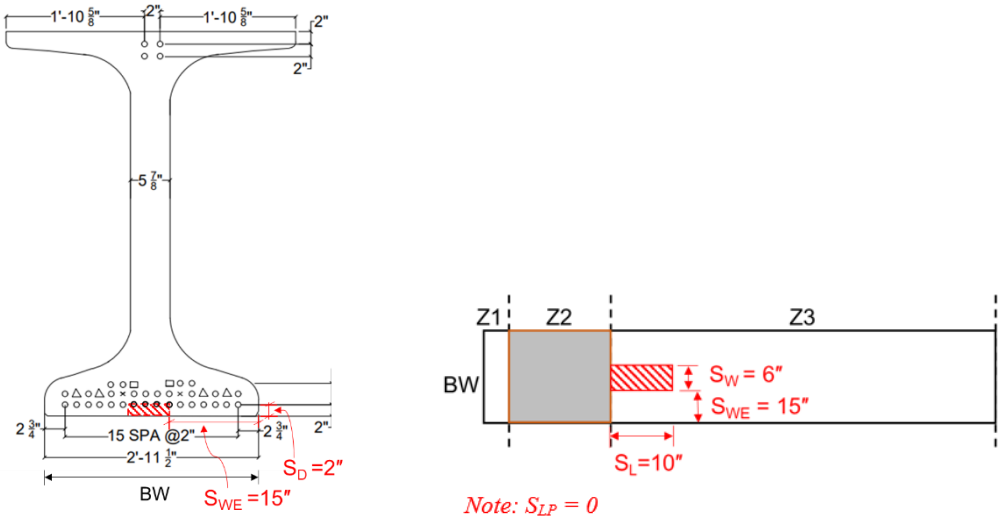

(a) Cross-section (b) Beam soffit

Figure 4-28. Beam soffit section loss corresponding to points B and C in Figure 4-26(a).

4.5.2 Beam End Shear Capacity with Spalls at the Bottom Flange

Figure 4-29 to Figure 4-31 show spalls at the bottom flange. Morcous et al. (2020) define spalls at the beam end as moderate, extensive, and severe based on the following conditions.

- Moderate: spall greater than 1 in. but less than 2 in. deep and less than 6 in. in diameter
- Extensive: spall greater than 2 in. but less than 4 in. deep or greater than 6 in. in diameter
- Severe: spall deeper than 4 in.

Figure 4-29 shows examples of section loss in front of the bearing and above the sole plate without exposed steel and/or bearing area loss. Figure 4-30(a) and (b) show moderate and extensive spall with bearing area loss but without exposed strands or steel. Figure 4-31(a) and (b) show moderate

spall with exposed strands. Figure 4-31(c) and (d) show severe spall with exposed strands. Inspection guidelines and templates were developed to document such conditions during scoping and RFA inspections (Figure 4-32). The section loss is defined as the length of section loss in the width direction relative to the total flange width. The bearing area loss is calculated as the loss of area within the bearing footprint relative to the total bearing area. The percentage of strand loss is defined as the ratio of exposed strands to the total number of straight bonded strands in the bottom flange and the lower part of the web.

(a) Section loss in front of the bearing (b) Section loss at the beam end

Figure 4-29. Section loss without exposed steel and bearing area loss.

(a) Moderate spall (b) Extensive spall

Figure 4-30. Spalls with bearing area loss.

(a) Moderate spall

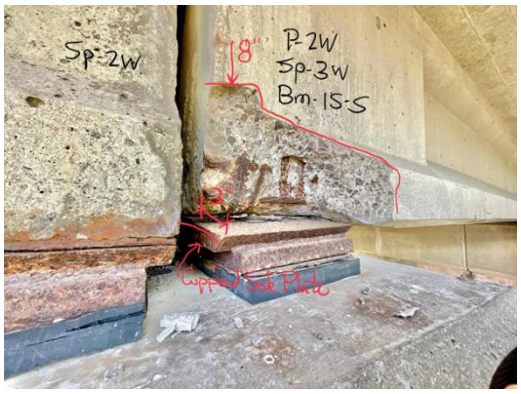

(b) Moderate spall

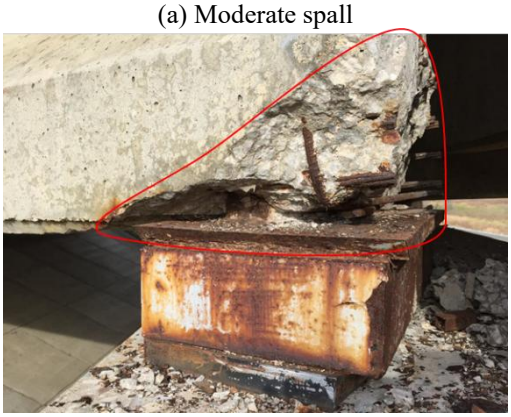

(c) Severe spall

(d) Severe spall

Figure 4-31. Bearing area loss with exposed strands and stirrups.

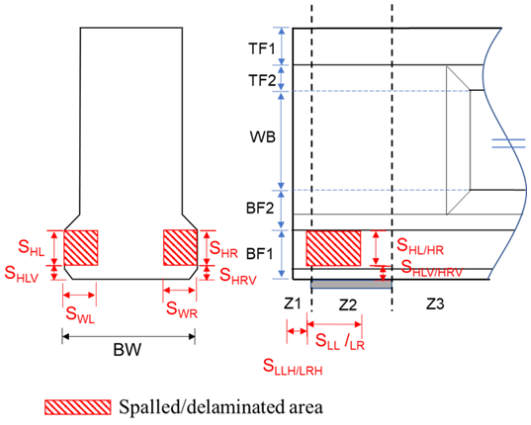

S_{HL}: height of spall/delamination on the left side
S_{HR}: height of spall/delamination on the right side
S_{HLV}: vertical distance from the beam soffit to the spall/delamination on the left side
S_{HRV}: vertical distance from the beam soffit to the spall/delamination on the right side
S_{LLH}: horizontal distance from the beam end to the spall/delamination on the left side
S_{LRH}: horizontal distance from the beam end to the spall/delamination on the right side
S_{LL}: length of spall/delamination on the left side
S_{LR}: length of spall/delamination on the right side
S_{WL}: depth of spall/delamination on the left side
S_{WR}: depth of spall/delamination width/depth on the right side

Figure 4-32. Beam end discretization and variables for documenting section loss and/or delamination at the beam bottom flange.

4.5.2.1 Thresholds for Bearing Area Loss

For sections similar to the one shown in Figure 4-20(b), a large section of the bottom flange outer portion could spall without exposing strands. For such sections, the maximum width of the concrete spall over the bearing is calculated by considering the factored bearing face resistance using Eq. 4-10 and listed in Table 4-9. For this calculation, beam sections and minimum bearing

length listed in Table 4-7 are used. The maximum factored shear for each section is taken from Table 4-8. The resistance factor of 0.7, confinement modification factor of 1, concrete efficiency factor of 0.45, and concrete compressive strength of 7.5 ksi are considered. The maximum factored shear listed in column (d) of Table 4-9 is used as P_{r1} in Eq. 4-11. The resulting minimum concrete bearing width for each section is calculated and listed in column (e). The maximum width of the concrete spall is calculated and shown in columns (f) and (g). As per the results shown in Table 4-9, irrespective of the beam type, the maximum width of concrete spall of 39% is possible at the bottom flange over the bearing without compromising the beam end factored shear resistance. For cases with spalls on only one side of the bottom flange, a maximum width of concrete spall of 20% is recommended.

Eq. 4-10 → $P_{r1} = \phi_c \times f_{cu1} \times l_b \times w_p$

Required minimum concrete bearing width = $P_{r1} / (\phi_c \times f_{cu1} \times l_b)$ *Eq. 4-19*

Table 4-9. Thresholds for Maximum Width of Concrete Spall

Beam section	Bottom flange width (in.)	Min. bearing length from Table 4-7 (in.)	Max. factored shear from Table 4-8 (kips)	Required min. concrete bearing width (in.)	Max. width of concrete spall	
					(in.)	(%)
(a)	(b)	(c)	(d)	(e)	(f) ≅ (b)–(e)	(g) ≅ (f)/(b)
MI 1800	35.5	7	357	21.35	14	39
BT 60 × *49*	40	8	335	17.72	22	55
Type III	22	8	167	8.84	13	59
Type II	18	8	106	5.61	12	66
Type I	16	8	102	5.40	10	62

4.5.2.2 Impact of Section and Strand Loss

Figure 4-33 presents the impact of bottom flange section loss and strand loss on beam end shear capacity. These three graphs present the following information:

(i) The vertical axis represents the capacity reduction as a percentage.

(ii) The top horizontal axis shows the section loss and bearing area loss as a percentage. The section loss is calculated as $(S_{WL} + S_{WR})/BW$. The bearing area loss is calculated as $(S_{WL} \times S_{LL} + S_{WR} \times S_{LR})$/(Bearing Area).

(iii) The bottom horizontal axis represents the percentage of exposed strands, calculated relative to the total number of straight strands located in the bottom flange and lower portion of the web.

(iv) Capacity reduction is approximately proportional to the percentage of exposed strands (i.e., ineffective strands due to spall, delamination, cracking, or a combination thereof).

(v) As discussed in Section 4.5.2.1, except for certain beams with bottom flange strands located within the footprint of the web, as shown in Figure 4-20(b), a large section loss without exposing prestressing strands is not possible. As shown in Figure 4-34, a 2-in. wide spall on both the left and right sides resulted in a 10% section loss without exposing strands. This section loss did not result in a capacity reduction as indicated by point A in Figure 4-33(b). However, when a 20% section loss, as shown in Figure 4-35, exposes 7% of the strands (two bonded strands in the bottom flange), beam end shear capacity decreases by 6%, as indicated by point B in Figure 4-33(b). A similar capacity reduction is represented by point C, which is the combined effect of a 20% section loss and a 7% strand loss.

(vi) As shown in Figure 4-36, a 2-in. wide and 8-in. long spall on both the left and right sides of the web resulted in a 9% bearing area loss without exposing strands. This bearing area loss did not result in a capacity loss as indicated by point D in Figure 4-33(b). This calculation used an 8-in. long and 40-in. wide bearing, and excluded the section loss within Z1 (one-inch long segment). As shown in Figure 4-37, a 26% bearing area loss exposes 15% of the strands (4 bonded strands in the bottom flange). As represented by point E in Figure 4-33(b), the 15% strand loss alone contributes to a 15% reduction in the capacity. When the combined effect of 26% bearing area loss and 15% strand loss is considered, the reduction of beam end shear capacity remains at 15%, as indicated by point F on the graph. This highlights the impact of exposed strands on the capacity compared to the significance of the bearing area loss. As indicated by point G on the graph, the bearing area loss of 11% also results in a 15% reduction of beam end shear capacity. This is because the bearing area loss of 11% represented by $S_{WR/WL}$ = 6 in. and $S_{LL/LR}$ = 4 in. also exposes 15% of the strands (4 bonded strands in the bottom flange).

(vii) *The above results and the calculations presented in Section 4.5.2.1 indicate that the width of the spall over the bearing (i.e., S_{WL} and S_{WR}) as a percentage with respect to the bottom flange width is a better measure than the bearing area loss for developing RFA guidelines.*

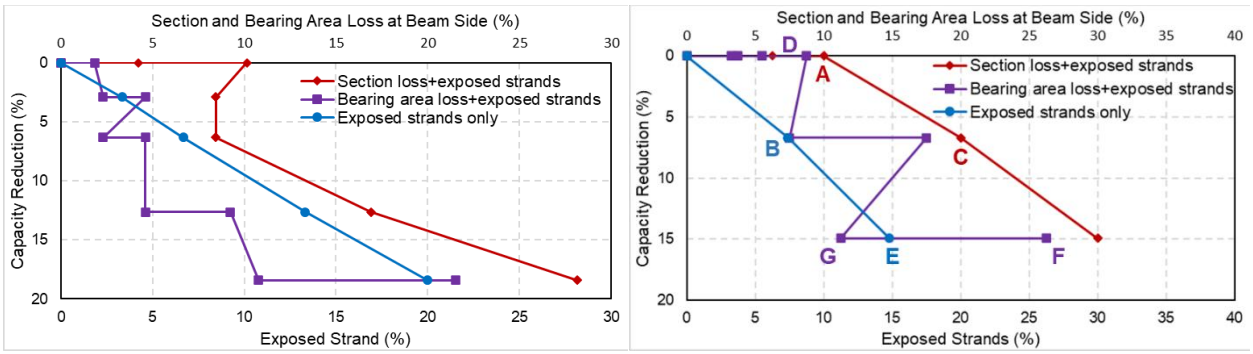

(a) MI 1800 (b) BT 36×49

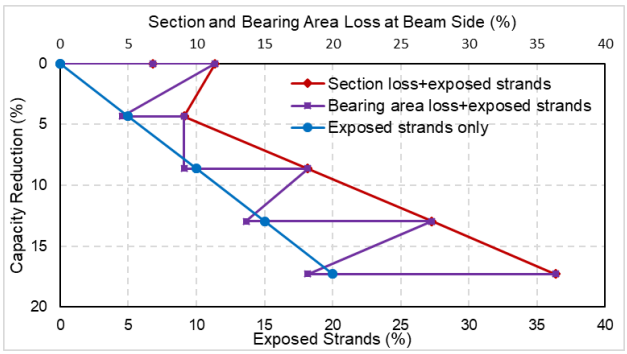

(c) Type III

Figure 4-33. Capacity reduction due to bottom flange section loss.

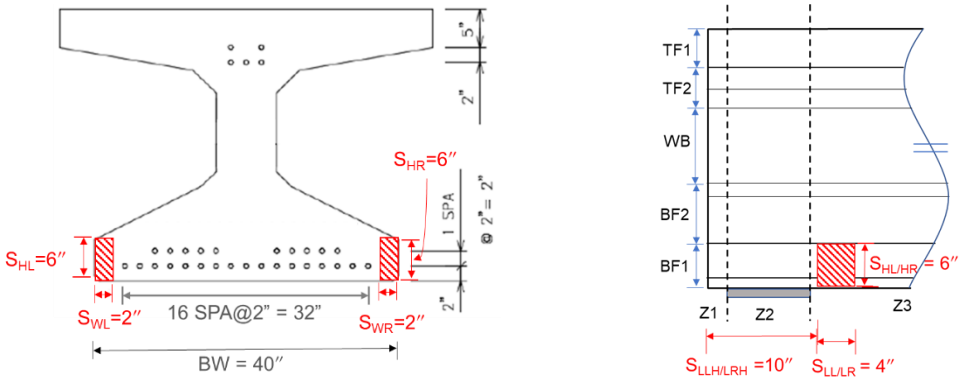

(a) Cross-section (b) Beam elevation

Figure 4-34. Bottom flange section loss corresponding to point A in Figure 4-33(b).

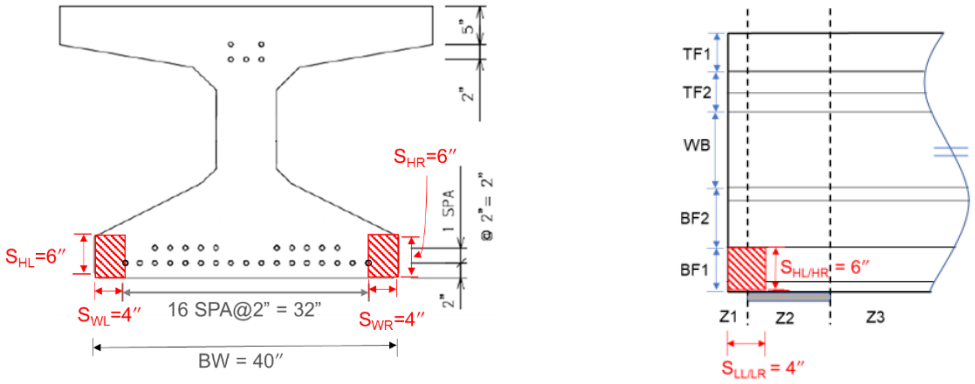

(a) Cross-section (b) Beam elevation

Figure 4-35. Bottom flange section loss corresponding to points B and C in Figure 4-33(b).

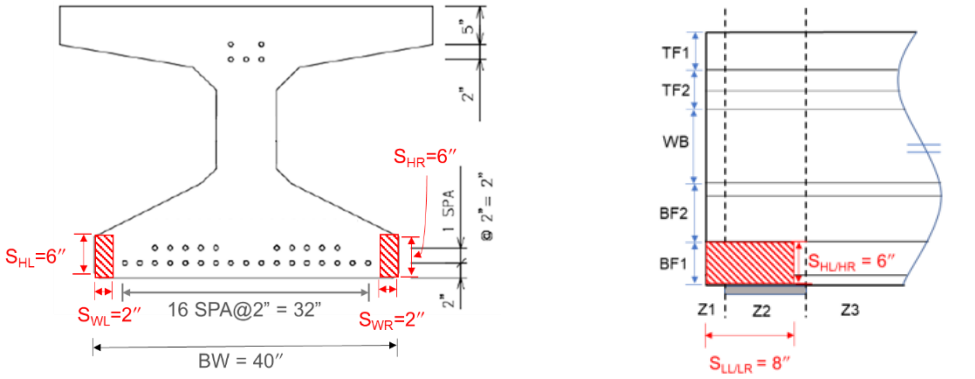

(a) Cross-section (b) Beam elevation

Figure 4-36. Bottom flange section loss corresponding to point D in Figure 4-33(b).

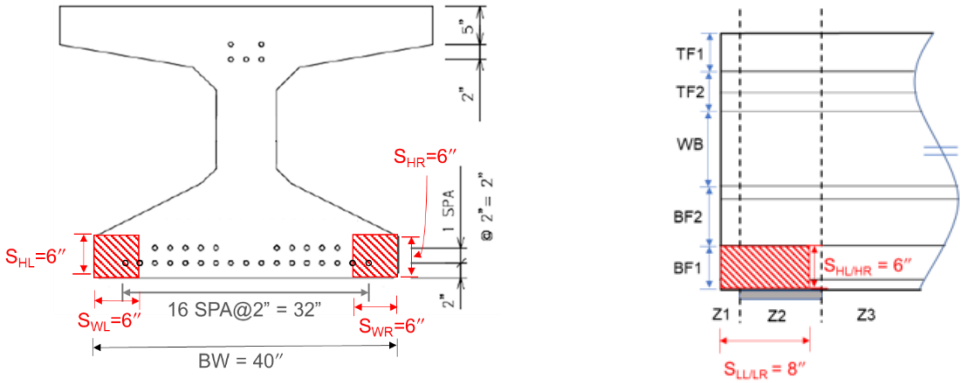

(a) Cross-section (b) Beam elevation

Figure 4-37. Bottom flange section loss corresponding to points E and F in Figure 4-33(b).

4.5.3 Summary of Sensitivity Analysis

As indicated by the sensitivity analysis, longitudinal tie failure is the governing failure mode in all the analysis cases. The capacity reduction due to exposed strands is proportional to the percentage of exposed strands. The beam end shear capacity is not affected by the section loss and/or bearing area loss without exposed strands, since it is not practical to have a significant section loss in typical PSC I-beams without exposing prestressing strands. As previously discussed, *a 15% capacity reduction is used as the threshold for RFA decisions. Based on the sensitivity analysis, deterioration thresholds corresponding to this 15% capacity reduction have been established for various beam types (Table 4-10).* For example, a 15% capacity reduction is observed if 17–18% of the strands are exposed at the beam soffit. To expose 17–18% of the strands at the beam soffit requires a section loss in the range of 22–37%. This variation is observed because the relationship between section loss and strand exposure depends on the arrangement of the strands within the beam cross-section.

Since the use of the width of the spall over the bearing (i.e. S_{WL} and S_{WR}) as a percentage with respect to the bottom flange width is a better measure than the bearing area loss for developing RFA guidelines, only the strand loss and section loss are considered for defining the thresholds to set the limits beyond which a detailed assessment is required to establish the load capacity. As long as the conditions remain within these limits, the beam can be considered to perform safely without requiring an RFA.

Table 4-10. The Threshold for Different Beam End Conditions Corresponding to the 15% Capacity Reduction

Location	Condition+	MI 1800 (%)	BT 36×49 (%)	Type III (%)	Range (%)
Beam soffit	Exposed strands	17	17	18	17-18
	Section loss with exposed strands	23	22	37	22-37
Beam side	Exposed strands	17	15	17	15-17
	Section loss with exposed strands	22	30	32	22-32
	Section loss only	39	55	59	39-59
+ Exposed strands include ineffective strands due to longitudinal cracking.					

4.6 CLASSIFICATION OF BEAM END DETERIORATION

The classification of beam end deterioration shown in Table 4-11 is based on the type, location, and extent of damage. It is used to determine the appropriate CS in accordance with inspection guidelines. The range for CSs is decided based on the analysis presented in Section 4.5, which evaluates the impact of various deterioration scenarios on beam end capacity.

Table 4-11. Classification of Beam End Deterioration by Condition State (CS)

Type of Deterioration	Location	Case	Range[1]	Zone	Condition State (CS)
Spall/ Delamination	Beam soffit[2]	(A) Depth < clear cover of stirrups	N/A	Z3	CS2
		(B) Depth = clear cover of stirrups	No strands are exposed, but section loss < 20%		CS2
		(C) Depth = clear cover of strands	< 15% of bottom flange strands are exposed and < 35% section loss		CS3
			≥ 15% of bottom flange strands are exposed		CS4
	Bottom flange side[3]	(A) Depth < clear cover of stirrups	N/A	Z1, Z2, Z3	CS2
		(B) Depth = clear cover of stirrups	Section loss < 10% and no strands are exposed		CS2
		(C) Depth = clear cover of strands	< 40% section loss without exposed strands[4]		CS2
			< 15% of the bottom flange strands are exposed and < 30% section loss		CS3
			≥ 15% of bottom flange strands are exposed		CS4
		(D) Depth > clear cover of strands	< 15% of bottom flange strands are exposed and <30% section loss		CS3
			Section loss ≥ 40% and no strands are exposed.		CS4
			≥ 15% of bottom flange strands are exposed		CS4

[1] Do not use these limits for MI 1800 beams. The capacity of MI 1800 beams should be evaluated on a case-by-case basis using the provided Mathcad calculation sheets and compared with the factored demands.
[2] Clear cover is measured from the beam soffit.
[3] Clear cover is measured from the vertical side of the bottom flange.
[4] Use 20% as the limit when the bottom flange spall is only on one side.

4.7 CONDITIONS REQUIRING A REQUEST FOR ACTION (RFA)

The RFA thresholds are developed based on the analysis results that account for the impact of deterioration, along with applicable inspection and rating criteria discussed throughout the report. Specifically, the thresholds outlined in Table 4-12 are aligned with the CS definitions established in Section 4.6, where capacity reductions were directly correlated with the extent of strand exposure and section loss.

Table 4-12. PSC I-Beam End Conditions Requiring a Request for Action (RFA)

Request for Action	PSC I-Beam End
In-depth inspection required	X
Element conditions at CS4	X
Exposed (ineffective) strands ≥ 15% of the bottom flange strands	X
Section loss ≥ 40% and no strands are exposed. (Section loss >20% and no strands are exposed if the spall is on one side of the bottom flange)	X
Shear cracks impacting the beam end capacity	X

5 PERFORMANCE OF BEAM END REPAIR AND PRESERVATION METHODS

5.1 OVERVIEW

This section describes the evaluation of repair and preservation methods for deteriorated PSC beam ends. The corrosion of prestressing strands and mild steel leads to concrete delamination and spalling, conditions predominantly observed at the beam ends. Traditional patching techniques have proven to be short-term solutions that do not contribute to capacity. The review of MDOT inspection data and literature suggests that concrete patching contributes to concealed corrosion at a faster rate, ultimately leading to delamination and spalling of the repairs. According to the MDOT Special Provision for Prestressed Concrete Beam End Repair (20RC712(A385)), Latex Modified Concrete (LMC) is commonly used for beam end repairs (MDOT 2021b). Further, MDOT recently decided to use penetrating sealants instead of concrete surface coatings (CSCs) to protect concrete. The use of a zinc-rich epoxy primer to protect exposed steel is also a more recent practice introduced in the Special Provision for Maintenance Repair of Prestressed Concrete Beam for Contract Identification 25031-214869, 20SM712(A175) (MDOT 2021a). This study was initiated to assess the effectiveness of these repair and preservation methods and develop recommendations through accelerated corrosion testing conducted using a modified version of the Bureau of Standards M-82 Protocol for Topical and Patch Repairs (Bureau of Reclamation 2014).

A total of ten (10) concrete slab specimens of 1 ft × 1 ft × 5.5 in. were fabricated using a typical concrete mix with Type 1 cement. Each specimen includes Grade 60, three #4 rebars at the top mat and a 4 × 4 heavy steel mesh at the bottom mat, acting as a cathode for the macrocell setup. Figure 5-1(a) shows the arrangement of #4 rebars within the specimens. Figure 5-1(b) shows a cross-section of the specimen perpendicular to the rebars.

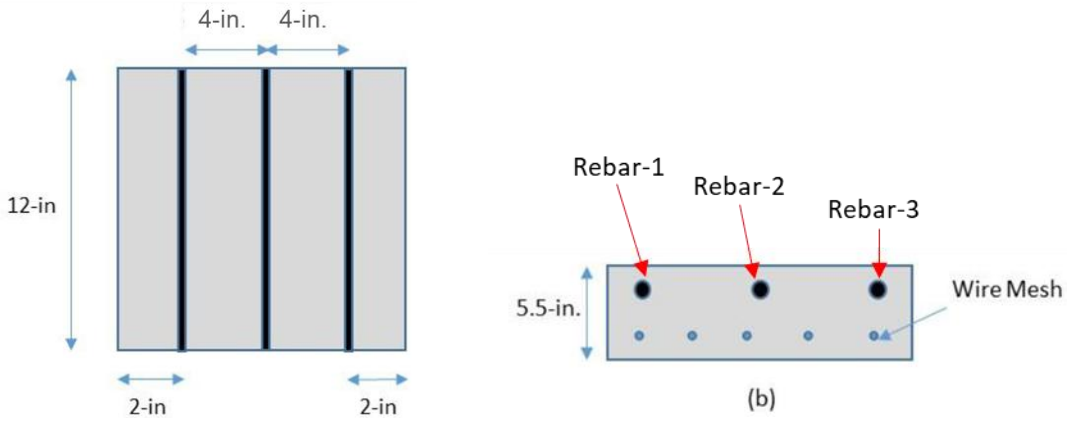

(a) Top view showing rebar locations (b) Cross-section

Figure 5-1. Schematic of concrete slab specimens.

Table 5-1lists repair and preservation methods and materials selected for this study. Two slab specimens were used for each test case. The first two test cases were to evaluate the performance of LMC as a repair material, both with and without penetrating sealants. The other three test cases were designed to assess the performance of zinc-rich epoxy primer, both with and without penetrating sealants and CSC. For these three cases, a regular concrete mix with Type I cement was used as the repair material to avoid the influence of LMC on the performance of the zinc-rich epoxy primer. The concrete surface coating, silane penetrating sealer, and the zinc-rich epoxy primer were selected from the MDOT Materials Source Guide (MDOT 2024). ZINC CLAD® 4100 was selected due to its high zinc content (≈89 wt%), which was expected to provide adequate protection against steel corrosion even when the coating is damaged. The specific CSC and penetrating sealant were selected based on the recommendations in Attanayake et al. (2022). Protectosil® BH-N silane penetrating sealant forms a breathable hydrophobic barrier and prevents moisture and chloride ingress. Benjamin Moore Ultra Spec® Masonry Elastomeric Waterproofing Coating Flat 0359 was selected because its 100% acrylic elastomeric formulation can bridge minor surface cracks (up to 0.03 in.) and create a flexible, breathable coating to protect concrete from moisture intrusion.

Table 5-1. Test Cases, Repair and Preservation Methods, Materials, and Specimen Labels

Test Case	Repair and Preservation	Selected Materials	Specimen Label
1	Patch repair w/o concrete surface treatment	Latex Modified Concrete (LMC) with unprotected rebar.	S1 S6
2	Patch repair + concrete surface treatment 1	LMC with unprotected rebar and silane penetrating sealer (Protectosil® BH-N)	S2 S7
3	Patch repair + zinc-rich epoxy primer on exposed steel	Type 1 concrete mix as the patch repair material and zinc-rich epoxy primer (ZINC CLAD® 4100) as the rebar protector	S3 S8
4	Patch repair + zinc-rich epoxy primer on exposed steel + concrete surface treatment 1	Type 1 concrete mix as the patch repair material, zinc-rich epoxy primer (ZINC CLAD® 4100), and silane penetrating sealer (Protectosil® BH-N)	S4 S9
5	Patch repair + zinc-rich epoxy primer on exposed steel + concrete surface treatment 2	Type 1 concrete mix as the patch repair material, zinc-rich epoxy primer (ZINC CLAD® 4100), and coating surface coating (Benjamin Moore Ultra Spec® Masonry Elastomeric Waterproofing Coating Flat 0359)	S5 S10

5.2 SPECIMEN PREPARATION

The process started with the assembly of formwork with inside dimensions of 1 ft × 1 ft × 5.5 in. A total of 30 pieces of #4 rebars were cut to a length of 16 in., and a wire wheel was used to ease and smooth the edges at both ends of the rebars. Both ends of the Rebar-2 and one end of all other rebars (Rebar-1 and Rebar-3) were drilled. Threads were tapped to a depth of ½ in. Stainless steel hex-head bolts (1/4-20 thread, 1.5 in. length) with two nuts were installed at the threaded ends, as shown in Figure 5-2(a). A wire wheel was used to remove mill scale for up to 3 in. at both ends of each rebar. All rebars were then cleaned with xylene and air-dried for at least 30 minutes. Next, a 3-in. length was marked from both ends to define a 10-in. long central region that would remain uncovered between the two shrink tube terminations. Electroplater tape, approximately 2-in. wide, was wrapped starting at the 3-in. mark and extended toward the end of the rebar, as shown in Figure 5-2(b). Shrink tubing was then applied using a heat gun. Green shrink tubes are used for Rebar-2, while black ones are used for the other rebars for identification purposes (Figure 5-2(c)). The shrink tube extended approximately ½ in. beyond the end of the rebar to enclose the retaining nut, providing a space for epoxy sealing.

(a) Rebars with bolts and nuts at the ends

(b) Electroplater tape wrapping at both ends

(c) Rebars with shrink tubes at both ends

Figure 5-2. Rebar preparation.

As shown in Figure 5-3, a 4 × 4 heavy steel mesh was placed at the bottom of each specimen, maintaining a 0.5 in. cover from the panel's bottom surface. A 12 in. long copper wire was welded to each steel mesh to serve as an electrical connection. Top rebars were placed in the formwork, maintaining a 1-in. clear cover from the top surface to accelerate the corrosion process.

(a) Top view

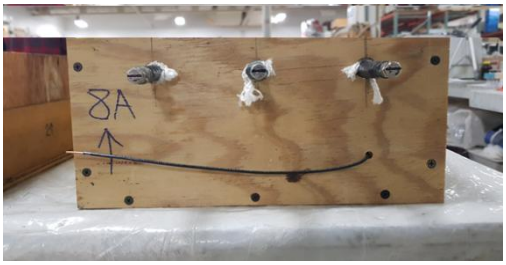

(b) Side view

Figure 5-3. A formwork with rebar and wire mesh arrangement.

Table 5-2 shows the design of the concrete mix used for specimen fabrication. The specimens were moist cured for the first 7 days and dry cured for 21 days. At the end of the moist curing period, all surfaces, except the top and bottom, were sealed with an epoxy paint. All cylinders prepared for compressive strength testing were kept in a 100% moist condition until the day of testing.

Table 5-2. Typical Concrete Mix Design with Type I Cement

Material	Quantity (per yd^3)
Coarse aggregate (SSD) (lb)	1,488
Fine aggregate (SSD) (lb)	1,557
Cement–Type I (lb)	656
Air entraining admixture (fl oz)	5.07
Water reducing admixture (fl oz)	58.67
Water (lb)	246
Water-cementitious material ratio	0.38

Two ponds were attached to the top of the specimen, one covering the entire top surface and the other isolating the area over Rebar-2. At 28 days of concrete age, the entire top surface area was ponded with a 5% NaCl solution for two weeks. Afterwards, only the top surface area over Rebar-2 was ponded with the same solution. A constant current of 30 mA was applied starting at 42 days of concrete age to accelerate the corrosion of Rebar-2, and this voltage supply was maintained until the cracks were visible on the surface. Approximately six weeks after the start of ponding, cracks were visible on both sides and the top surface over Rebar-2 (Figure 5-4).

(a) Front view (b) Top view

Figure 5-4. Concrete cracking near the corroded Rebar-2.

5.3 IMPLEMENTATION OF REPAIR AND PRESERVATION METHODS

Following concrete cracking, the ponding was removed and two 2.5-in. deep saw cuts were made parallel to Rebar-2, isolating a 2-in. wide concrete section with Rebar-2 to facilitate the removal of Rebar-2 and the surrounding concrete (Figure 5-5).

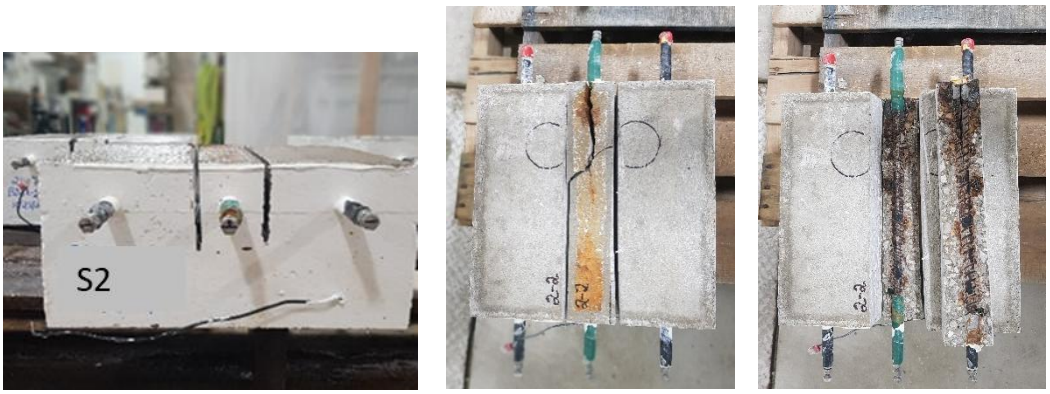

(a) Front view (b) Top view (c) Removed concrete

Figure 5-5. The removal of corroded Rebar-2r and the surrounding concrete.

Following concrete removal, two core samples were extracted from each specimen, as shown in Figure 5-6 to evaluate chloride content at the rebar depth. One core was extracted starting from the surface that was exposed after the removal of Rebar-2. Another was taken from an area near Rebar-1. The cores were sliced at 0.5 in. intervals and oven-dried for 24 hours, as shown in Figure 5-6(c). The slices were ground into powder, and the particles passing the US sieve #20 were used for chloride testing. The chloride content was evaluated using the acid-soluble chloride content test method described in ASTM C1152 (ASTM C1152 2023). The core holes were filled with Sikadur® VPC mix to restore integrity before continuing with the repair and preservation activities.

(a) Coring locations (b) A core sample (c) 0.5 in. thick slices

Figure 5-6. Coring before repair.

Before placing the repair materials, the vertical sawcut surfaces were chipped and cleaned to enhance bonding. Since the same Rebar-2 was used in the repair, it was cleaned before being placed in the repair. A wire wheel was used to effectively remove rust and corrosion products. Chemicals were not used for cleaning the rebar to replicate typical field cleaning conditions encountered during bridge repair work. The condition of Rebar-2 before and after cleaning is shown in Figure 5-7.

(a) Before cleaning (b) After cleaning

Figure 5-7. The condition of Rebar-2 before and after cleaning.

For test cases 3, 4, and 5, the cleaned Rebar-2 was coated with a zinc-rich epoxy primer to provide additional corrosion protection, as shown in Figure 5-8. The primer comprises three components (Parts A, B, and F-zinc dust), as shown in Figure 5-8(a). Parts A and B were thoroughly mixed with a Jiffy Mixer before adding the zinc dust (Figure 5-8(b)). A brush was used to apply the primer (Figure 5-8(c)).

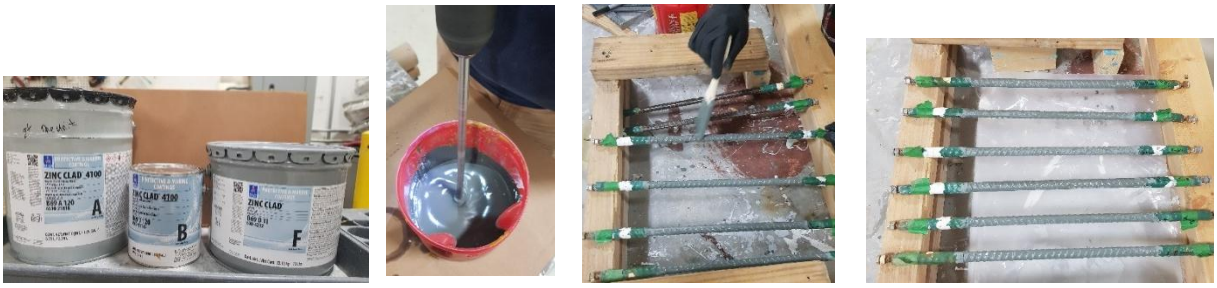

(a) Mixing components (b) Mixing (b) Coating application (c) Drying

Figure 5-8. Preparation and application of the zinc-rich epoxy primer coating on Rebar-2.

After coating Rebar-2, the patch repair was performed by casting the designated repair material to restore the original cover thickness. Figure 5-9 shows the specimen after patch repair.

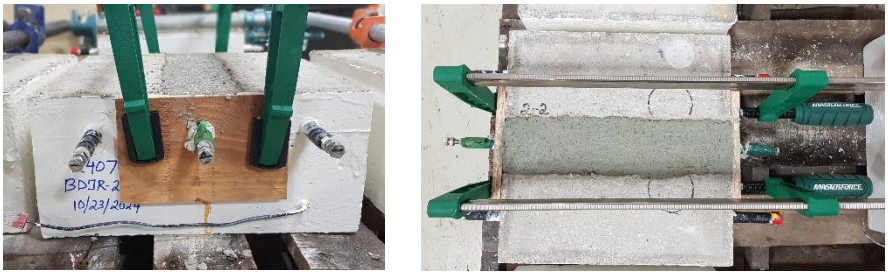

(a) Front view (b) Top view

Figure 5-9. Specimen after patch repair.

Specimens for Test Cases 2 and 4 were protected using a silane penetrating sealer (Protectosil® BH-N), which requires a 28-day curing period for the substrate concrete before application. The

application of the selected CSC requires a minimum of 7 days of curing of substrate concrete. The concrete top surface was sandblasted at the end of the required curing ages. Both the penetrating sealant and the CSC were applied using a brush (Figure 5-10).

(a) Silane penetrating sealer application (b) Coating application

Figure 5-10. Application of silane penetrating sealer and CSC on the top surface of the specimens.

Following the application of concrete surface treatments to the top surface, all the side surfaces were sealed using an epoxy paint. A pond was attached to the entire top surface of each specimen, and a junction box was connected to the rebars (Figure 5-11). At 28 days of patching, the entire panel was ponded with a 5% NaCl solution for two weeks. The NaCl solution was drained for a short period after one day to take the initial reading of the half-cell potential and the voltage across the 1 Ω resistor. Afterwards, the wet-dry cycles were continued, and the data were collected at 14, 42, 70, 98, 126, 154, 182, and 210 days after the start of ponding over the repaired specimens. Therefore, the ages of the concrete patch repairs at the time of data collection are 29, 42, 70, 98, 126, 154, 180, 210, and 238 days.

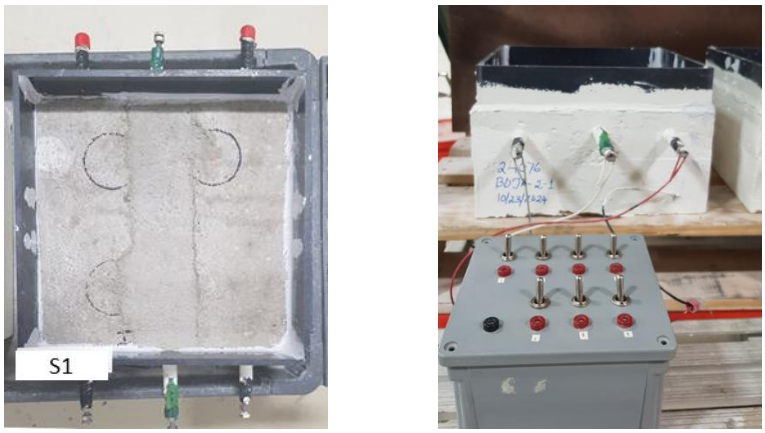

(a) Pond (b) Junction box

Figure 5-11. Repaired specimen with a pond and a junction box.

5.4 RESULTS AND DISCUSSION

5.4.1 Concrete Strength

The concrete mix with Type 1 cement was used to fabricate the slabs and repair six out of 10 slabs. This concrete mix is referred to as R1 in this report. The same mix used for the repairs is referred to as R1-Repair. The LMC mix was used to repair four slabs and is referred to as LMC-Repair. Standard 4×8 in. cylinders were prepared from each mix to perform compressive strength tests in accordance with ASTM C39. The cylinders were kept in 100% moist conditions until the day of testing. Table 5-3 presents concrete compressive strength results. The R1 mix developed a compressive strength of 6030 psi in 3 days and 8100 psi in 28 days. The R1-Repair mix reached a strength of 5900 psi in 7 days and 8420 psi in 28 days. The LMC-Repair mix developed a compressive strength of 5960 psi in 7 days and 7530 psi in 28 days. Both repair mixes exceeded the required 7-day and 28-day compressive strengths of 3200 psi and 4500 psi, respectively. The required minimum strengths are defined in Table 1004-1 of the MDOT Standard Specifications for Construction (MDOT 2020). These results indicate that both R1-Repair and LMC-Repair mixes develop sufficient compressive strength over time to be viable for beam end repairs.

Table 5-3. Compressive Strength of Concrete Used for Specimens and Repairs

Mix ID	Age (Days)	Strength (psi)
R1	3	6030
	7	6660
	14	7300
	28	8100
R1-Repair	7	5900
	14	7860
	28	8420
LMC-Repair	7	5960
	14	7220
	28	7530

5.4.2 Chloride Content in Concrete

Several methods are available to measure chloride content in concrete. The acid-soluble and water-soluble chloride contents are evaluated following ASTM C1152 and C1218 procedures, respectively. The ASTM C1152 procedure is used to measure the total chloride content. This includes the amount freely available to contribute to steel corrosion and the amount bound to aggregates and hydrated cement. The threshold total chloride content to initiate steel corrosion is 500 ppm (parts per million). The ASTM C1218 procedure is used to measure the water-soluble chloride content, the amount freely available to cause steel corrosion. This test does not evaluate the bound chloride in aggregates and hydrated cement. The chloride content evaluated according

to ASTM C1218 can yield higher chloride content and highly variable data, depending on factors such as aggregate crushing, particle size, core extraction time, and temperature (Concrete Construction 1998). For this study, the acid-soluble chloride content is evaluated in accordance with ASTM C1152.

Table 5-4 presents the average total chloride content evaluated within 1 to 1.5 in. depth from the top surface before and after repair. The total chloride content at Rebar-2 exceeded the threshold value of 500 ppm before the concrete was removed for repair, indicating active corrosion at this location. In contrast, the chloride content at Rebar-1 remained below the threshold, ranging from a minimum of 49 ppm to a maximum of 191 ppm. This indicates that while the Rebar-2 was exposed to chloride levels high enough to initiate corrosion, the adjacent areas had relatively lower chloride concentrations.

After repair, chloride test results reveal that chloride concentrations at Rebar-2 locations were consistently higher, ranging from 408 ppm to 2096 ppm, compared to those near Rebar-1 locations. Except for two specimens (one from each Test Cases 4 and 5), all Rebar-2 values exceeded the 500 ppm threshold, indicating a potential risk of corrosion. In contrast, chloride levels at Rebar-1 remained below the threshold, ranging from 139 ppm to 383 ppm. The type of concrete surface treatment, the steel protection system, or a combination thereof applied to these specimens influenced the chloride content at Rebar-1 and Rebar-2.

Test Case 5, which included CSC on the top surface, exhibited the lowest chloride concentrations at both Rebar-2 (408 ppm) and Rebar-1 (139 ppm), indicating the effectiveness of CSC in mitigating chloride ingress. A similar trend was observed in Test Case 4, which used a silane penetrating sealer, further supporting the benefits of surface treatments in reducing chloride intrusion. In contrast, Test Cases 1 and 3, where no surface protection was applied, showed elevated chloride concentrations, reaching up to 1025 ppm at Rebar-2 and 383 ppm at Rebar-1, highlighting the importance of applying concrete surface protection. Notably, Test Case 2 showed the highest chloride content (2096 ppm) despite the use of a penetrating sealer. This anomaly is attributed to the presence of a cold joint between the repair and existing concrete, as shown in Figure 5-12, which likely compromised the effectiveness of the surface treatment.

Table 5-4. Total Chloride Content Test Data

Test Case	Sample ID	Average Total Chloride Content Within 1 to 1.5 in. Depth from the Top Surface (ppm)	
		Before Repair	After Repair
1	S1-B2*	543	720
	S1-B1	173	189
	S6-B2	1267	932
	S6-B1	189	383
2	S2-B2	1732	1202
	S2-B1	157	172
	S7-B2	1380	2096
	S7-B1	182	157
3	S3-B2	761	1025
	S3-B1	160	189
	S8-B2	668	550
	S8B1	163	175
4	S4-B2	1547	443
	S4-B1	191	166
	S9-B2	1562	557
	S9-B1	167	139
5	S5-B2	1176	408
	S5-B1	49	188
	S10-B2	1065	612
	S10-B1	163	168

**S1-B2: S1 = specimen number 1; B2 = rebar number (Rebar-2)*

(a) Front view (b) Top surface

Figure 5-12. Specimen S7 with a cold joint on the top surface.

5.4.3 Half-Cell Potential (ASTM C876)

ASTM C876 (2015) defines the limits for the potentials measured with a copper-copper sulfate reference electrode to identify the probability of reinforcing steel corrosion. Table 5-5 presents a summary of the ASTM limits and definitions. As shown in the table, the likelihood of not having corrosion is greater than 90% when the half-cell potential is more positive than -200 mV. When

the measurements show more negative potentials than -350 mV, the probability of having steel corrosion is greater than 90%.

Table 5-5. Half-Cell Potential Limits for Evaluating Corrosion Potential (ASTM C876)

Half-Cell Potential (mV)	Corrosion Potential for the Copper-Copper Sulfate Reference Electrode
> -200	Probability of no corrosion > 90%
-200 to -350	Uncertain
< -350	Probability of corrosion > 90%

The half-cell potential of the top three rebars for each specimen is presented in Figure 5-13. Before repair, across all test cases, Rebar-2 showed a more negative value than -350 mV, confirming active corrosion activity in the deteriorated region. In contrast, Rebars 1 and 3 (side bars) mostly showed values more positive than -350 mV, indicating a lower likelihood of corrosion before repair.

After repair, Test Case 1, showed that Rebar-2 continued to show half-cell potentials more negative than -350mV, with the time exceeding -500 mV, as shown in Figure 5-13(a). This indicates the presence of corrosion activity at Rebar-2 and confirms that LMC patching alone is insufficient to mitigate corrosion. In contrast, Rebars 1 and 3 remained near the -350 mV threshold, suggesting a lower likelihood of corrosion with time. In Test Case 2, a similar pattern of half-cell potentials is observed, as shown in Figure 5-13(b). Rebar-2 showed a more negative value, and other bars showed more positive values compared to Test Case 1, which is due to the application of the penetrating silane sealer on the top surface. In Test Case 3, Rebar-2 from specimen S3 exceeded the corrosion threshold of half-cell potentials. At the same time, the other rebars showed improved performance due to the application of the zinc-rich epoxy primer, as shown in Figure 5-13(c). As discussed later in Section 5.4.5 of this report, Rebar-2 exhibits corrosion over 25% of the surface area. This variation in the results of Test Case 3 highlights the need for more careful and consistent application of the zinc-rich epoxy primer coating on the rebar to ensure adequate corrosion protection. Test Cases 4 and 5 showed similar results in terms of corrosion protection. Test Case 5 performed the best among all cases, with all bars showing more positive than -350 mV threshold of half-cell potential, indicating no active corrosion, as shown in Figure 5-13(e). Test Case 4 showed comparable performance, except for Rebar-3 in specimen S9, which exceeded the corrosion threshold, as shown in Figure 5-13(d). The combination of zinc-rich epoxy primer and elastomeric surface coating provided the most effective protection.

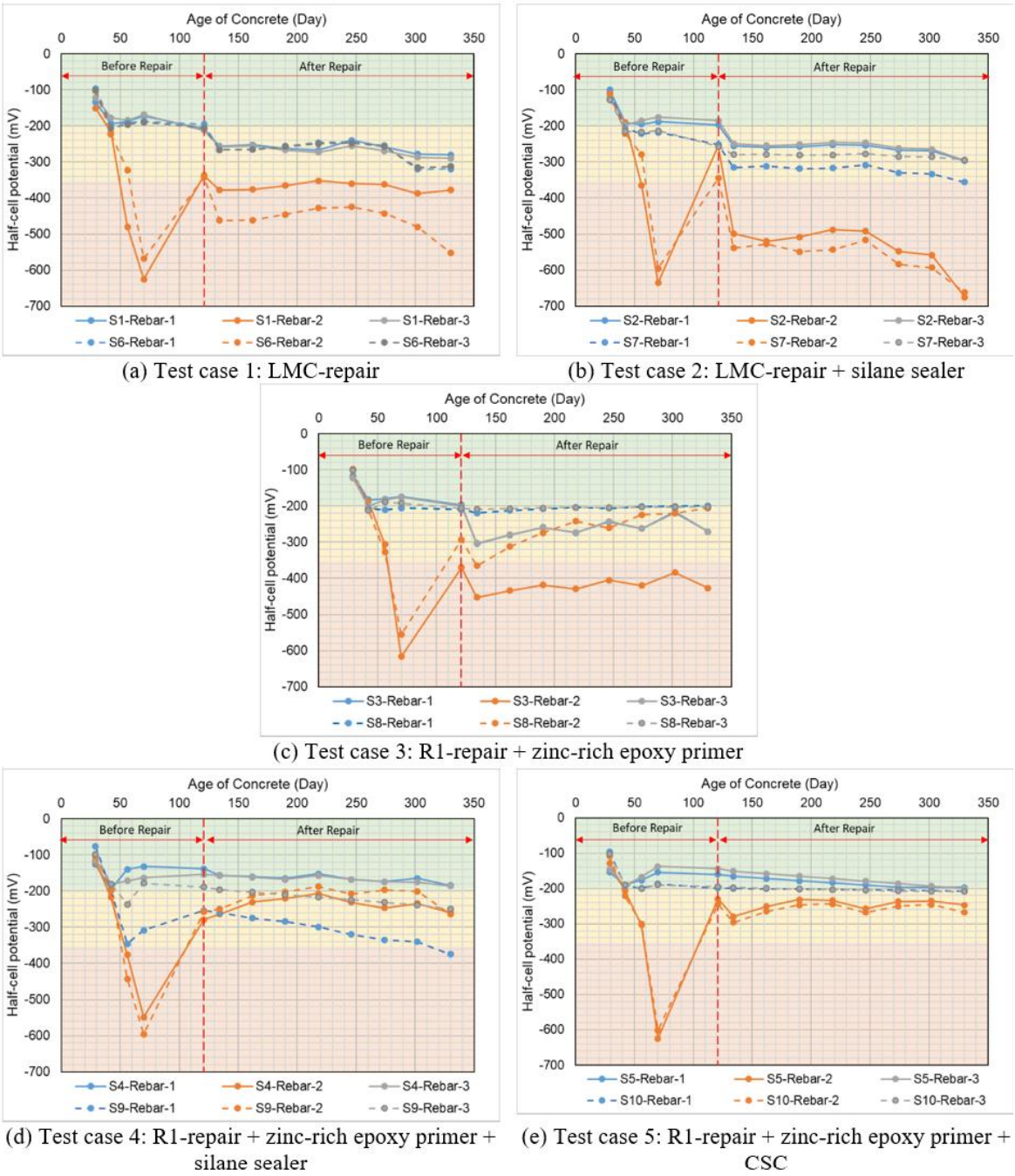

(a) Test case 1: LMC-repair

(b) Test case 2: LMC-repair + silane sealer

(c) Test case 3: R1-repair + zinc-rich epoxy primer

(d) Test case 4: R1-repair + zinc-rich epoxy primer + silane sealer

(e) Test case 5: R1-repair + zinc-rich epoxy primer + CSC

Figure 5-13. Variation of half-cell potential with respect to the age of concrete.

5.4.4 Integrated Current

Following the Bureau of Standards M-82 procedures, the top rebars were connected to the WWR through 1 ohm (Ω) resistors through switches in a junction box. The voltage across the 1 Ω resistor was measured. The current passing through the resistor was calculated and recorded as a time series. The data was used to calculate the integrated current. According to ASTM G109 (2023),

an integrated current of 150° C is sufficient to produce an adequate amount of corrosion for visual evaluation. An integrated current above zero represents anodic current, meaning the steel is losing electrons and starting to corrode. Conversely, an integrated current below zero indicates a cathodic current, where the steel is gaining electrons, and this can restrain or protect the bar receiving the current.

In Test Case 1, where LMC repair was used without any protective treatment on the rebar, Rebar-2 consistently exhibited anodic behavior, with a positive integrated current reaching approximately 2100 C, while the adjacent side bars (Rebars 1 and 3) showed cathodic responses, with negative integrated currents up to -600 C (Figure 5-14a). A similar trend was observed in Test Case 2, where LMC repair was protected with a silane-penetrating sealer. Rebar-2 demonstrated more noticeable anodic behavior, with integrated current values exceeding 8000 C, and the side bars exhibited stronger cathodic responses, with integrated currents reaching up to -2000 C (Figure 5-14b). Rebar-2 of both Test Cases 1 and 2 reached the integrated current threshold of 150 C at 40 days and 35 days of repair, respectively.

In Test Case 3, the R1-Repair patch was used in combination with a zinc-rich epoxy primer applied to the rebar without any additional surface protection on the concrete. Specimen S8 demonstrated the expected behavior, with the epoxy primer effectively protecting Rebar-2 and enhancing the performance of the side bars against corrosion. The center bars exhibited slightly positive integrated current at the beginning, and gradually started showing negative integrated current, while the side bars showed steady negative integrated current, indicating the effectiveness of the primer (Figure 5-14). In contrast, specimen S3 showed behavior similar to that observed in Test Cases 1 and 2. Despite the application of zinc-rich epoxy primer to the center bar, it consistently exhibited anodic behavior with a positive integrated current reaching approximately 2000 C at 240 days of repair, while the adjacent side bars showed cathodic responses with negative integrated current values up to -700 C (Figure 5-14). As discussed later in Section 5.3.5 of this report, Rebar-2, removed from the S3 specimen, exhibited corrosion over 25% of the surface area. This variation of Test Case 3 demands additional investigations to identify the possible reasons for this observation.

In Test Case 4, where R1-Repair was combined with zinc-rich epoxy primer and a penetrating silane sealer, both center and side bars exhibited a steady increase in integrated current (Figure 5-14). The center bars initially exhibited a slightly positive integrated current, and then gradually began to show a negative integrated current, indicating the effectiveness of the primer. However, the Rebar-1 showed a minimal positive integrated current of 53 C at 238 days of repair, suggesting the initiation of corrosion. As discussed late in Section 5.4.5 of this report, Rebar-1, removed from the S9 specimen, exhibited corrosion over 5% of the surface area.

Test Cases 4 and 5 results show a similar pattern for all four specimens. In Test Case 5, where a surface coating was used instead of a silane sealer, the integrated current values in the bars exhibited cathodic responses, with negative integrated currents reaching up to -200 C at 238 days of repair, as shown in Figure 5-14e. Yet none of the rebars showed any positive current at the end of the test cycle, which indicates that the coating provided slightly better corrosion protection than the silane penetrating sealer, resulting in more stable electrochemical performance throughout the specimen.

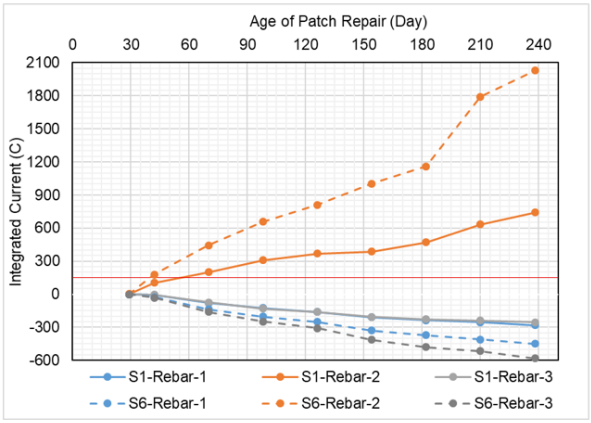

(a) Test case 1: LMC-repair

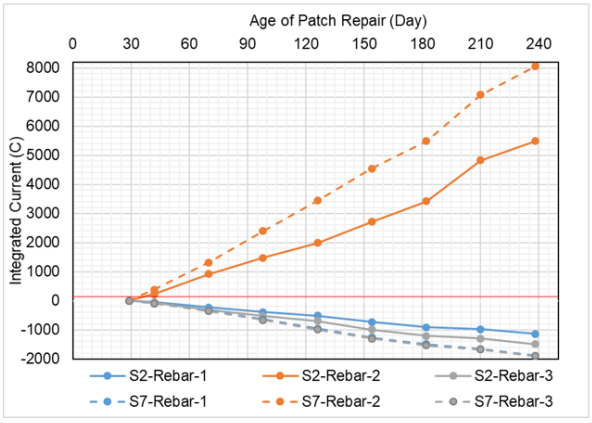

(b) Test case 2: LMC-repair + silane sealer

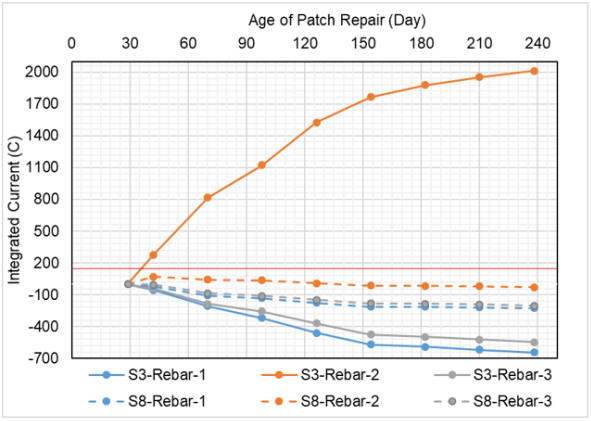

(c) Test case 3: R1-repair + zinc-rich epoxy primer

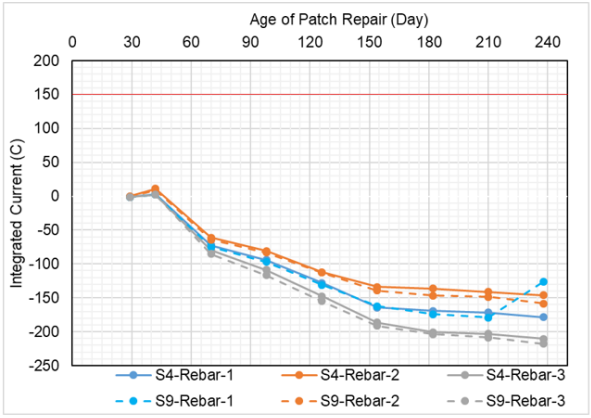

(d) Test case 4: R1-repair + zinc-rich epoxy primer + silane sealer

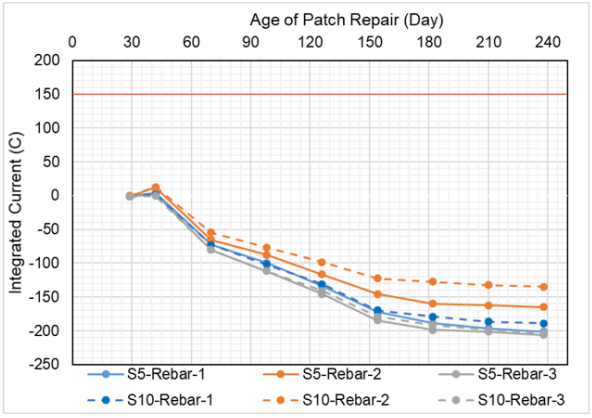

(e) Test case 5: R1-repair + zinc-rich epoxy primer + coating

Figure 5-14. Variation of integrated current against the age of patch repair.

5.4.5 Rebar Condition at the End of Testing

Test results of Cases 1 and 2 exhibited chloride contents exceeding 500 ppm within a 1.0 to 1.5 in. depth near Rebar-2, half-cell potential more negative than -350 mV, and integrated current values greater than 150 C. Based on these observations, Rebar-2 in Test Cases 1 and 2 was classified as having 100% of its surface area corroded. As shown in Figure 5-15, Rebar-2 removed from those

four specimens (S1, S6, S2, and S7) confirms the conditions. Similarly, in Test Case 3, only Rebar-2 from S3 specimen showed signs of corrosion, with approximately 25% of the surface area affected under light to moderate corrosion conditions (Figure 5-15). Rebar-2 recovered from the other test specimens showed no signs of corrosion, indicating the effectiveness of the applied preservation methods.

(a) Top view (b) Bottom view

Figure 5-15. Condition of Rebar-2 removed from the repaired area.

Visual inspection revealed no signs of corrosion on Rebars 1 and 3. However, Rebar-1 from specimen S7 exhibited light corrosion over approximately 10% of the surface area (Figure 5-16). Rebar-1 from specimen S9 showed less than 5% corrosion over the surface area (Figure 5-17). In both specimens, the half-cell potentials were more negative than -350 mV, but the integrated current and chloride content values were below the corrosion threshold limit.

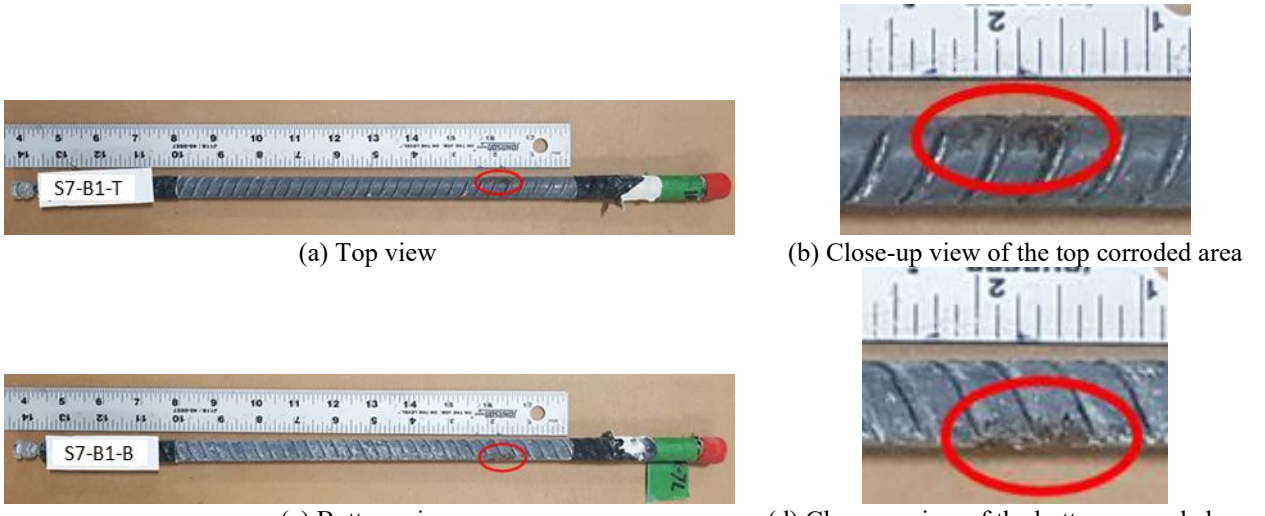

(a) Top view (b) Close-up view of the top corroded area

(c) Bottom view (d) Close-up view of the bottom corroded area

Figure 5-16. Condition of Rebar-1 from S7 specimen.

(a) Bottom view (b) Close-up view of corroded area

Figure 5-17. Condition of Rebar-1 from S9 specimen.

5.5 CONCLUSIONS AND RECOMMENDATIONS

The findings indicate that patch repair with only LMC (Test Case 1) or LMC with a silane penetrating sealer (Test Case 2) is not effective in protecting embedded steel from corrosion. In Test Cases 1 and 2, the corrosion threshold of an integrated current of 150 C was reached at 40 and 35 days after patch repair, respectively. The application of a zinc-rich epoxy primer protects the coated bars within the repaired area. It also reduces the corrosion potential of the surrounding rebars. The combination of the zinc-rich epoxy primer with a concrete surface treatment, either a silane penetrating sealer or CSC, demonstrated improved performance compared to other methods. Considering the surface treatments used in this study, the elastomeric coating provided a slightly better corrosion control relative to the silane penetrating sealer. Overall, the integration of patch repair, zinc-rich epoxy primer, and surface coating yielded the most consistent and effective corrosion mitigation across all test cases and is recommended for implementation. Additionally, it is recommended that further testing be conducted to validate the findings, as this study was limited to a small number of specimens.

6 BEAM END REPAIR DETAILS AND CAPACITY IMPROVEMENT

6.1 OVERVIEW

The MiSIM (2019) Table 5.13.12 lists the recommended actions for deteriorated or damaged concrete beams, such as providing temporary support, crack injection, beam end patching, and overcasting (encasement). The published literature provides an extensive list of maintenance and repair options for deteriorated PSC I-beam ends, including epoxy injection, patching, overcasting, cleaning and coating of exposed steel, fiber-reinforced polymer (FRP) wrapping, cathodic protection for widespread corrosion, and the application of waterproof coatings or silane penetrating sealers. Section 712.3(U) of the MDOT Standard Specifications for Construction describes the epoxy injection procedures for crack repair (MDOT 2020). Moreover, Appendix A4: Concrete Standard Repair Program of the Structural Fabrication Quality Manual (SFQM) outlines a standard procedure for repairing concrete cracks using epoxy injection during fabrication (MDOT 2023). Section 712.03(O) of the MDOT Standard Specifications for Construction describes the procedures for concrete patching on bridge decks and other surfaces (MDOT 2020). Needham (1999) presents repair details and procedures for overcasting deteriorated PSC I-beam ends. Needham (2000) describes construction challenges associated with overcasts and suggests guidelines to overcome them. Section 6.4 of this report describes the field performance of concrete patch repair and overcasting documented during field inspections. MDOT typically uses Latex Modified Concrete (LMC) as a PSC beam end repair material, and the Special Provision for Prestressed Concrete Beam End Repair with LMC, 20RC712(A385) outlines the requirements (MDOT 2021b). The mix design of LMC is provided in Table 703-1 of the MDOT Standard Specifications for Construction (MDOT 2020). The MDOT Special Provision for Fiber Reinforced Polymer Shear Strengthening System, 20BR712(A295), provides guidelines for furnishing and installing fiber-reinforced polymer (FRP) sheets for the repair of prestressed concrete bridge beams (MDOT 2021c). The MDOT Special Provision for Maintenance Repair of Prestressed Concrete Beam for Contract Identification 25031-214869, 20SM712(A175) directs contractors to remove delaminated and unsound concrete and apply a zinc-rich epoxy primer to protect exposed reinforcement (MDOT 2021a). This special provision lacks clear guidelines for handling beam end conditions with exposed strands and advises the contractor to seek additional consultation for handling such situations. The typical MDOT practice is to patch repair beam ends with exposed strands. The Special Provision for Maintenance Repair

of Prestressed Concrete Beam for Contract Identification 25031-214869, 20SM712(A175) is new, and the performance of zinc-rich epoxy primer for protecting steel with and without concrete repairs is unknown. Therefore, an experimental program was developed, utilizing a modified, lower cost version of the Bureau of Standards M-82 Protocol for Topical and Patch Repairs, to evaluate the durability performance of zinc-rich epoxy primers, repair materials, concrete surface coatings, and silane penetrating sealers. Chapter 5 presents the experimental program details, results, and recommendations. The MDOT Special Provision for Concrete Surface Coatings, 20RC710(A285), outlines the requirements for applying concrete surface coatings as well as guidelines for selecting suitable coating materials (MDOT 2021d).

Shield and Bergson (2018) presented full-depth overcast repair details and procedures using shotcrete. Shafei et al. (2020) evaluated the bond strength of concrete patch repairs using ultra-high-performance concrete (UHPC) and high-early-strength concrete (HESC). However, the repair procedure demonstrated by Shafei et al. (2020) is not practical to implement under field conditions due to the lack of space at the beam ends. Harries et al. (2009) present various repairs for high-load-hits (HLHs), including concrete patching, epoxy injection, fiber reinforced polymer (FRP) wrapping, near-surface mounted FRP, steel jacketing, tendon splicing, external posttensioning, or a combination thereof. NCHRP Reports 226 and 280 (Shanafelt and Horn 1980 and 1985), Feldman et al. (1996), Waheed et al. (2005), and Tabatabai and Nabizadeh (2019) present repair methods for different levels of PSC beam damages at mid span. Aktan et al. (2002) and Morcus et al. (2020) classified the deterioration levels of PSC I-beams and listed preventative maintenance or repair methods. Table 6-1 lists different repair methods applicable to deteriorated PSC I-beam ends. The type of repair for each beam end must be selected on a case-by-case basis due to the varying details, conditions, and space constraints of each beam end.

Table 6-1. Repair Methods for PSC I-Beam Ends

Repair Method	Application	Figure
Epoxy injection	Seal structural or hairline cracks	Figure 6-1
Concrete patching	Shallow localized spalls and minor delamination.	Figure 6-2
Partial-depth overcast	Deteriorated concrete is removed up to a specified depth and replaced with new concrete with or without additional steel reinforcement.	Figure 6-3
Partial-depth overcast with FRP wraps		Figure 6-4
Full-depth overcast	Deteriorated concrete is removed up to the full beam height and a specified length (typically, the greater of beam height or 3 ft.). Overcast the end with new concrete and steel reinforcement.	Figure 6-5
Full-depth overcast with FRP wraps	Full-depth overcast is provided as described above, and FRP is applied externally to increase shear strength and/or maintain the integrity of the overcast.	Figure 6-6
FRP wraps		Figure 6-7
Cleaning and coating of steel	Exposed strands and mild steel are cleaned and coated with zinc-rich epoxy primer. The beam end is either cleaned and protected with a concrete surface coating or with an overcast, depending on the impact of beam end deterioration on shear capacity.	Figure 6-8
Silane penetrating sealers and/or concrete surface coatings	Applied to prevent moisture and chloride ingress.	Figure 6-6 Figure 6-7

(a) General view (b) A close-up view

Figure 6-1. Epoxy injected cracks in a PSC I-beam.

(a) The sole plate is in good condition (b) Corroded sole plate

Figure 6-2. Concrete patching at the beam end soffit and in front of the sole plate.

(a) Overcast with a varying height (b) Overcast at the bottom flange

Figure 6-3. Partial-depth overcast.

(a) Overcast up to the top flange (b) Overcast up to mid-height

Figure 6-4. Partial-depth overcast with FRP wraps.

(a) Elevation

(b) Isometric view

Figure 6-5. Full-depth overcast.

(a) Isometric view

(b) Isometric view showing a leaky deck

Figure 6-6. Full-depth overcast with FRP wraps.

(a) Elevation view

(b) Bottom surface

Figure 6-7. FRP repair without overcast.

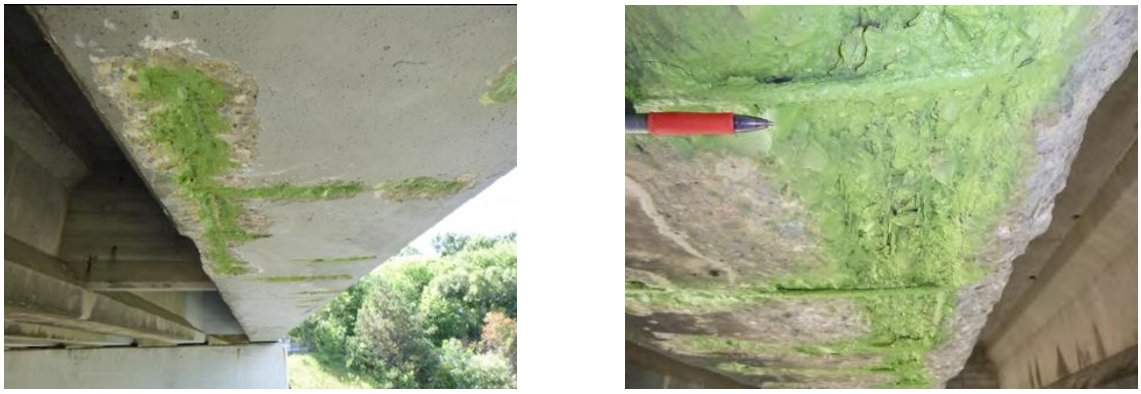

(a) General view (b) A close-up view

Figure 6-8. Cleaning and coating of exposed steel at the beam soffit.

6.2 BEAM END DETAILS

The load transfer mechanism, rate of deterioration, and the selection of various repair methods largely depend on the beam end details. Beam end details can be classified into two groups based on their location: abutment ends and pier ends. At the abutment, as shown in Figure 6-9, three different configurations are commonly used (1) independent backwall, (2) dependent backwalls, and (3) independent backwall with sliding slab. When the beam end is not embedded into the backwall, it is considered as a bridge with an independent backwall, as shown in Figure 6-9(a), or an independent backwall with a sliding slab shown in Figure 6-9(c). When the beam ends are embedded into the backwall, it becomes a dependent backwall, as shown in Figure 6-9(b). Dependent backwalls are used in integral or semi-integral abutments. The dowel bars used in integral abutments are expected to transfer shear from the bridge superstructure to the substructure.

Three different superstructure details are used at the piers: (1) expansion joints, (2) link slabs, and (3) beam ends encased in end diaphragms (Figure 6-10). Expansion joints and link slabs are used in simple span bridges. Typically, full-depth or partial-depth concrete end diaphragms, as shown in Figure 6-11, are provided with these simple spans. Full-depth end diaphragms extend from the underside of the deck to the bottom flange (Figure 6-11a). The partial-depth diaphragm is provided within the web (Figure 6-11(b). These concrete end diaphragms hinder ventilation around beam ends and make it challenging to inspect and repair them. Although it is possible to use steel end diaphragms, this is not a common practice. The use of steel end diaphragms enhances ventilation around beam ends and provides adequate space for inspection and repair.

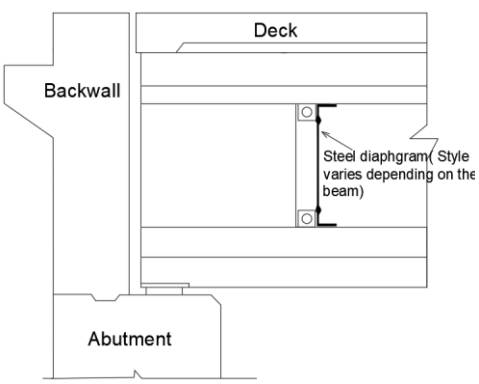

(a) Independent backwall

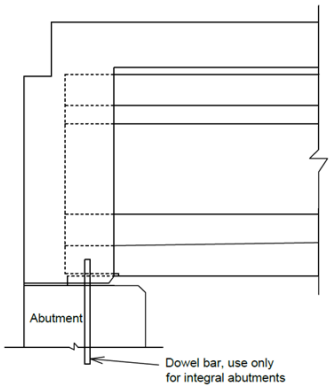

(b) Dependent backwalls in integral or semi-integral abutments

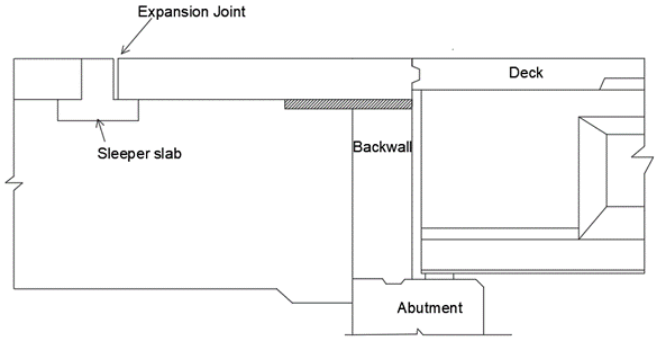

(c) Independent backwall with sliding slab

Figure 6-9. Various details at the bridge abutments.

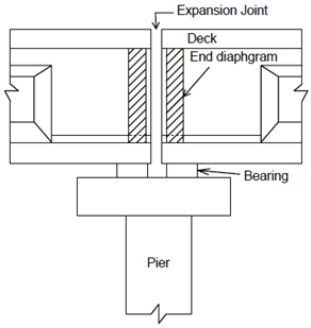

(a) Simple span superstructure with an expansion joint

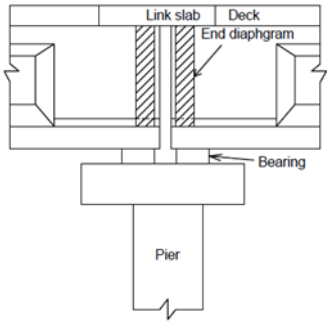

b) Simple span superstructure with a link slab

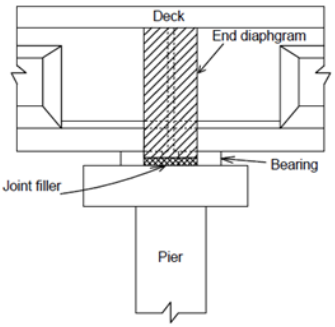

(c) Continuous for live load superstructure with beam ends embedded in the end diaphragm

Figure 6-10. Superstructure details at the pier.

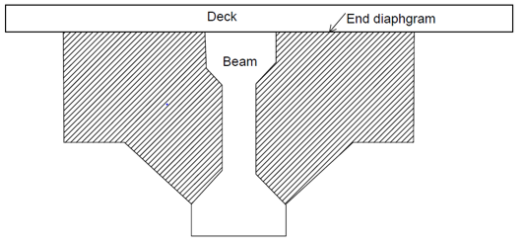

(a) Full-depth concrete end diaphragm

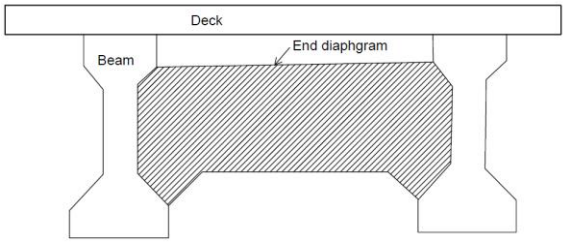

(b) Partial-depth concrete end diaphragm

Figure 6-11. Concrete end diaphragm configurations at piers.

6.3 REPAIR DETAILS

6.3.1 Epoxy Injection

Epoxy is a high-strength adhesive material commonly used for bonding concrete surfaces (ACI 2003). It forms a durable bond that enhances structural integrity and is particularly effective for sealing cracks. By sealing cracks, epoxy prevents moisture and chloride ingress through the cracks, thereby reducing the risk of corrosion to prestressing strands and reinforcing steel. Tests have shown that epoxy-repaired cracks are often stronger than the surrounding concrete; therefore, if the underlying cause of distress is not addressed, new cracks could develop adjacent to the repaired ones (Mansur and Ong 1985). Epoxy injection has been a popular and effective repair strategy for decades. A survey conducted more than four and half decades ago by Shanafelt and Horn (1980) revealed that twenty state Departments of Transportation (DOTs) in the U.S. used epoxy injection to seal cracks in prestressed beam bridges. The study recommended using epoxy injection for cracks wider than 0.003 in. Additionally, durability can be improved by applying a preload prior to epoxy injection. Various highway agencies define different crack width limits for epoxy injection. Attanayake et al. (2022) reviewed crack sealing and epoxy injection guidelines published by multiple agencies and developed the summary shown in Figure 6-12.

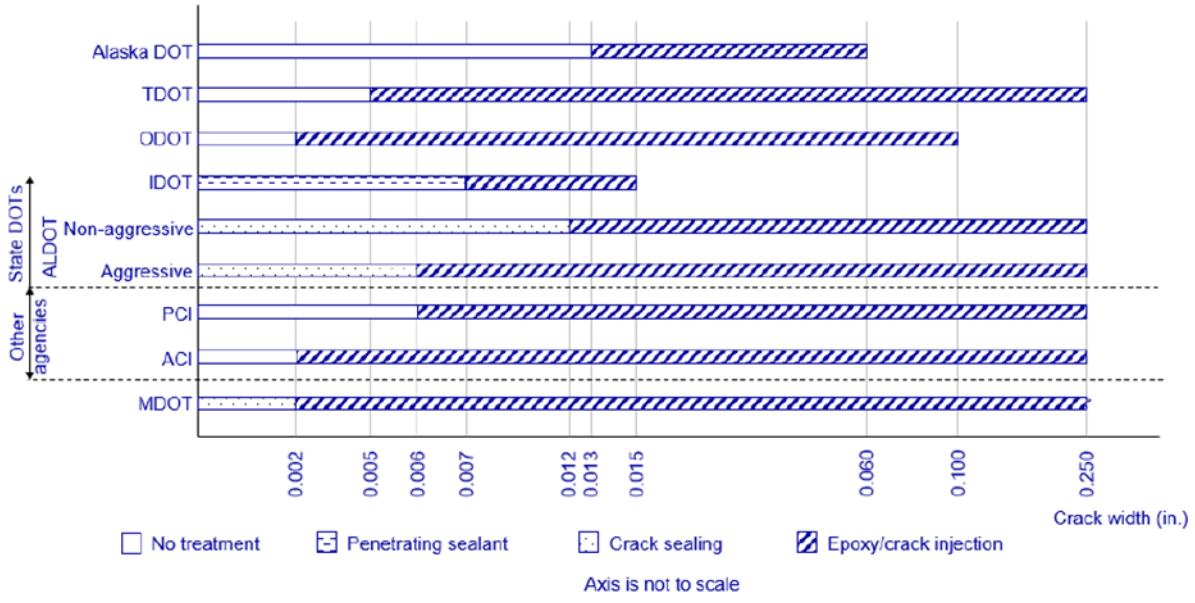

Figure 6-12. Crack sealing and epoxy injection practices of state highway and other agencies (Attanayake et al. 2022).

The Ohio DOT (ODOT 2019), Tennessee DOT (TDOT 2018), and Alaska DOT (Alaska DOT 2016) do not require treating cracks narrower than 0.002 in., 0.005 in., and 0.013 in., respectively. The IDOT (2020) requirement is to apply a protective coating or a concrete penetrating sealer for

beam ends and the visible surfaces of the fascias when the cracks are narrower than 0.007 in. and the short-term visible crack growth has subsidized. ALDOT (2015) defines crack repair methods based on aggressive and non-aggressive exposure conditions. An aggressive environment shall be considered to be a marine environment or an environment with the potential for sulfate or acid attack. For a non-aggressive environment, ALDOT recommends using epoxy injection for crack widths between 0.012 in. and 0.025 in. For aggressive exposure, cracks wider than 0.006 in. are treated with epoxy injection. ACI (2023) recommends repairing 0.002 to 0.250 in. wide cracks using epoxy injection. Section 712-3.9 of the MDOT Construction Manual (MDOT 2025) includes recommendations for epoxy injection of cracks when the crack width is equal to or greater than 0.002 inches. Even though several DOTs define an upper limit for crack widths, MDOT has not defined such a limit. Section 712.3(U) of the MDOT Standard Specifications for Construction (MDOT 2020) describes the epoxy pressure injection procedure for crack repair. The Structural Fabrication Quality Manual (SFQM), Appendix A4: Concrete Standard Repair Program (MDOT 2023), outlines the standard procedure for epoxy injection of cracks in precast beams at the fabrication yard.

6.3.2 Patch Repair

The patch repair is a common method documented in the literature for deteriorated PSC beam ends. Patching is typically used for shallow-depth repairs. MDOT uses patch repair of beam ends when strands are exposed, but the load capacity is not compromised. It is intended to restore the surface condition and enhance durability without increasing the beam capacity. Section 712.03(O) of the MDOT Standard Specifications for Construction (MDOT 2020) describes concrete patching procedures for bridge decks and other surfaces. Cracking and spalling of shallow patches and unreinforced repairs are documented in biennial inspection reports, scoping reports, and the observations summarized in Appendix D, following inspections of several bridges with beam end repairs. For beam ends with shallow spalls, MDOT prefers to clean and protect both steel and concrete surfaces with coatings, as outlined in the Special Provisions for Maintenance Repair of Prestressed Beams 20SM712(A175) and the Special Provision for Concrete Surface Coatings, 20RC710(A285). Attanayake et al. (2022) evaluated the breathability and crack-bridging ability of concrete surface coatings and recommended the application of breathable coatings with crack-bridging ability for improved durability. Attanayake et al. (2022) also suggested using hybrid protective systems, incorporating penetrating sealers and concrete surface coatings, to enhance

durability. Where needed, patch repairs can be protected with FRP sheets installed in accordance with the MDOT Special Provision for Fiber Reinforced Polymer Shear Strengthening System, 20BR712(A295).

6.3.3 Overcast Repair

Overcast is typically used for severe beam end deterioration and involves placing a new reinforced or unreinforced layer of concrete over the existing surface after removing damaged material. Unlike patching, overcast increases the cross-sectional area at the beam end. The types of overcasts can be classified as follows from the information gathered from literature, MDOT scoping reports, field inspections, and the survey of bridge inspection engineers, construction and field services engineers, and design and load rating engineers:

(i) full-depth reinforced concrete overcasts,

(ii) full-depth reinforced concrete overcasts with FRP wraps,

(iii) partial-depth unreinforced concrete overcasts,

(iv) partial-depth reinforced concrete overcasts, and

(v) partial-depth concrete overcasts with FRP wraps.

6.3.3.1 Full-Depth Reinforced Concrete Overcasts

The MDOT's current full-depth reinforced concrete overcast (FDRCO)repair details for PSC I-beam ends reflect the recommendations by Needham (2000). The recommended overcast length is the greater of beam height (H) or 3 feet. The overcast typically extends 3 inches beyond the bottom flange of the original cross-section. Figure 6-13 illustrates the overcast repair details in Needham (2000) for a PSC I-beam with an end block.

Figure 6-14 presents the FDRCO repair detail used in the bridge (STR 3832) carrying Williamston Road over I-96 EB, located in the city of Lansing in Ingham County, Michigan. The repair was performed at the ends of AASHTO Type III beams. For an unknown reason, the overcast length is limited to 2.5 feet, which is shorter than the recommended minimum length of 3.75 feet (the height of the beam) by Needham (2000).

Shield and Bergson (2018) documented FDRCO repair details and procedures implemented by the Minnesota DOT for AASHTO Type III beam ends. They used shotcrete instead of cast-in-place concrete, as shown in Figure 6-15.

The capacity contribution of an FDRCO repair depends on several factors, including the development length of reinforcement, the configuration and anchorage details of the added reinforcement, and the number and length of the exposed strands re-embedded within the overcast concrete. These factors collectively influence the effectiveness of the repair in restoring or enhancing beam end capacity. Section 6.5.1 of this report provides a detailed discussion about the capacity improvements achieved through overcast repairs.

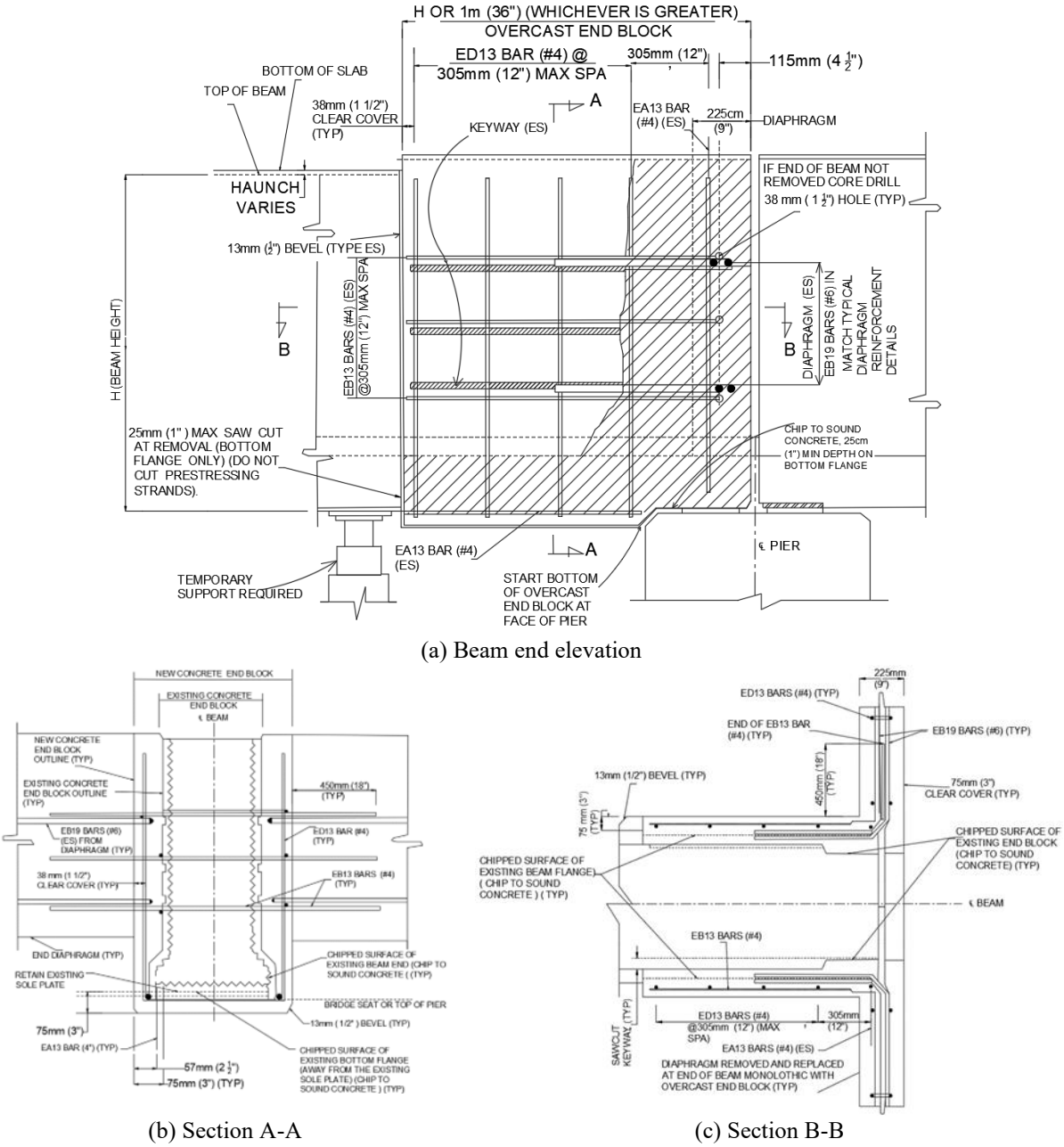

(a) Beam end elevation

(b) Section A-A

(c) Section B-B

Figure 6-13. FDRCO repair details (Needham 2000).

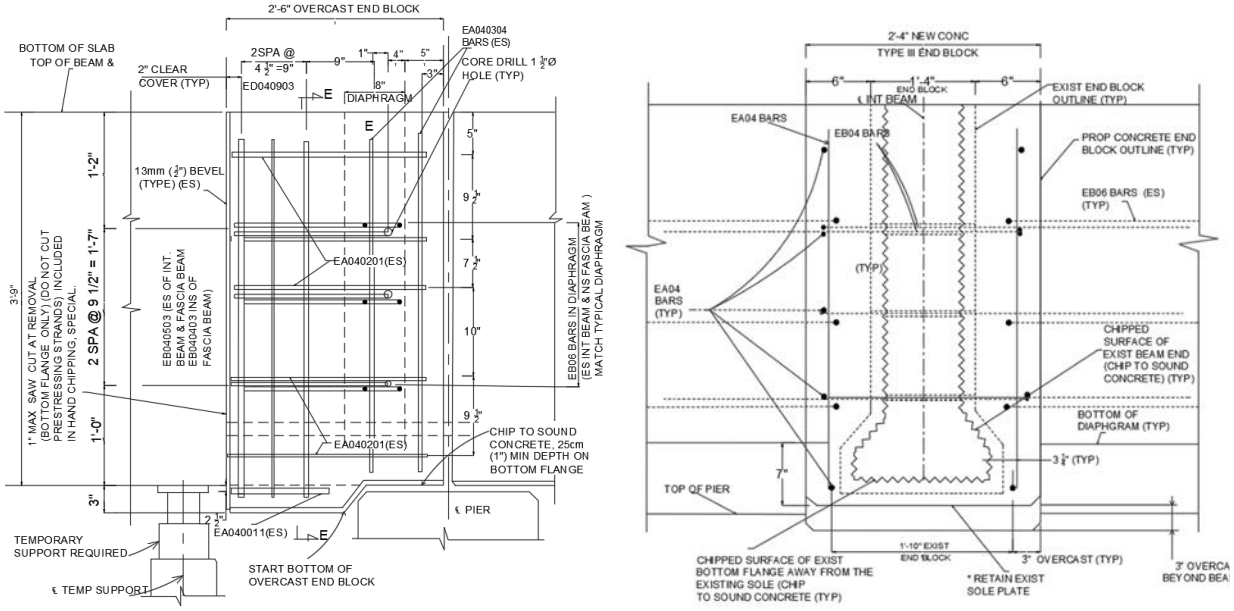

(a) Full-depth beam end repair: elevation (b) Full-depth beam end repair: Section E-E

Figure 6-14. FDRCO repair details.

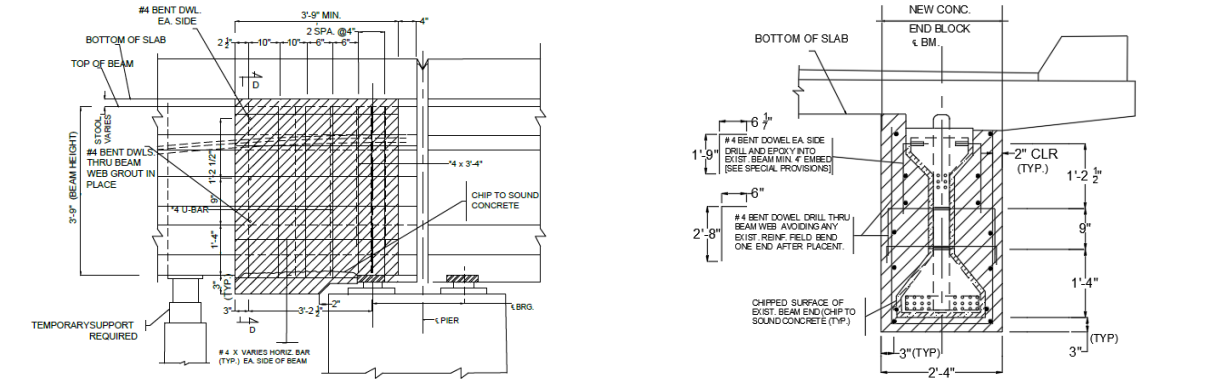

(a) Beam end elevation (b) Section D-D

(c) Interior face of the fascia beam with end diaphragm (d) Exterior face of the fascia beam

Figure 6-15. FDRCO repair using shotcrete (Shield and Bergson 2018).

6.3.3.2 Full-Depth Reinforced Concrete Overcasts with FRP Wraps

FDRCO repairs with FRP U-wraps have been used in the bridge (STR 7412) that carries US-131 SB and M-46 SB over Tamarack Creek, located in Montcalm County, Michigan. Figure 6-16 presents the repair details of AASHTO Type III beams. It is not recommended to use FRP strips on new concrete until the new concrete has reached 28 days of age. As discussed later in Section 6.3.4, FRP U-wraps that are located within a length equal to the height of the beam measured from the bearing centerline (i.e., within a span-to-depth (a/d) ratio of one) do not contribute to the shear capacity. These U-wraps control the development of shrinkage cracks and prevent concrete spall. FRP wraps with a concrete surface coating serve as a protective layer, reducing the risk of moisture and chloride ingress, and subsequently preventing the corrosion of embedded reinforcement, thereby extending the service life of the overcast repair.

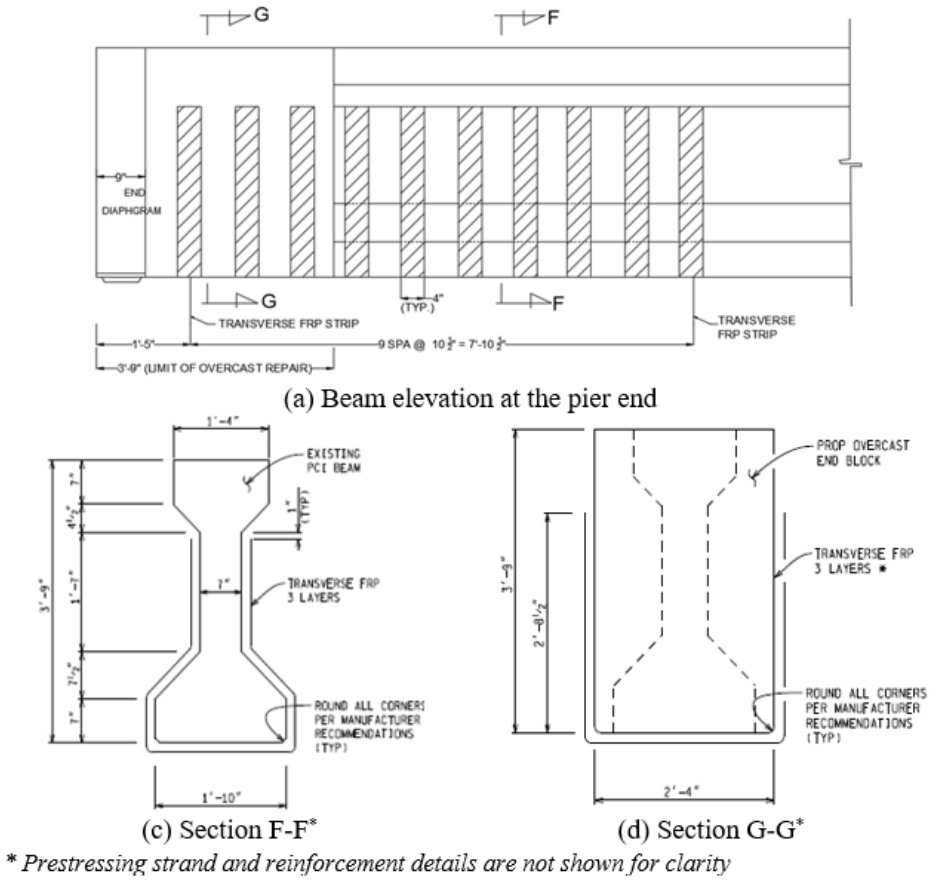

Figure 6-16. FDRCO repair with FRP U-wraps.

6.3.3.3 Partial-Depth Unreinforced Concrete Overcasts

Twelve and 36 beam ends of the bridge (STR 3832) have been repaired with FDRCOs and partial-depth unreinforced overcasts, respectively Figure 6-17 presents the partial-depth unreinforced overcast details. This repair is not expected to improve the structural capacity of the beam ends.

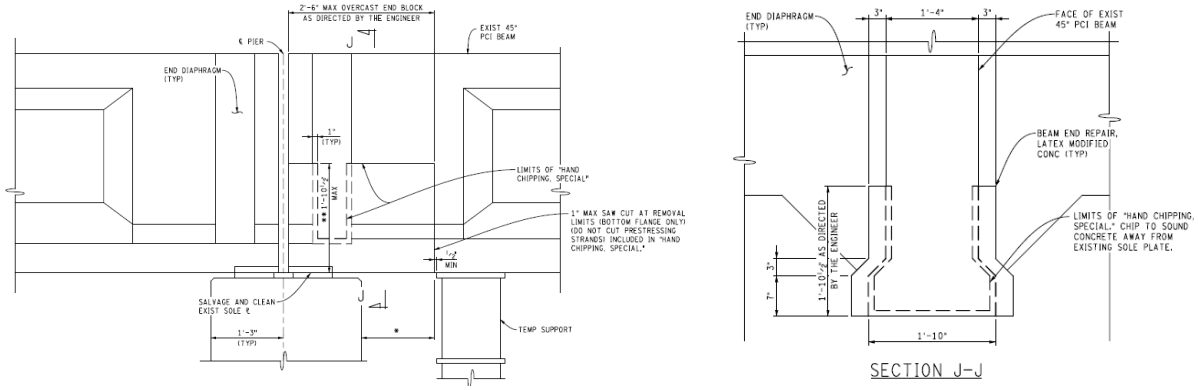

(a) Elevation (b) Section J-J

Figure 6-17. Partial-depth unreinforced concrete overcasts.

6.3.3.4 Partial-Depth Reinforced Concrete Overcasts

Figure 6-18 presents the partial-depth reinforced overcast repair details implemented in the bridge (STR 8012) that carries Giddings Road over I-75 in the city of Auburn Hills in Oakland County. As shown in the figure, rebars are inserted through the holes in the web. This repair includes closed-loop confining steel for the bottom flange section located in front of the bearing, as well as an inverted U-shaped steel over the bearing.

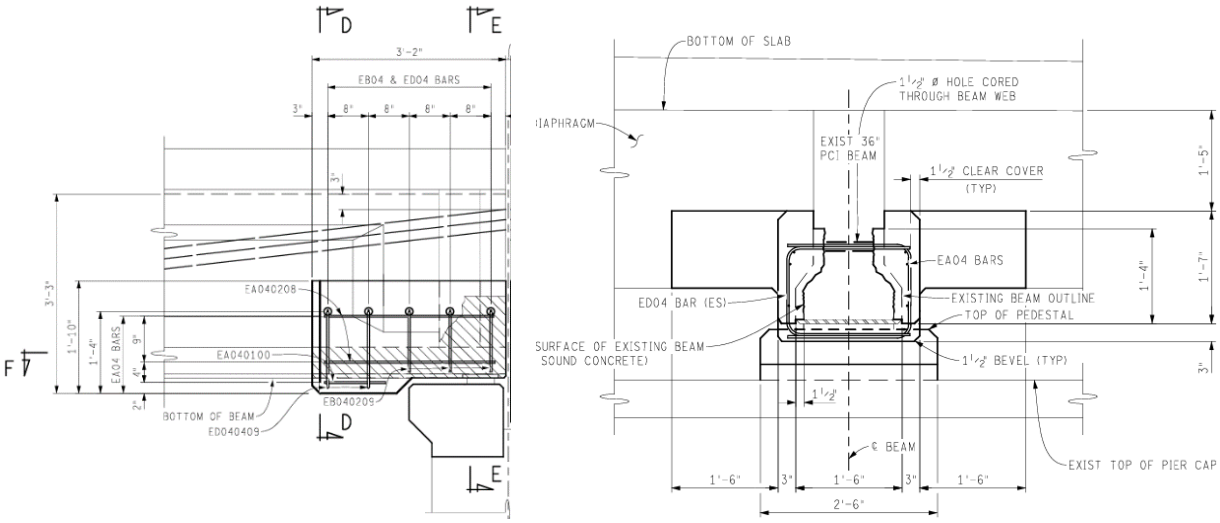

(a) Interior beam end repair elevation (b) Section D-D

Figure 6-18. Partial-depth reinforced concrete overcast.

Rich et al. (2023) repaired an AASHTO Type I beam end using a reinforced concrete partial-depth overcast. As shown in Figure 6-19, the width of the overcast is 34 in. and provides an adequate space to use 7 in. wide bearings at each end, thereby developing an alternative load path to avoid the transfer of loads through the original bearing because of severe concrete deterioration and sole plate corrosion. The total bearing area of these two pads equals the total area provided by the original design. The repair extended 24 inches along the length of the beam to cover the deteriorated section at the end. However, this repair did not perform well due to a lack of confining steel and failed at a much lower load than the original design load. The design details shown in Figure 6-19 and the failure pattern shown in Figure 6-20 highlight the impact of not having properly designed and fabricated confining steel at the end.

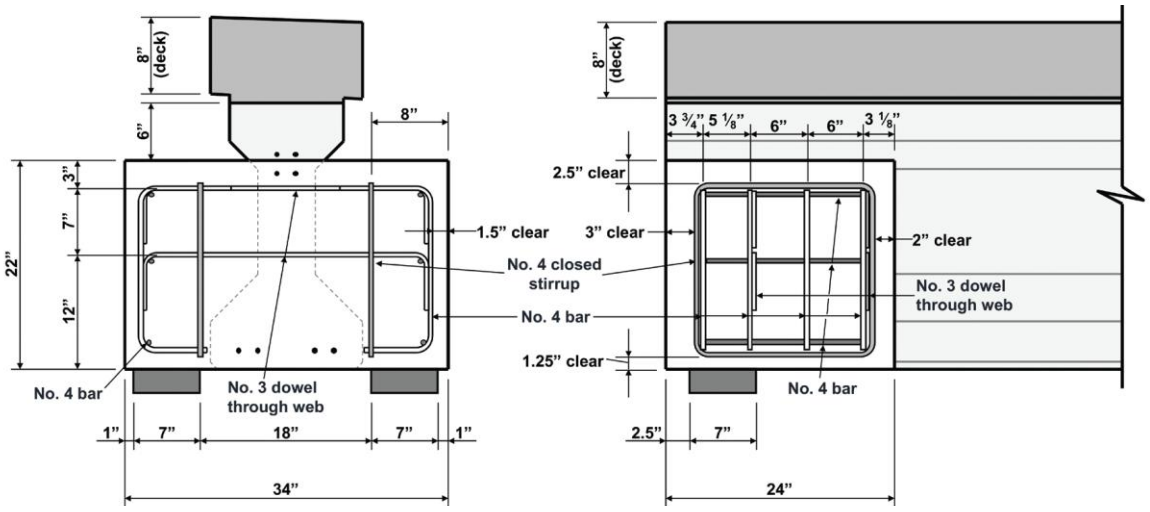

Figure 6-19. Partial-depth overcast with alternative load path (Rich et al. 2023).

(a) Side view (b) End view

Figure 6-20. The failure of the repaired beam end (Rich et al. 2023).

6.3.3.5 Partial-Depth Concrete Overcasts with FRP Wraps

Partial-depth overcasts with FRP wraps have been used to repair the ends of AASHTO Type II beams of the I-94 EB over the Dancer Road bridge (STR 10942) in Washtenaw County, Michigan. Figure 6-21 presents the details of the partial-depth unreinforced overcast. This repair method does not improve the structural capacity of deteriorated beam ends.

(a) South elevation (b) Bottom flange soffit

Figure 6-21. Partial-depth unreinforced concrete overcast with FRP wraps.

6.3.4 FRP Repair

MDOT repairs PSC beams using FRP sheets following the directions in the Special Provision for Fiber Reinforced Polymer Shear Strengthening System, 20BR712(A295) (MDOT 2021c). MDOT has utilized FRP systems at beam ends, both with and without repairs. Figure 6-22 presents the details of an FRP system used for AASHTO Type III beam ends over the abutments of the US-131SB and M-46SB over Tamarack Creek bridge (STR 7412) in Montcalm County, Michigan. Typical FRP beam end repairs involve a combination of FRP configurations, anchorage systems, and application techniques. To determine the most appropriate FRP system for a given repair, it is essential to understand the configuration types, anchorage methods, long-term durability, and structural capacity contributions of the system. The following sections of this report provide a detailed discussion of these aspects.

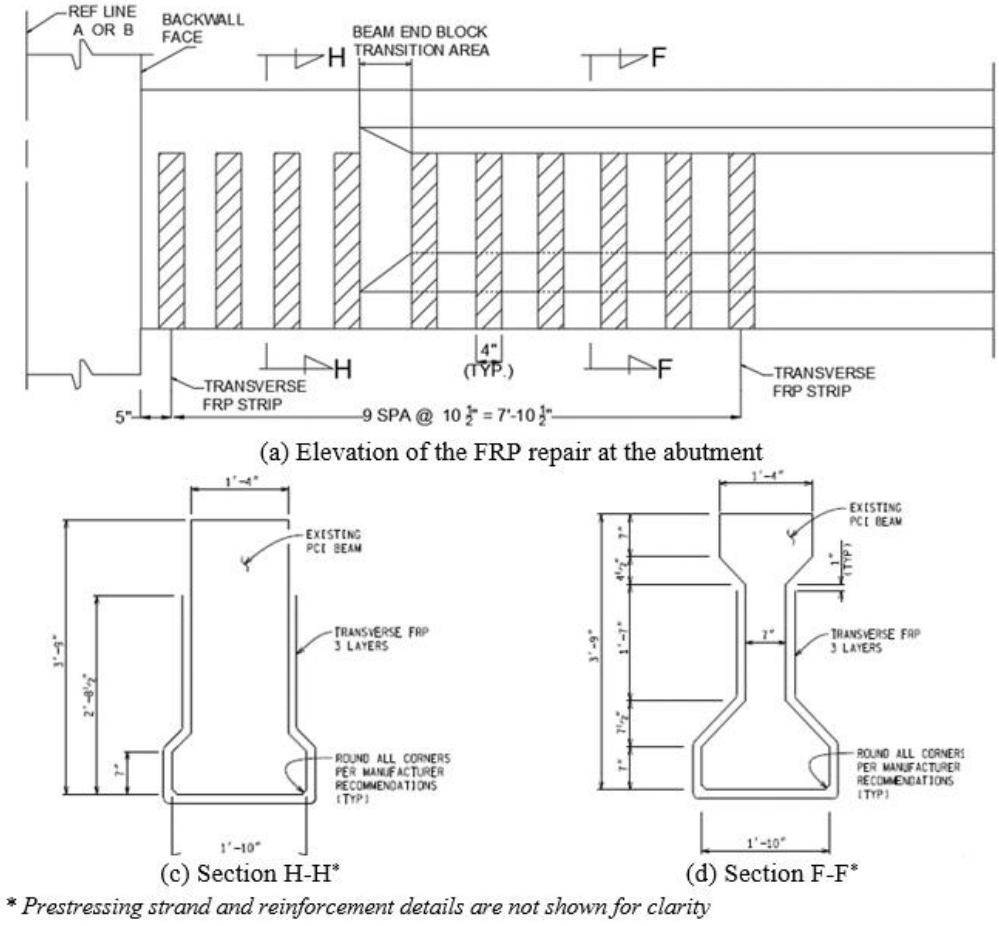

Figure 6-22. The application of FRP strips at beam ends.

6.3.4.1 FRP Configurations

Figure 6-23 shows three different FRP configurations commonly used at beam ends: (1) side-bonding, FRP sheets are bonded to the sides, (2) U-wrap, FRP sheets are bonded to the sides and soffit, and (3) complete wrap, FRP sheets are wrapped around the entire cross-section. A complete wrap is the most efficient and effective method for enhancing shear strength at beam ends (Bae and Belarbi 2013, ACI 2017). U-wraps, also known as U-shaped wraps, involve wrapping FRP fabrics or sheets around a structural element in a U-shaped configuration. Side bonding is the least effective one for increasing the shear capacity of a structure (Kang and Ary 2012, ACI 2017).

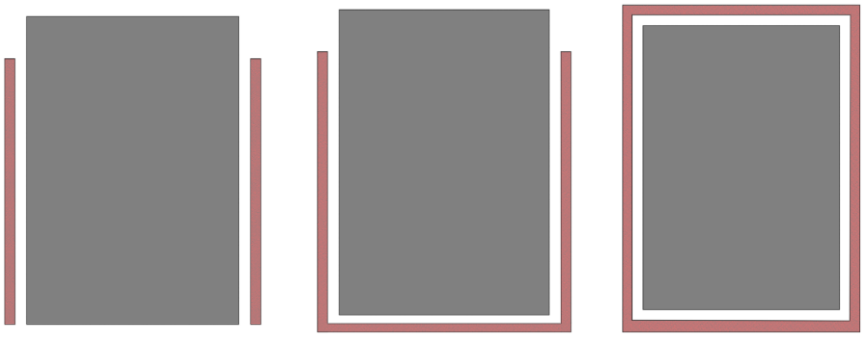

(a) Side bonding (b) U-wrap (c) Complete wrap

Figure 6-23. Commonly used FRP laminate configurations at beam ends.

The implementation of FRP systems on in-service bridges experiences unique challenges, often necessitating changes to standard procedures to accommodate site-specific conditions. For example, the presence of bearing plates and end diaphragms can prevent complete wrapping of beam ends with FRP. As a result, alternative anchorage techniques must be employed to ensure effective load transfer and long-term performance.

6.3.4.2 Anchorage Systems

Anchorage systems can delay debonding or prevent premature failure of bonded FRP sheets. These systems offer various mechanisms for transferring load from one member to another (Muciaccia et al. 2022). Of all anchor types, FRP spike anchors are efficient and can be applied to various geometric shapes. Experimental investigations support the usage of spike anchors shown in Figure 6-24 (AASHTOO FRP 2023, del Ray Castillo et al. 2019, and Girotti 2017).

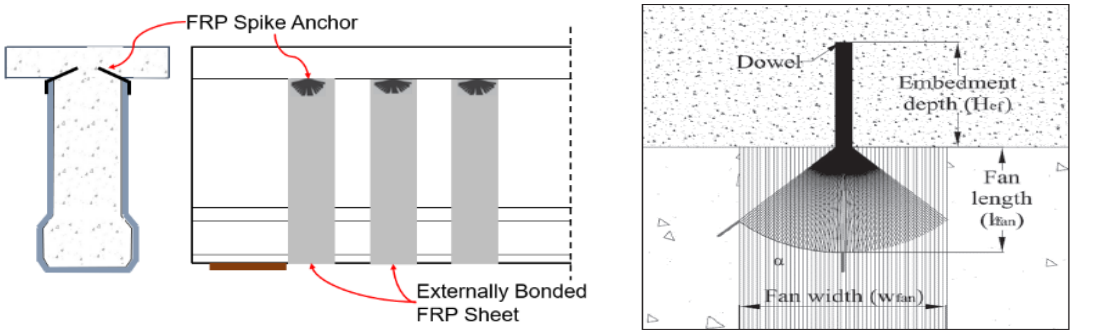

(a) CFRP with spike anchors (b) Front view (del Rey Castillo et al. 2019)

Figure 6-24. FRP spike anchorage system.

The near-surface mounted (NSM) anchorage systems are used, as shown in Figure 6-25, to maintain the transfer length of FRP wraps due to geometric constraints, or to shorten the required FRP length by improving stress transfer efficiency (Grelle and Sneed 2013).

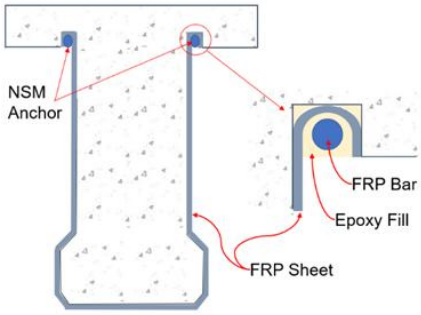

Figure 6-25. NSM anchorage system.

Murphy et al. (2012) investigated four different anchorage systems (i) CMA - continuous mechanical anchorage system (Figure 6-26a), (ii) DMA - discontinuous mechanical anchorage system (Figure 6-26b), (iii) SDMA - sandwich panel discontinuous mechanical anchorage system (Figure 6-26c), and (iv) HS - horizontal strips (Figure 6-27).

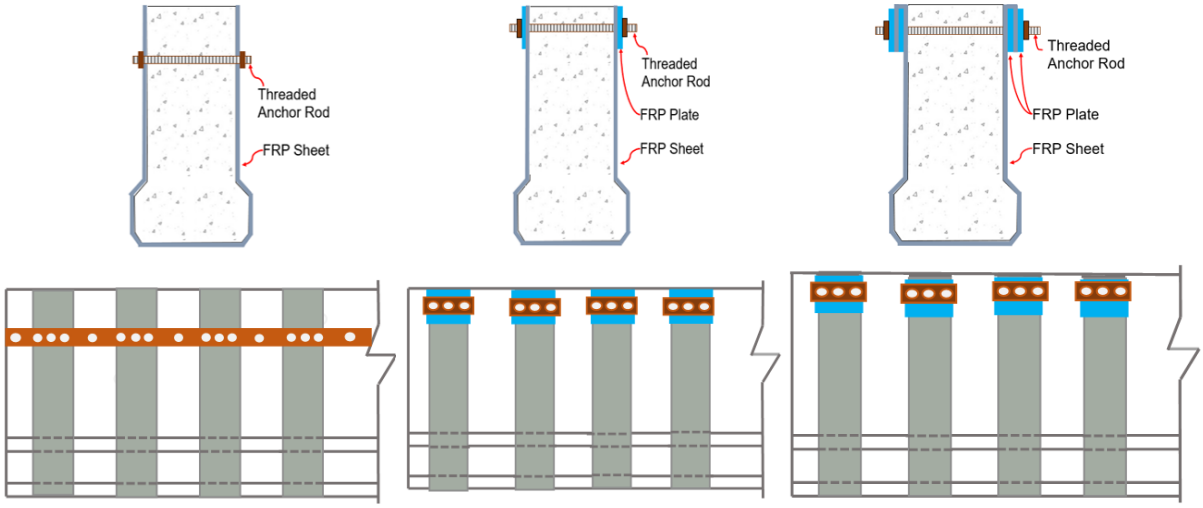

(a) CMA (b) DMA (c) SDMA

Figure 6-26. Mechanical and metallic anchorage systems.

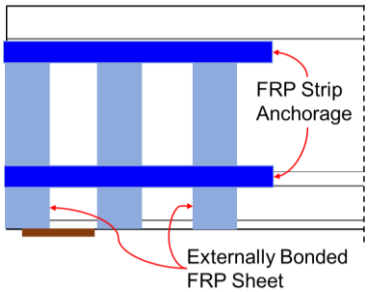

Figure 6-27. Horizontal strips (HS) anchorage system.

The CMA system uses continuous, precured CFRP plates secured with threaded anchor rods over the ends of U-wraps. The DMA system employs discontinuous precured CFRP plates secured with threaded anchor rods over the ends of U-wraps. The SDMA system is similar to DMA but features sandwich-wrapped plate ends, which are also secured with threaded anchor rods. The HS system incorporates CFRP strips applied longitudinally along the beam. These strips are provided across the free edges of vertical CFRP sheets and at the intersection of the web and bottom flange, the areas prone to debonding. They are installed immediately after the vertical strips to enhance bonding between the vertical and horizontal layers of CFRP. The performance of these anchorage systems is described below.

- The CMA anchorage system exhibited poor performance, failing prematurely due to buckling of the horizontal strip.
- The DMA system did not entirely prevent FRP debonding, but it did delay debonding and outperformed the CMA system.
- The HS system provided moderate improvements in delaying debonding but was still less effective than the DMA system.
- The SDMA system achieved the best results by successfully preventing debonding to cause failure due to FRP rupture.

6.3.4.3 Laboratory Performance of Beam Ends Repaired with FRP Systems

The shear capacity of beam ends repaired with FRP systems is influenced by several key factors, including the FRP layer configuration, anchorage method, and bond quality with the concrete substrate. Shear span-to-depth (a/d) ratio is an important geometric parameter that significantly affects the capacity of repaired beam ends. The a/d ratio is calculated by dividing the shear span (a) by the effective depth (d) of the beam, as shown in Figure 6-28. In this study, an a/d ratio of one is considered for capacity evaluation using the Strut-and-Tie Method (STM). Limited studies have evaluated the FRP contribution to shear capacity when the a/d ratio is one. The studies conducted by Pevey et al. (2021), Jirsa et al. (2017), Murphy et al. (2012), and Kim et al. (2011) showed that the FRP contribution to shear capacity increases when the a/d ratio increases. This highlights the need for careful consideration of beam geometry when evaluating the performance or designing FRP strengthening systems for beam ends.

Kim et al. (2011) conducted an experimental study on reinforced concrete T-beams strengthened with carbon fiber reinforced polymer (CFRP) layers. Figure 6-28 shows the cross-section and

CFRP layout on a 24 in. deep T-beam. The study evaluated the influence of the a/d ratio on the effectiveness of shear strengthening by testing three different a/d ratios: 1.5, 2.1, and 3.0.

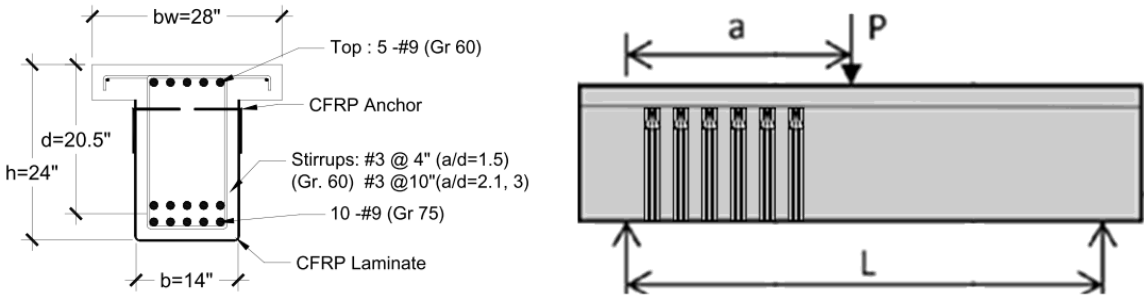

(a) Cross-section of 24 in. T-beams (b) Elevation of T-beam with CFRP layers

Figure 6-28. Cross-section and CFRP layout on a 24 in. deep T-beam (Kim et al. 2012).

The shear capacity contribution of concrete (F_c), CFRP (F_f), and reinforcing steel (F_s) for three different a/d ratios is shown in Figure 6-29. The study uses a naming convention for test specimens. For example, "24-1.5-4" refers to the fourth specimen of a set of 24-in. deep beams that were loaded to simulate an a/d ratio of 1.5. To evaluate the influence of the a/d ratio, the load test results of the same CFRP layout (i.e., 5-in. wide strips spaced at 10-in. on center) were compared across all three a/d ratios. Figure 6-29 (a) to (c) present the shear capacity contribution of concrete and steel against a/d ratios of 1.5, 2.1, and 3.0. Figure 6-29 (d) to (f) present the shear capacity contribution of concrete, steel, and CFRP against a/d ratios of 1.5, 2.1, and 3.0. As shown in Figure 6-29 (d), the shear capacity contribution of CFRP is minimum for an a/d ratio of 1.5 when compared to the other a/d ratios.

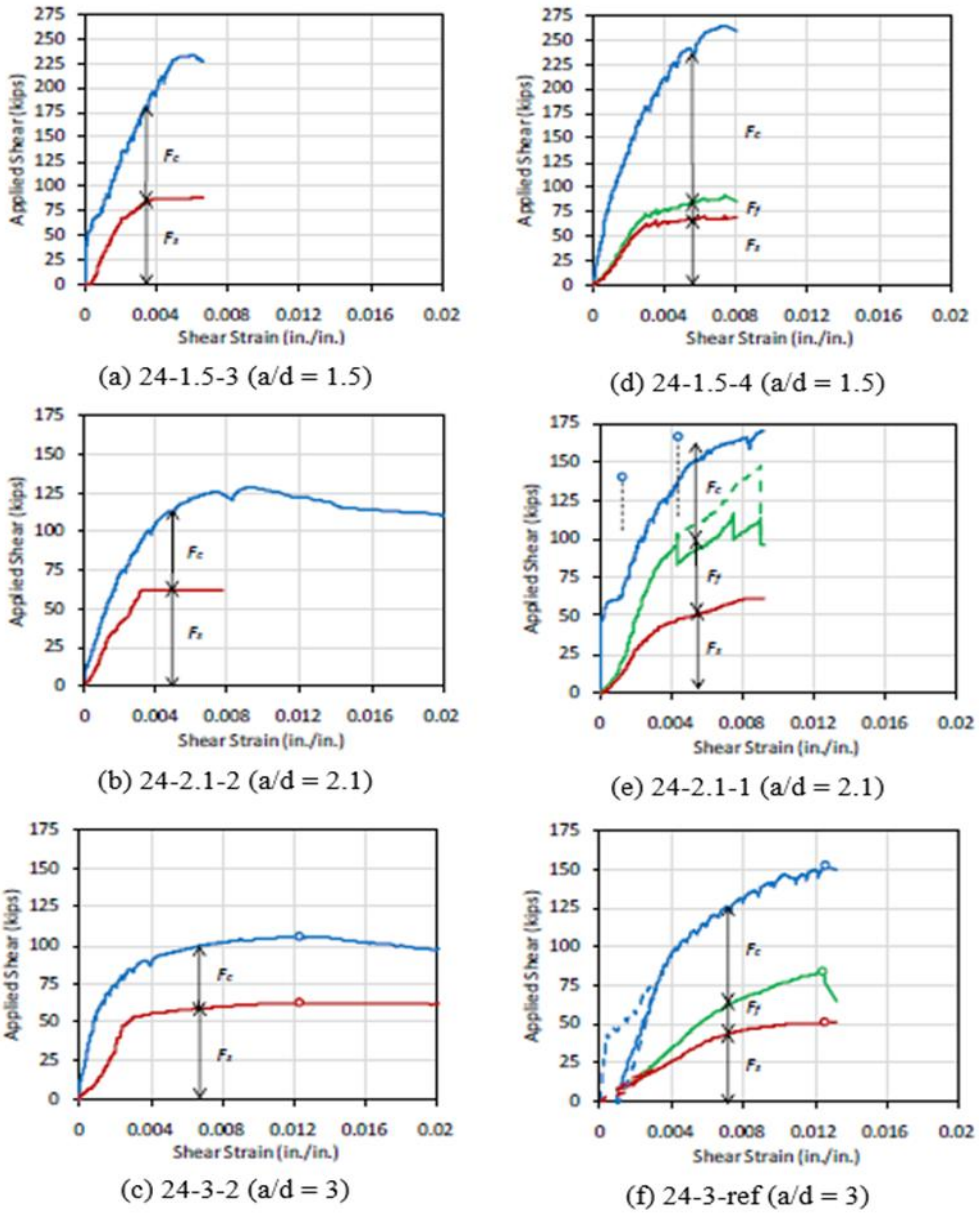

Figure 6-29. Shear capacity contribution of concrete (blue), CFRP (green), and steel (red) with different a/d ratios (Kim et al. 2012).

Figure 6-30 shows the capacities of strengthened and control beams with three different a/d ratios. The results show that the shear contribution from CFRP increases with a/d ratios. Specifically, for a/d ratios of 1.5, 2.1, and 3.0, the CFRP contribution to shear capacity improved by 13% (31 kip), 32% (41 kip), and 44% (46 kip), respectively.

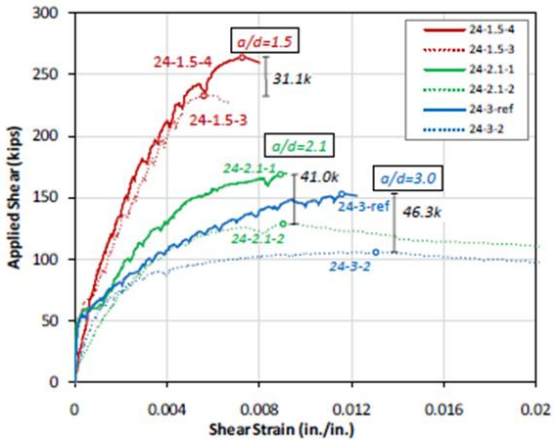

Figure 6-30. The comparison of shear capacity contribution by CFRP in strengthened beams against the control beams and the a/d ratios. (Kim et al. 2012).

Kim et al. (2012) also performed CFRP strengthening on prestressed AASHTO Type IV beams. Four tests were conducted on beams identical to those in Texas bridges. Figure 6-31 shows the cross-section, shear reinforcement, and the tendon profile.

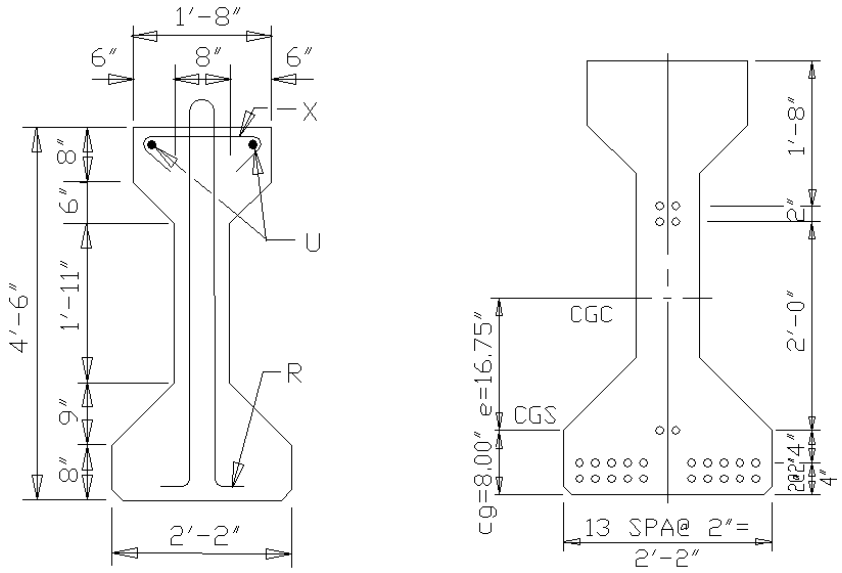

(a) (b)

Figure 6-31. Cross-section showing (a) shear reinforcement and (b) tendon profile (Kim et al. 2012).

Specimen I-1 served as the control without CFRP strengthening. Figure 6-32 presents the elevation views of specimens I-2, I-3, and I-4, highlighting the CFRP configurations and anchor layouts. The a/d ratios of these specimens ranged from 3.8 to 4.15. Specimens I-3 and I-4 incorporated intermediate horizontal anchors in addition to end anchors. Specimens I-2 and I-4 have vertical CFRP strips. Specimen I-3 has a complete wrap. The CFRP in I-2 extended only to the top of the web, whereas in I-4 it continued up to the top of the beam.

(a) I-2 with vertical strips.

(b) I-3 with a complete wrap in the vertical direction and sheets in the horizontal direction.

(c) I-4 with vertical and horizontal strips.

Figure 6-32. Elevation views of specimens I-2, I-3, and I-4 (Kim et al. 2012).

The unidirectional (vertical) application of CFRP strips increased shear strength by just 2% compared to the control specimen I-1. In contrast, specimens I-3 and I-4, which were strengthened using bi-directional CFRP (in both horizontal and vertical directions), achieved approximately 38% greater shear resistance than the control. Notably, I-4 contained only about half the amount of CFRP used in I-3, suggesting that the strength gain is not directly proportional to the quantity of CFRP applied. These findings highlight that bi-directional CFRP application is more effective for this type of beam.

According to Kim et al. (2012), for beams with an a/d ratio of approximately 4, the CFRP contribution to shear strength is about 38%. In comparison, Murphy et al. (2012) reported a maximum CFRP contribution of 24% for AASHTO Type IV beam ends with an a/d ratio of 2.9. The findings of Kim et al. (2012) for different a/d ratios showed that the shear strength contribution of CFRP decreases as the a/d ratio decreases. Therefore, for an I-beam with an a/d ratio of 1, the increase in shear strength due to CFRP strengthening is expected to be negligible. However, the application of FRP wraps over overcast repairs can enhance the durability of the overcast repair, as observed during field inspection. Section 6.4 of this report includes a further discussion on the field performance.

According to AASHTO LRFD 5.8.2.2, the angle between the strut and tie should be greater than 25°. To evaluate the influence of a/d ratio on FRP performance, the strut angle is considered to be within the 25° to 45° range, as illustrated in Figure 6-33. An a/d ratio of 2 corresponds to a strut angle of approximately 25°, while a ratio of 1 corresponds to an angle of 45°. As the strut angle approaches 25°, more FRP strips intersect the crack path, increasing their effectiveness. Conversely, when the strut angle is 45° (i.e., a/d = 1), fewer FRP strips are aligned to intercept the shear cracks, resulting in a negligible contribution of CFRP to the shear strength. This geometry-

dependent alignment is a key reason why FRP shear strengthening tends to be less effective on PSC I-beams with a lower a/d ratio.

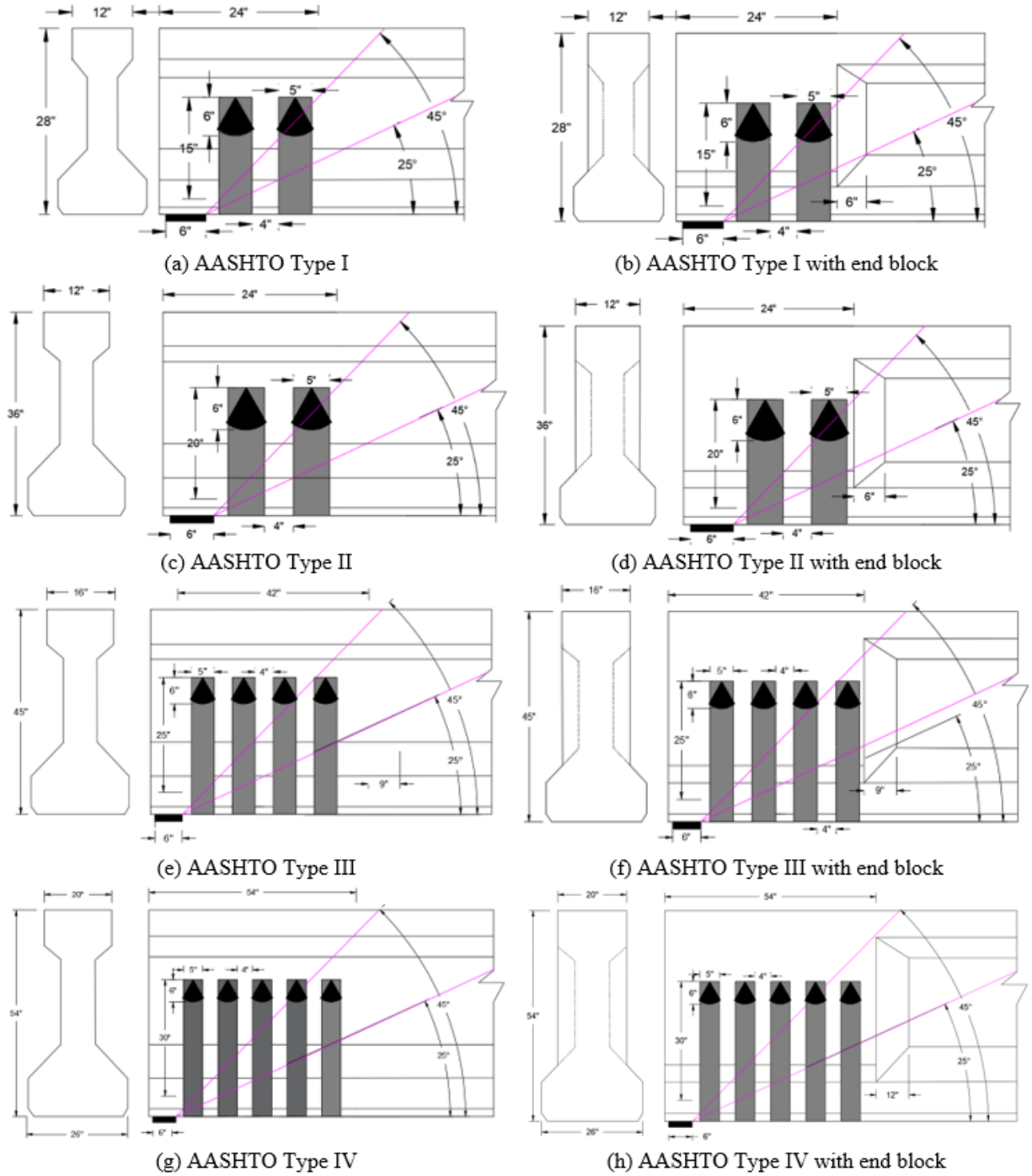

Figure 6-33. AASHTO I-beams with or without end blocks showing the number of effective FRP strips as the a/d ratio ranges between 1 and 2.

Rich et al. (2023) evaluated the effectiveness of a multi-layer FRP configuration to enhance the capacity contribution of a deteriorated beam end under laboratory conditions. The test results showed that the strengthened beam end achieved 1.34 times the capacity of the control undamaged beam end and 2.36 times that of the damaged beam end. The load test was conducted with an a/d ratio of 1.25. The test specimen was a composite section consisting of an AASHTO Type I beam and its original 8-inch-thick reinforced concrete deck. The repair system included three FRP layer configurations and anchors, as shown in Figure 6-34. The first configuration included two horizontal U-wraps and two strips with fibers aligned parallel to the girder's longitudinal axis. Only the horizontal U-wraps were secured with spike anchors (Figure 6-34a). The second configuration is identical to the first. Still, it includes two additional vertical U-wraps and two strips along the beam's side surfaces, anchored in place using spike anchors to secure both the longitudinal strips and vertical sheets (Figure 6-34b). The vertical strips were utilized over the bearings due to space constraints for U-wraps. The third configuration is an enhancement to the second configuration, which includes externally bonded FRP patches over the spike anchor locations to complete the system (Figure 6-34c).

The significant increase in capacity documented by Rich et al. (2023) was due to the two longitudinal U-wraps installed in all three configurations. These U-wraps, particularly the one along the bottom flange, helped restore the tensile capacity of the beam that had been reduced due to deterioration of the prestressing strands. However, implementing this FRP configuration on in-service bridges may be challenging due to the end diaphragms and adjacent beam ends that restrict access behind the beam ends. Further, MDOT does not permit drilling PSC beams closer to the strands. This will restrict the installation of anchors at the bottom flange. However, the use of overcasts to provide adequate cover for installing anchors, removal of concrete end diaphragms during repair, and the use of steel end diaphragms will minimize challenges for implementing this system in in-service bridges.

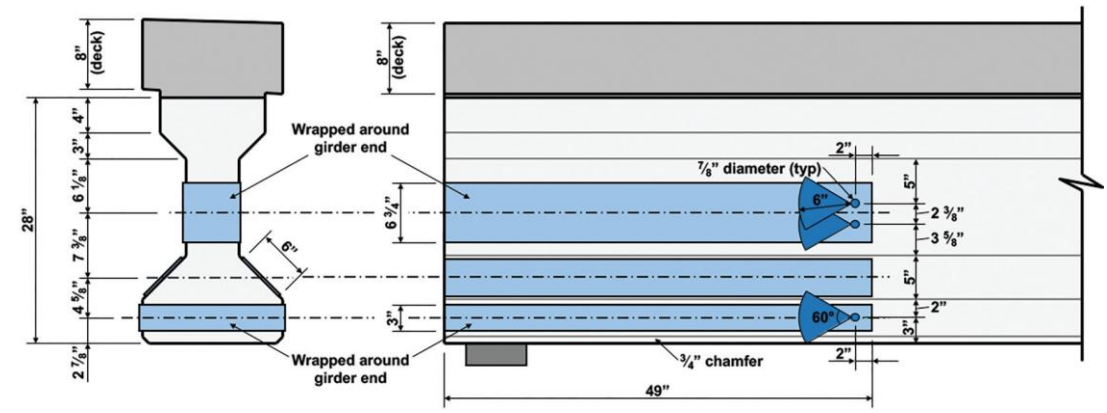

(a) First layer (two longitudinal U-wraps with spike anchors and two horizontal strips)

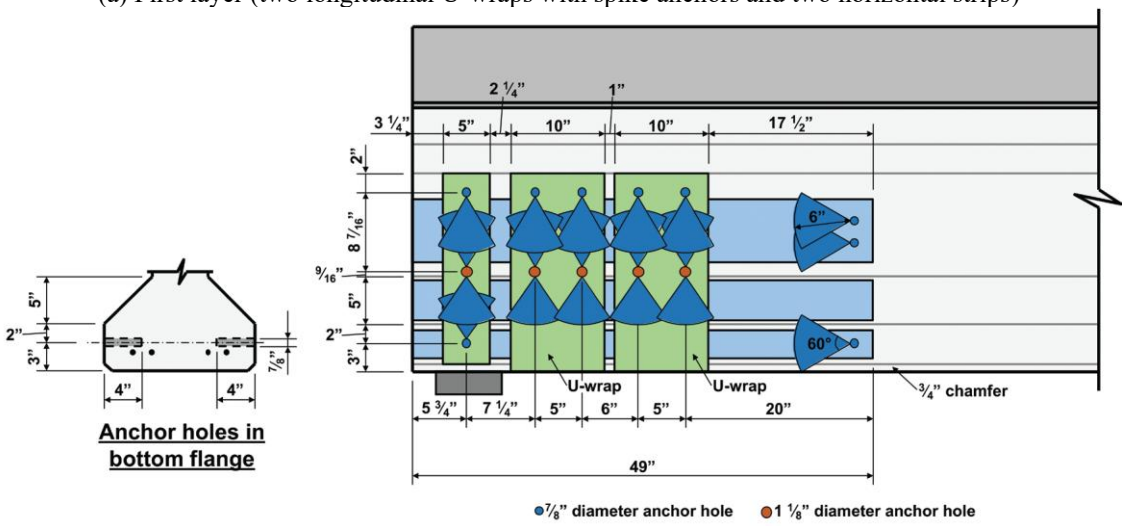

(b) Second layer (two vertical U-wraps and two vertical strips with spike anchors)

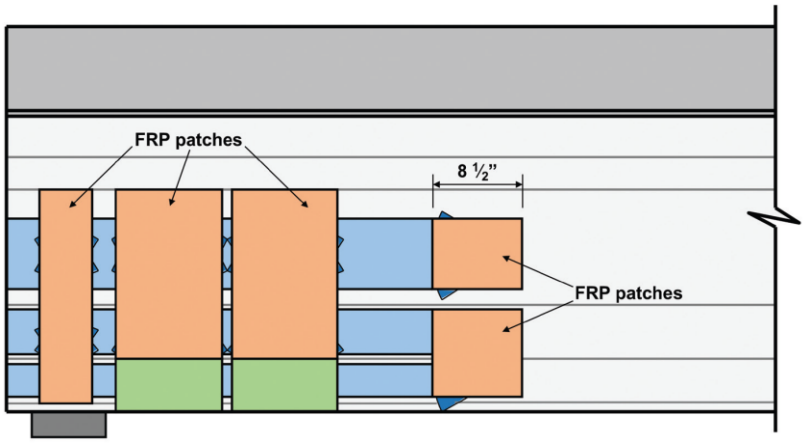

(c) Third layer (patches covering spike anchors)

Figure 6-34. Three-layer FRP strengthening system with spike anchors (Rich et al. 2023).

6.3.5 Alternative Repair Details

The typical beam end overcast repair, shown in Figure 6-14, results in a rectangular section that is 6 in. wider than the bottom flange and 3 in. deeper than the original beam section. However, for bulb tee beams or beams with wider flanges, this approach requires adding a significantly large concrete volume to make a rectangular section. Therefore, the details shown in Figure 6-35 provide an alternative to maintain the I-shaped geometry, the original beam depth, and the required capacity. As shown in Figure 6-35, this repair uses a galvanized 2 × 2 W1.4/W1.4 welded wire fabric in areas where the bottom flange has been chipped out to remove the unsound concrete. The repair also uses adhesive anchoring for stirrups. Typically, this type of repair is performed within the span because of high load hits and to maintain vertical clearance. This detail can be modified by extending the welded wire fabric towards the web to satisfy the development length requirements in Article 5.10.8.2.5 of AASHTO LRFD Bridge Design Specifications (AASHTO 2020) and to provide adequate confinement for the bottom flange. Also, adhesive anchoring and welded wire fabrics can be incorporated into the overcast details discussed in Section 6.3.3. for enhanced performance.

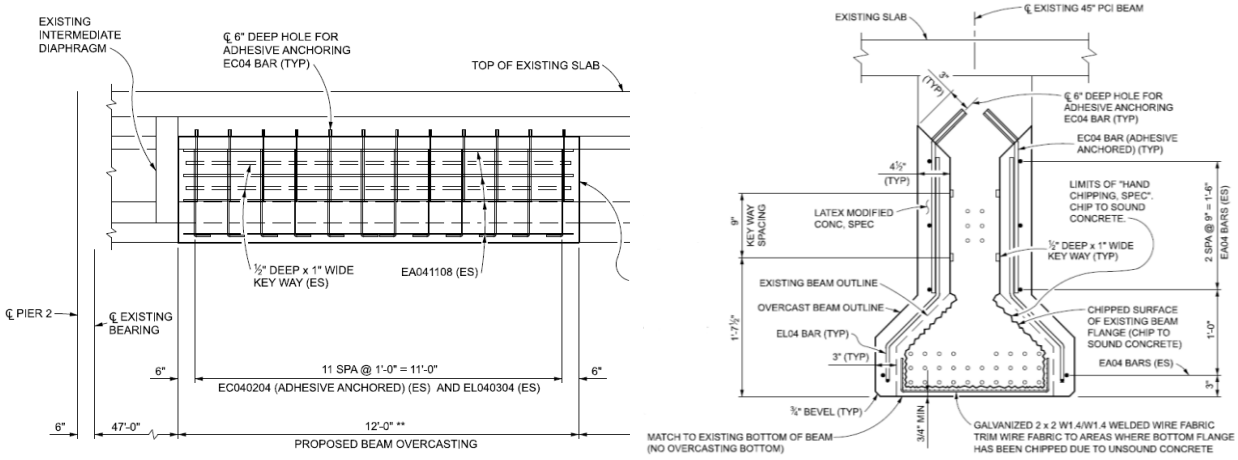

(a) Elevation of the beam (b) Cross-section of the beam

Figure 6-35. Overcast repair detail with welded wire fabric and adhesive anchoring for stirrups.

6.4 FIELD PERFORMANCE OF REPAIRS

6.4.1 Overcast Repair Performance

A review of beam end overcast repair performance for eight Michigan bridges reveals a range of outcomes, influenced by the scope of the repair, time in service, and follow-up inspections. Most beam ends had full-depth or partial-depth overcast repairs, often in response to critical deterioration identified through condition ratings and Requests for Action (RFAs). Table 6-2

summarizes the observed field performance of beam end overcast repairs. Appendix D presents a comprehensive discussion on beam end repair details and the performance of each bridge.

Table 6-2. Field Performance of Overcast Repairs

Bridge ID	Year Repaired	Repair Type	Age of Repair (Years)	Observations
STR 1413	2006	Full-depth reinforced overcasts (22 @ piers, 1 @ abutment)	17	Reported cracking within 2 years of repair.
STR 2538	2008	Full-depth reinforced overcasts + coating (8 @ piers)	11	Cracking in 6 of 8 fascia beams; poor condition after 11 years.
STR 3810/ 3811	2016	Full-depth reinforced overcasts + coating	8	Minor cracking and coating issues; functionally effective.
STR 3832	2020	Full-depth reinforced (12) + partial-depth unreinforced (36) overcasts	4	Localized cracking, mostly in good condition.
STR 3830	2020	Full-depth reinforced (2) + partial-depth unreinforced (15) overcasts	4	Reported cracking in partial-depth repair.
STR 8012	2021	Partial-depth reinforced overcasts (25) + patching + coating	2	Minor spalls/delamination
STR 5753	1999/ 2016	Full-depth reinforced (24) + partial-depth (4) overcasts	25/8	Reported cracking, delamination, and spall in full-depth repair within 10 years. Two (2) were re-repaired after 14 years.
STR 5754	1999/ 2016	Full-depth reinforced (31) + partial-depth (9) overcasts	25/8	Reported cracking and spall in full-depth repair within 16 years. Nine (9) beam ends were re-repaired after 17 years.

Common issues, such as early-age cracking, coating failure, and delamination, highlight the importance of proper detailing, material selection, and the use of FRP sheets or strips, as well as regular maintenance.

6.4.2 FRP Repair Performance

Four bridges were inspected to document the performance of FRP repairs at beam ends. FRP sheets or strips were used in most bridges with overcasts and protected with concrete surface coatings (CSC). Table 6-3 summarizes the observed field performance of FRP repairs. Appendix D presents a comprehensive discussion on beam end repair details and performance for each bridge.

Table 6-3. Field Performance of FRP Repairs at PSC I-Beam Ends

Bridge ID	Year Built	Repaired Year	Repair Type	Performance
STR 1213	1968	2021	Partial-depth unreinforced overcast, FRP U-wraps, CSC, epoxy coating	Good overall condition after 2 years; minor deficiencies (e.g., FRP debonding, sole plate corrosion).
STR 1215	1968	2021	Partial-depth unreinforced overcast, FRP U-wraps, CSC, epoxy coating	CSC and FRP areas performed well; cracks in unreinforced overcasts suggest limited durability.
STR 7412	1972	2012	Full-depth reinforced overcast, FRP, CSC, epoxy injection	Good condition after 12 years; FRP and CSC effective; minor issues with uncoated surfaces.
STR 10942	1961	2021	Partial-depth unreinforced overcast with FRP, CSC	FRP debonding; peeling off of CSC. The deteriorated beam end over the bearing was not repaired.

The field inspection was limited to four bridges, with most FRP repairs being relatively recent, while the overcast repairs without FRP appeared to be older. In summary, beam end repairs that combined reinforced overcasts with FRP and concrete surface coating (CSC) demonstrated better performance. In contrast, unreinforced overcasts and repairs lacking surface coatings consistently demonstrated poor durability performance, underscoring the importance of providing adequate protection for concrete using CSC, which offers breathability and crack-bridging ability, as well as long-term maintenance planning.

6.5 REPAIR DETAILS AND RECOMMENDATIONS

The full-depth reinforced overcast repair enhances the structural capacity of deteriorated beam ends. In contrast, the application of FRP wraps primarily contributes to improved durability, rather than increasing load-carrying capacity. This study uses the Strut-and-Tie Model (STM) to quantify the capacity improvement achieved through the overcast repairs. The STM framework considers the failure modes and capacities associated with longitudinal ties, bearing faces, strut-to-node interfaces, and transverse ties to determine the overall beam end capacity while ensuring that the minimum anchorage capacity is maintained. The failure of longitudinal tie is consistently identified as the critical failure mode controlling the capacity of deteriorated beam ends.

The development of a longitudinal tie force resulting from the applied load at an a/d ratio of one is illustrated in Figure 6-36(a). The longitudinal tie force, T, is calculated using Eq. 6-1.

$$T = A_{ps} \times f_{pe} \times l_x/l_t \qquad \textit{Eq. 6-1}$$

where,

A_{ps} = *total area of bonded prestressing strands in the bottom flange, in.*^{2}

f_{pe} = *effective stress in prestressing steel after losses, ksi*

l_t = *transfer length, in.*

l_x = *distance from the beam end to the location of the critical section for the development of the tie, in., as shown in* Figure 6-36(b)

The factored shear resistance at the beam end with straight strands, controlled by the longitudinal tie failure mode, V_{uLT_S}, is calculated using Eq. 6-2.

$$V_{uLT\_S} = \phi \times T \times \tan\theta \qquad \textit{Eq. 6-2}$$

where,

θ = *the angle between the strut and tie, degrees*

ϕ = *the resistance factor for tension-controlled members in STM*
= *1.0 (Article 5.5.4.2 of AASHTO LRFD 2020)*

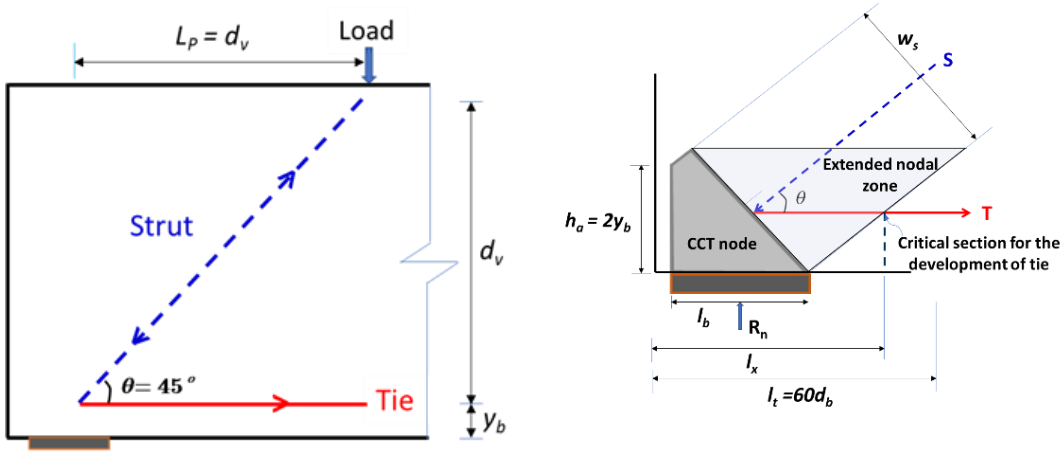

(a) Strut and tie forces (b) CCT node geometry

Figure 6-36. STM model for a beam end with straight strands.

As shown in Figure 6-37(a), concrete spall exposes several prestressing strands. Consequently, the bonded prestressing strand area (A_{ps}) is reduced, leading to a decrease in beam end capacity. Even though the exposed strands are re-embedded into the overcast, the extent of capacity recovery from the re-embedded strands depends on their embedment length within the region between the beam end and the critical section required for tie force development, as shown in Figure 6-36(b). The typical MDOT full-depth reinforced overcast repair also includes additional reinforcement closer to the bottom flange, which terminates just ahead of the bearing area, as shown in Figure 6-37(b). Such reinforcement does not contribute to the longitudinal tie capacity due to insufficient development length. This study suggests modifications to beam end overcast details to maintain the minimum required capacity of the repaired beam end.

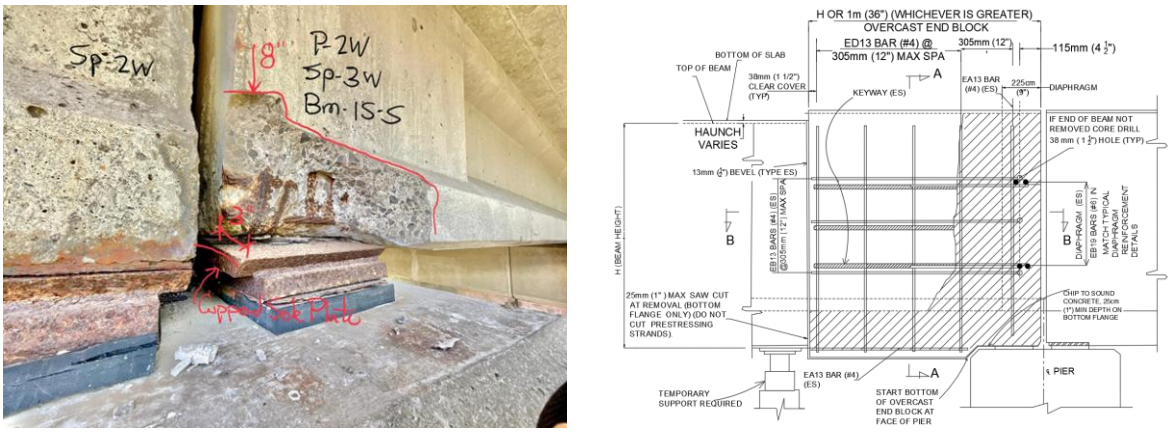

(a) (b)

Figure 6-37. (a) Deteriorated beam end with exposed strands and (b) typical overcast repair details.

6.5.1 Recommended Full-Depth Reinforced Concrete Overcast Repair Details

Appendix F presents the typical procedures implemented in the field for full-depth reinforced concrete overcast (FDRCO) repair. The overcast length is the greater of 3 ft or the beam height (H). The typical full-depth overcast for beams with end blocks results in a rectangular cross-section as shown in Figure 6-38.

Typical details of an FDRCO repair are shown in Figure 6-39. The capacity contribution of the FDRCO depends on the added longitudinal rebar (A_{s_ADD}) closer to the beam soffit, undamaged bonded prestressing strands (A_{ps_UD}), and the re-embedded exposed strands (A_{ps_exp}). The capacity contribution of A_{s_ADD} and A_{ps_exp} depends on the available development lengths. Therefore, certain exposed strands can be spliced to extend their lengths and bent up to 90 degrees to provide an adequate anchorage before being re-embedded in the overcast ($A_{ps\_exp\_bent}$).

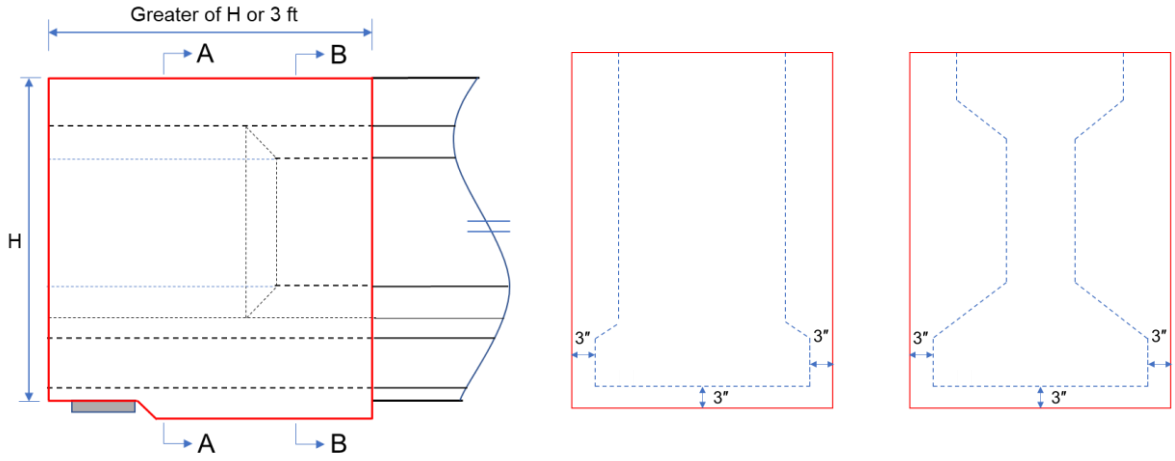

(a) Elevation (b) Section A-A (c) Section B-B

Figure 6-38. Geometry of a typical FDRCO repair (a) elevation, (b) section A-A, and (c) section B-B.

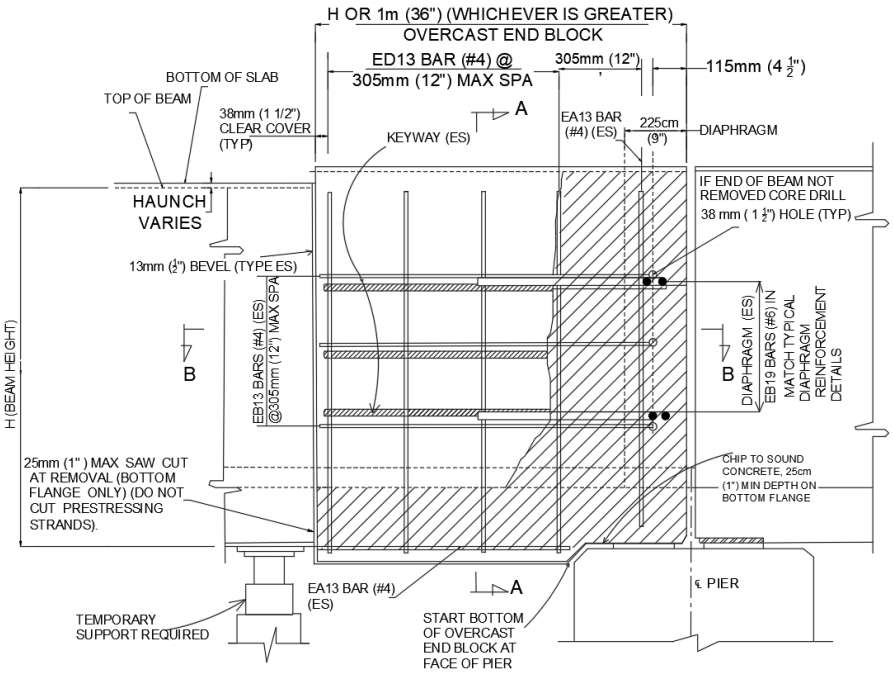

(a) Beam end elevation

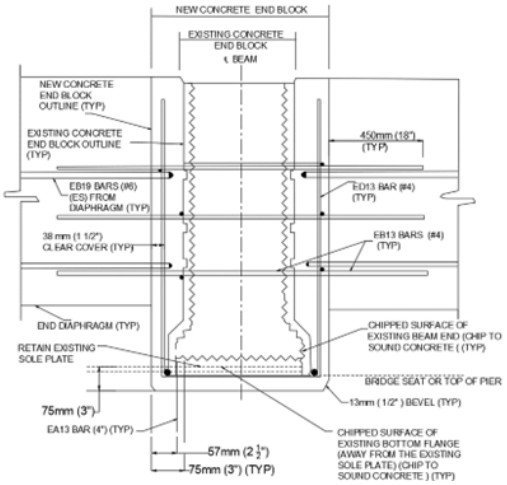

(b) Section A-A

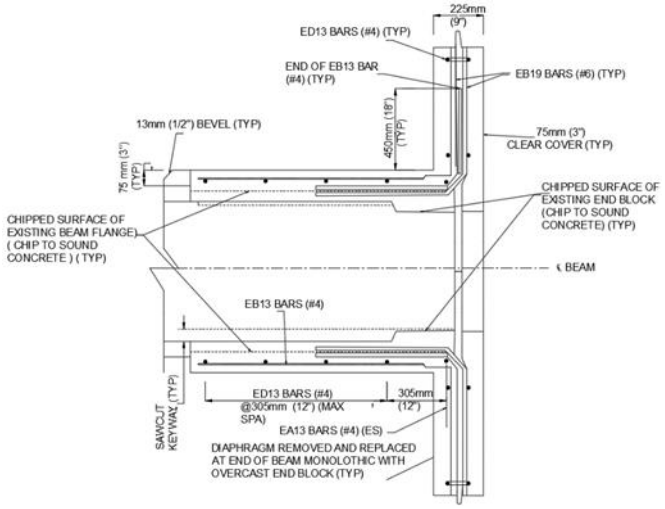

(c) Section B-B

Figure 6-39. FDRCO details for an I-beam with end blocks (Needham 2000).

An example is provided in this section to illustrate the capacity contributions of different reinforcement details in FDRCO repairs. A deteriorated PSC I-beam end is selected from a 46.58 ft wide and 33.5 ft span. Each span has seven AASHTO Type beams. Figure 6-40 shows the condition of the AASHTO Type I beam with an end block. The beam end has 16 strands in the bottom flange. Each strand has a diameter of 0.438 in. and a cross-sectional area of 0.115 in². Four out of 16 strands are exposed. Since all four exposed strands are in good condition, they are re-embedded in the overcast, and the total area of those four strands, A_{ps_exp}, is considered in the capacity calculation.

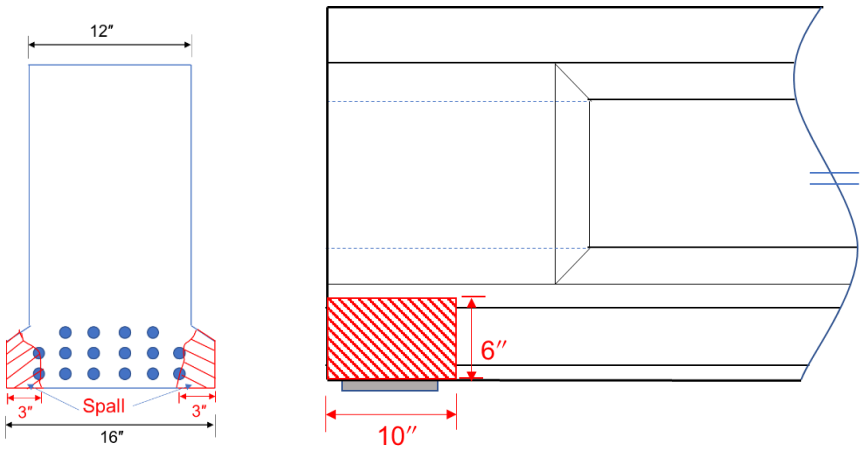

(a) Cross-section (b) Elevation

Figure 6-40. Beam end with exposed strands.

The as-designed shear capacity (factored shear resistance) of the beam calculated using STM is 144 kips. Because of the deteriorated conditions shown in Figure 6-40, the shear capacity is reduced to 110 kips. An FDRCO repair is selected for this beam end. Before erecting the rebar cage and pouring concrete, it is required to remove delaminated concrete and clean the exposed steel. It has been observed that additional strands are exposed during the chipping and cleaning. Figure 6-41 shows the beam end condition after preparing the end up to 3 ft for the overcast. In total, eight out of the 16 strands in the bottom flange are exposed. Because of the additional strands exposed during the process, the remaining beam end capacity with only eight bonded strands is 79 kips. Despite this significant reduction in capacity, the beam end did not exhibit any signs of failure because of the temporary support placed prior to chipping. The following sections present alternative details for an FDRCO repair, along with their respective capacities.

(a) After chipping out the delaminated concrete (b) Exposed strands

Figure 6-41. Condition after chipping out and cleaning the end.

6.5.1.1 FDRCO Repair - Alternative 1

Alternative 1 detail is the typical MDOT overcast repair detail suggested by Needham (2000). This detail includes two additional longitudinal rebars at the bottom flange, as shown in Figure 6-42. These additional longitudinal rebars (A_{s_ADD}) terminate in front of the bearing and do not contribute to the longitudinal tie capacity. The area of exposed strands (A_{ps_exp}) re-embedded in the overcast partially contributes to the capacity. The extent of capacity recovery from the re-embedded strands depends on their embedment length within l_x, which is the region between the beam end and the critical section required for tie force development, as shown in Figure 6-36(b).

The PCI Strand Bond Fast Team (2025) recommended Eq. 6-3 to calculate the minimum length to fracture a strand, L_{ult}, during a pull-out test.

$$L_{ult} = f_{pu} \times A_{ps} \times L_b / F \qquad \text{Eq. 6-3}$$

where,

A_{ps} = *area of strands, in.*^{2}

F = *average measured force in the strand corresponding to 0.10 in. slip at the dead end of the pull-out test specimen, kip*

f_{pu} = *minimum tensile strength of strand, ksi*

L_b = *bonded length of strand, in.*

Typically, L_{ult} is less than the strand development length, l_{d_PS}. For the calculation of repaired beam end capacities with re-embedded strands, Eq. 6-3 is rearranged as shown in Eq. 6-4 to calculate the force in the re-embedded strand, F, and the strand development length, l_{d_PS}, is used instead of L_{ult}, to yield conservative results.

$$F = f_{pu} \times A_{ps\_exp} \times l_x / l_{d\_PS} \qquad \text{Eq. 6-4}$$

Therefore, the longitudinal tie capacity of this *Alternative 1* detail, T_1, is:

$$T_1 = (A_{ps\_UD} \times f_{pe} \times l_x/l_t) + (A_{ps\_exp} \times f_{pu} \times l_x/l_{d\_PS}) \qquad \text{Eq. 6-5}$$

where,

A_{ps_UD} = *undamaged bonded prestressing strand area in the bottom flange, in.*^{2}

A_{ps_exp} = *exposed bottom flange strand area re-embedded in the overcast, in.*^{2}

f_{pe} = *effective stress in prestressing steel after losses, ksi*

f_{pu} = *ultimate strength of strands, ksi*

l_{d_PS} = *development length of strand, in.*

l_t = *prestress transfer length, in.*

l_x = *distance from the beam end to the location of the critical section for the development of the tie force, in.*

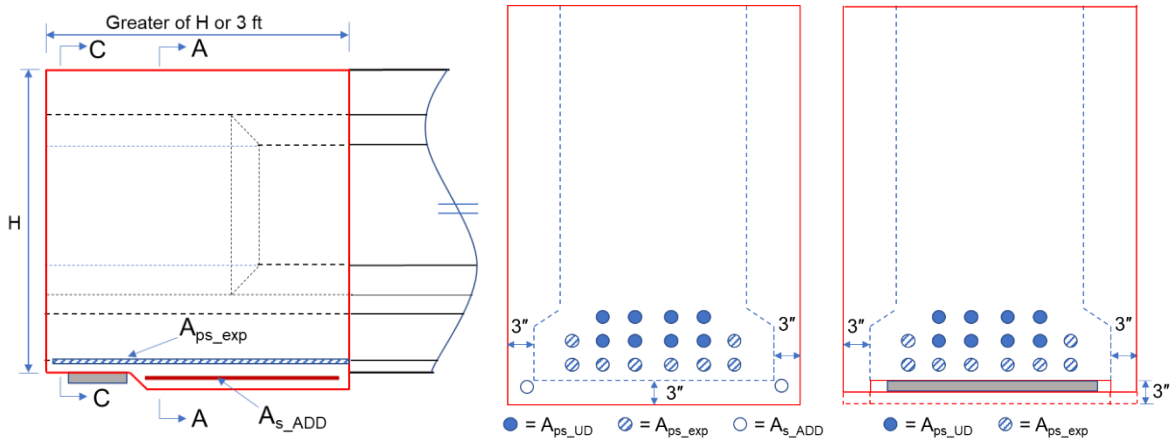

(a) Elevation view (b) Section A-A (c) Section C-C

Figure 6-42. ***Alternative 1*** **detail for FDRCO repairs.**

The longitudinal tie capacity of the repaired section is calculated considering two different scenarios. First, it is assumed that no additional strands are exposed during the chipping and cleaning process. As a result, the repaired section includes 12 bonded strands and four re-embedded strands. Therefore, the longitudinal tie capacity of the overcast repair is calculated using Eq. 6-5 as follows.

$$T_{l\_1} = (A_{ps\_UD} \times f_{pe} \times l_x/l_t) + (A_{ps\_exp} \times f_{pu} \times l_x/l_{d\_PS})$$

$$= (1.38 \times 162 \times 13/26.28.) + (0.46 \times 270 \times 13/109.7)$$

$$= 110.59 + 14.72 = 125.31 \text{ kip}$$

The second scenario assumes that four additional strands are exposed during the chipping and cleaning process, resulting in a total of eight exposed strands. As a result, the repaired section includes eight bonded strands and eight re-embedded strands. The longitudinal tie capacity of this overcast repair is calculated using Eq. 6-5 as follows.

$$T_{l\_2} = (A_{ps\_UD} \times f_{pe} \times l_x/l_t) + (A_{ps\_exp} \times f_{pu} \times l_x/l_{d\_PS})$$

$$= (0.92 \times 162 \times 14/26.28) + (0.92 \times 270 \times 14/109.7)$$

$$= 79.4 + 31.7 = 111.1 \text{ kip}$$

Note: The value of l_x changes due to modifications in the number of strands and their centroidal distance from the beam soffit.

As demonstrated by the above two calculations, exposing additional strands during the chipping and cleaning process reduces the tie force capacity, thereby decreasing the beam end capacity. Therefore, it is recommended to take utmost care to avoid exposing additional strands during the chipping and cleaning process.

6.5.1.2 FDRCO Repair - Alternative 2

The additional longitudinal rebar at the bottom flange is extended up to the beam end and terminated with a 90-degree hook to provide the required development length (Figure 6-43). According to Article 5.10.2.1 of AASHTO LRFD Bridge Design Specifications (AASHTO LRFD 2020), a 90-degree hook on a longitudinal reinforcing bar must include an extension of $12d_b$, where d_b is the diameter of the bar. Therefore, both the added rebar and the re-embedded strands contribute to the longitudinal tie capacity as follows:

$$T_2 = (A_{ps\_UD} \times f_{pe} \times l_x/l_t)+(A_{ps\_exp} \times f_{pu} \times l_x/l_{d\_PS})+[A_{s\_ADD} \times \{(f_{pu} \times l_x/l_{d\_PS}) \leq f_y\}] \quad \text{Eq. 6-6}$$

where,

A_{s_ADD} = *total area of longitudinal rebar in the bottom flange, in.*^{2}

f_y = *yield strength of longitudinal reinforcement, ksi*

Due to strain compatibility requirements, both the added rebar and the re-embedded strands are expected to have a similar strain magnitude. Therefore, $(f_{pu} \times l_x/l_{d\_PS})$ is used as the third term of Eq. 6-6 in place of the yield strength of the longitudinal reinforcement, f_y.

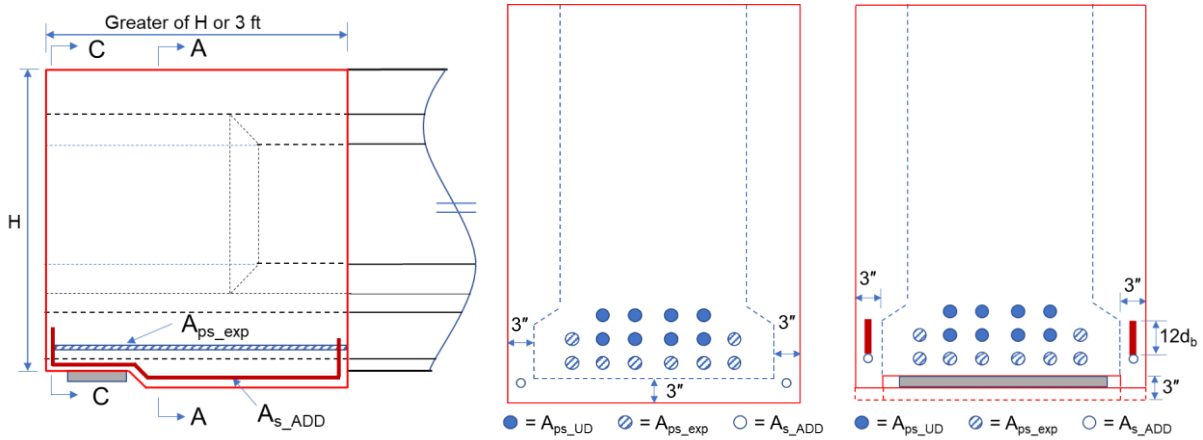

(a) Elevation view (b) Section A-A (c) Section C-C

Figure 6-43. Alternative 2 detail for FDRCO repairs.

The longitudinal tie capacity of the overcast repair with eight exposed strands is calculated using Eq. 6-6 as follows:

$$T_2 = (A_{ps\_UD} \times f_{pe} \times l_x/l_t) + (A_{ps\_exp} \times f_{pu} \times l_x/l_{d\_PS}) + [A_{s\_ADD} \times \{(f_{pu} \times l_x/l_{d\_PS}) \leq f_y\}]$$
$$= (0.92 \times 162 \times 14/26.28) + (0.92 \times 270 \times 14/109.7) + [0.4 \times \{(270 \times 14/109.7) \leq 60\}]$$
$$= 79.4 + 31.7 + 13.8 = 124.9 \text{ kip}$$

The inclusion of a hook in the longitudinal rebar increases the capacity of the overcast repair by 12.4% compared to configurations without a hook. This is because the hook provides sufficient anchorage, allowing the rebar to develop its full tensile capacity within the overcast concrete, thereby enhancing the overall effectiveness of the repair.

6.5.1.3 FDRCO Repair - Alternative 3

Figure 6-44 shows *Alternative 3* details. While the longitudinal rebar configuration remains the same as in the *Alternative 2* detail with hooked ends, a selected number of exposed strands are spliced, bent up 90 degrees, and re-embedded into the overcast to enhance their capacity contribution. Depending on the exposed strand length, location, and available space, a strand splice device can be used to extend the strand length to make a 90-degree bend at the end. Therefore, *Alternative 3*, which details the addition of rebars with 90-degree hooks, re-embedded straight strands, and re-embedded strands with 90-degree bents, can be designed to provide a capacity similar to the as-designed capacity, provided that an adequate number of exposed strands is available to extend using splice chucks and make 90-degree bents.

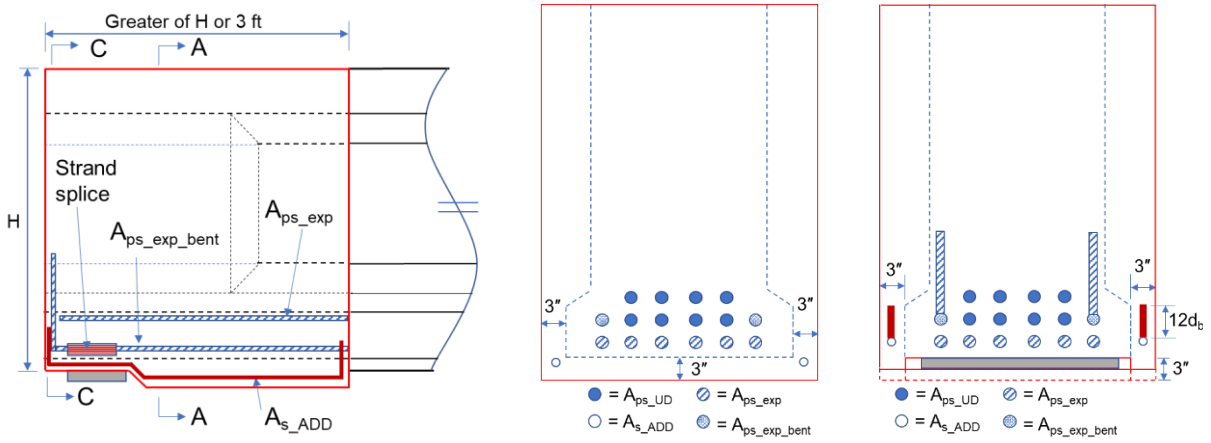

(a) Elevation view (b) Section A-A (c) Section C-C

Figure 6-44. Alternative 3 detail for FDRCO repairs.

Tadros and Jongpitaksseel (2003) evaluated the required embedment length and corresponding pullout strength developed in strands embedded in concrete with 90-degree bents. They recommended that the total embedment length (L_e) should be at least 30 in. for 0.5 in. diameter strands and at least 36 in. for 0.6 in. diameter strands to achieve a strand stress of $0.8f_{pu}$. The total embedment length, L_e, beyond the bearing centerline includes the embedded horizontal length (L_h) and the vertical length (L_v), as illustrated in Figure 6-45.

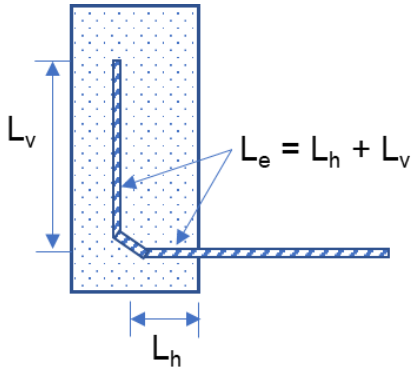

Figure 6-45. A strand with a 90-degree bent.

Figure 6-46 shows a strand splice chuck assembly that can be used at beam ends to splice exposed strands to provide an extended length with 90-degree bents to enhance the load carrying capacity. The diameter and length of each chuck are 1.25 in. and 4.75 in., respectively (PSI 2025, GTI 2025).

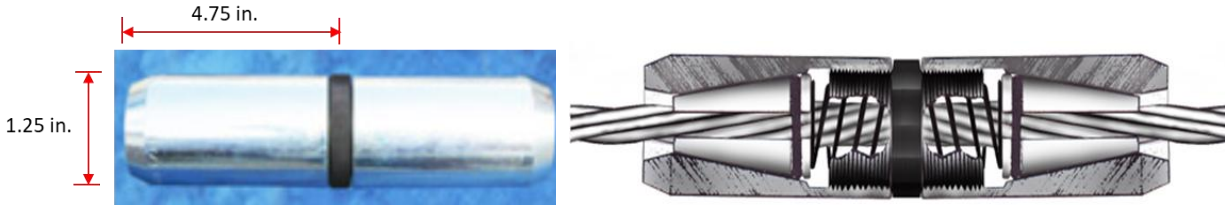

(a) Splice chuck (b) Cross-section of splice chuck

Figure 6-46. Strand splice assembly detail (PSI 2025).

Both the rebars with 90-degree hooks and re-embedded strands with 90-degree bents could provide greater capacities if they are subjected to a minimum of 0.002 με, the yield strain of mild steel. However, concrete cracks before steel reaches this strain limit, resulting in a pull-out failure of existing bonded strands. Therefore, the *Alternative 3* details shown in Figure 6-44 are expected to result in multi-stage failures, as shown in Figure 6-47.

The condition before exceeding the prestressed concrete cracking strain limit is considered as *Stage 1*. Until the undamaged bonded strands fail, the capacity contribution of A_{s_add}, A_{ps_exp}, and $A_{ps\_exp\_bent}$ is proportional to the strain levels of the undamaged strands. Therefore, the capacity of

the repaired beam end is the same as that of *Alternative 2*. As shown in Figure 6-47, A_{ps_UD}, A_{s_add}, A_{ps_exp}, and $A_{ps\_exp\_bent}$ contribute to the total capacity. During *Stage 2*, only A_{s_add} and $A_{ps\_exp\_bent}$ contribute to the total capacity. Forces in longitudinal rebars with hooks increase until yielding. The force in the embedded strands with 90-degree bents increases continuously until the steel reaches a stress limit of $0.80\,f_{pu}$.

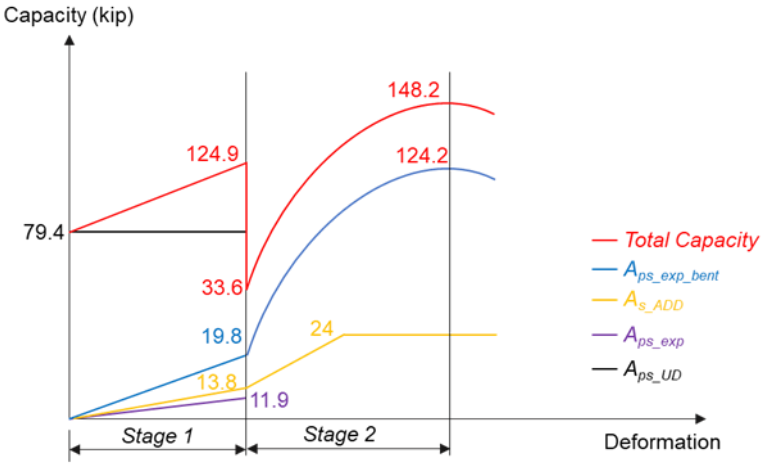

Figure 6-47. Capacity contribution of *Alternative 3* details during different failure stages.

Assume that *Alternative 3* details include eight undamaged strands, three re-embedded strands, five re-embedded strands with 90-degree bents, and two longitudinal bars with hooks. The *Stage 1* longitudinal tie capacity of this detail is calculated as follows:

$$T_{3\text{-}1} = (A_{ps\_UD} \times f_{pe} \times l_x/l_l) + (A_{ps\_exp} \times f_{pu} \times l_x/l_{d\_PS}) + [A_{s\_ADD} \times \{(f_{pu} \times l_x/l_{d\_PS}) \leq f_y\}] + [A_{ps\_exp\_bent} \times \{(f_{pu} \times l_x/l_{d\_PS}) \leq f_y\}] \quad \text{Eq. 6-7}$$

$$= (0.92 \times 162 \times 14/26.28) + (0.345 \times 270 \times 14/109.7) + [0.4 \times \{(270 \times 14/109.7) \leq 60\}] + [0.575 \times \{(270 \times 14/109.7) \leq 60\}]$$

$$= 79.4 + 11.9 + 13.8 + 19.8 = 124.9 \text{ kip } (\underline{\text{Same as Alternative 2 capacity}})$$

Upon the failure of eight bonded strands, the three re-embedded strands also become ineffective. Therefore, only five re-embedded strands with 90-degree bents and two longitudinal bars with hooks are left to provide capacity during *Stage 2*. The longitudinal tie capacity during *Stage 2* is calculated as follows:

$$T_{3\text{-}2} = (A_{s\_ADD} \times f_y) + (A_{ps\_exp\_bent} \times 0.80\,f_{pu}) \quad \text{Eq. 6-8}$$

$$= (0.4 \times 60) + (0.58 \times 0.80 \times 270)$$

$$= 24 + 124.2 = 148.2 \text{ kip}$$

Alternative 3 details can be selected to increase the beam end ultimate capacity to equal or exceed the as-designed capacity. In this example, the details chosen for *Alternative 3* increased the repaired beam end capacity by 33% compared to *Alternative 1.*

6.5.1.4 Comparison of FDRCO Repair Capacity Contributions

This section summarizes the results from the three FDRCO repair examples presented earlier. The as-designed AASHTO Type I beam had a total of 16 strands at the bottom flange. Initially, four of the 16 strands were exposed due to spalling, and an additional four strands were exposed after chipping and cleaning. Thus, a total of eight out of 16 strands were exposed before repair. Table 6-4 summarizes the FDRCO repair capacities of different alternatives.

Table 6-4. Capacity of Beam Ends with FDRCO Repair

Beam End Condition	Strands				Longitudinal Rebar with 90-deg. Hook	Capacity (kip)	Comparing Capacity Change w.r.t (%) ↑↓[1]	
	Exposed	Bonded[2]	Re-embedded[3]				As-designed	D_2
			Straight	90-deg. Bent				
As-designed		16				144	N/A	82.3(↑)
Deteriorated (D_1)	4	12				110	23.6 (↓)	39.2(↑)
After chipping and cleaning (D_2)	8	8				79	45.1 (↓)	0
Alternative 1 ($T_{1\text{-}1}$)		12	4			125	13.2 (↓)	N/A
Alternative 1($T_{1\text{-}2}$)		8	8			111	22.9 (↓)	40.5(↑)
Alternative 2		8	8		2	125	13.2 (↓)	58.2(↑)
Alternative 3		8	6	2	2	148	2.8(↑)	87.3(↑)

[1]Capacity changes are calculated relative to the as-designed capacity, and the beam end condition after chipping and cleaning (D_2); ↑= increase, ↓=decrease
[2] Bonded strands are undamaged and prestressed.
[3] Re-embedded strands are not prestressed.

6.5.2 Preservation and Repair Recommendations

The following preservation and repair methods are recommended based on their field performance, performance during laboratory studies documented in Chapter 5, performance reported in Attanayake et al. (2022), and the capacity contributions documented in this chapter. The listed methods can be combined for improved performance. For example, for beam ends with shallow spalls that do not expose steel, a breathable concrete surface coating (CSC) with crack-bridging ability, a silane penetrating sealer, or a combination thereof can be used to protect the member. For a beam end with exposed steel and adequate load capacity, a breathable CSC with crack-bridging ability or a silane penetrating sealer can be applied after cleaning and protecting the exposed steel with a zinc-rich epoxy primer. As noted in Attanayake et al. (2022), the use of a

breathable CSC with crack-bridging ability is better than using a penetrating sealant to protect concrete.

1. Breathable CSC with crack-bridging ability or silane penetrating sealers
2. Cleaning and protecting exposed steel with zinc-rich epoxy primer
3. Concrete Patching*
4. Epoxy injection**
5. Full-depth reinforced concrete overcast (FDRCO)***
    A. Alternative 1
    B. Alternative 2
    C. Alternative 3
6. Overcast with welded wire fabric and adhesive-anchored stirrups

** Concrete patching does not increase the structural capacity of deteriorated beam ends. Option 1 (breathable concrete surface coatings with crack-bridging ability or silane penetrating sealers) and 2 (cleaning and protecting exposed steel with zinc-rich epoxy primer) often serve a similar protective function and, in some cases, provide a better corrosion resistance than patching alone. Patching should be selected primarily when aesthetic restoration of the damaged area is required. If patching is used, it is recommended to use FRP strips to maintain the integrity of the repaired section and use a breathable CSC with crack-bridging ability for improved durability.*

*** Epoxy injection is required for cracks with widths of 0.002 inches or greater. Structural cracks in beams should be repaired by epoxy injection prior to overcasting to ensure structural integrity.*

**** Full-depth reinforced concrete overcast (FDRCO) repair includes three different detail options (A, B, and C). The most suitable detail needs to be selected based on the required capacity improvement and site-specific conditions. The use of FRP strips and breathable CSCs with crack-bridging ability is recommended.*

Table 6-5 outlines repair recommendations for deteriorated PSC I-beam ends based on the type, location, and severity of damage.

Table 6-5. Repair Recommendations for Deteriorated PSC I-Beam Ends

Type of Deterioration	Location	Case	Range[1]	Zone	Condition State (CS)	Repair Options
Spall/ Delamination	Beam soffit[2]	(A) Depth < clear cover of stirrups	N/A	Z3	CS2	1, 3
		(B) Depth = clear cover of stirrups	No strands are exposed, section loss < 20%		CS2	1, 2, 3
		(C) Depth = clear cover of strands	< 15% of the bottom flange strands are exposed and < 35% section loss		CS3	1, 2, 3, 5A, 6
			≥ 15% of the bottom flange strands are exposed		CS4	5B, 5C
	Bottom flange side[3]	(A) Depth < clear cover of stirrups	N/A	Z1, Z2, Z3	CS2	1, 3
		(B) Depth = clear cover of stirrups	Section loss < 10% and no strands are exposed		CS2	1, 2, 3
		(C) Depth = clear cover of strands	< 40% section loss without exposed strands[4]		CS2	1, 2, 3
			< 15% of the bottom flange strands are exposed and < 30% section loss		CS3	1, 2, 3, 5A, 6
			≥ 15% of the bottom flange strands are exposed		CS4	5B, 5C
		(D) Depth > clear cover of strands	< 15% of the bottom flange strands are exposed, and <30% section loss		CS3	1, 2, 3, 5A, 6
			Section loss ≥ 40% and no strands are exposed.		CS4	5A
			≥ 15% of the bottom flange strands are exposed		CS4	5B, 5C

[1] Do not use these limits for MI 1800 beams. The capacity of MI 1800 beams should be evaluated on a case-by-case basis using the provided Mathcad calculation sheets and compared with the factored demands.
[2] Clear cover is measured from the beam soffit.
[3] Clear cover is measured from the vertical side of the bottom flange.
[4] Use 20% as the limit when the bottom flange spall is only on one side.

7 CAPACITY OF STEEL BEAM ENDS WITH HOLES

7.1 OVERVIEW

As discussed in Chapter 2, 62% of beam end deteriorations are associated with the web. The web area of a beam in the vicinity of a support can be divided into two zones: bearing zone and shear zone (Figure 7-1). The width of the bearing zone at a beam end and away from a beam end is defined as N+2.5k and N+5k, respectively. The evaluation of typical failure modes within the bearing zone and the associated capacities requires the application of the theory of buckling. In typical multi-beam, simple span bridges, the beam top flange is monolithically connected to the cast-in-place concrete deck. The bottom flange over the bearing is welded to the sole plate and connected to the abutment or pier using various mechanisms limiting bottom flange deformations. Therefore, the buckling capacity is primarily controlled by the web and the stiffeners.

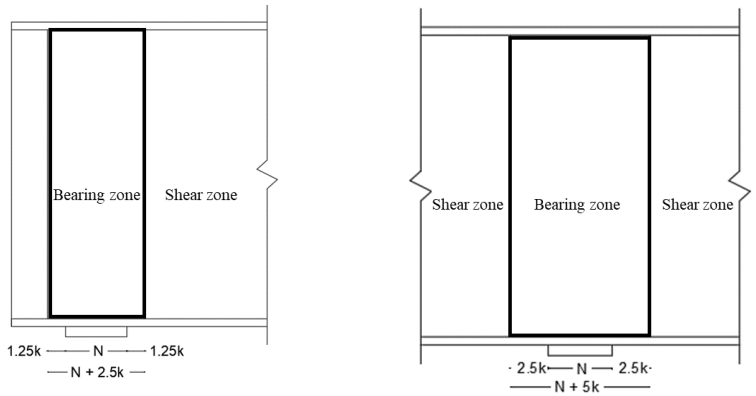

(a) Bearing zone near the beam end (b) Bearing zone away from the beam end

Figure 7-1. Bearing and shear zones of a steel beam

This chapter describes the beam geometry selected for analysis, material properties, modeling and analysis of beam ends with holes, analysis results, and recommendations for assessing the capacities of unstiffened and stiffened beam ends with holes.

7.2 BEAM GEOMETRY

The analysis model represents the most commonly used beam section in Michigan bridges, W30×108 (Table 7-1). The other parameters considered for the model include beam length, bearing length, the geometry of diaphragms and stiffeners, and the beam overhang length, which is the distance between the beam end and the exterior edge of the bearing. Cross-section properties are shown in Table 7-2. The span length of the W30×108 section ranges between 29 and 54 ft.

Pier bearing length ranges between 6 in. and 9 in. Typically, the beam ends are offset about one inch beyond the edge of the bearing. This segment is referred to as the overhang in this report.

Table 7-1. Beam Sections Used in Michigan Bridges

Beam Section	Number of Members per Type	Total
30" deep plate girder	24	24
36" Plate girder	9	9
48" deep plate girder	138	138
54" deep plate girder	24	24
60" deep plate girder	58	58
63" deep plate girder	24	24
66" deep welded plate girder	24	24
66.5" deep riveted plate girders	16	16
72" deep plate girder	24	24
CB27×137	36	36
W18×50	8	8
W21×62	12	12
W24×100	55	97
W24×110	40	
W24×68	1	
W24×84	1	
W27×102	104	240
W27×84	30	
W27X94	84	
W27×98	22	
W30×108	220	402
W30×116	93	
W30×124	80	
W30×99	9	
W33×118	14	181
W33×130	77	
W33×132	11	
W33×141	66	
W33×152	13	
W36×135	112	202
W36×150	90	

Table 7-2. W30×108 Section Properties

Geometry	Dimensions
Depth (in.)	29.8
Thickness of the bottom flange (in.)	0.76
Thickness of the top flange (in.)	0.76
Thickness of the web (in.)	0.545
Width of the bottom flange (in.)	10.5
Width of the top flange (in.)	10.5
Fillet radius (in.)	0.65
Distance from the outer face of the flange to the web toe of the fillet, *k* (in.)	1.41

The end diaphragms are partial depth, 12 inches deep, and are typically located at 12 inches from the beam end. The intermediate diaphragms are mostly 20 inches deep and equally spaced between the end diaphragms. The number of intermediate diaphragms in a span depends on the span length, as shown in Table 7-3.

Table 7-3. Number of Intermediate Diaphragms in a Span

Span Length, L (ft)	Number of Intermediate Diaphragms
L < 40 ft	1
40 ft ≤ L ≤ 70 ft	2
L > 70 ft	3

As shown in Figure 7-2, most interior beams have only one bearing stiffener on each side of the web. In the analysis model, the bearing stiffener is placed at the bearing centerline.

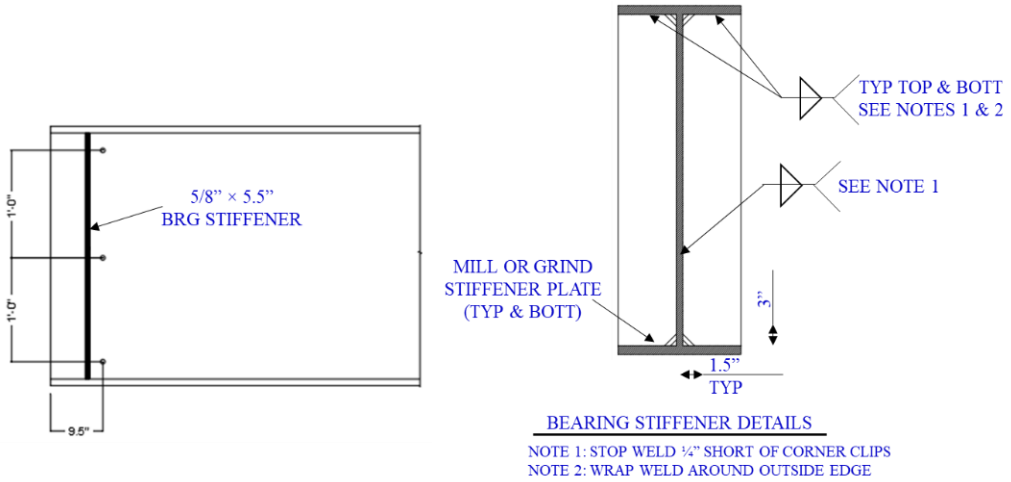

Figure 7-2. A typical bearing stiffener.

7.3 STEEL PROPERTIES

Table 7-4 summarizes the steel properties used for analysis.

Table 7-4. Steel Properties

Material Properties	Values
Modulus of Elasticity, E (ksi)	29,000
Yield strength, F_y (ksi)	50
Poisson's ratio, ν	0.3
Unit weight (lb/ft^3)	490
Density, ρ (slug/in.^{3})	0.0088
Mass per unit area, γ (slug/in.^{2})	0.0048

7.4 CAPACITY OF AS-DESIGNED I-BEAM SECTION

Figure 7-3 shows the failure modes considered for evaluating beam end capacities of unstiffened and stiffened beam ends and the corresponding articles of the AASHTO (2020). The unstiffened beam end capacity is the minimum of shear, web local yielding, and web crippling capacities. For stiffened beam ends, capacity is the minimum of shear resistance and bearing and axial resistances of the bearing stiffeners.

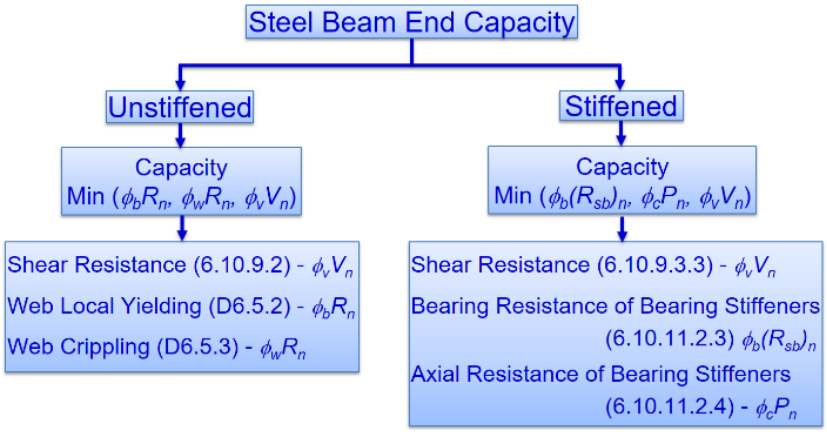

Figure 7-3. Steel beam end capacity as per AASHTO (2020)

7.4.1 Nominal Resistance of an Unstiffened Beam End

7.4.1.1 Shear Resistance

To prevent shear yielding or shear buckling, an unstiffened web must possess a nominal resistance of V_n, calculated using Eq. 7-1. The shear resistance is calculated without considering the tension-field action.

$$V_n = V_{cr} = CV_p = C[0.58F_{yw}Dt_w] \quad \text{Eq. 7-1}$$

where,

C = the ratio of shear-buckling resistance to shear-yielding resistance calculated using Eq. 7-2, 7-3, or 7-4, as applicable, with the shear-buckling coefficient of k taken equal to 5.0.

$$\text{if } \frac{D}{t_w} \leq 1.12\sqrt{\frac{Ek}{F_{yw}}}, \text{ then } C = 1.0 \qquad \text{Eq. 7-2}$$

$$\text{if } 1.12\sqrt{\frac{Ek}{F_{yw}}} < \frac{D}{t_w} \leq 1.40\sqrt{\frac{Ek}{F_{yw}}}, \text{ then } C = \frac{1.12}{\left(\frac{D}{t_w}\right)}\sqrt{\frac{Ek}{F_{yw}}} \qquad \text{Eq. 7-3}$$

$$\text{if } \frac{D}{t_w} > 1.4\sqrt{\frac{Ek}{F_{yw}}}, \text{ then } C = \frac{1.57}{\left(\frac{D}{t_w}\right)^2}\left(\frac{Ek}{F_{yw}}\right) \qquad \text{Eq. 7-4}$$

D = web depth (in.)

V_{cr} = shear-yielding or shear-buckling resistance (kip)

Vp = plastic shear resistance (kip)

V_u = factored shear in the web at the section under consideration (kip) $\leq \varphi_v V_n$

ϕ_v = resistance factor for shear specified in Article 6.5.4.2

7.4.1.2 Web Local Yielding

To prevent web local yielding, a beam end needs to possess a nominal resistance of R_n calculated using either Eq. 7-5 or 7-6. The Eq. 7-5 is valid only when the concentrated load (i.e., an internal pier reaction or an applied load) is located at a distance greater than d from the beam end.

$$R_n = (5k+N) F_{yw} t_w \qquad \text{Eq. 7-5}$$

Otherwise:

$$R_n = (2.5k+N) F_{yw} t_w \qquad \text{Eq. 7-6}$$

where:

d = depth of the steel section (in.)

k = distance from the outer face of the flange resisting the concentrated load or bearing reaction to the web toe of the fillet (in.)

t_w = thickness of the web resisting the concentrated load or bearing reaction (in.)

F_{yw} = yield strength of web (ksi)

N = length of bearing (in.)

R_u = factored concentrated load or bearing reaction (kip) $\leq \varphi_b R_n$

ϕ_b = resistance factor for bearing specified in Article 6.5.4.2

7.4.1.3 Web Crippling

To prevent web crippling, a beam end needs to possess a nominal resistance of R_n calculated using either Eq. 7-7, 7-8 or 7-9. The Eq. 7-7 is valid only when the concentrated load (i.e., an internal pier reaction or an applied load) is located at a distance greater than or equal to *d/2* from the beam end.

$$R_n = 0.8t_w^2\left[1 + 3\left(\frac{N}{d}\right)\left(\frac{t_w}{t_f}\right)^{1.5}\right]\sqrt{\frac{EF_{yw}t_f}{t_w}} \qquad \text{Eq. 7-7}$$

- Otherwise:
  - When $\frac{N}{d} \leq 0.2$

$$R_n = 0.4t_w^2\left[1 + 3\left(\frac{N}{d}\right)\left(\frac{t_w}{t_f}\right)^{1.5}\right]\sqrt{\frac{EF_{yw}t_f}{t_w}} \qquad \text{Eq. 7-8}$$

  - When $\frac{N}{d} > 0.2$

$$R_n = 0.4t_w^2\left[1 + \left(\frac{4N}{d} - 0.2\right)\left(\frac{t_w}{t_f}\right)^{1.5}\right]\sqrt{\frac{EF_{yw}t_f}{t_w}} \qquad \text{Eq. 7-9}$$

where,

t_f = thickness of the flange resisting the concentrated load or bearing reaction (in.)

R_u = factored concentrated load or bearing reaction (kip) $\leq \varphi_w R_n$

ϕ_w = resistance factor for web crippling specified in Article 6.5.4.2

Note: A concentrated load acting on a rolled shape or a built-up section is assumed critical at the toe of the fillet located a distance k from the outer face of the flange resisting the concentrated load or bearing reaction, as applicable. For a rolled shape, k is published in the available tables giving dimensions for the shapes. For a built-up section, k may be taken as the distance from the outer face of the flange to the web toe of the web-to-flange fillet weld. (AASHTO LRFD 2020)

7.4.1.4 Nominal Resistance of an Unstiffened Beam End

Table 7-5 shows the summary of nominal and factored resistances calculated for an unstiffened W30×108 beam end section. The dominant failure mode is web crippling, with a nominal resistance of 231 kips.

Table 7-5. Nominal Resistance of an Unstiffened W30×108 Beam End Section

Failure Mode	Nominal Resistance, R_n (kips)	Resistance factor, ϕ	Factored Resistance, ϕR_n (kips)
Shear	447	1.0	447
Web local yielding	260	1.0	260
Web crippling	231	0.8	185

7.4.2 Nominal Resistance of a Stiffened Beam End

7.4.2.1 Shear Resistance

The nominal shear resistance of a stiffened web end panel is calculated using Eq. 7-1. The value of C is calculated using Eq. 7-2, 7-3 or 7-4. The shear buckling coefficient, k, is calculated using Eq. 7-10. The shear resistance is calculated without considering the tension-field action. This assumption is valid for the beam ends with a single bearing stiffener on each side of the web, the configuration used for the analysis cases considered in this study.

$$k = 5 + \frac{5}{\left(\frac{d_0}{D}\right)^2} \qquad \text{Eq. 7-10}$$

where:

d_o = transverse stiffener spacing (in.)

Note: The shear-buckling coefficient, k, to be used in determining the constant C in Eq. 7-1 is to be calculated based on the spacing from the support to the first stiffener adjacent to the support, which may not exceed 1.5D. (AASHTO LRFD 2020)

7.4.2.2 Bearing Resistance of Bearing Stiffeners

Stiffeners are provided at bearing locations and other locations subjected to concentrated loads. In the absence of stiffeners, the bearing resistance is not evaluated when the unstiffened web satisfies the provisions of AASHTO (2020) Article D6.5.

To prevent bearing failure at the fitted ends, bearing stiffeners must possess a nominal resistance of $(R_{sb})_n$, calculated using Eq. 7-11.

$$(R_{sb})_n = 1.4\, A_{pn}\, F_{ys} \qquad \text{Eq. 7-11}$$

where,

A_{pn} = area of the projecting elements of the stiffener outside of the web-to-flange fillet welds but not beyond the edge of the flange (in.^{2})

$(R_{sb})_r$ = factored bearing resistance for the fitted ends of bearing stiffeners (kip)

$\leq \phi_b (R_{sb})_n$

ϕ_b = resistance factor for bearing specified in Article 6.5.4.2 = 1.0

To prevent local buckling of the bearing stiffener plates the contact width, b_t, of each stiffener plate shall satisfy:

$$t_p \geq b_t/0.48\ (E/F_{ys})^{1/2} \qquad \text{Eq. 7-12}$$

where:

b_f = flange width (in.)

b_t = contact width of the projecting stiffener element (in.) ≤ $[(b_f - t_w)/2 - (k - t_f)]$

k = distance from the outer face of the flange resisting the concentrated load or bearing reaction to the web toe of the fillet (in.)

t_f = flange thickness (in.)

t_p = thickness of the projecting stiffener element (in.)

t_w = web thickness (in.)

E = modulus of elasticity (ksi)

F_{ys} = specified minimum yield strength of the stiffener (ksi)

If the condition given in Eq. 7-12 is not satisfied during the design, the section thickness needs to be increased. During an assessment of an existing detail, the buckling analysis provides a capacity after incorporating the beam end conditions and details. Therefore, when the conditions are not met, a refined finite element model must be used for buckling analysis. Please refer to Section 7.5.3 of this report for further details on such analysis.

7.4.2.3 Axial Resistance of Bearing Stiffeners

Even though flexural buckling, torsional buckling, or flexural-torsional buckling are the possible failure modes of a component under compression, flexural buckling is the failure mode for bearing stiffeners. Eq. 7-13 is used to calculate the factored resistance of a component under compression, P_r.

$$P_r = \phi_c P_n \qquad \text{Eq. 7-13}$$

where:

P_n = nominal compressive resistance (kip)

ϕ_c = resistance factor for compression as specified in Article 6.5.4.2

Bearing stiffeners used in typical bridges are nonslender elements. Therefore, the nominal compressive resistance is calculated using either Eq. 7-14 or Eq. 7-15.

If $P_e/P_o \geq 0.44$, then:

$$P_n = \left[0.658^{\left(\frac{P_o}{P_e}\right)}\right] P_o \qquad \text{Eq. 7-14}$$

If $P_e/P_o < 0.44$, then:

$$P_n = 0.877 P_e \qquad \text{Eq. 7-15}$$

The elastic critical buckling resistance, P_e, is calculated using Eq. 7-16.

$$P_e = \frac{\pi^2 E}{\left(\frac{Kl}{r_s}\right)^2} A_g \qquad \text{Eq. 7-16}$$

The nominal yield resistance, P_o, is calculated using Eq. 7-17.

$$P_o = F_y A_g \qquad \text{Eq. 7-17}$$

where,

r_s = radius of gyration in the plane of buckling (in.)

A_g = gross sectional area of the member (in.^{2})

D = web depth (in.)

I_s = moment of inertia of the effective column section (in.^{4})

K = effective length factor in the plane of buckling = 0.75 D

l = unbraced length in plane of buckling (in.)

The effective section for axial resistance calculation is determined as follows:

1) For stiffeners bolted to the web:
   - the effective section is represented only by the stiffeners.
2) For stiffeners welded to the web:
   - a portion of the web shall be included as part of the effective column section.
   - for stiffeners consisting of two plates welded to the web, the effective column section includes the two stiffener elements and a centrally located strip of web extending not more than $9t_w$ on each side of the stiffeners, as shown in Figure 7-4.

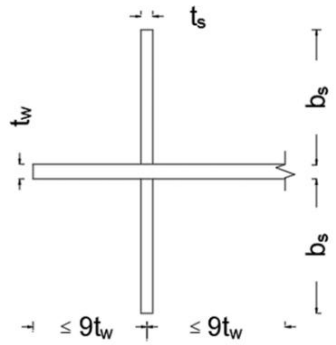

Figure 7-4. Effective column section when two stiffener plates are welded to the web

7.4.2.4 Nominal Resistance of a Stiffened Beam End

Table 7-6 shows the summary of nominal and factored resistances calculated for a stiffened W30×108 beam end section. The dominant failure mode is bearing, with a nominal resistance of 260 kips.

Table 7-6. Nominal Resistance of a Stiffened W30×108 Beam End Section

Failure modes	Nominal Resistance, R_n (kips)	Resistance factor, ϕ	Factored Resistance, ϕR_n (kips)
Shear	447	1.0	447
Bearing	260	1.0	260
Axial	470	0.95	446

7.5 NUMERICAL ANALYSIS OF BEAM ENDS

After conducting a series of parametric analyses, a 25-ft-long beam, both without and with stiffeners, was modeled using S9R5 elements. The beam is simply supported and includes 6-in. long bearings at each end. Abaqus, a general-purpose finite element software, is used for this analysis because it provides eigenvalue buckling analysis and post-buckling analysis capabilities necessary to evaluate beam end capacity. Eigenvalue analysis provides mode shapes to calculate buckling loads. The Riks method considers the buckling modes to calculate postbuckling load capacity. The Riks method can incorporate imperfection for postbuckling load capacity calculation. This is important because it allows introducing web out-of-plane deformation documented during inspection in the capacity calculation.

Figure 7-5 shows the web out-of-plane deformation of a W30×108 section documented during inspections. Such deformations reduce the beam end capacity compared to the capacities calculated using AASHTO equations, which assume a perfectly vertical (plumb) web and perfect geometries. The original thickness of the web is 0.605 in. The out-of-plane deformation magnitude of 0.25 in. represents a 41% imperfection (i.e., 0.25/0.605×100), which is typically presented as a percentage of the component thickness in buckling analysis and referred to as the imperfection amplitude.

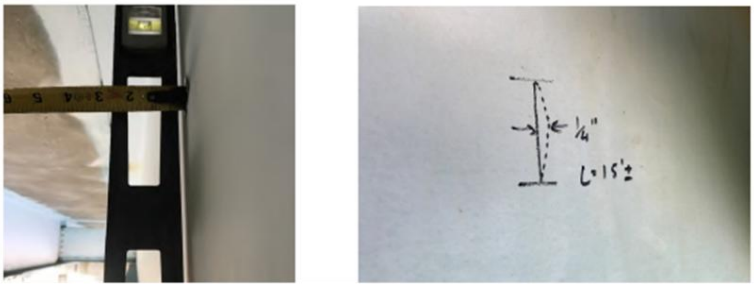

Figure 7-5. Web out-of-plane deformation measured during field inspection.

7.5.1 Unstiffened Beam Ends Without Holes

Figure 7-6 shows the first five mode shapes of the beam end without bent plates. The first mode shape being the controlling mode for buckling, it is scaled as an imperfection when using Riks method for postbuckling capacity analysis (Kanakamedala et al. 2023 and Tzortzinis, et al. 2019).

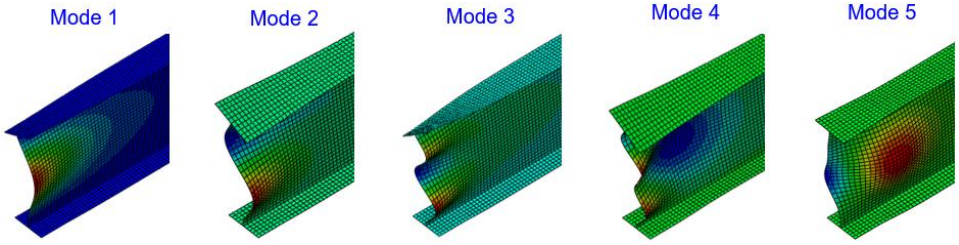

Figure 7-6. Mode shapes at the beam end

Beam end geometry was modified to include bent plates and evaluate their impact on buckling modes and postbuckling capacity. Figure 7-7 shows a typical end diaphragm connection. While the bent plate is welded to the girder, the diaphragm is either bolted or welded to the bent plate. Two models were developed representing an exterior beam with a single bent plate and an interior beam with bent plates on both sides of the web. A bent plate thickness of 0.375 in. was used in the model. The distance between the top surface of the end diaphragm and the top surface of the top flange ranges between 2 and 4 inches. Since most of the deteriorations are observed at the bottom of the web, it is vital to maintain the largest gap between the end of the bent plate and the top of the bottom flange to allow the longest unsupported length of the web, a critical parameter for buckling. Figure 7-8 shows the geometry of the bent plate and the connection details.

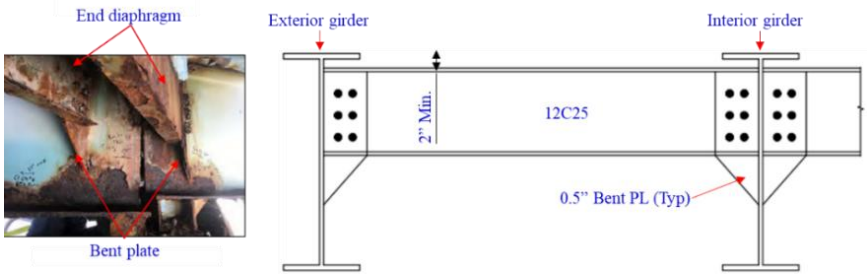

Figure 7-7. End diaphragm and connection details.

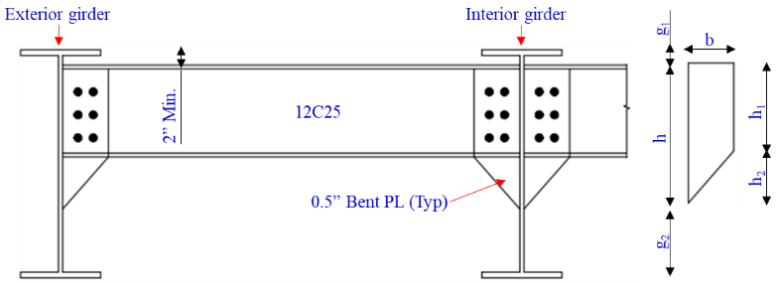

Figure 7-8. Bent plate and connection details.

Figure 7-9 and Figure 7-10 show the first five mode shapes of an exterior beam with one bent plate and an interior beam with two bent plates, respectively. Both beam ends produced the same mode shapes since the bent plates are located 12 inches from the ends. Furthermore, they are similar to those observed without bent plates, as shown in Figure 7-6.

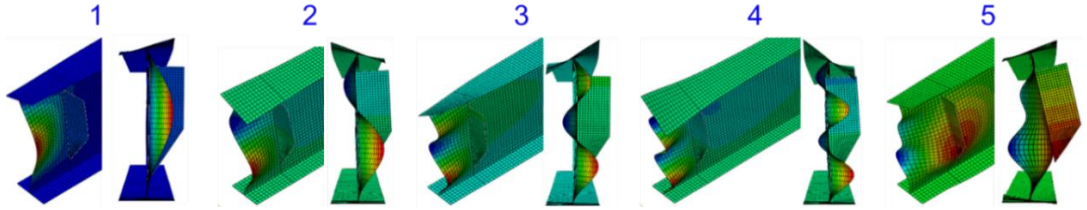

Figure 7-9. Mode shapes of an exterior beam end with one bent plate.

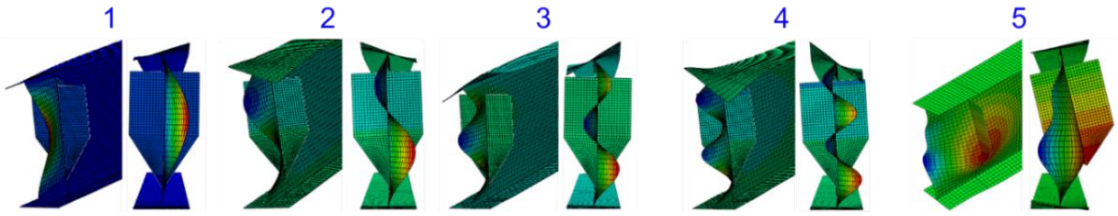

Figure 7-10. Mode shapes of an interior beam with two bent plates.

Table 7-7 summarizes the analysis results for all the cases: beams without and with bent plates, as well as exterior and interior beams. Web crippling is the failure mode identified in Section 7.4.1.4 for an unstiffened beam end, with a nominal resistance of 231 kips. Numerical analysis results are compared with the nominal resistance calculated using AASHTO (2020) equations. Two parameters are introduced to compare the results, as shown below,

LPF_{BL} = the ratio between the postbuckling load (failure load) and the buckling load.

LPF = the ratio between the postbuckling load (failure load) and the nominal resistance.

As shown in the following table, the failure load calculated for a beam end without bent plates is only 3% more than the nominal resistance calculated using the AASHTO (2020) equations for web crippling [i.e., (239-231)/231×100]. This shows an excellent correlation between the numerical and analytical solutions. The impact of web out-of-plane deformations on web crippling capacity

was evaluated by incorporating a range of imperfection amplitudes. The results are presented in Table 7-7. The variation of LPF against the imperfection magnitude for a beam without bent plates is shown in Figure 7-11. As indicated by the analysis results, even a web out-of-plane deformation magnitude equal to 0.1% of the web thickness (t_w) could reduce the load capacity by 15%. When the same beam end has an imperfection amplitude of 50% of the web thickness, the failure load is decreased by 33%. The failure loads of interior and exterior beam ends with bent plates are also listed in the table.

Table 7-7. LPF for Nominal Web Crippling Resistance of Beams Ends Without and With Bent Plates

FE Models	Analysis Cases	Buckling Load (kip)	LPF_{BL}	Failure load (kip)	LPF
	As designed (nominal resistance)	231		231	
Beams without bent plates	Beam without imperfection	197	1.22	239	1.03
	Beam with 0.1% imperfection	197	0.99	196	0.85
	Beam with 5% imperfection	197	0.90	177	0.77
	Beam with 25% imperfection	197	0.82	161	0.69
	Beam with 50% imperfection	197	0.79	155	0.67
	Beam with 75% imperfection	197	0.74	146	0.63
	Beam with 100% imperfection	197	0.70	138	0.60
	Beam with 150% imperfection	197	0.62	122	0.53
	Beam with 200% imperfection	197	0.57	112	0.49
Beams with bent plates	Exterior beam without imperfection	283	0.82	231	1.00
	Exterior beam with 25% imperfection	283	0.68	192	0.83
	Exterior beam with 50% imperfection	283	0.64	180	0.78
	Exterior beam with 75% imperfection	283	0.60	170	0.73
	Exterior beam with100% imperfection	283	0.58	164	0.71
	Interior beam without imperfection	289	0.83	240	1.04
	Interior beam with 25% imperfection	289	0.67	194	0.84
	Interior beam with 50% imperfection	289	0.63	183	0.79
	Interior beam with 75% imperfection	289	0.60	173	0.75
	Interior beam with 100% imperfection	289	0.57	165	0.71

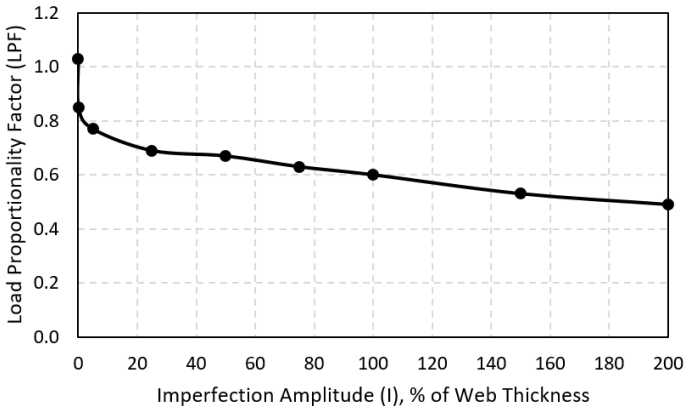

Figure 7-11. Variation of LPF against the imperfection amplitude.

7.5.2 Unstiffened Beam Ends with Holes

The models include beam ends with and without bent plates. The model with bent plates includes only one plate, similar to an exterior beam. Hole configurations are decided based on deteriorations documented in the scoping reports. A few common deteriorations are shown in Figure 7-12.

Tzortzinis et al. (2019) investigated the impact of holes on beam end capacity, finding that the change in capacity is insignificant when the hole height exceeds 10% of the web height and the hole length exceeds 70% of the bearing length. Based on this study, MassDOT developed simplified methods for calculating web local yielding and web local crippling capacities. The application of these simplified methods for load rating is recommended by MassDOT when the web section loss within the bottom 4 in. of the web height is equal to or exceeds an average of 1/8 in. over that height (MassDOT 2025). Considering the recommendations in the literature and the conditions recorded in the inspection reports, the analysis presented in this section includes holes up to 14% of the web height (i.e., 4 in.), measured from the bottom of the web. The heights of the holes are defined as 3.5%, 7%, 10.5%, and 14% of the web height. The hole length is determined based on the overhang length and the bearing length. The location of the holes is defined as follows:

- Case 1: Holes within the overhang, Figure 7-12(a)
- Case 2: Holes starting from overhang and extending to the bearing, Figure 7-12(b)
- Case 3: Holes starting at the exterior bearing edge closer to the end and extending towards the span, Figure 7-12(c)
- Case 4: Holes starting at the middle of the bearing and extending toward the span, Figure 7-12(d).

(a) Complete section loss within the overhang

(b) Complete section loss within the overhang and above the bearing

(c) Complete section loss above the bearing

(d) Complete section loss starting from the middle of the bearing and extending towards the span

Figure 7-12. Hole configurations documented during bridge inspection.

7.5.2.1 Holes Within the Overhang

Figure 7-13 shows different configurations of holes within the overhang (OH). With the overhang being one inch, the hole length (HL) is one inch. The hole heights considered are those mentioned above as a percentage of the web height (3.5%, 7%, 10.5%, 14%). For the holes in the overhang, the loss of the entire web is also considered (i.e., HH = 100% of the web height).

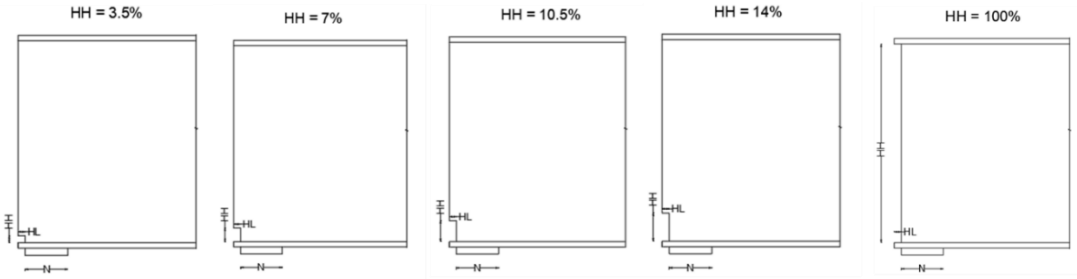

Figure 7-13. Holes within the overhang.

A beam end without a bent plate and an exterior beam end with one bent plate were considered for the analyses to understand the impact of holes on beam end capacity. The model included a 6-inch bearing and an imperfection amplitude (I) of 50%, 75%, and 100% of the web thickness. Table 7-8 summarizes the numerical results. As shown in the table, when there are no holes in the beams without and with bent plates, the LPF is 0.67 and 0.78, respectively. When the entire overhang is lost due to corrosion (i.e., HH = 100%), the LPF is 0.61 and 0.67 for beams without

and with bent plates. The table also shows the capacity calculated using the equations provided in MassDOT (2025) for HH = 100%, which yield comparable results to our analysis without a bent plate.

The average web thickness (t_{ave}) calculation in the MassDOT procedure accounts for the hole length and imperfection amplitude, as shown in Eq. 7-18. The factor used for the imperfection amplitude is constant for imperfections greater than $0.1t_w$ (Table 7-9). Therefore, the t_{ave} values shown in Table 7-8 are the same for all the imperfection cases listed in the table. However, the coefficients defined in the MassDOT Bridge Manual for web crippling capacity calculations differ for imperfections greater than 50%, between 50% and 10%, and less than 10% of the web thickness (Table 7-10). Therefore, the web crippling capacities and LPF values calculated using the MassDOT procedure with 50% imperfection and imperfections greater than 50% are different (Table 7-8). The results also show that the beam end capacity is insensitive to the hole height.

$$t_{ave} = [(N + md - H) \times t_w]/(N + md) \quad \text{Eq. 7-18}$$

where,

N = bearing length (in.)

H = hole length (in.)

d = web depth (in.)

m = factor given in Table 7-9

t_w = web thickness (in.)

Table 7-8. LPF for Nominal Web Crippling Resistance of Beam Ends with Holes Located within the Overhang, N = 6 in., I=0.5t_w, 0.75t_w, 1t_w

	HL (in.)	I (%)	Hole Height, HH (% of the web height)						MassDOT Bridge Manual Part I 100th Anniversary Edition		
			0	3.50	7	10.5	14	100	t_{ave} (in.)	Capacity (kip)	LPF
LPF for beams without a bent plate	1	50	0.67	0.66	0.66	0.66	0.65	0.61	0.48	142	0.62
		75	0.63	0.62	0.62	0.62	0.62	0.59	0.48	138	0.60
		100	0.60	0.59	0.59	0.59	0.59	0.56	0.48	138	0.60
LPF for beams with a bent plate	1	50	0.78	0.77	0.76	0.76	0.76	0.67	0.48	142	0.62

Table 7-9. Values of Factor (m) for Average Web Thickness Calculation (MassDOT 2025)

	Imperfection Amplitude (I)*		
	$I > 0.5t_w$	$0.5t_w \geq I > 0.1t_w$	$I \leq 0.1t_w$
$N/d > 0.2$	0.2	0.2	0.1
$N/d \leq 0.2$	0.1	0.1	0.0

* Values shall not be interpolated

Web crippling capacity, $R_n = \left(a\sqrt{EF_y t_f}\, t_{ave}^{1.2} + b\left(\frac{N-H}{d}\right)\sqrt{\frac{EF_y t_f}{t_f^{1.5}}}\, t_{ave}^{3} \right)\left(\frac{t_{ave}}{t_w}\right)^h$ Eq. 7-19

where,

a = factor from Table 7-10

b = factor from Table 7-10

h = factor from Table 7-10

E = modulus of elasticity (ksi)

F_y = yield strength (ksi)

t_f = flange thickness (in.)

Table 7-10. Factors for Calculating Rn When N/d ≤ 0.2 (MassDOT 2025)

	Imperfection Amplitude (I)*		
	$I > 0.5t_w$	**$0.5t_w \geq I > 0.1t_w$**	**$I \leq 0.1t_w$**
a	0.33	0.32	0.38
b	0.00	0.17	0.0
h	0.40	0.20	0.15

* Values shall not be interpolated

7.5.2.2 Holes Starting from Overhang and Extending to the Bearing

The hole length over the bearing is calculated as N/3, 2N/3, and N. With the overhang length of one inch and the bearing length of 6 inches, the lengths of the holes are 3, 5, and 7 inches. Figure 7-14 shows the position of the holes. The results are presented in Table 7-11 in terms of LPF. Even though a slight capacity increase is observed with having a bent plate, the capacity of the beam end is the same when the hole is located over the entire bearing. When the hole is located over a maximum of 83% of the bearing length, the beam end capacity is about 58% of the as-designed capacity. When the hole extended over the entire bearing, at least 41% of the as-designed capacity remains. As indicated by the results, hole height does not affect the load capacity. Hole length has a significant impact on the beam end capacity. Web imperfections exceeding 50% have a minimal impact on the beam end capacity. When the hole is over the entire bearing length, the beam end capacity is insensitive to the imperfection amplitude (i.e., the web out-of-plane deformation).

The capacity of a beam end with 14% hole height, various hole lengths as defined in Table 7-11, and the imperfection amplitudes of 50%, 75%, and 100% of t_w, are calculated using the equations in the MassDOT Bridge Manual. A significant difference is observed between the values calculated using MassDOT (2025) equations and those obtained from the buckling analysis

conducted in this study. The possible reasoning for this difference is discussed in Section 7.5.2.3 of this report.

Table 7-11. LPF for Nominal Web Crippling Resistance of Beam Ends with Holes Located Within the Overhang and Over the Bearing, N = 6 in., I=0.5t_w, 0.75t_w, 1t_w

	I (%)	HL = (OH + x)		Hole Height, HH (% of the web height)					MassDOT Bridge Manual Part I 100th Anniversary Edition		
		OH (in.)	x (in.)	0	3.50	7	10.5	14	t_{ave} (in.)	Capacity (kip)	LPF
LPF for beams without a bent plate	50	1	N/3	0.67	0.64	0.64	0.64	0.64	0.36	94	0.40
			2N/3	0.67	0.61	0.60	0.59	0.58	0.24	52	0.22
			N	0.67	0.41	0.41	0.41	0.41	0.12	20	0.08
	75		N/3	0.63	0.61	0.61	0.61	0.61	0.36	87	0.38
			2N/3	0.63	0.58	0.58	0.57	0.56	0.24	45	0.20
			N	0.63	0.41	0.41	0.41	0.41	0.12	15	0.06
	100		N/3	0.60	0.57	0.57	0.57	0.58	0.36	87	0.38
			2N/3	0.60	0.56	0.56	0.56	0.56	0.24	45	0.20
			N	0.60	0.41	0.41	0.41	0.41	0.12	15	0.06
LPF for beams with a bent plate	50	1	N/3	0.78	0.72	0.72	0.72	0.71	0.36	94	0.40
			2N/3	0.78	0.63	0.62	0.61	0.60	0.24	52	0.22
			N	0.78	0.41	0.41	0.41	0.41	0.12	20	0.08

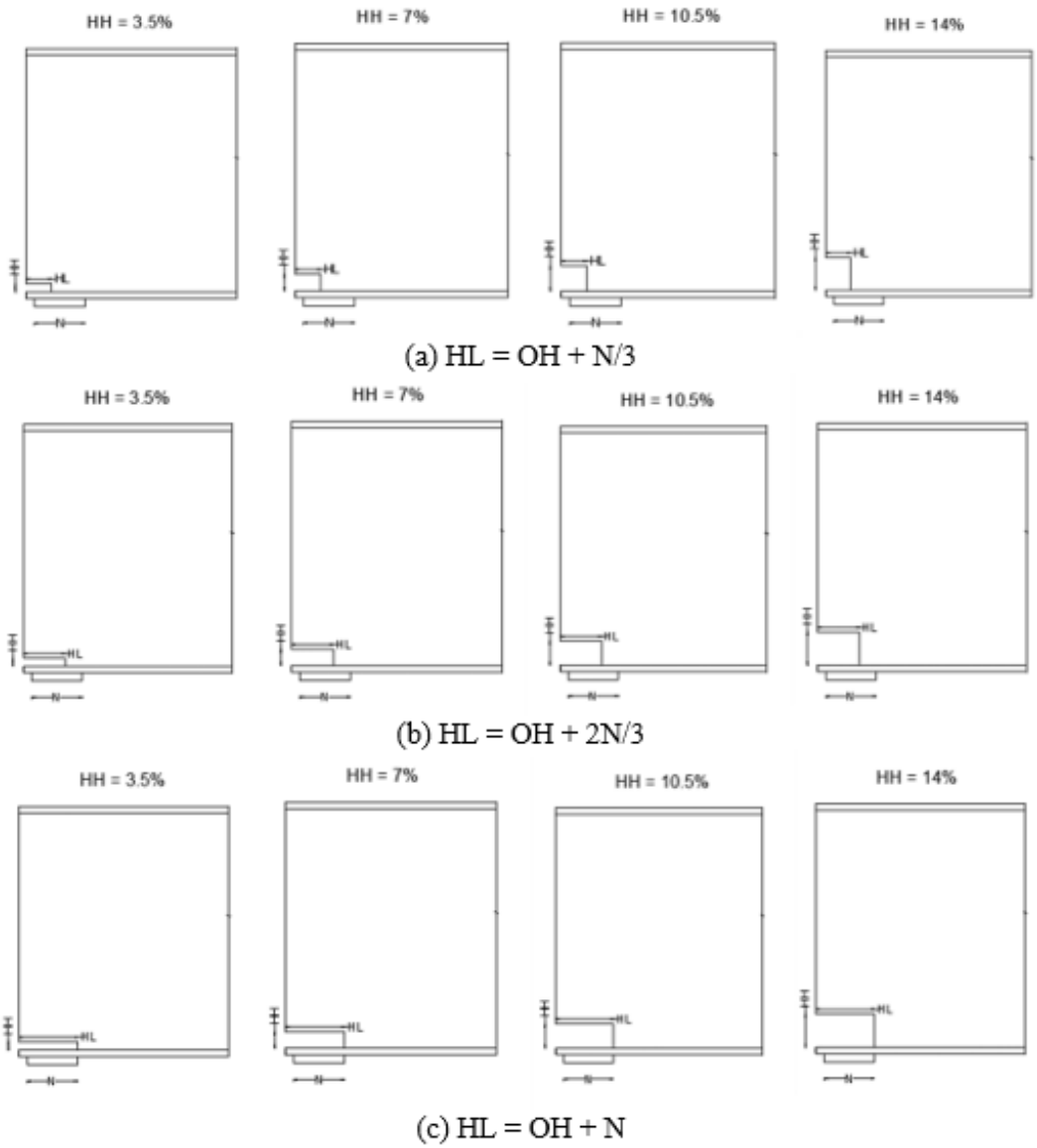

Figure 7-14. Holes located within the overhang and over the bearing.

7.5.2.3 Holes Located Over the Bearing

Figure 7-15 shows the position of the holes over the bearing. The hole length over the bearing is calculated as N/3, 2N/3, and N. With a bearing length of 6 inches, the lengths of the holes are 2, 4, and 6 inches. The results are presented in Table 7-12 in terms of LPF. Even though a slight capacity increase is observed with having a bent plate, the capacity of the beam end with and without a bent plate is the same when the hole is located over the entire bearing length. When the hole extended over the entire bearing, at least 46% of the as-designed capacity remains. The magnitude of imperfection greater than 50% has a minimal impact on the beam end capacity.

When the hole is located over the entire length of the bearing, the beam end capacity is not affected by the magnitude of the imperfection.

As presented in the table, the remaining capacity of the beam end is 63% when the hole length over the bearing is 4 in. (2N/3 or 67%N). There is a 37% reduction in capacity. Tzortzinis et al. (2019) obtained similar results when evaluating the impact of holes on beam end capacity. According to their experience with finite element analysis, a 30% capacity reduction was observed when using a hole length of 70% of the bearing length and a hole height of 10% of the web height. Their findings on specific analysis cases are similar to the results presented in this section. However, a significant difference is observed between the values calculated using MassDOT (2025) equations and those obtained from the buckling analysis conducted in this study. Even though the equations and procedures presented in the MassDOT Bridge Manual (MassDOT 2025) are an outcome of the Tzortzinis et al. work, the results for many cases presented in this report do not correlate well with the values calculated using the MassDOT (2025) equations. This is because Tzortzinis et al. established the factors and derived the equations covering an extensive array of hole configurations, including several extreme cases that are not practically possible when structural deformation limits are considered.

Table 7-12. LPF for Nominal Web Crippling Resistance of Beam Ends with Holes Located Over the Bearing, N = 6 in., I=0.5t_w, 0.75t_w, 1t_w

	I (%)	HL (in.)	Hole Height, HH (% of the web height)					MassDOT Bridge Manual Part I 100th Anniversary Edition		
			0	3.50	7	10.5	14	t_{ave} (in.)	Capacity (kip)	LPF
LPF for beams without a bent plate	50	N/3	0.67	0.65	0.65	0.65	0.65	0.42	117	0.50
		2N/3	0.67	0.63	0.63	0.63	0.63	0.30	71	0.31
		N	0.67	0.51	0.49	0.47	0.47	0.18	35	0.15
	75	N/3	0.63	0.62	0.62	0.62	0.62	0.42	112	0.48
		2N/3	0.63	0.60	0.59	0.59	0.59	0.30	65	0.28
		N	0.63	0.51	0.48	0.46	0.46	0.18	29	0.12
	100	N/3	0.60	0.58	0.58	0.58	0.58	0.42	112	0.48
		2N/3	0.60	0.57	0.57	0.57	0.57	0.30	65	0.28
		N	0.60	0.51	0.48	0.46	0.46	0.18	29	0.12
LPF for beams with a bent plate	50	N/3	0.78	0.75	0.75	0.75	0.75	0.42	117	0.50
		2N/3	0.78	0.70	0.69	0.67	0.66	0.30	71	0.31
		N	0.78	0.51	0.50	0.47	0.47	0.18	35	0.15

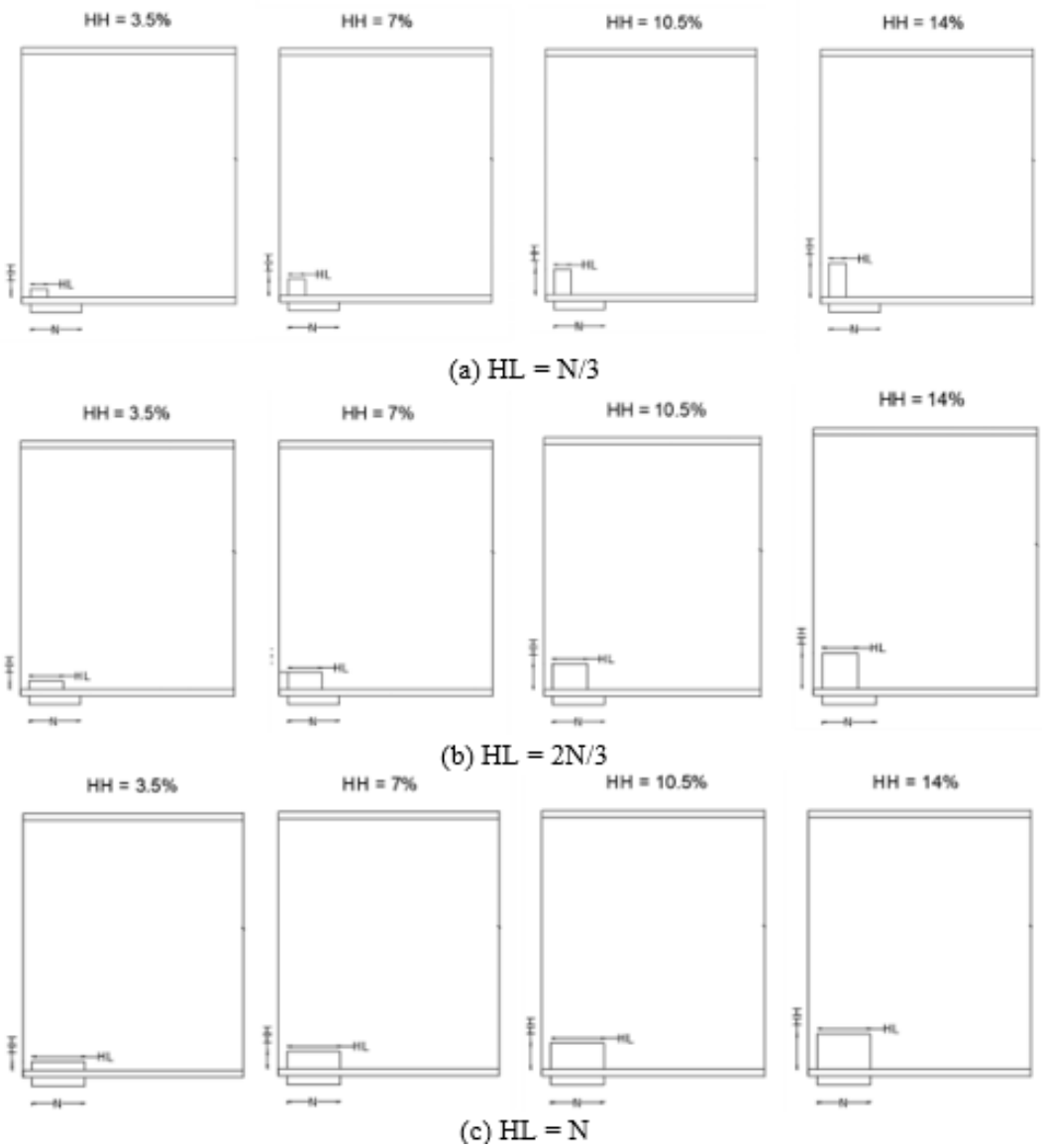

Figure 7-15. Holes located over the bearing.

7.5.2.4 Holes Starting at the Middle of the Bearing

Figure 7-16 shows the position of the holes over the bearing. The hole length is set to be half the bearing length, N/2, and extended by a length proportional to the bearing length, N/3 and 2N/3. Therefore, the ratio between the hole length HL and the bearing length *N* is: 0.50 (HL = N/2), 0.83 (HL = N/2 + N/3 = 5N/6), and 1.16 (N/2 + 2N/3 = 7N/6). The results are presented in Table 7-13 in terms of LPF. The results are similar to those in the previous cases, with the least capacity being 38% of the as-designed capacity.

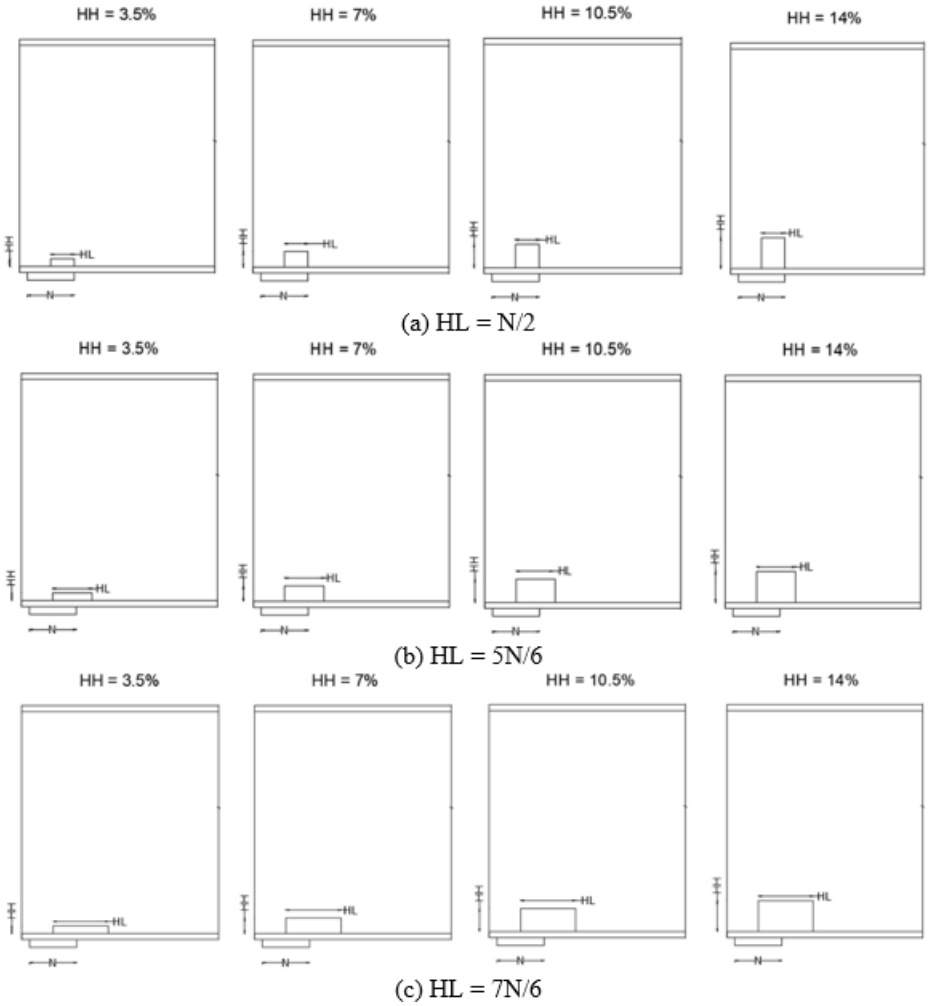

Figure 7-16. Holes starting at the middle of the bearing and extending towards the span.

Table 7-13. LPF for Nominal Web Crippling Resistance of Beam Ends with Holes Starting at the Middle of the Bearing and Extending Towards the Span, N = 6 in., I=0.5t_w, 0.75t_w, 1t_w

	I (%)	HL (in.)	Hole Height, HH (% of the web height)					MassDOT Bridge Manual Part I 100th Anniversary Edition		
			0	3.50	7	10.5	14	t_{ave} (in.)	Capacity (kip)	LPF
LPF for beams without a bent plate	50	N/2	0.67	0.62	0.62	0.62	0.62	0.36	93	0.40
		5N/6	0.67	0.57	0.56	0.54	0.52	0.24	52	0.23
		7N/6	0.67	0.51	0.49	0.47	0.40	0.12	20	0.09
	75	N/2	0.63	0.59	0.59	0.58	0.58	0.36	87	0.38
		5N/6	0.63	0.55	0.54	0.53	0.51	0.24	45	0.20
		7N/6	0.63	0.50	0.47	0.46	0.38	0.12	15	0.06
	100	N/2	0.60	0.57	0.57	0.56	0.56	0.36	87	0.38
		5N/6	0.60	0.53	0.53	0.51	0.50	0.24	45	0.20
		7N/6	0.60	0.48	0.47	0.45	0.38	0.12	15	0.06
LPF for beams with a bent plate	50	N/2	0.78	0.69	0.69	0.68	0.67	0.36	93	0.40
		5N/6	0.78	0.60	0.58	0.56	0.53	0.24	52	0.23
		7N/6	0.78	0.52	0.50	0.47	0.44	0.12	20	0.09

7.5.2.5 Recommendations for Unstiffened Beam Ends with Holes

The above analysis cases showed that the hole length has a significant impact on the beam end capacity. Considering that the hole is located within the bottom 4 inches of the web height, and the web crippling resistance is controlling, the remaining capacity can be calculated by multiplying the capacity of the as-designed beam by the following resistance factors. These factors are suggested based on the largest hole size and the web out-of-plane deformation (i.e., 100% imperfection) used for the analysis.

- If $\frac{HL}{N} \leq 0.80$

  $\phi = 0.50$

- Otherwise

  $\phi = 0.38$

The implementation of these recommendations requires accurate documentation of the hole sizes and their locations. When the holes are not located within the bottom 4 inches of the web height, a refined analysis is needed to assess the capacity. When the beam end capacity is controlled by web yielding, the beam end capacity can be calculated using the average web thickness defined in Eq. 7-18.

7.5.3 Stiffened Beam Ends with Holes

The beam end was modeled with one stiffener on each side over the bearing, as shown in Figure 7-2 and Figure 7-17. The stiffener has a thickness of 7/16 in. = 0.4375 in., which is the minimum thickness recommended in the MDOT Bridge Design Manual Art. 7.02.11.A. The stiffener width is 5.25 in. and 1 in. × 1 in. corners at the top and bottom were clipped for the fillet weld.

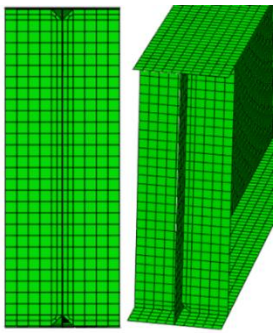

Figure 7-17. Finite element model of a beam end with bearing stiffeners.

7.5.3.1 As-Designed Beam End with Bearing Stiffeners

The beam model used for previous analyses was modified by adding two stiffeners, one on each side of the web at the bearing centerline. Figure 7-18 shows the first five mode shapes and the first mode shape contribution to the buckling capacity. Table 7-14 presents analysis results without imperfections and with an imperfection amplitude ranging from 25% to 100% of the web thickness. The load proportionality factor, LPF, is calculated as the ratio of the capacity calculated using finite element models and the theoretical solution (axial resistance). The numerical results are slightly greater than the theoretical solution, primarily due to the contribution of an additional cross-sectional area that is not considered in the theoretical calculations. Also, the imperfection amplitudes greater than 25% do not impact the axial resistance of the bearing stiffeners defined in Section 7.4.2.3 of this report.

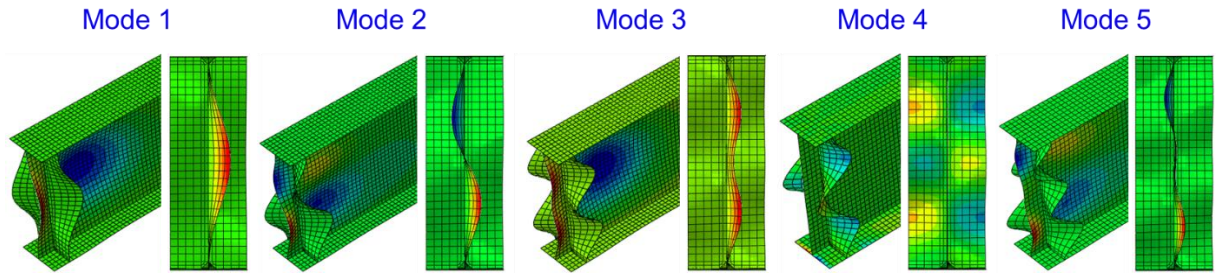

Figure 7-18. Mode shapes of a stiffened beam end.

Table 7-14. LPF for the Nominal Axial Resistance of Stiffened Beam Ends

Stiffened Beam End	Failure Load (kips)	LPF
Nominal axial resistance (theoretical)	470	
Without imperfection	507	1.08
With 25% imperfection	500	1.06
With 50% imperfection	500	1.06
With 75% imperfection	500	1.06
With 100% imperfection	500	1.06

7.5.3.2 Stiffened Beam End with Holes

Figure 7-19 shows the locations of holes at the stiffened beam ends. Rectangular shapes were used in the finite element models to represent these holes. The hole heights are taken as a percentage of the web height (3.5%, 7%, 10.5%, and 14%).

(a) Web section loss between the beam end and the stiffener

(b) Web section loss towards the span of the stiffener

(c) Web section loss on both sides of the stiffener

(d) Stiffener section loss at the bottom flange

Figure 7-19. Holes at stiffened beam ends.

7.5.3.2.1 Holes Located between the Beam End and the Stiffener

Figure 7-20 defines the length and height of the hole located between the beam end and the bearing stiffeners. With a stiffener thickness of 0.4375 in., a bearing length of 6 in., and an overhang of 1 in., the hole length is approximately 3.78 in. The results are presented in Table 7-15 in terms of LPFs calculated with respect to the axial resistance of 507 kips. As shown in the table, the remaining capacity of the beam end is 76%, even with a complete section loss that is 4 inches tall and 3.78 inches long.

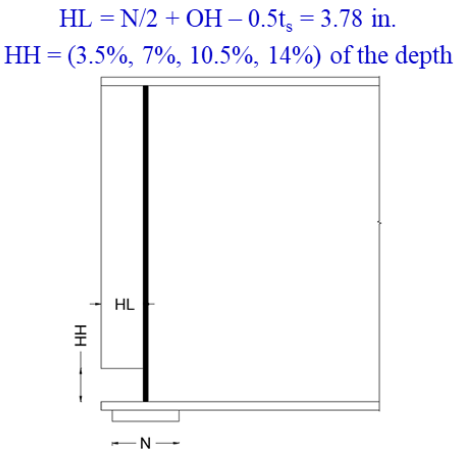

Figure 7-20. Holes located between the beam end and the stiffener.

Table 7-15. LPF for the Nominal Axial Resistance of Beam Ends with Holes Located between the Beam End and the Stiffener, N = 6 in., I=0.5t_w, 0.75t_w, 1t_w

HL (in.)	I (%)	Hole Height, HH (% of the web height)				
		0	3.50	7	10.5	14
3.78	50	0.98	0.78	0.78	0.77	0.76
	75	0.98	0.77	0.77	0.77	0.76
	100	0.98	0.77	0.77	0.77	0.76

7.5.3.2.2 Holes Located Towards the Span from the Stiffener

Figure 7-21 shows two configurations of holes used in this analysis. The results are presented in Table 7-16 in terms of LPFs. As shown in the table, the remaining capacity of the beam end is 74%, even with a complete section loss that is 4 inches tall and 4.78 inches long.

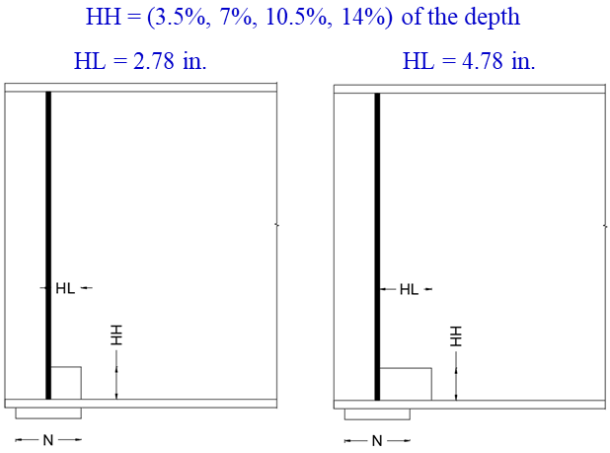

Figure 7-21. Holes located towards the span from the stiffener.

Table 7-16. LPF for the Nominal Axial Resistance of Beam Ends with Holes Located Towards the Span from the Stiffener, N = 6 in., I=0.5t_w, 0.75t_w, 1t_w

HL (in.)	I (%)	Hole Height, HH (% of the web height)				
		0	3.50	7	10.5	14
2.78	50	0.98	0.83	0.83	0.82	0.82
	75	0.98	0.80	0.79	0.79	0.79
	100	0.98	0.80	0.79	0.79	0.79
4.78	50	0.98	0.74	0.74	0.74	0.74
	75	0.98	0.74	0.74	0.74	0.74
	100	0.98	0.74	0.74	0.74	0.74

7.5.3.2.3 Holes Located on Both Sides of the Stiffener

In this configuration, the hole starts at the beam end and extends beyond the stiffener towards the span (Figure 7-22). One hole ends at the edge of the bearing on the span side. The other hole extends by N/3 beyond the bearing towards the span. With the bearing length of 6 in. and the stiffener thickness of 0.4375 in., the hole lengths are 6.5625 in. and 8.5625 in., respectively.

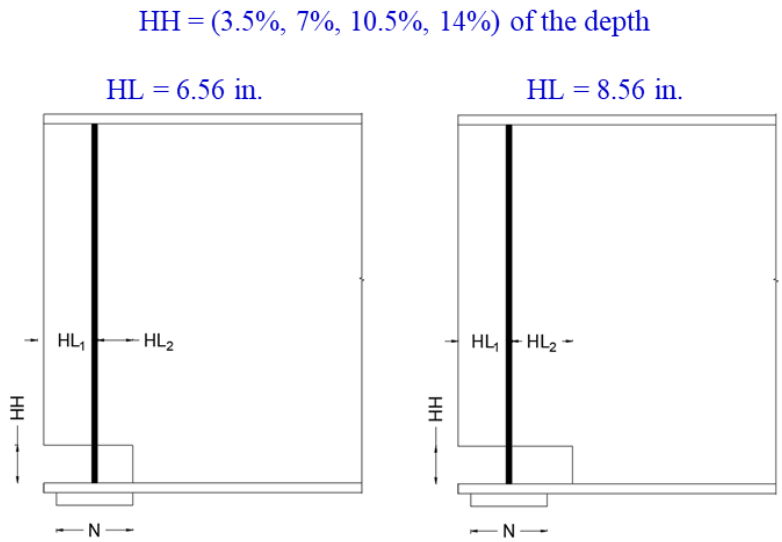

Figure 7-22. Holes located on both sides of the stiffener.

The results are presented in Table 7-17 in terms of LPFs calculated with respect to the axial resistance of 507 kips. As shown in the table, the remaining capacity of the beam end is 39% with a complete section loss that is 4 inches tall and 8.56 inches long. This hole extends 1.56 inches beyond the bearing towards the span.

Table 7-17. LPF for the Nominal Axial Resistance of Beam Ends with Holes Located on Both Sides of the Stiffener, N = 6 in., I=0.5t_w, 0.75t_w, 1t_w

HL (in.)	I (%)	Hole Height, HH (% of the web height)				
		0	3.50	7	10.5	14
6.5625	50	0.98	0.62	0.61	0.44	0.42
	75	0.98	0.59	0.59	0.42	0.41
	100	0.98	0.59	0.58	0.42	0.41
8.5625	50	0.98	0.52	0.50	0.41	0.39
	75	0.98	0.52	0.50	0.41	0.39
	100	0.98	0.52	0.50	0.41	0.39

7.5.3.2.4 Holes at the Bottom of the Stiffener

Figure 7-23 shows a hole located at the bottom of one of the stiffeners. This particular configuration is selected because extensive damage to both stiffeners results in an unstiffened beam end. According to the results shown in Table 7-18, with only one stiffener being damaged, the beam end still possesses 79% of the nominal axial resistance of the undamaged beam end.

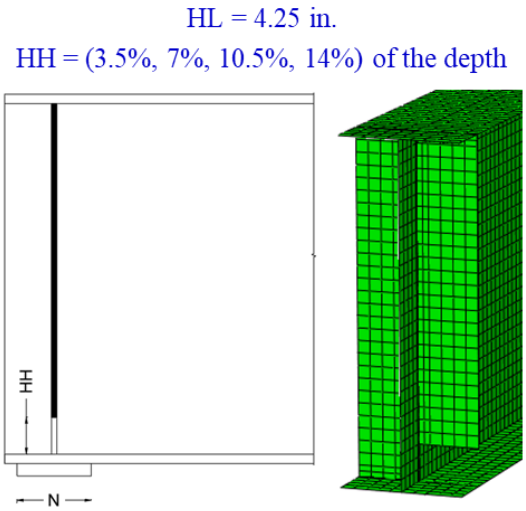

Figure 7-23. A hole at the bottom of one stiffener.

Table 7-18. LPF for the Nominal Axial Resistance of Beam Ends with Holes Located at the Bottom of a Stiffener, N = 6 in., I=0.5t_w, 0.75t_w, 1t_w

HL (in.)	I (%)	Hole Height, HH (% of the web height)				
		0	3.50	7	10.5	14
4.25	50	0.98	0.81	0.79	0.79	0.79
	75	0.98	0.78	0.78	0.77	0.76
	100	0.98	0.78	0.78	0.77	0.76

7.5.3.3 Recommendations for Stiffened Beam Ends with Holes

From the above four analysis cases, the remaining capacity can be estimated by multiplying the capacity of the as-designed beam by a load factor, ϕ, as per the following criteria. These factors are suggested based on the largest hole size and the web out-of-plane deformation (i.e., 100% imperfection) used for the analysis.

- When the hole is located on both sides of the bearing stiffener,

  $\phi = 0.39$

- Otherwise

  $\phi = 0.74$

The implementation of these recommendations requires accurate documentation of the hole sizes and their locations. When the holes are not located within the bottom 4 inches of the web height, a refined analysis is needed to assess the capacity. The *MDOT Web Deterioration Check* spreadsheet was updated using the factors presented in this chapter and submitted as a deliverable of this project.

8 LONGEVITY AND FATIGUE PREDICTION OF BOLTED STEEL REPAIRS

Scoping inspections documented cracking at beam ends with bolted repairs, as shown in Figure 8-1 and Figure 8-2. As discussed in Chapter 2, bolted repairs are provided due to section loss at the beam ends. Section loss increases the surface roughness of the section, increasing the potential for fatigue cracking. This required developing a procedure for evaluating the fatigue life of the steel beam end with bolted repairs.

4" long crack in bottom of web w/ arrestor hole; 63% loss of section in web; 38% loss of section in bottom flange

Beam 7s
Pier 1w
Span 1w

Figure 8-1. Beam end with a 4 in. long crack (STR 10907).

4.5" long crack in bottom of web w/ arrestor hole; 34% loss of section in web

Beam 8s
Pier 1w
Span 1w

Figure 8-2. Beam end with a 4.5 in. long crack (STR 10907).

The above details are taken from the bridge STR 10907. According to the original plans, this bridge has three spans, each with eight W30×108 steel beams, a beam spacing of 6 ft, and a span length of 53.07 ft.

The fatigue life can be defined as the predicted period of time to cause fatigue failure under the application of the design or assessment load spectrum (Kühn et al. 2008). The stress-life (S-N) curves and fracture mechanics-based approaches are commonly used for evaluating fatigue life. The stress-life method uses alternating stress cycles to calculate fatigue life using Miner's Rule. Fracture mechanics can characterize the fatigue life, from an observable crack or flaw, to complete failure of the component (Skoglund 2022). A crack initiates when the stress intensity factor K is greater than the threshold stress intensity factor, K_{th}. Once a crack has initiated, Paris Law utilizes the stress intensity factor and material constants, C and m, to determine the number of cycles to propagate a crack a certain distance (Lozano and Riveros 2021). During this stage, the fatigue life is usually determined by using the following Paris Law formula:

$$\frac{da}{dN} = C(\Delta K)^m$$

where:

a = crack size

ΔK = range of the stress intensity factor

C and m are constants based on the material, stress ratio, and environment

As discussed in Bannantine et al. (1990), the environment, surface treatment, surface finish, temperature, and loading influence fatigue life. As will be shown later, it is possible to consider the surface finish/treatment by defining the surface finish factor, K_t, which is related to the manufacturing process (i.e., hot rolling) or the surface roughness, R_a. As shown in Figure 8-3, the AASHTO LRFD (2020) recommends maintaining a surface roughness of 1,000 μ-in. or less to minimize the impact on the fatigue life. Based on R_a and the specified minimum tensile strength, F_u, the surface factor, K_f (i.e., $1/K_t$), can be determined from the plot shown in Figure 8-4. For 58 ksi ultimate tensile strength of steel and the surface roughness of 1000 μ-in., $K_f \cong 0.8$, and the corresponding $K_t = 1/0.8 \cong 1.3$. In fact, K_f and K_t represent the same characteristics. However, K_t, is the value used in *fe-safe*, the fatigue life calculation software, to match the program algorithm. It should also be noted that the fatigue life evaluation performed in *fe-safe* provides the *LOGLife-Repeats* contours, showing the critical locations/regions. The surface finish factor can be used to highlight a critical location/region in a component. For the evaluation of fatigue life of beam ends with bolted steel repair, surface finish factors of 1, 1.3, and 1.5 are considered, representing

polished surfaces, the surface roughness of 1000 μ-in., and the surface roughness slightly greater than 2000 μ-in. In this study, the fatigue life evaluation was conducted in *fe-safe* using finite element analysis (FEA) results from Abaqus.

Description	Category	Constant A $(ksi)^3$	Threshold $(\Delta F)_{TH}$ ksi	Potential Crack Initiation Point	Illustrative Examples
Section 1—Plain Material away from Any Welding					
1.1 Base metal, except noncoated weathering steel, with rolled or cleaned surfaces, or base metal with thermal-cut edges with a surface roughness value of 1,000 μ-in. or less, but without re-entrant corners.	A	250×10^8	24	Away from all welds or structural connections	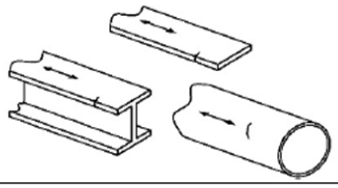
1.2 Noncoated weathering steel base metal with rolled or cleaned surfaces designed and detailed in accordance with FHWA (1989), or noncoated weathering steel base metal with thermal-cut edges with a surface roughness value of 1,000 μ-in. or less, but without re-entrant corners.	B	120×10^8	16	Away from all welds or structural connections	

Figure 8-3. Surface roughness for specific fatigue detail categories (LRFD Table 6.6.1.2.3-1).

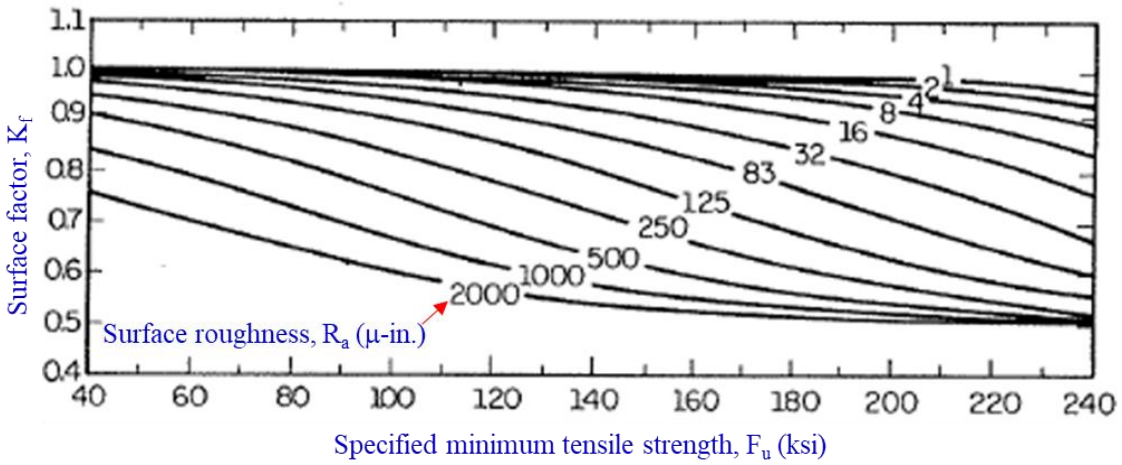

Figure 8-4. Variation of surface factor against surface finish and tensile strength of steel (Bannantine et al. 1990).

8.1 MODELING AND ANALYSIS OF STEEL BEAM ENDS WITH BOLTED REPAIRS

8.1.1 Geometry and Material Properties

The cross-sectional dimensions of the W30×108 section are summarized in Table 8-1.

Table 8-1. W30×108 Steel Beam Section Properties

Geometry	Dimensions
Depth (in.)	29.8
Thickness of the bottom flange (in.)	0.76
Thickness of the top flange (in.)	0.76
Thickness of the web (in.)	0.545
Width of the bottom flange (in.)	10.5
Width of the top flange (in.)	10.5
Fillet radius (in.)	0.65

The repair has eight bolts, as shown in Figure 8-5, and an end diaphragm is connected to the stiffener. For the bolted steel repair, the following dimensions are considered:

- Bolt diameter = 0.75 in. (19 mm)
- Bolt hole diameter = 0.825 in. (21 mm)
- Space between centerline of bolts = 2.95 in. (75 mm)
- Thickness of the plate = 0.375 in.

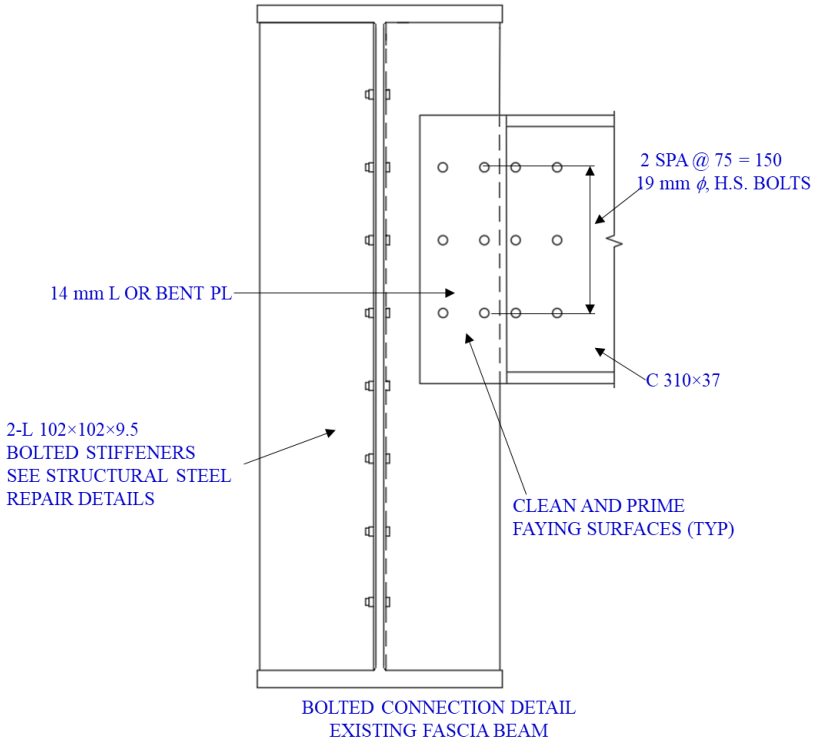

Figure 8-5. Bolted repair detail (STR 10907).

Table 8-2 shows the suggested material properties in literature for this particular steel beam. After the table, the selected material properties for analysis are listed.

Table 8-2. Material Properties for ASTM A373 steel (FHWA-HRT-21-020, Table 2)

ASTM	Year	Yield strength, F_y (ksi)	Tensile strength, F_u (ksi)
A 373	1954-1966	32	58-75

- Specified minimum yield strength, F_y = 32 ksi
- Specified minimum tensile strength, F_u = 58 ksi
- Unit weight = 490 lb/ft^3
- Modulus of elasticity, E_s = 29,000 ksi

The following properties are considered for the concrete deck.

- Unit weight = 150 lb/ft^3
- Modulus of elasticity, E_c = 3,987 ksi

8.1.2 Finite Element Modeling

A simply supported beam was modeled with a 50 ft length, as shown in Figure 8-6. At each end, the beam is supported by a steel block of 6 in. (along the length of the girder), as shown in Figure 8-7. The overhang between the beam end and the edge of the bearing is 1 in. An interior beam was considered, and it was assumed that the effective width of the deck was similar to the beam spacing of 6 ft. C3D8R element types are used for all the components. Four elements are used to represent the flange width. The element length of one inch is used along the beam length.

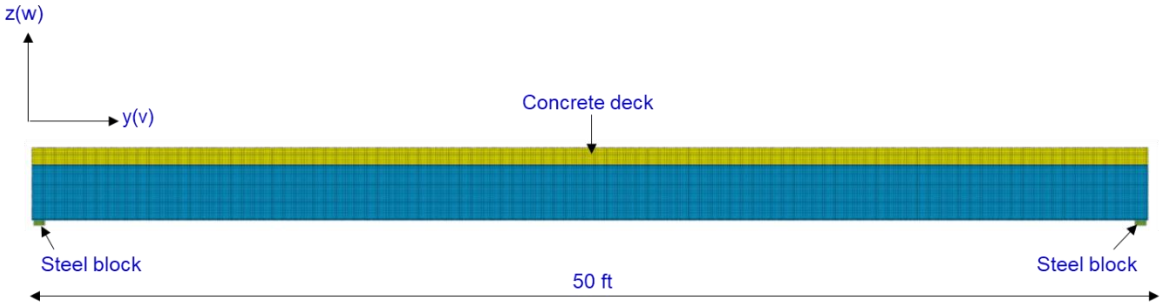

Figure 8-6. Elevation view of the beam.

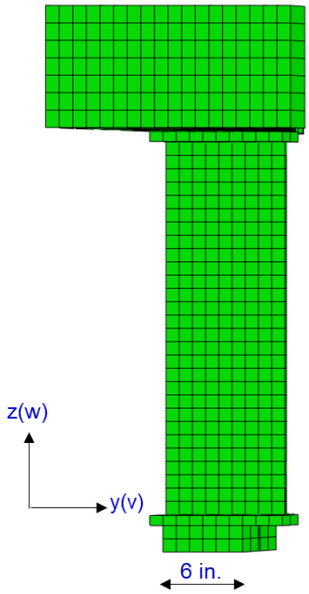

Figure 8-7. Bearing dimension along the length of the beam.

Dead and live loads are considered for this analysis. The dead loads consist of the self-weight of the beam, the self-weight of the deck, the barrier load, and the future wearing surface (FWS). The AASHTO LRFD fatigue truck and 28 Michigan legal truck loads are considered for live loads. As shown in Figure 8-8, only the normal loading was considered for Michigan legal trucks.

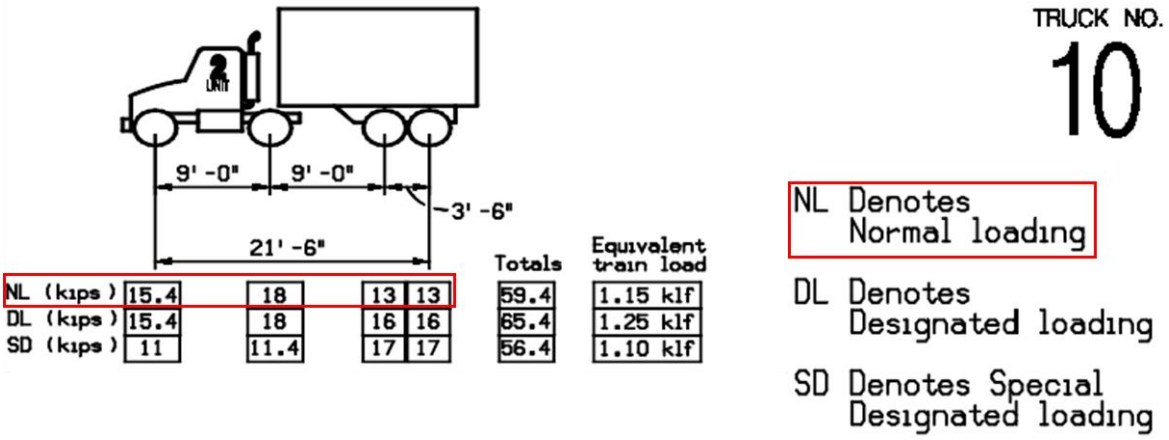

Figure 8-8. Normal loading for the truck No. 10 (MDOT 2009).

Apart from the steel beam and concrete deck, a Type 4 New Jersey barrier, and a 25 lb/ft^2 FWS are considered. The barrier and FWS loads are applied as area loads on the top of the deck. The self-weight of the barrier is distributed equally among all the beams. Since the flexural behavior of the beam with restraints provided by the thick sole plates at the bearing develops tensile stresses to cause fatigue cracking, truck loads are placed within the span to generate the maximum rotation at the bearing. Hence, the distribution factor for the moment, defined in the AASHTO LRFD (2020), is used. For live loads, the following parameters are considered:

- Distribution factor for moment, DFM
- Dynamic load allowance for fatigue and fracture limit state, IM = 15% (LRFD Table 3.6.2.1-1)
- Load factor for fatigue = 1.75 as per the AASHTO LRFD Fatigue I limit state

As for the boundary conditions, the bottom surface of each steel block is restrained to represent a simply supported beam. The bottom surface of one block had all the translations restrained, and the other bottom surface was allowed to move in the longitudinal direction, as shown in Figure 8-9.

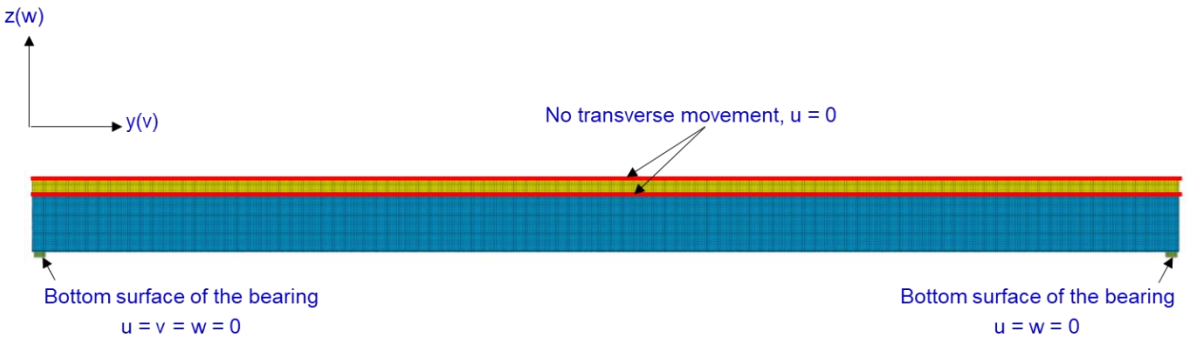

Figure 8-9. Boundary conditions.

8.1.3 Fatigue Life Evaluation Procedure

The scope of work included determining the fatigue life of an uncracked section and identifying the location of any potential cracking. The software, *fe-safe*, provides the fatigue life as the number of cycles. The process begins with importing FEA results and defining material properties, loading conditions, and a fatigue algorithm. The Brown-Miller strain-based fatigue-life algorithm was selected for steel, a ductile material. An important step is to define the loading, which can be based on a stress dataset or a combination of stress and strain datasets. Since the Brown-Miller model can handle plasticity issues, only a stress dataset (elastic) associated with a load history was considered.

As shown in Figure 8-10, *fe-safe* results can be used to identify the critical location and the number of cycles for crack initiation. Results can be validated if the damaged region/critical location corresponds to the one provided by the experiments or FEA results. In this work, FEA results and *LOGLife-Repeats* contours are provided to compare the critical locations identified by the two analyses. In addition to the features described above, *fe-safe* has various options to scale the load

or load history, combine different load histories, and modify surface roughness by defining a surface finish factor.

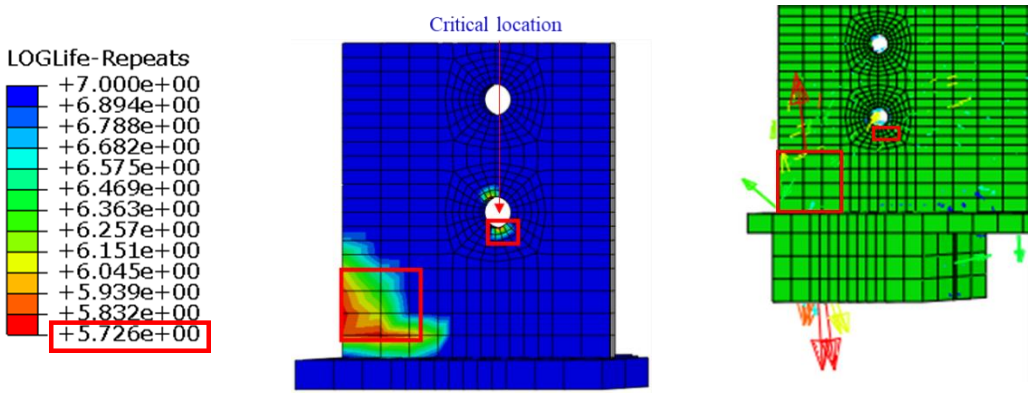

(a) Legend (b) LOGLife-Repeats contour from fe-safe (c) Maximum principal stress symbol plot from Abaqus

Figure 8-10. *LOGLife-Repeats* contour plot and Abaqus results.

8.1.4 Analysis Results

The simply supported beam was modeled with the boundary conditions shown in Figure 8-9. Live loads were applied based on the configuration and position of trucks that provided the greatest rotation at the beam end. For each truck, the critical configuration was determined using SAP2000, and the same configuration was used in Abaqus by placing the axle loads at the corresponding positions. The analysis cases included:

- As-designed beam
- Beam with bolt holes at the ends
- Beam with bolt holes having a pre-existing crack
- Beam with a pre-existing crack beneath the bolted steel repair

8.1.4.1 As-Designed Beam

The beam was analyzed using the current AASHTO LRFD fatigue truck and all 28 Michigan legal trucks. A surface finish factor of one is used to represent a smooth surface. Figure 8-11 shows the maximum principal stress at the beam end. The *LOGLife-Repeats* contour is shown in Figure 8-12. The red color and the lowest number indicate the critical area and the fatigue life. According to the results, this beam end could develop a crack after being subjected to 783,429 cycles of Truck #6 loads (i.e., $N = 10^{5.894}$). The critical region shown in the analysis matches the typical crack locations of beam ends without holes, as shown in Figure 8-12(b). The same process was followed for all 28 Michigan legal trucks, and the calculated load cycles for each truck are provided in Table

8-3. The corresponding load cycles under the current AASHTO LRFD fatigue truck were also evaluated, and the results are provided at the end of Table 8-3.

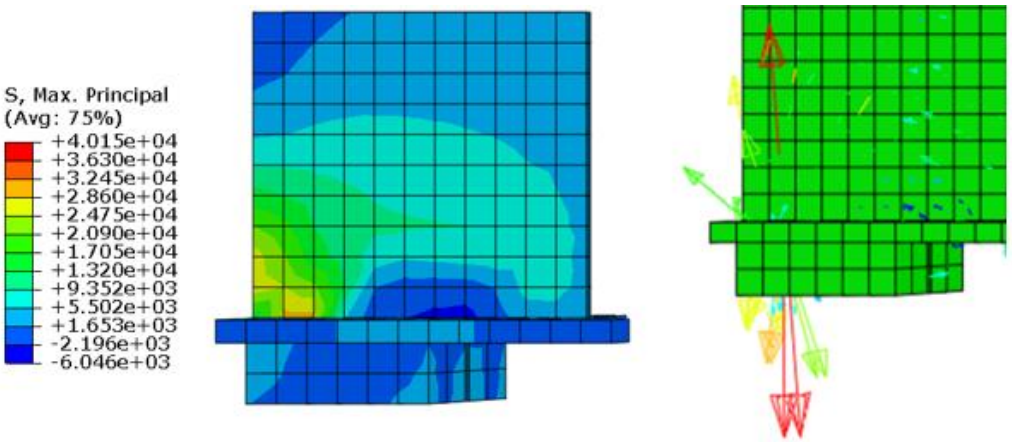

Figure 8-11. The maximum principal stress at the as-designed beam end under truck # 6.

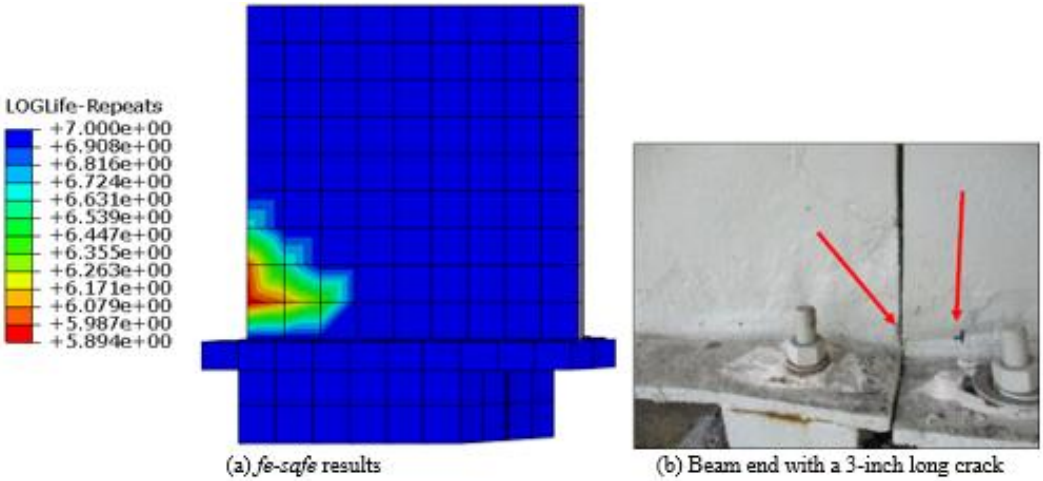

Figure 8-12. *LOGLife-Repeats* plot showing the critical location in red at the beam end.

Table 8-3. Load Cycles for Developing Fatigue Cracking at the As-Designed Beam End Under MI Legal Loads and the AASHTO Fatigue Truck

Truck No.	Number of Cycles, N
1	1.05E+06
2	8.43E+05
3	7.71E+05
4	7.71E+05
5	7.65E+05
6	7.83E+05
7	7.83E+05
8	7.73E+05
9	8.39E+05
10	7.74E+05
11	7.76E+05
12	7.82E+05
13	7.81E+05
14	7.52E+05
15	7.56E+05
16	7.44E+05
17	7.46E+05
18	7.72E+05
19	7.78E+05
20	7.63E+05
21	7.55E+05
22	7.48E+05
23	7.58E+05
24	7.61E+05
25	7.55E+05
26 (AASHTO Type 3)	8.01E+05
27 (AASHTO Type 3S2)	8.11E+05
28 (AASHTO Type 3-3)	9.18E+05
AASHTO Fatigue Truck	8.74E+05

8.1.4.2 Beam End with Bolt Holes

Figure 8-1 shows a crack that started from a bolt hole. The details shown in Figure 8-13 were used to evaluate the potential for developing a fatigue crack at a bolt hole and calculate the number of load cycles required to initiate a crack under MI legal loads and the AASHTO fatigue truck. A surface finish factor of one is used to represent a smooth surface. Greater stresses are developed at the beam end and around the bottom bolt hole, as indicated by the principal stresses shown in Figure 8-14 and the *LOGLife-Repeats* contour shown in Figure 8-15. The number of load cycles required to develop fatigue cracking at the beam end with bolt holes was calculated using 28 Michigan legal trucks and the AASHTO LRFD fatigue truck. As per the results shown in Table 8-4, this detail could develop a fatigue crack with 538,000 load cycles under Truck #6. When

compared with the numbers shown in Table 8-3, the presence of bolt holes alters the stress patterns at the beam end and reduces the number of Truck #6 load cycles required to initiate a crack by 245,000 (i.e., 7.83E+05 – 5.38E+05).

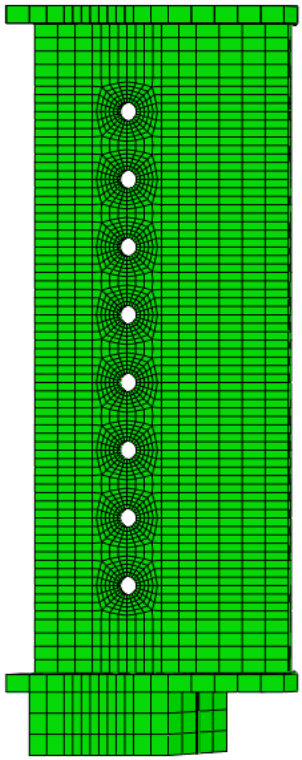

Figure 8-13. Beam end with bolt holes.

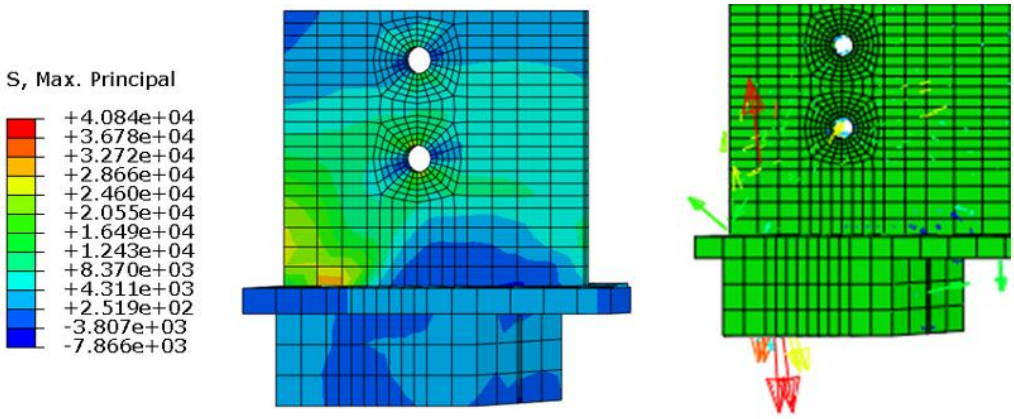

Figure 8-14. Maximum principal stress at the beam end with bolt holes.

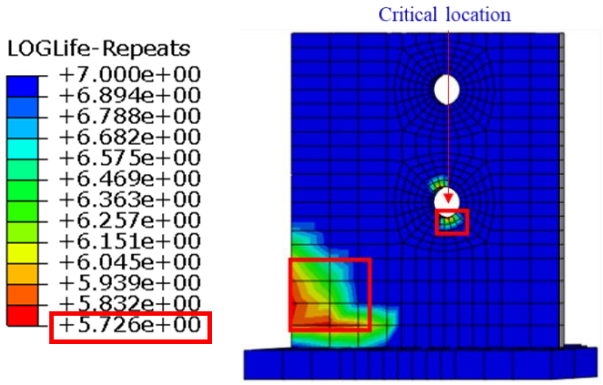

Figure 8-15. ***LOGLife-Repeats*** **plot showing the critical locations in red at the beam end with bolt holes.**

Table 8-4. Load Cycles for Developing Fatigue Cracking at the Beam End with Bolt Holes Under MI Legal Loads and the AASHTO Fatigue Truck

Truck No.	Number of Cycles, N
1	8.47E+05
2	5.70E+05
3	5.65E+05
4	5.22E+05
5	5.17E+05
6	5.38E+05
7	5.38E+05
8	5.27E+05
9	5.68E+05
10	5.69E+05
11	5.51E+05
12	4.83E+05
13	4.81E+05
14	4.59E+05
15	4.57E+05
16	4.54E+05
17	4.51E+05
18	4.76E+05
19	5.08E+05
20	5.45E+05
21	4.78E+05
22	4.99E+05
23	4.55E+05
24	5.41E+05
25	4.81E+05
26 (AASHTO Type 3)	6.03E+05
27 (AASHTO Type 3S2)	6.51E+05
28 (AASHTO Type 3-3)	6.36E+05
AASHTO Fatigue Truck	5.77E+05

8.1.4.3 Beam End with Bolt Holes and a Pre-existing Crack

This analysis case considers a crack at the bolt hole without the influence of bolts and the other repair details. As shown in Figure 8-16, two different crack sizes based on the thickness of the web, t_w, are considered: $0.15t_w$ and t_w. A surface finish factor of one is used to represent a smooth surface.

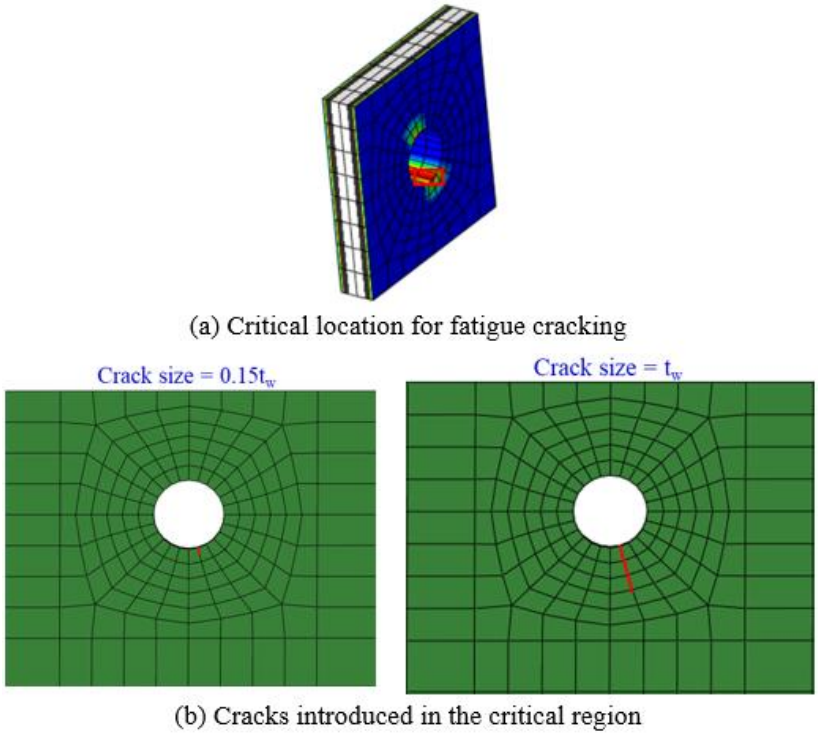

Figure 8-16. Cracks introduced within the critical region of the model.

8.1.4.3.1 Crack size a = $0.15t_w$

Figure 8-17 and Figure 8-18 show analysis results. The STATUSXFEM shows a completely cracked element next to the bolt hole (STATUSXFEM = 1) and a partially cracked element representing an active crack. Additionally, the crack surface is indicated by the PHILSM. It was observed that a crack initiating near the bolt hole can propagate towards the span, as shown in Figure 8-17. As expected, the maximum principal stress contour shows higher stresses at the beam end over the bearing and above the bolt hole, with the highest stress at the crack.

Moreover, the *LOGLife-Repeats* contours shown in Figure 8-18 indicate a greater potential for damage at the beam end over the bearing, top of the bolt hole, and next to the crack tip. The number of load cycles required to develop fatigue cracking at the beam end with bolt holes and pre-existing cracks was calculated using 28 Michigan legal trucks and the AASHTO LRFD fatigue truck. The results are summarized in Table 8-5.

When compared with a section without bolt holes and a section with bolt holes, the presence of a $0.15t_w$ pre-existing crack at the lower bolt hole reduces the number of Truck #6 load cycles required to initiate a crack by 676,000 (i.e., 7.83E+05 – 1.07E+05) and 431,000 (5.38E+05 – 1.07E+05), respectively.

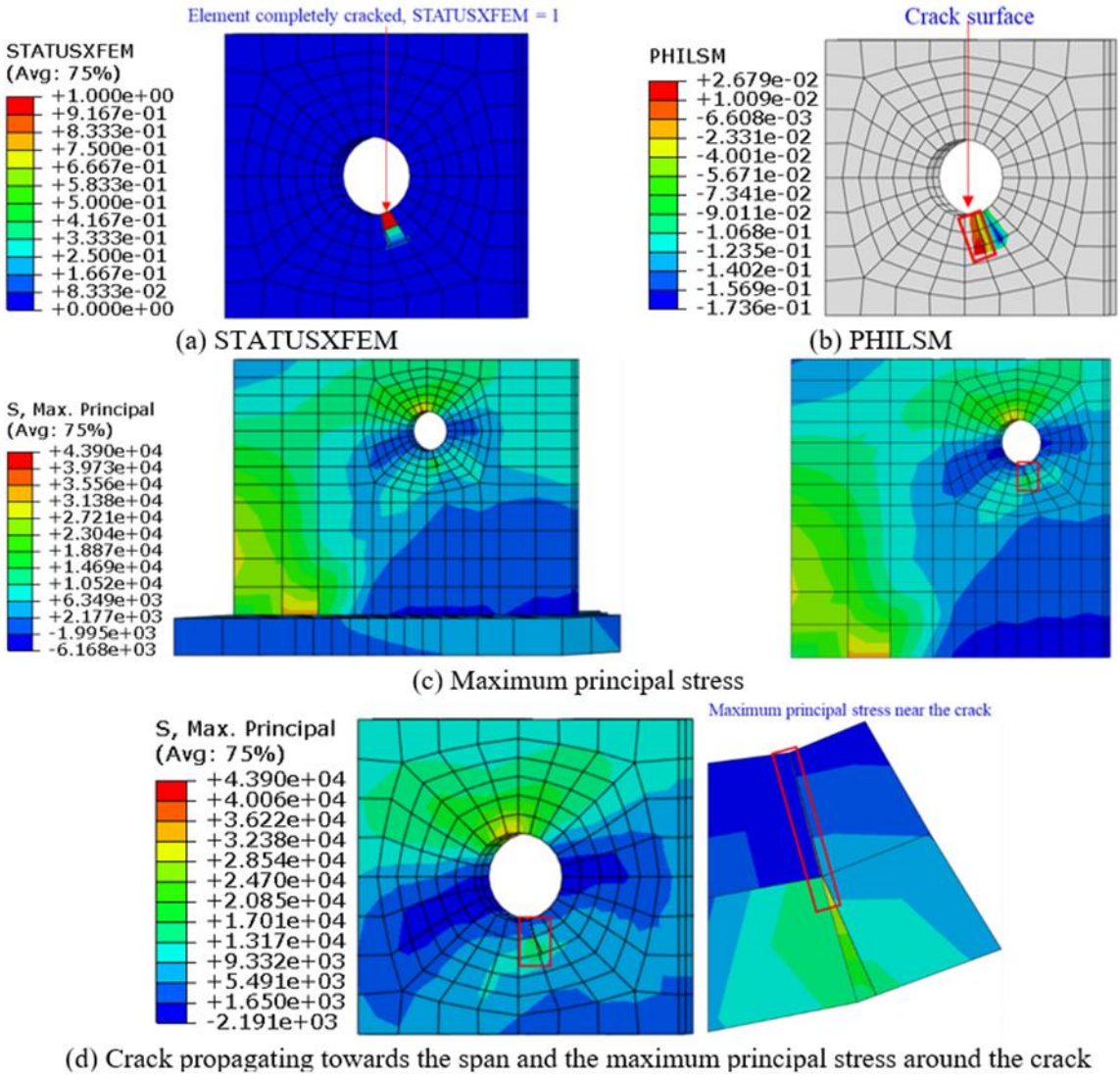

Figure 8-17. FEA results showing an active crack.

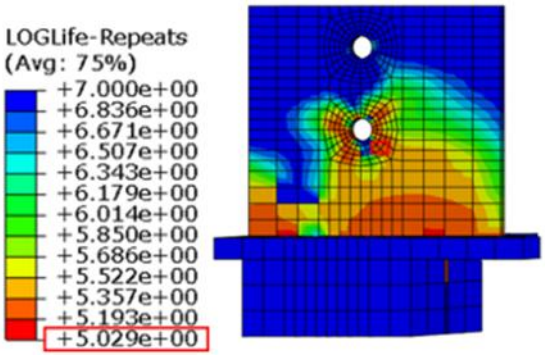

Figure 8-18. *LOGLife-Repeats* contours around a bolt hole with a crack.

Table 8-5. Load Cycles for Developing Fatigue Cracking at the Beam End with Bolt Holes and Pre-existing Crack (a = 0.15t_w) Under MI Legal Loads and the AASHTO Fatigue Truck

Truck No.	Number of cycles, N
1	1.06E+05
2	1.05E+05
3	1.04E+05
4	1.03E+05
5	1.05E+05
6	1.07E+05
7	1.07E+05
8	1.06E+05
9	1.04E+05
10	1.04E+05
11	1.04E+05
12	1.05E+05
13	1.05E+05
14	1.04E+05
15	1.05E+05
16	1.04E+05
17	1.05E+05
18	1.04E+05
19	1.04E+05
20	1.06E+05
21	1.04E+05
22	1.04E+05
23	1.04E+05
24	1.06E+05
25	1.04E+05
26 (AASHTO Type 3)	1.05E+05
27 (AASHTO Type 3S2)	1.06E+05
28 (AASHTO Type 3-3)	1.06E+05
AASHTO Fatigue Truck	1.05E+05

8.1.4.3.2 Crack size a = t_w

As shown in Figure 8-19, the STATUSXFEM shows completely cracked elements along the introduced crack, and the PHILSM shows the crack surface to the left of the crack. It can also be observed that the maximum principal stress is higher at the crack tip, the girder end, and the top of the bolt hole. Figure 8-20 shows the *LOGLife-Repeats* contours. The number of load cycles

required to develop fatigue cracking at the beam end with bolt holes and pre-existing cracks was calculated using 28 Michigan legal trucks and the AASHTO LRFD fatigue truck. The results are summarized in Table 8-6.

When compared with a section without bolt holes, a section with bolt holes, and a section with bolt holes and a $0.15t_w$ long pre-existing crack, the presence of an pre-existing crack at the lower bolt hole with an equivalent crack length of t_w reduces the number of Truck #6 load cycles required to initiate a crack by 764,800 (i.e., 7.83E+05 – 1.82E+04), 519,800 (5.38E+05 – 1.82E+04), and 88,800 (1.07E+05 – 1.82E+04), respectively.

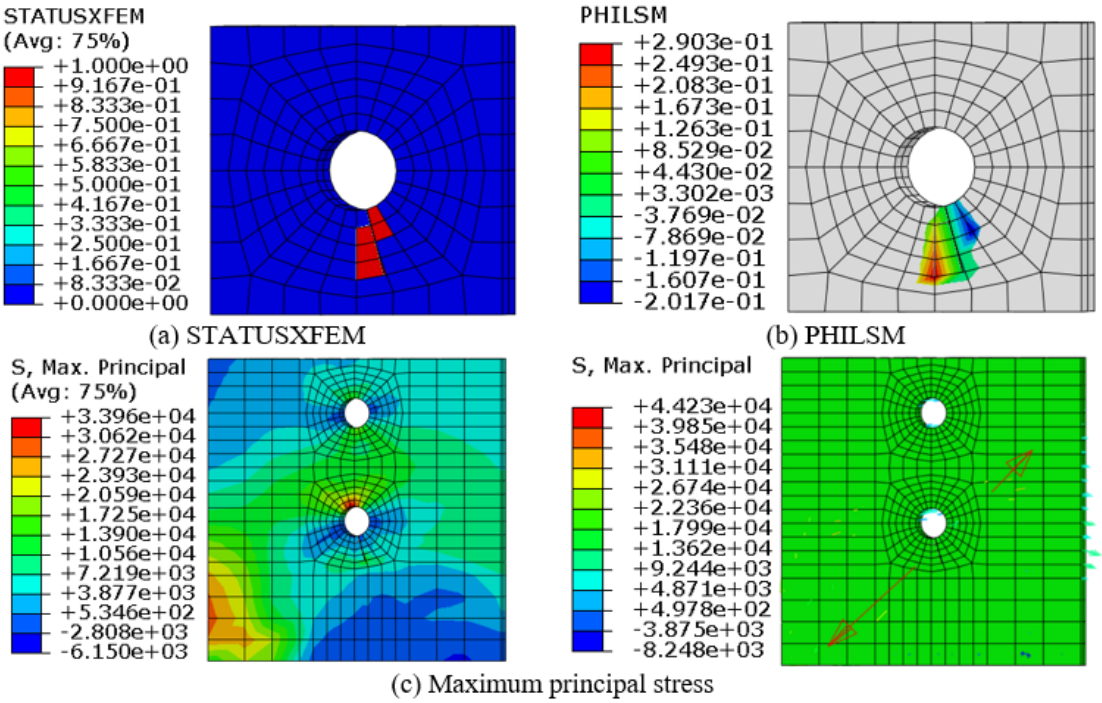

Figure 8-19. FEA results showing an active crack.

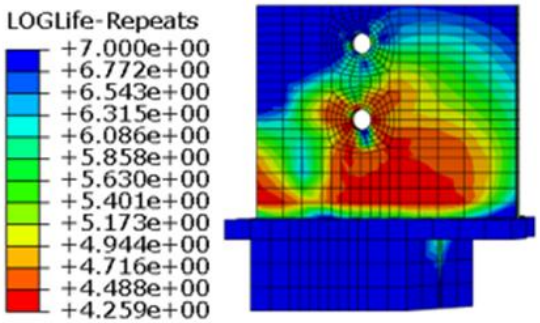

Figure 8-20. *LOGLife-Repeats* contours around a bolt hole with a crack.

Table 8-6. Load Cycles for Developing Fatigue Cracking at the Beam End with Bolt Holes and Pre-existing Crack ($a = t_w$) Under MI Legal Loads and the AASHTO Fatigue Truck

Truck No.	Number of cycles, N
1	2.14E+04
2	1.97E+04
3	1.83E+04
4	1.81E+04
5	1.81E+04
6	1.82E+04
7	1.82E+04
8	1.81E+04
9	1.83E+04
10	1.82E+04
11	1.81E+04
12	1.81E+04
13	1.81E+04
14	1.93E+04
15	1.81E+04
16	1.93E+04
17	1.89E+04
18	1.89E+04
19	1.90E+04
20	1.81E+04
21	1.89E+04
22	1.92E+04
23	1.95E+04
24	1.81E+04
25	1.98E+04
26 (AASHTO Type 3)	1.83E+04
27 (AASHTO Type 3S2)	1.83E+04
28 (AASHTO Type 3-3)	1.84E+04
AASHTO Fatigue Truck	1.99E+04

8.1.4.4 Beam End with a Pre-existing Crack and Bolted Repair

The analysis discussed in Section 0 showed the possibility of initiating a crack at the bottom bolt hole. This section presents the analysis results of a beam end with bolted repair and a pre-existing crack. Figure 8-21 and Figure 8-22 show the beam end with bolted repair and pre-existing cracks. Two crack sizes are considered: $0.15t_w$ and t_w. Unlike in the previous analysis cases, the impact of surface finish, smooth, as-designed (1000 μ-in.), and rough (≅ 2000 μ-in.), is considered by using K_t of 1, 1.3, and 1.5.

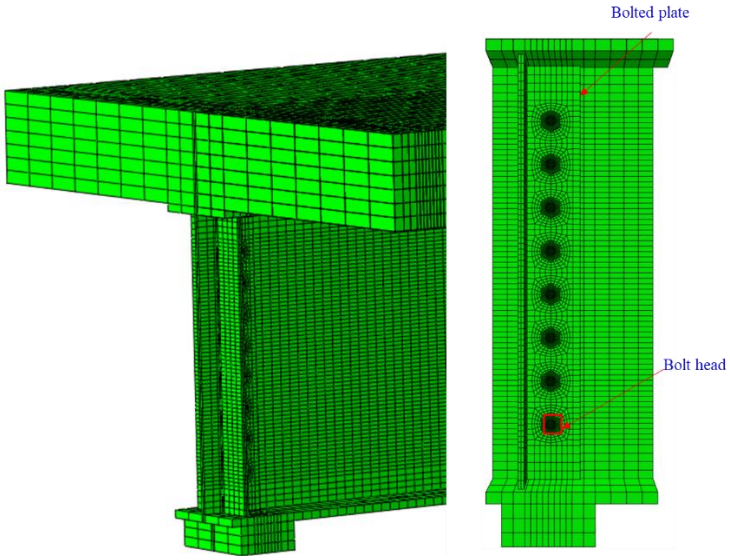

Figure 8-21. Beam end with a bolted repair.

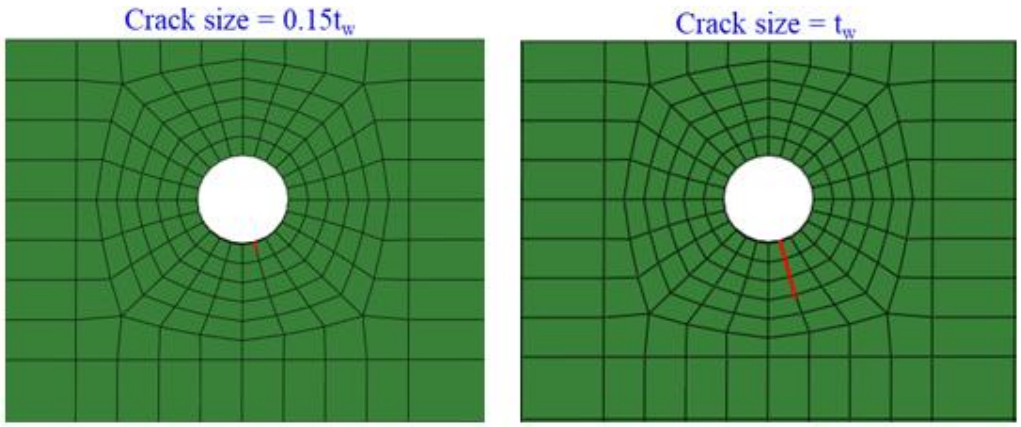

Figure 8-22. Cracks introduced within the critical region to simulate pre-existing cracks.

8.1.4.4.1 Crack size, a = 0.15t_w

The STATUSXFEM, the PHILSM, and the maximum principal stress are shown in Figure 8-23. The *LOGLife-Repeats* contours shown in Figure 8-24 indicate the impact of surface roughness on crack initiation. As shown in the figure, the potential for fatigue crack development increases with the increasing surface roughness around the bolt hole. For example, Figure 8-24(c) features brighter colors just below the bolt hole and extending toward the span, indicating the potential for growing a crack within that region. The number of load cycles required to develop fatigue cracking at the beam end with bolted repairs and pre-existing cracks was calculated using 28 Michigan legal trucks and the AASHTO LRFD fatigue truck. The results are summarized in Table 8-7. Additionally, a chart emulating the format of AASHTO LRFD fatigue curves was developed using the results for different surface finish factors, as shown in Figure 8-25. Having access to weigh-

in-motion data to determine the annual average daily truck traffic (AADTT) on a bridge with similar details, the values in the table or chart can be used with Miner's rule to calculate the fatigue life. An example calculation is provided in Section 8.1.5.

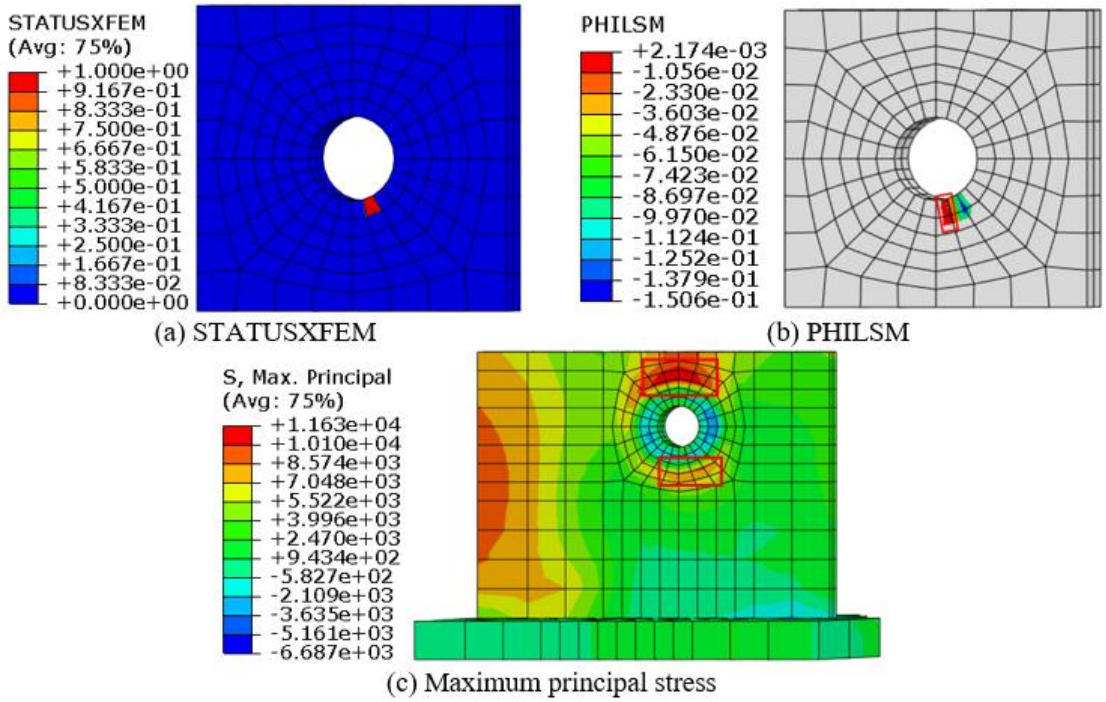

Figure 8-23. FEA stress contours for a beam end with a bolted repair and a pre-existing crack.

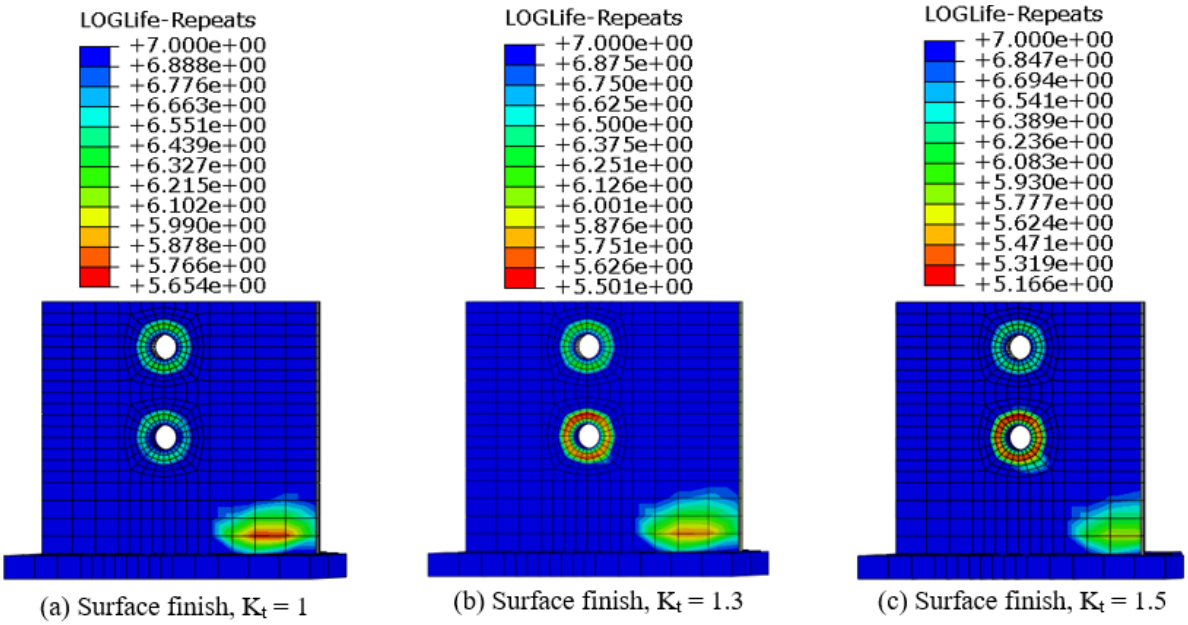

Figure 8-24. *LOGLife-Repeats* contours for beam ends with bolted repairs, pre-existing cracks, and different surface roughness.

Table 8-7. Load Cycles for Developing Fatigue Cracking at the Beam End with Bolted Repair, a Pre-existing Crack (a = 0.15t_w), and Different Surface Roughness Under MI Legal Loads and the AASHTO Fatigue Truck

Truck No.	Number of cycles, N, based on the surface finish factor, K_t		
	K_t = 1	K_t = 1.3	K_t = 1.5
1	8.90E+05	3.54E+05	1.64E+05
2	8.20E+05	3.51E+05	1.62E+05
3	7.43E+05	3.42E+05	1.58E+05
4	7.07E+05	3.25E+05	1.50E+05
5	5.47E+05	3.20E+05	1.48E+05
6	4.50E+05	3.17E+05	1.46E+05
7	4.50E+05	3.17E+05	1.41E+05
8	4.28E+05	3.18E+05	1.41E+05
9	7.64E+05	3.47E+05	1.60E+05
10	7.40E+05	3.41E+05	1.58E+05
11	4.30E+05	3.27E+05	1.51E+05
12	3.84E+05	1.58E+05	1.37E+05
13	4.14E+05	1.70E+05	1.38E+05
14	3.44E+05	1.26E+05	1.26E+05
15	3.95E+05	1.94E+05	1.38E+05
16	3.53E+05	1.29E+05	1.27E+05
17	3.15E+05	1.17E+05	1.17E+05
18	3.19E+05	1.18E+05	1.18E+05
19	4.12E+05	2.65E+05	1.47E+05
20	3.71E+05	3.20E+05	1.48E+05
21	3.52E+05	2.18E+05	1.41E+05
22	3.46E+05	1.72E+05	1.37E+05
23	3.70E+05	1.35E+05	1.35E+05
24	3.44E+05	3.18E+05	1.47E+05
25	3.62E+05	1.51E+05	1.36E+05
26 (AASHTO Type 3)	7.75E+05	3.47E+05	1.61E+05
27 (AASHTO Type 3S2)	7.82E+05	3.46E+05	1.60E+05
28 (AASHTO Type 3-3)	8.33E+05	3.49E+05	1.62E+05
AASHTO Fatigue Truck	8.33E+05	3.52E+05	1.63E+05

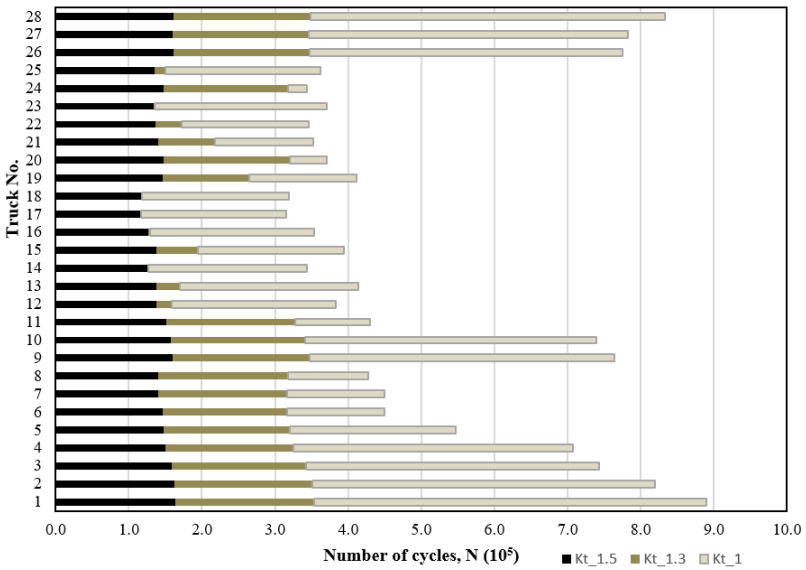

Figure 8-25. Load cycles for developing fatigue cracking at the beam end with bolted repair, a pre-existing crack (a = 0.15t_w), and different surface roughness under MI legal loads.

8.1.4.4.2 Crack size, a = t_w

The STATUSXFEM shows completely cracked elements along the crack. The crack surface is highlighted in the PHILSM. The highest maximum principal stress is also at the crack surface, as shown in Figure 8-26. As shown in Figure 8-27, the crack surface with the highest maximum principal stress is the critical location. The number of load cycles required to develop fatigue cracking at the beam end with bolted repairs and pre-existing cracks was calculated using 28 Michigan legal trucks and the AASHTO LRFD fatigue truck. The results are summarized in Table 8-8. Additionally, a chart emulating the format of AASHTO LRFD fatigue curves was developed using the results for different surface finish factors, as shown in Figure 8-28.

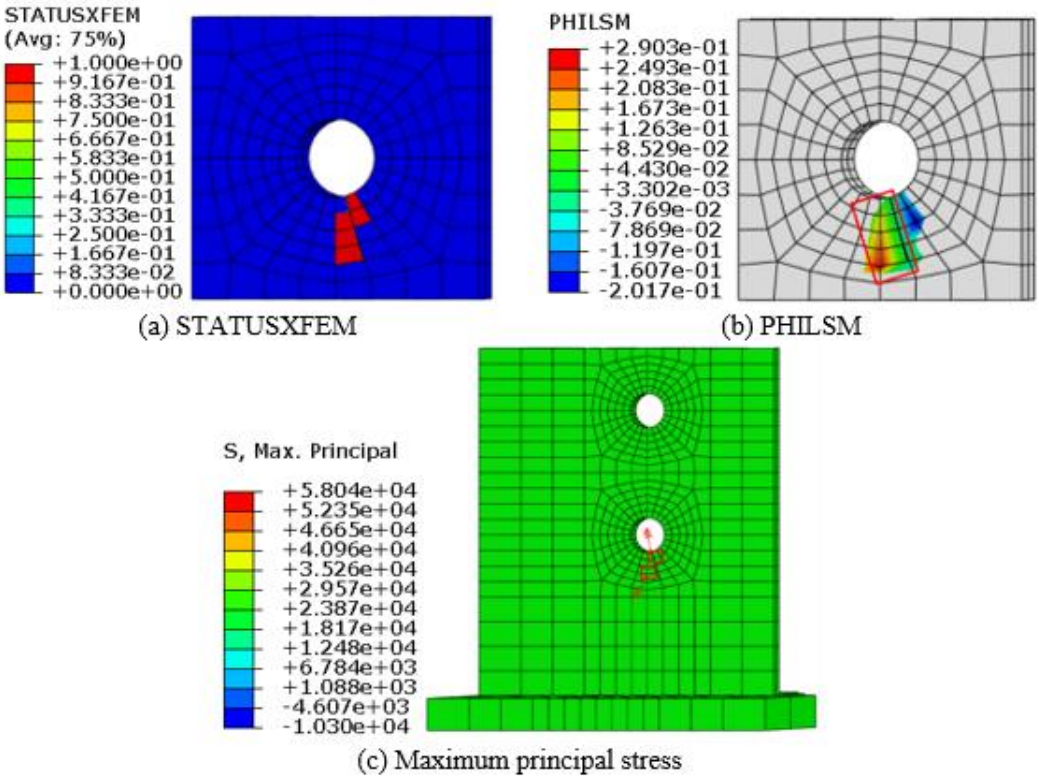

Figure 8-26. FEA stress contours for a beam end with a bolted repair and a pre-existing crack.

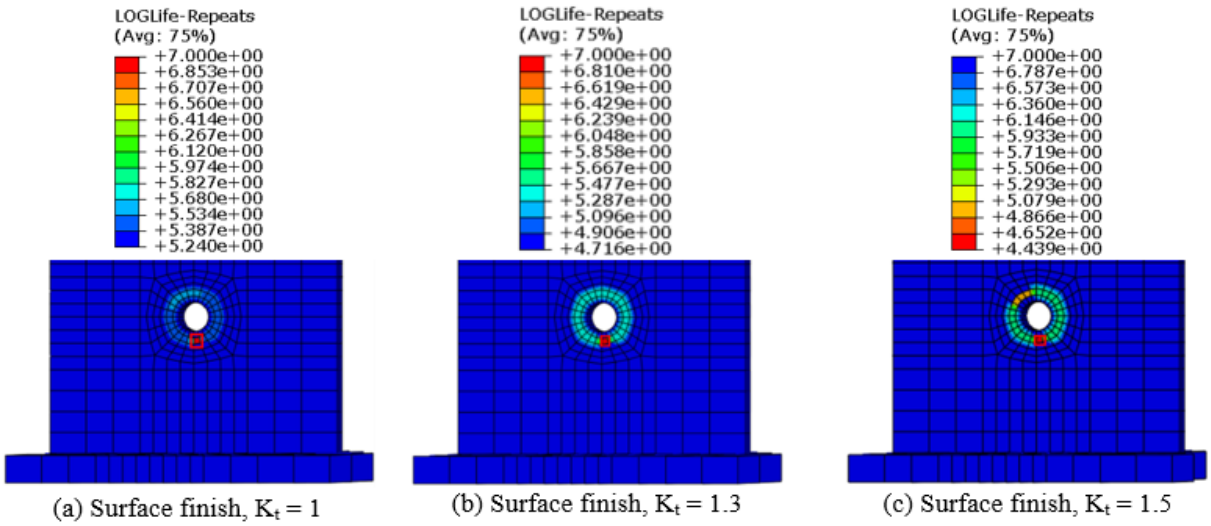

(a) Surface finish, $K_t = 1$ (b) Surface finish, $K_t = 1.3$ (c) Surface finish, $K_t = 1.5$

Figure 8-27. *LOGLife-Repeats* contours for beam ends with bolted repairs, pre-existing cracks, and different surface roughness.

Table 8-8. Load Cycles for Developing Fatigue Cracking at the Beam End with Bolted Repair, a Pre-existing Crack ($a = t_w$), and Different Surface Roughness Under MI Legal Loads and the AASHTO Fatigue Truck

Truck No.	Number of cycles, N, based on the surface finish factor, K_t		
	$K_t = 1$	$K_t = 1.3$	$K_t = 1.5$
1	1.78E+05	5.41E+04	2.88E+04
2	1.78E+05	5.41E+04	2.88E+04
3	1.77E+05	5.40E+04	2.88E+04
4	1.80E+05	5.56E+04	2.98E+04
5	1.96E+05	5.94E+04	3.16E+04
6	1.74E+05	5.20E+04	2.75E+04
7	1.74E+05	5.20E+04	2.75E+04
8	1.89E+05	5.67E+04	3.00E+04
9	1.78E+05	5.41E+04	2.88E+04
10	1.78E+05	5.42E+04	2.89E+04
11	1.85E+05	5.65E+04	3.02E+04
12	1.86E+05	5.79E+04	3.12E+04
13	1.83E+05	5.72E+04	3.08E+04
14	1.80E+05	5.60E+04	3.02E+04
15	1.83E+05	5.72E+04	3.09E+04
16	1.72E+05	5.19E+04	2.75E+04
17	1.71E+05	5.16E+04	2.74E+04
18	1.75E+05	5.29E+04	2.81E+04
19	1.97E+05	5.68E+04	2.96E+04
20	1.85E+05	5.58E+04	2.96E+04
21	1.80E+05	5.39E+04	2.85E+04
22	1.74E+05	5.28E+04	2.81E+04
23	1.85E+05	5.49E+04	2.89E+04
24	1.86E+05	5.61E+04	2.98E+04
25	1.83E+05	5.45E+04	2.88E+04
26 (AASHTO Type 3)	1.88E+05	5.65E+04	2.99E+04
27 (AASHTO Type 3S2)	2.03E+05	5.98E+04	3.15E+04
28 (AASHTO Type 3-3)	1.98E+05	5.86E+04	3.09E+04
AASHTO Fatigue Truck	1.80E+05	5.44E+04	2.89E+04

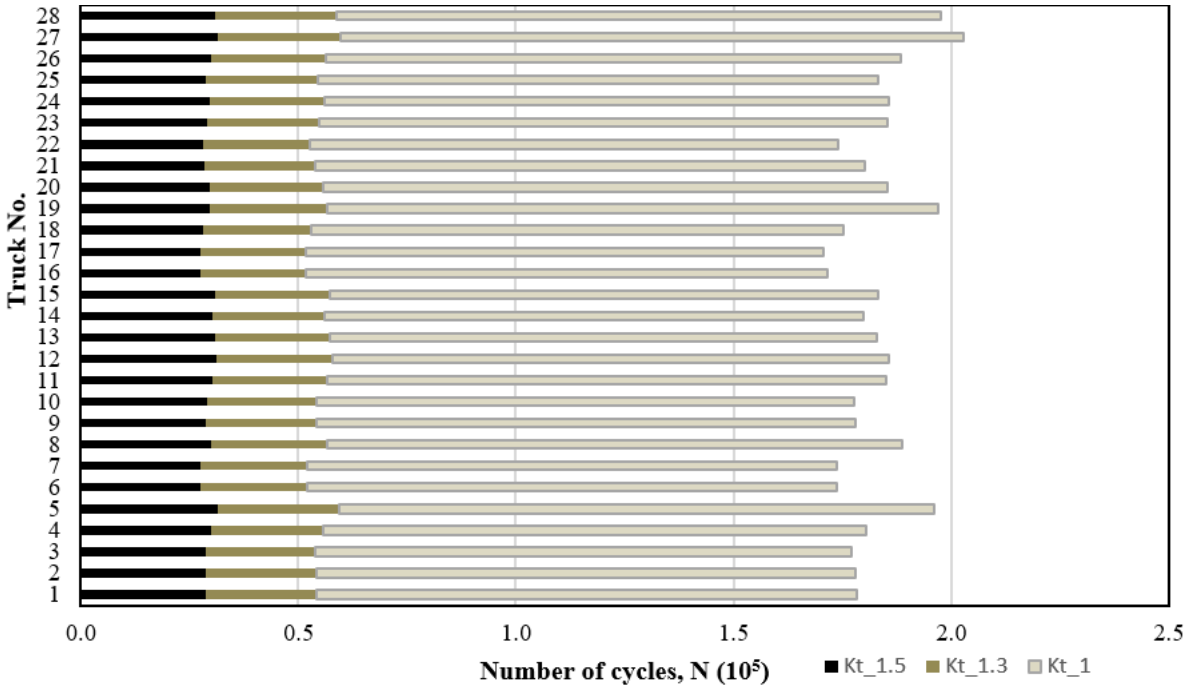

Figure 8-28. Load cycles for developing fatigue cracking at the beam end with bolted repair, a pre-existing crack (a = t_w), and different surface roughness under MI legal loads.

8.1.5 Remaining Fatigue Life

The analysis discussed in this chapter used a 50 ft long span and details that have already shown fatigue cracks. The remaining fatigue life can be estimated using Miner's rule, the load cycles presented in this chapter for Michigan legal loads, and average daily truck traffic from weigh-in-motion (WIM) data for the specific bridge. To illustrate the process, an example is presented in this section. Table 8-9 shows the calculation. Column (a) presents the truck number. Columns (b) and (c) present the number of Truck type (i) travelling over this bridge, n_i. Column (d) presents the values in Table 8-7 for K_t = 1.3, the load cycles (N_i) required under Truck type (i) to develop a 0.5t_w long crack in an as-designed beam to reach the critical crack length. Column (e) presents the damage accumulated under each Truck type, n_i/N_i. When column (c) and (d) values are used, the damage accumulated under each truck is calculated per year. Following Miner's rule, the total damage is calculated as follows:

Accumulated damage, $D = \sum_{i=1}^{n} \frac{n_i}{N_i}$ = 6.085/year

Remaining fatigue life, t = 1/D = 1/6.085 = 0.16 years ≅ 2 months

Therefore, having an initial crack length of 0.2725 in. (i.e., $0.5t_w = 0.5\times0.545$) in a W30×108 section used in a bridge, similar to the one considered in this chapter, and subjected to the loading in Table 8-9, the time it requires for that crack to develop into the critical crack length is about 2 months.

Table 8-9. Miner's Rule for Remaining Fatigue Life Evaluation

Truck No.	Load cycles		Crack = 0.15 t_w	Damage, (n_i/N_i)
	n_i/day	n_i/year	N_i for K_t = 1.3	0.423
1	410	149,566	3.54E+05	0.331
2	319	116,329	3.51E+05	0.291
3	273	99,711	3.42E+05	0.204
4	182	66,474	3.25E+05	0.104
5	91	33,237	3.20E+05	0.105
6	91	33,237	3.17E+05	0.115
7	100	36,561	3.17E+05	0.110
8	96	34,899	3.18E+05	0.240
9	228	83,092	3.47E+05	0.146
10	137	49,855	3.41E+05	0.203
11	182	66,474	3.27E+05	0.315
12	137	49,855	1.58E+05	0.284
13	132	48,194	1.70E+05	0.237
14	82	29,913	1.26E+05	0.222
15	118	43,208	1.94E+05	0.064
16	23	8,309	1.29E+05	0.014
17	5	1,662	1.17E+05	0.028
18	9	3,324	1.18E+05	0.094
19	68	24,928	2.65E+05	0.109
20	96	34,899	3.20E+05	0.198
21	118	43,208	2.18E+05	0.271
22	127	46,532	1.72E+05	0.296
23	109	39,884	1.35E+05	0.141
24	123	44,870	3.18E+05	0.309
25	127	46,532	1.51E+05	0.402
26 (AASHTO Type 3)	382	139,595	3.47E+05	0.418
27 (AASHTO Type 3S2)	396	144,581	3.46E+05	0.409
28 (AASHTO Type 3-3)	391	142,919	3.49E+05	0.423
Damage accumulation per year, D				6.085

This chapter presents a detailed procedure for calculating the fatigue life of bridge components that are not included in the AASHTO LRFD (2020). This procedure can be implemented for other details to calculate their fatigue lives.

9 SUMMARY, CONCLUSIONS, AND RECOMMENDATIONS

9.1 SUMMARY

The Michigan Department of Transportation (MDOT) uses the Agency-Developed Element (ADE) 826 to document the condition of a beam end only when deterioration or repair meets the definitions in Condition State (CS) Table 9 of the Michigan Bridge Element Inspection Manual (MiBEIM 2017). The quantity is reported per beam end when the deterioration or repair is within 5 ft of the bearing. Bridge inspection engineers and consultants submit requests for action (RFAs) due to safety concerns associated with steel and PSC beam end conditions. Region bridge engineers review RFAs and submit them to the Bridge RFA Coordination Committee (BRFACC) for deliberation. The RFA and subsequent decisions are made based on the currently available inspection guidelines and the experience of inspection engineers, region bridge engineers, and BRFACC members. Having focused guidelines and tools for bridge inspection engineers, region bridge engineers, and other members of the BRFACC can streamline the RFA submission and evaluation process. Additionally, the availability of beam end maintenance and repair guidelines, including repair details and their impact on load capacity, is vital to overcoming programming and resource allocation challenges while ensuring public safety and avoiding potentially unnecessary restrictions on the motoring public. To accomplish project objectives, this project was organized into 11 tasks, and the findings are summarized in this chapter.

9.2 CONCLUSIONS AND RECOMMENDATIONS

9.2.1 Steel Beam Ends

9.2.1.1 Preference for Bolted Repairs over Welded Repairs

Thirty-two (32) scoping reports, inspector comments, bridge plans, and other associated documents were reviewed to collect condition data on 431 beam ends. Welded repairs are typically recommended for sections with cracks, buckled webs, buckled flanges, or a combination of these defects. Repairs recommended at 98% of the 431 beam ends were bolted repairs. The data indicate a strong preference for bolted repairs due to the challenges associated with field welding requirements, fatigue concerns, and the difficulty in finding qualified welders.

9.2.1.2 Section Loss Limits for Repair Recommendations

The review of the literature and the survey of highway agencies indicated inconsistency in the guidelines used for submitting RFAs for steel beam ends. Considering the statistics presented in Chapter 2, it is recommended to use a 20% web section loss as the limit for determining the need for repairs on webs up to 0.625 inches thick, unless unique conditions at the specific beam end dictate otherwise. Similarly, it is recommended to use a 10% flange section loss as the limit for determining the need for repairs on flanges up to 1.25 inches thick when a beam end has both web and flange section losses.

9.2.1.3 Capacity Prediction of Beam Ends with Holes

Sixty-two percent (62%) of beam end deteriorations are associated with the web area, particularly affecting the bearing and shear zones near beam supports. The capacity of beam ends with holes resulting from corrosion was studied, focusing on the most commonly used beam section in Michigan bridges—the W30×108. Both unstiffened and stiffened beam ends with various hole configurations documented during bridge inspections were used in this study.

For unstiffened W30×108 beam ends, web crippling controls the failure mode with a nominal resistance of 231 kips. The finite element analysis showed excellent correlation with AASHTO (2020) analytical solutions, with failure loads within 3% of the nominal resistance. For stiffened beam ends, bearing resistance controls with a nominal resistance of 260 kips, while axial resistance provides a capacity of 470 kips. When holes are located within the bottom 4 inches of the web height with web crippling controlling, the remaining capacity of the beam end with 100% imperfection can be calculated using the following load factors:

If $HL/N \leq 0.80$: $\varphi = 0.50$ (retains 50% of original capacity)

If $HL/N > 0.80$: $\varphi = 0.38$ (retains 38% of original capacity)

Where HL is the hole length and N is the bearing length.

For stiffened beam ends, the location of holes relative to the bearing stiffener is critical:

- When holes are located on both sides of the bearing stiffener: $\varphi = 0.39$ (retains 39% of original capacity)
- For all other hole configurations: $\varphi = 0.74$ (retains 74% of original capacity)

Stiffened beam ends generally maintain higher capacity than unstiffened ends when subjected to localized deterioration. The MDOT load rating spreadsheet was also updated to incorporate the effects of holes at beam ends. The following recommendations are derived for practice:

- *Load Rating*: Apply the recommended load factors when evaluating beam ends with documented section loss, considering both hole length and stiffener presence.
- *Maintenance Planning*: Beam ends with hole length-to-bearing length ratios exceeding 0.80 should receive priority for rehabilitation due to significant capacity reductions.
- *Design Considerations*: The presence of end diaphragms with bent plates provides minimal improvement in capacity for beams with deterioration, suggesting that resources may be better allocated to direct web repair or stiffener installation.
- *Further Research*: Additional investigation is recommended for holes exceeding 14% of web height and for the long-term effects of progressive deterioration on beam end capacity.

9.2.1.4 Longevity and Fatigue Prediction of Bolted Steel Repairs at Beam Ends

Scoping inspections documented fatigue cracking at beam ends with bolted repairs. These bolted repairs were implemented to address section loss at beam ends, which increases surface roughness and increases the potential for fatigue crack development. The fatigue life of steel beam ends with bolted repairs was evaluated using finite element analysis (FEA) and the fe-safe fatigue analysis software. A W30×108 steel beam with a 50 ft span and 6 ft beam spacing was selected. The Brown-Miller strain-based fatigue-life algorithm was employed to represent the behavior of the steel material.

The investigation examined multiple analysis cases, including as-designed beams, beams with bolt holes, beams with pre-existing cracks of varying sizes ($0.15t_w$ and t_w), and beams with bolted repairs and pre-existing cracks. Surface finish effects were incorporated through surface finish factors (K_t) of 1.0, 1.3, and 1.5, representing polished surfaces, 1000 μ-in. surface roughness, and approximately 2000 μ-in. surface roughness, respectively.

The presence of bolt holes significantly reduces fatigue life compared to as-designed beam conditions. The critical locations identified through analysis corresponded well with observed crack patterns in field inspections. The study provides detailed fatigue life calculation tables for all 28 Michigan legal truck configurations and AASHTO fatigue trucks. Using Miner's rule with

actual traffic data, engineers can estimate the remaining fatigue life of similar details. The example calculation demonstrated that a $0.5t_w$ initial crack on the web of W30×108 with bolt holes could reach critical crack length in approximately 2 months under the loading spectrum considered for the structure. The comprehensive procedure developed in this study can be applied to other structural details not covered in the AASHTO LRFD specifications, providing engineers with valuable tools for assessing the fatigue life of steel bridge members.

9.2.1.5 Impact of Pack Rust on Beam End Capacity

The comprehensive review of literature and practice revealed that the impact of pack rust on beam capacity is the least studied topic. This is primarily due to the challenge of quantifying the section loss by measuring component deformation, which depends on the section thickness, boundary conditions (bolt or weld patterns), the amount of corrosion products, the type of corrosion, and the relationship between the amount of corrosion and the section loss. The current practice is to clean the corroded details and measure the remaining thickness for capacity calculation.

9.2.2 PSC I-beam Ends

9.2.2.1 RFA and Scoping Inspection Guidelines

MDOT currently uses various templates and guidelines to document PSC I-beam end distress and deterioration during inspections. A comprehensive review of nineteen scoping inspection reports, Bridge Safety Inspection Report (BSIR) reports of 267 bridges, several RFA reports, and related documents from the MiBRIDGE database revealed that existing inspection guidelines are insufficient for collecting the minimum required data to assess beam end capacity and make informed decisions regarding maintenance, repair, or load posting.

To address these shortcomings, inspection guidelines and templates specifically designed for PSC I-beam ends were developed. The guidelines include a systematic approach to beam end discretization and detailed documentation procedures for delamination, spalls, and cracking. These guidelines were developed with consideration for the future implementation of drone and computer vision technologies to enhance traditional visual inspection methods.

9.2.2.2 RFA Decision Matrix

MDOT required improved decision-making tools for evaluating PSC beam end deterioration to enhance the identification of bridges requiring RFAs. Current RFA guidelines rely on general condition ratings and visual inspection criteria that lack clear correlations with structural performance, creating challenges in determining when deteriorated beam ends require immediate attention versus continued monitoring.

This project addressed the need for a rational, capacity-based assessment method by developing a comprehensive beam end deterioration classification system using the Strut-and-Tie Method (STM). The study focused on evaluating the PSC I-beam end capacity, particularly addressing deterioration factors such as exposed prestressing strands, bearing area loss, and structural cracking that significantly impact structural performance but are inadequately addressed by current inspection protocols using Agency Developed Element (ADE) 826.

The research analyzed disturbed regions (D-regions) at beam ends, where complex load paths violate conventional design assumptions, developing mathematical frameworks for four primary failure modes: longitudinal tie failure, bearing face failure, strut-to-node interface failure, and transverse tie failure. Capacity calculations were validated using experimental data from 16 PSC I-beam specimens.

STM was successfully implemented to model complex load transfer mechanisms at PSC beam ends, providing a superior representation of failure modes compared to conventional flexural design assumptions. Sensitivity analysis revealed that beam end shear capacity is primarily controlled by longitudinal tie failure and is directly proportional to the percentage of exposed prestressing strands. Section loss without strand exposure has minimal impact on capacity. A comprehensive set of Mathcad calculation sheets was developed and delivered to MDOT for calculating capacities of as-designed, deteriorated, and repaired beam ends.

A 15% capacity reduction was established as the critical threshold for RFA decisions based on structural safety considerations. The developed capacity-based deterioration classification system should replace current condition state definitions that rely solely on section loss measurements. Specific RFA thresholds include: spalls deeper than 1 inch with ≥15% bottom flange strand

exposure at beam soffits, spalls deeper than 2 inches with ≥15% strand exposure at beam sides, section loss ≥40% without strand exposure, and any shear cracking affecting beam end capacity.

For all beam types, except MI 1800, a minimum reserved capacity of 115% should be maintained. MI 1800 beams require individual assessment due to variable performance characteristics and Capacity-to-Demand Ratio values below 1.0 in some cases. The implementation of this system is expected to enhance bridge safety while optimizing maintenance resource allocation by providing rational correlations between visual inspection data and structural performance.

9.2.2.3 Performance of Beam End Preservation and Repair Methods

MDOT has observed that traditional concrete patching methods for PSC beam ends provide only short-term solutions and may contribute to accelerated concealed corrosion. In response, MDOT developed Special Provision for Maintenance Repair of Prestressed Concrete Beam for Contract Identification 25031-214869, 20SM712(A175), which requires the cleaning of exposed steel reinforcement and the application of a zinc-rich epoxy primer to enhance durability. However, the performance of this preservation approach had not been evaluated before this study.

This investigation was initiated to assess the effectiveness of various preservation and repair techniques for deteriorated PSC beam ends through accelerated corrosion testing. The study examined four different preservation and repair methods, including latex modified concrete (LMC), zinc-rich epoxy primer for steel, a silane penetrating sealer, and a breathable concrete surface coating with crack bridging abilities.

The findings indicate that patch repair with latex modified concrete (LMC) provides protection only to the reinforcing steel within the repaired area and offers no protection to adjacent steel elements. A similar limitation was observed when a silane penetrating sealer was applied over patch repairs using a regular concrete mix, suggesting limited effectiveness in preventing corrosion beyond the immediate repair zone. Based on the current findings, the integration of patch repair with a zinc-rich epoxy primer and an elastomeric concrete surface coating with crack bridging abilities is recommended. This combined approach demonstrated the most consistent performance in delaying corrosion activity compared to the other methods evaluated during this study.

Additional testing with a larger number of specimens is recommended to validate these preliminary findings, as this study was limited in scope.

9.2.2.4 PSC I-beam End Repair and Capacity Improvement

MDOT recognizes that deteriorated PSC beam ends require systematic repair approaches to restore structural capacity and extend service life. The repair methods examined during this study range from basic crack sealing and concrete patching to more comprehensive solutions such as full-depth reinforced concrete overcasts and fiber-reinforced polymer (FRP) strengthening systems.

The study utilized the Strut-and-Tie Model (STM) to quantify capacity improvements achieved through overcast repairs, consistently identifying longitudinal tie failure as the critical failure mode controlling beam end capacity. Three alternative Full-Depth Reinforced Concrete Overcast (FDRCO) repair details were developed and analyzed: *Alternative 1* (typical MDOT detail), *Alternative 2* (with hooked longitudinal reinforcement), and *Alternative 3* (incorporating strand splicing with 90-degree bents). *Alternative 3* FDRCO details, which incorporate strand splicing and 90-degree bents, can restore and potentially exceed the original design capacity. An alternative repair detail with welded wire fabric and adhesive anchoring is suggested for situations where maintaining the original beam geometry and vertical clearance is critical. It is recommended to experimentally evaluate the performance of *Alternative 2* and *Alternative 3* details before implementing them on in-service bridges.

Field performance reviews revealed that beam end repairs, which combined reinforced overcasts with FRP U-wraps and breathable concrete surface coatings, demonstrated the best long-term performance. In contrast, unreinforced overcasts and repairs without protective coatings consistently show poor performance, with common issues including early-age cracking and delamination within 2 to 11 years of installation. For beam ends with a/d ratios near 1, FRP U-wraps provide minimal improvement in structural capacity. Still, they can enhance the durability of overcast repairs by bridging cracks and providing protective barriers against moisture and chloride ingress.

Careful preparation during repair construction is critical to avoid exposing additional prestressing strands, which can compromise the effectiveness of the repair. The use of strand splicing devices and 90-degree bent strands offers significant capacity improvements for deteriorated beam ends.

The study presented alternative repair details, including modified overcast repairs with welded wire fabric and adhesive anchoring, for situations where maintaining the original beam geometry and vertical clearance is critical. Regular inspection and maintenance of repaired beam ends, particularly monitoring of protective coatings and early detection of cracking, is essential for long-term repair performance and service life extension.

10 REFERENCES

1. AASHTO LRFD (2020). *AASHTO LRFD bridge design specifications*. American Association of State Highway and Transportation Officials, Washington, D.C.
2. AASHTO FRP (2023). *Guide Specifications for Design of Bonded FRP Systems for Repair and Strengthening of Concrete Bridge Elements. FRPS-1*, American Association of State Highway and Transportation Officials, Washington, D.C.
3. ACI (2003). *ACI 503R-93: Use of Epoxy Compounds with Concrete* (Reapproved 2003). Farmington Hills, MI.
4. ACI (2017). *Guide for the design and construction of externally bonded FRP systems for strengthening concrete structures (ACI 440.2R-17)*. American Concrete Institute, Farmington Hills, MI.
5. ACI (2023). *Material Selection for Concrete Repair - Guide*, Report No. ACI 546.3-23, American Concrete Institute (ACI), 38800 Country Club Drive, Farmington Hills, Detroit, Michigan 48331.
6. Aktan, H., Attanayake, U., & Ulku, E. (2008). *Combining Link Slab, Deck Sliding over Backwall, and Revising Bearings* (Research Report No. RC-1514). Michigan Department of Transportation, Construction and Technology Division, Lansing, MI.
7. Aktan, H., Ahlborn, T., Koyuncu, Y., Rutyna, J., and Kasper, J. (2002). *Causes and Cures for Prestressed Concrete I-Beam End Deterioration,* Report No. 1412, Michigan Department of Transportation, Lansing, MI.
8. Alaska DOT (2016). *Statewide Special Provisions*, Alaska Department of Transportation, Juneau, Alaska 99811-2500, pp 60-61.
9. ALDOT (2015). *ALDOT-367 Production and Inspection of Precast Non- Prestressed and Prestressed Concrete*, Alabama Department of Transportation, 1409 Coliseum Blvd #2060, Montgomery, Alabama 36130.
10. ASTM *C1152* (2023). *Standard test method for acid-soluble chloride in mortar and concrete.* ASTM International, West Conshohocken, PA.
11. ASTM C876 (2015). *Standard Test Method for Corrosion Potentials of Uncoated Reinforcing Steel in Concrete*, American Society of Testing and Materials (ASTM) International, 100 Barr harbor Drive, West Conshoshocken, PA 19428.
12. ASTM G109 (2023). Standard Test Method for Determining Effects of Chemical Admixtures on Corrosion of Embedded Steel Reinforcement in Concrete Exposed to Chloride Environments. ASTM International, West Conshohocken, PA.
13. Attanayake, U., Berke, N., Amunugama, H., and Basnayake, K (2022). *Concrete Deterioration of Prestressed Bridge Beams.* Final Report, submitted to the Michigan Department of Transportation, Western Michigan University, Kalamazoo, MI.

14. Bae, S. W. and Belarbi, A. (2013). "Behavior of Various Anchorage Systems Used for Shear Strengthening of Concrete Structures with Externally Bonded FRP Sheets." *J. of Bridge Engineering*, 18(9), 837–847.

15. Bannantine, J. A., Comer, J. J., and Handrock, J. L. (1990). *Fundamentals of Metal Fatigue Analysis*, Prentice Hall, Englewood Cliffs, New Jersey 07632.

16. MnDOT BIFM (2016). *Bridge Inspection Manual*. Minnesota Department of Transportation, https://www.dot.state.mn.us/bridge/pdf/insp/bridgeinspectionmanual.pdf. (Last Accessed July 15, 2025).

17. Bureau of Reclamation (2014). *M-82: Standard protocol to evaluate the performance of corrosion mitigation technologies in concrete repairs*. U.S. Department of the Interior, Bureau of Reclamation, Denver, CO.

18. Concrete Construction (1998). *Chloride Limits in the ACI 318 Building Code Requirements*, Publication No. J980869, P.O. Box 3494, Northbrook, IL 60065.

19. del Rey Castillo, E., Kanitkar, R., Smith, S. T., Griffith, M. C., and Ingham, J. M. (2019). "Design approach for FRP spike anchors in FRP-strengthened RC structures." *Composite Structures, Elsevier*. https://doi.org/10.1016/j.compstruct.2018.11.076

20. Feldman, L. R., Jirsa, J. O., Fowler, D. W., and Carrasquillo, R. L. (1996). *Current practice in the repair of prestressed bridge girders.* Center for Transportation Research, The University of Texas at Austin, Texas 78712-1075.

21. FHWA (2021). *Historical Changes to Steel Bridge Design, Composition, and Properties*, Publication No. FHWA-HRT-21-020, Federal Highway Administration (FHWA), Research, Turner-Fairbank Highway Research Center, McLean, VA.

22. GTI (2025). GTI Reusable Splice Chucks Data Sheet, General Technologies, https://gti-usa.net/post-tensioning/reusable-components/gti-reusable-splice-chucks/. (Last accessed: September 26, 2025)

23. Girotti, L. (2017). *CFRP anchors for external reinforcement: Methodology for structural and material testing*. M.S. thesis, Politecnico di Milano, Milano, Italy.

24. Grelle, S. V. and Sneed, L. H. (2013). "Review of Anchorage Systems for Externally Bonded FRP Laminates." *Int. J. Concrete Struct. Mater.*, 7(1), 17–33. DOI:10.1007/s40069-013-0029-0

25. Harries, K. A., Kasan, J., and Aktas, J. (2009). *Repair Method for Prestressed Girder Bridges,* Report No. FHWA-PA-2009-008-PIT 006, Pennsylvania Department of Transportation, Bureau of Planning and Research, PA, 17120.

26. Hawkins, N. M. and Kuchma, D. A (2007). *Application of LRFD Bridge Design Specifications to High-Strength Structural Concrete: Shear Provisions.* Washington, DC: The National Academies Press. https://doi.org/10.17226/17616.

27. IDOT (2020). *Manual for Fabrication of Precast Prestressed Concrete Products*, Illinois Department of Transportation, Bureau of Materials and Physical Research, 126 E Ash St, Springfield, Illinois 62704.

28. Jang, H., Webb, Z., Choi, J., Wang, H. C., and Bayrak, O. (2022). Analyze Shear Capacity of Texas Standard Prestressed Beams from Strut-and-Tie Models of Beam Ends: Final Report. University of Texas at Austin. Center for Transportation Research. Austin, TX.

29. Jirsa, J. O., Ghannoum, W. M., Kim, C. H., Sun, W., Shekarchi, W. A., Alotaibi, N. K., Pudleiner, D. K., Zhu, J., Lui, S., and Wang, H. (2017). *Use of carbon fiber reinforced polymer (CFRP) with CFRP anchors for shear-strengthening and design recommendations/quality control procedures for CFRP anchors.* Center for Transportation Research, Univ. of Texas at Austin.

30. Kanakamedala, D., Seo, J., Varma, A. H., Connor, R. J., and Tarasova, A. (2023). *Shear and bearing capacity of corroded steel beam bridges and the effects on load rating* (Joint Transportation Research Program Publication No. FHWA/IN/JTRP-2023/11). West Lafayette, IN: Purdue University. https://doi.org/10.5703/1288284317634

31. Kang, T. H. K. and Ary, M. I. (2012). "Shear-strengthening of reinforced & prestressed concrete beams using FRP: Part II - Experimental investigation." *International Journal of Concrete Structures and Materials*, 6(1), 49–57.

32. Kim, Y., Quinn, K., Satrom, N., Garcia, J., Sun, W., Ghannoum, W. M., and Jirsa, J. O. (2011). *Shear strengthening of reinforced and prestressed concrete beams using carbon fiber reinforced polymer (CFRP) sheets and anchors*. Center for Transportation Research, University of Texas at Austin, https://rosap.ntl.bts.gov/view/dot/23479.

33. Kühn, B., Lukić, M., Nussbaumer, A., Günther, H. P., Helmerich, R., Herion, S., Kolstein, M. H., Walbridge, S., Androic, B., Dijkstra, O., and Bucak, Ö. (2008). *Assessment of Existing Steel Structures: Recommendations for Estimation of Remaining Fatigue Life*, JRC Scientific and Technical Reports, EUR 23252 EN-2008.

34. Lozano, C. M. and Riveros, G. A. (2021). *Classical and Innovative Methods of Fatigue and Fracture Repairs in Navigation Steel Structures*, US Army Engineer Research and Development Center (ERDC), 3909 Halls Ferry Road, Vicksburg, MS 39180-6199.

35. Mansur, M.A. and Ong, K.C.G. (1985). "Epoxy-Repaired Beams." *Concrete International: Design and Construction*, Vol. 7, No. 10, pp. 46-50.

36. MassDOT (2025). Bridge Maual, Hundredth Anniversary Edition, the Massachusetts Department of Transportation. https://massdot.docs.mass.gov/hwy-bridge-manual/part-1/ch7-bridge-load-rating-guidelines-240906.pdf (Last accessed: July 18, 2025)

37. MDOT (2009). *Bridge Analysis Guide*, 2005 Edition with 2009 Interim Update, Part 1, Michigan Department of Transportation, 425 W. Ottawa St., Lansing, Michigan 48909.

38. MDOT (2017). *MDOT NBI Rating Guidelines*, Michigan Department of Transportation, 425 W. Ottawa St., Lansing, Michigan 48909.

39. MDOT (2020). *Standard Specifications for Construction,* Michigan Department of Transportation, 425 W. Ottawa St., Lansing, MI.

40. MDOT (2021a). *Special Provision for Maintenance Repair of Prestressed Beam for contract identification 25031-214869, 20SM712(A175)*. Michigan Department of Transportation, Lansing, MI.

41. MDOT (2021b). *Special Provision for Prestressed Concrete Beam End Repair with Latex Modified Concrete, 20RC712(A385)*. Michigan Department of Transportation, Lansing, MI.

42. MDOT (2021c). *Special Provision for Fiber Reinforced Polymer Shear Strengthening System, 20RC712(A295)*. Michigan Department of Transportation, Lansing, MI.

43. MDOT (2021d). *Special Provision for Concrete Surface Coatings, 20RC710(A285)*. Michigan Department of Transportation, Lansing, MI.

44. MDOT (2022). *Michigan structure inventory and appraisal coding guide*, Michigan Department of Transportation, Bridge Management Unit, 425 W. Ottawa St., Lansing, Michigan 48909.

45. MDOT (2023). *Structural Fabrication Quality Manual*, Michigan Department of Transportation, 425 W. Ottawa St., Lansing, MI.

46. MDOT (2024). *MDOT materials source guide*. Michigan Department of Transportation, Lansing, MI.

47. MDOT (2025). Construction Manual, Construction Field Services Division, MDOT. https://mdotwiki.state.mi.us/construction/index.php?title=712_-_Bridge_Rehabilitation,_Concrete#Crack_Injection. (Last accessed: September 20, 2025).

48. MiBEIM (2017). *Michigan Bridge Element Inspection Manual (MiBEIM)*, Michigan Department of Transportation, 425 W. Ottawa St., Lansing, Michigan 48909.

49. MiSIM (2019). *Michigan structure inspection manual: bridge inspection.* Michigan Department of Transportation, 425 W. Ottawa St., Lansing, Michigan 48909.

50. Morcous, G., Wood, R., L., and Kodsy, A., M., K., M. (2020). *Synthesis of Repair Practices of Damaged Precast/Prestressed Concrete Girders.* University of Nebraska – Lincoln, NE 68588.

51. Muciaccia, G., Khorasani, M., and Mostofinejad, D. (2022)." Effect of different parameters on the performance of FRP anchors in combination with EBR-FRP strengthening systems: A review." *Construction and Building Materials*, 354(September), 129181.

52. Murphy, M., Belarbi, A., and Bae, S. W. (2012). "Behavior of prestressed concrete I-girders strengthened in shear with externally bonded fiber-reinforced-polymer sheets." *PCI Journal*, 57(3), 63–82.

53. Needham, D. E. (1999). *Prestressed Concrete Beam End Repair (Interim Report).* Michigan Department of Transportation, Lansing, MI.

54. Needham, D. E. (2000). *Prestressed Concrete Beam End Repair.* Michigan Department of Transportation, Lansing, MI.

55. ODOT (2019). *Construction and Material Specifications*, Ohio Department of Transportation, Columbus, Ohio 43216, pp. 372 – 373.

56. Osborn, G. P., Barr, P. J., Petty, D. A., Halling, M. W., and Brackus, T. R. (2012). "Residual prestress forces and shear capacity of salvaged prestressed concrete bridge girders." J. Bridge Eng., 17(2), 302–309. https://doi.org/10.1061/(ASCE)BE.1943-5592.0000212.

57. PCI Strand Bond Fast Team (2025). "Recommended Practice to Assess and Control Strand/Concrete Bonding Properties of ASTM A416 Prestressing Strand." *PCI Journal*, 70(1), 23–36. https://doi.org/10.15554/pcij70.1-03.

58. Pevey, J. M., Rich, W. B., Williams, C. S., and Frosch, R. J. (2021). *Repair and strengthening of bridges in Indiana using fiber reinforced polymer systems: Volume*. Joint Transportation Research Program, Indiana Dept. of Transportation and Purdue University.

59. PSI (2025). GRABB-IT Cable Splice Installation Instructions, https://www.prestresssupply.com/technical-notes/ (Last accessed: July 07, 2025)

60. Rich, W. B., Williams, C. S., and Frosch, R. J. (2023), "Investigation of repair techniques for deteriorated end regions of prestressed concrete bridge girders", *PCI Journal,* March–April 2023.

61. Ross, B. E. (2012). *Function and design of confinement reinforcement in pretensioned concrete I-girders.* Ph.D. thesis, Univ. of Florida.

62. Ross, B. E., Hamilton, H. R., and Consolazio., G. R. (2013). "Design model for confinement reinforcement in pretensioned concrete I-girders." *Transp. Res.* 2331 (1): 59–67. https://doi.org/10.3141/2331-06.

63. Shahrooz, B. M., Miller, R. A., Harries, K. A., Yu, Q., and Russell. H. G. (2017). *Strand debonding for pretensioned girders.* NCHRP Rep. No. 849. Washington, DC: Transportation Research Board, National Research Council.

64. Shafei, B., Phares, B., and Shi., W. (2020). *Beam End Repair for Prestressed Concrete Beams.* Iowa Department of Transportation, 2711 South Loop Drive, Ames, IA 50010.

65. Shanafelt, G. O. and Horn, W. B. (1980). *Damage evaluation and repair methods for prestressed concrete bridge members.* NCHRP Report 226, Transportation Research Board, National Research Council, Washington, D. C.

66. Shanafelt, G. O. and Horn, W. B. (1985). *Guidelines for evaluation and repair of prestressed concrete bridge members.* NCHRP Report 280, Transportation Research Board, National Research Council, Washington, D. C.

67. Shield, C. and Bergson, P. (2018). *Experimental Shear Capacity Comparison Between Repaired and Unrepaired Girder Ends.* Minnesota Department of Transportation, St. Paul, MN.

68. Skoglund, O. (2022). *Fatigue Life Estimation Based on LEFM and the Study of Initial Parameters,* KTH Royal Institute of Technology, Department of Civil and Architectural Engineering, Division of Structural Engineering and Bridges, TRITA-ABE-RPT-2128, ISBN 978-91-8040-018-3.

69. TDOT (2018). *Procedures for Prestressed Concrete Construction (SOP 5-4)*, Division of Materials and Tests, Tennessee Department of Transportation (TDOT), James K. Polk Bldg., Suite 700 505 Deadrick Street Nashville, Tennessee 37243.

70. Tabatabai, H. and Nabizadeh, A. (2019). *Strength and serviceability of damaged prestressed girders.* Department of Civil and Environmental Engineering, University of Wisconsin – Milwaukee, WI 53211.

71. Tadros, M. K. and Jongpitaksseel, N. (2003). *Anchorage of 0.6" diameter strands*. Final Report, SPR-1 (03) P551, Nebraska Department of Roads, Bridge Division, Lincoln, NE.

72. Tuchscherer, R. G., Birrcher, D. B., and Bayrak, O. (2011). "Strut-and-tie model design provisions." *PCI J.*, 56(1), 155–177.

73. Tzortzinis, G., Gerasimidis, S., Brena, S., and Knickle, B. (2019). *Development of Load Rating Procedures for Deteriorated Steel Beam Ends*, Massachusetts Department of Transportation, Boston, MA 02116.

74. Waheed, A., Kowal, E., and Loo. T. (2005). *Repair manual for concrete bridge elements.* Version 2.0, Alberta Infrastructure and Transportation, Government of the Province of Alberta.

75. William B. R., Christopher S. W., and Robert J. F. (2023), "Investigation of repair techniques for deteriorated end regions of prestressed concrete bridge girders", *PCI Journal,* March–April 2023.

APPENDIX A: Survey questionnaire

A.1 PRESTRESSED CONCRETE (PSC) I-BEAM

This survey is conducted by Western Michigan University for the Michigan Department of Transportation-Sponsored Research Project OR23-001: Capacity Prediction of Repaired and Unrepaired Bridge Beams with Deteriorated Ends. Your response to the following questionnaire is greatly appreciated.

Please email the completed survey to sanjoykumar.bhowmik@wmich.edu. For questions/concerns, please contact Sanjoy at (269) 779-0936.

Name:

Position:

Employer:

Email:

Note: We will NOT publish or share your contact information. Such information will ONLY be used for contacting you for further information or clarifications to the information provided as a response to the survey.

A.1.1 PSC I-Beam End Condition Assessment

1(a) Do you have established procedures to estimate the depth of delaminated area in PSC beams?

Yes No

If *Yes*, please describe the procedure or provide weblinks to access relevant resources.

(b) Do you have established procedures to estimate the number of corroded/ineffective **strands**?

Yes No

If *Yes*, please describe the procedure or provide weblinks to access relevant resources.

(c) Do you have established procedures to estimate the number of corroded/ineffective **stirrups**?

Yes No

If *Yes*, please describe the procedure or provide weblinks to access relevant resources.

A.1.2 PSC I-Beam End Repair

2. Concrete *patching* is a PSC I-beam end repair method.

(a) Do you protect beam ends ***after patching*** using any of the following methods for enhanced durability?

Yes No

If *No*, do you observe any issues/concerns regarding the repair performance?

If *Yes*, please select the method(s) and provide information.

	Most commonly used product(s)	Implementation challenges	Performance	Additional comments
Penetrating sealants				
Concrete surface coating				
Penetrating sealants and concrete surface coatings (hybrid systems)				
Other techniques				

(b) Do you apply bonding agents on the prepared concrete surface before patching?

Yes No

If *Yes*, please provide information.

Most commonly used product(s)	Implementation challenges	Performance	Additional comments

3. Overcasting (or the use of end blocks) is a PSC I-beam end repair method.
(a) Do you protect *beam ends with overcasting* using any of the following methods for enhanced durability?

Yes No

If *No*, do you observe any issues/concerns regarding the repair performance?

If *Yes*, please indicate the additional protection method(s) and relevant information.

	Most commonly used product(s)	Implementation challenges	Performance	Additional comments
Penetrating sealants				
Concrete surface coating				
Penetrating sealants and concrete surface coatings (hybrid systems)				
Other techniques				

(b) Do you apply bonding agents on the prepared concrete surface before overcasting?

Yes No

If *Yes*, please provide the information.

Most commonly used product(s)	Implementation challenges	Performance	Additional comments

4. Various strategies can be implemented to protect exposed steel (strands/reinforcement) at damaged/deteriorated PSC I-beam ends. A few approaches are described below. Please share your experience with such approaches.

	Most commonly used product(s)	Implementation challenges	Performance	Additional comments
(i) applying coating(s) for corrosion protection and leaving the beam end without patching/overcasting				
(ii) applying coating(s) for corrosion protection before patching/overcasting				
(iii) using cathodic protection with patching/overcasting				
(iv) patching/overcasting without providing an additional protection for steel.				
(iv) implementing other methods, please describe.				

5. After chipping out and cleaning a deteriorated beam end, the cleaned concrete surface can be protected with penetrating sealants, concrete surface coatings, patching, or overcasting. Please share your experience with such approaches.

	Most commonly used product(s)	Implementation challenges	Performance	Additional comments
(i) applying a penetrating sealant and leaving the beam end without patching/overcasting				
(ii) applying a concrete surface coating and leaving the beam end without patching/overcasting				
(iii) applying a penetrating sealant and a concrete surface coating (hybrid systems) and leaving the beam end without patching/overcasting				
(iv) applying a penetrating sealant before patching/overcasting				
(v) implementing other methods, please describe				

6. Please share your field implementation experience with the following repair materials and construction methods.

Repair materials		Implementation challenges	Performance
Carbon fiber reinforced polymer (CFRP) sheets/strips			
Glass fiber reinforced polymer (GFRP) sheets/strips			
Near surface mounted (NMS) FRP bars/strips			
Proprietary ultra-high performance concrete (UHPC)			
Non-proprietary ultra-high performance concrete (UHPC)			
High early strength concrete (HESC)			
Other	Name the material		

Construction method	Application	Implementation challenges	Performance
Shotcrete	Patching		
	Overcasting		
Cast-in-place concrete	Patching		
	Overcasting		

7. PSC I-beam ends are embedded into backwalls or end diaphragms as shown in the following figures.

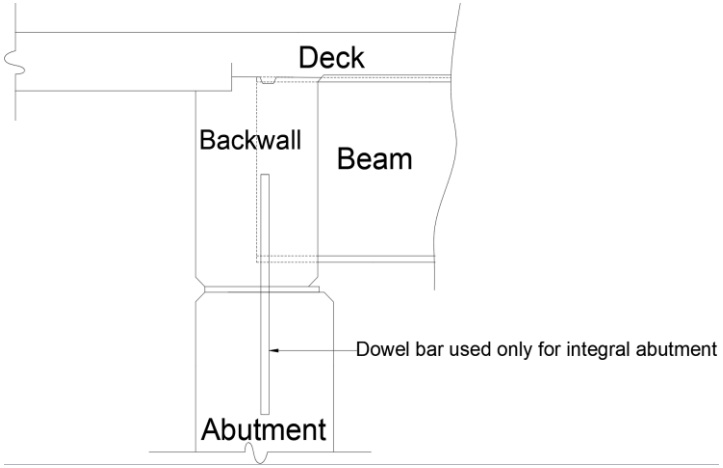

Integral and semi-integral abutment detail
(beam end embedded into the backwall)

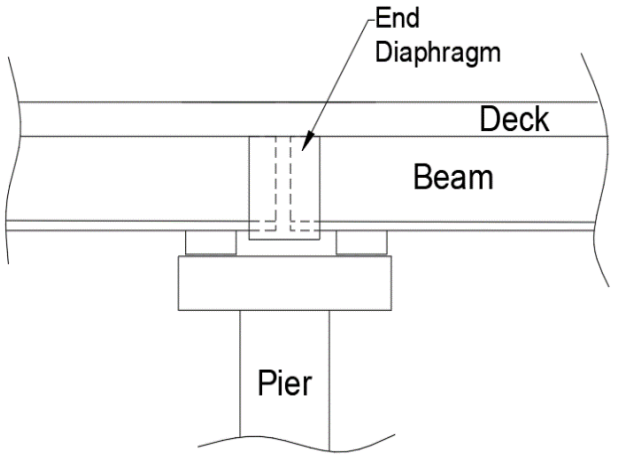

Continuous for live load detail over pier
(beam end embedded into the end diaphragm)

Please share your experience related to the repair of such beam ends.

Abutment and pier configuration	Beam end distress before repair	Possible causes of beam end distress	Beam end repair method	Implementation challenges	Possible long-term performance issues
Integral and semi-integral abutment					
Continuous for live load over pier					

8. Please share your experience with the following PSC I-beam end repair materials.

(a) Proprietary ultra-high performance concrete (UHPC)

Type of repair	Comment about the expected structural capacity contributions

(b) Non-proprietary ultra-high performance concrete (UHPC)

Type of repair	Comment about the expected structural capacity contributions

(c) High early strength concrete (HESC)

Type of repair	Comment about the expected structural capacity contributions

(d) Other repair materials

Name the material	

Type of repair	Comment about the expected structural capacity contributions

9. Concrete *patching* is a PSC I-beam end repair method. Sealants and/or coatings protect the repaired ends. Please comment on the ***long-term performance*** of the following implementations.

Concrete patching without additional protection	
Concrete patching protected with penetrating sealants	
Concrete patching protected with surface coating	
Concrete patching protected with penetrating sealants and concrete surface coatings (hybrid systems)	
Concrete patching protected with other techniques Please describe the techniques and performance	

10. Overcasting (or the use of end blocks) is a PSC I-beam end repair method. Please comment on the ***long-term performance*** of the following implementations.

End blocks without additional protection	
End blocks protected with penetrating sealants	
End blocks protected with surface coating	
End blocks protected with penetrating sealants and concrete surface coatings (hybrid systems)	
End blocks protected with other techniques Please describe the techniques and performance	

11. To minimize the failure of externally bonded Fiber-Reinforced Polymer (FRP) repair methods, various *anchorage systems* are used. A few examples are shown below:

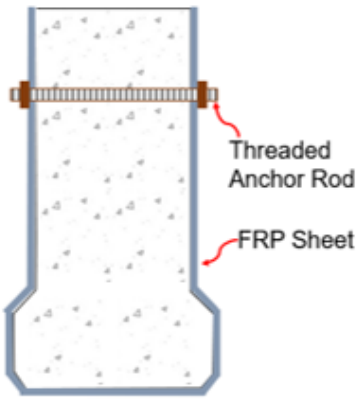

Threaded anchor rod

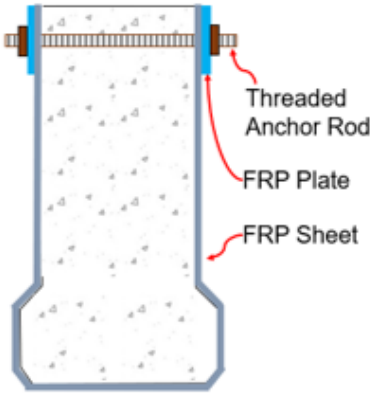

Typical FRP plate anchor

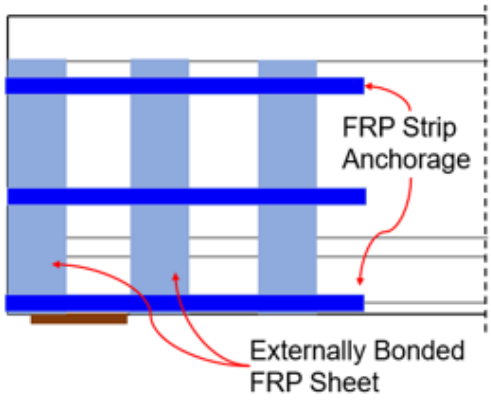

FRP strip

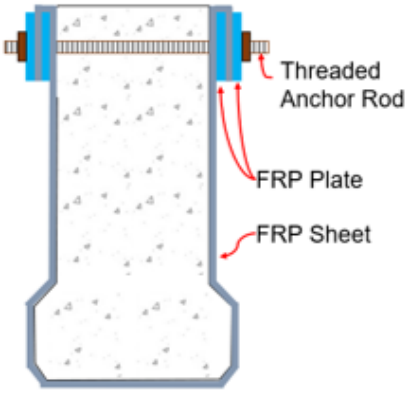

Sandwich FRP plate anchor

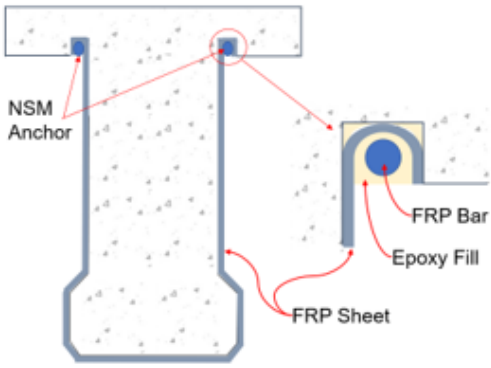

Near Surface Mounted (NSM) anchor rods

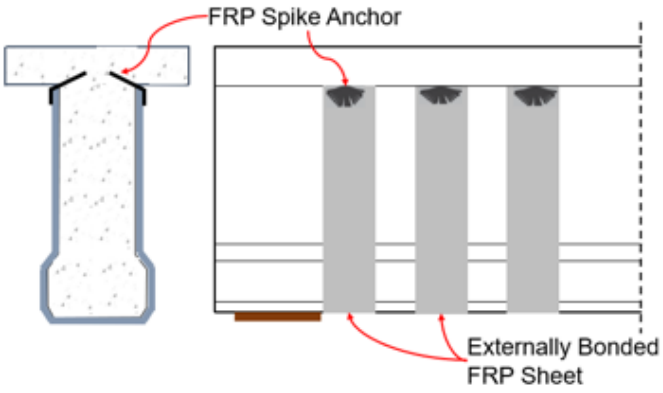

FRP spike anchor

The following figures show three different FRP configurations typically used at beam ends.

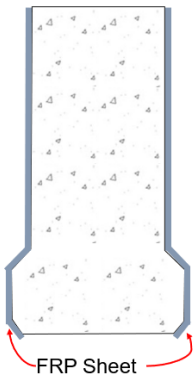

FRP side-bonding

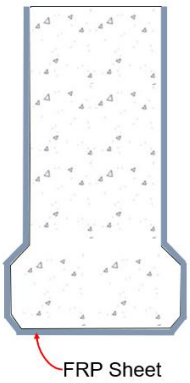

FRP U-wrap

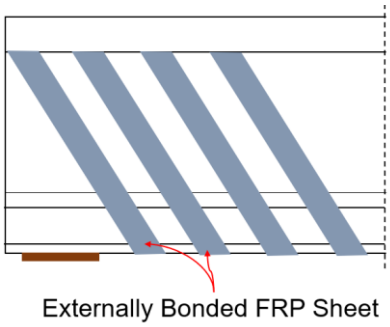

FRP strip at a 45° angle or perpendicular to shear cracks

Please select the FRP repair methods with different anchorage systems for PSC I-beam ends that you are familiar with and provide information.

FRP configuration	Anchorage systems	Implementation challenges	Performance
FRP side-bonding FRP U-wrap FRP strip at a 45° angle	None		
FRP side-bonding FRP U-wrap FRP strip at a 45° angle	Threaded anchor rod		
FRP side-bonding FRP U-wrap FRP strip at a 45° angle	Typical FRP plate anchor		
FRP side-bonding FRP U-wrap FRP strip at a 45° angle	Sandwich FRP plate anchor		
FRP side-bonding FRP U-wrap FRP strip at a 45° angle	FRP strip		
FRP side-bonding FRP U-wrap FRP strip at a 45° angle	FRP spike anchor		
FRP side-bonding FRP U-wrap FRP strip at a 45° angle	NSM anchor rods		

Other (please describe)	

A.1.3 PSC I-Beam End Capacity Calculation

12. Select the specifications/guides/references that you use for the design/capacity assessment of FRP repairs using Carbon Fiber Reinforced Polymer (CFRP), Glass Fiber Reinforced Polymer (GFRP) and Near-Surface Mounted (NSM) FRP bars.

Specifications/Guides/References	FRP Type	Remarks
AASHTO Guide Specifications for Design of Bonded FRP Systems for Repair and Strengthening of Concrete Bridge Elements, 1st Edition (AASHTO 2012) or 2nd Edition (AASHTO 2023)	CFRP GFRP NSM	
ACI 440R.2-17 Guide for the Design and Construction of Externally Bonded FRP Systems for Strengthening Concrete Structures (ACI Committee 440, 2017)	CFRP GFRP NSM	
ICRI Guideline No. 330.2 Guide Specifications for Externally Bonded FRP Fabric Systems for Strengthening Concrete Structures (ICRI 2016)	CFRP GFRP NSM	
Agency developed manuals/guides/calculation sheets (please specify and share links to access such publications)	CFRP GFRP NSM	
Other (please specify and share links to access such publications)	CFRP GFRP NSM	

13. Please select the method(s) used for calculating the shear and bearing capacities of deteriorated PSC I-beam ends.

In-house calculation tools based on the AASHTO Sectional Design Method (Please share links to access relevant documents and calculation tools)		
In-house calculation tools based on the Strut-and-Tie Method (Please share links to access relevant documents and calculation tools)		
Structural analysis software (Please list the name(s) of the software)		
AASHTOWare		
Other (Please describe)		

14. Please clarify any responses to this survey and/or provide additional information related to PSC beam end condition/capacity assessment with/without repairs.

A.2 STEEL I-BEAM

This survey is conducted for the MDOT-Sponsored Research Project OR23-001: Capacity Prediction of Repaired and Unrepaired Bridge Beams with Deteriorated Ends. Your response to the following questionnaire is greatly appreciated.

Please email the completed survey to kevinmakubuli.saleh@wmich.edu. For questions/concerns, please contact Kevin at (269) 267-7215.

Name:
Position:
Employer:
Email:

Note: We will NOT publish or share your contact information. Such information will ONLY be used for contacting you to get additional information or clarifications to the information provided as a response to the survey.

A.2.1 Inspection

1. Please share your experience with the section loss assessment. *Select all that apply*.

1(a). Thickness is measured using	Ultrasonic thickness gauge
	Calipers
	Other, specify
1(b). Web thickness loss is measured	Over the entire section loss area
	Only within a 4-in. strip from the bottom flange
	On a grid and reported as the average
	Randomly at several discrete points and reported as the average
	Other, specify

2. State the section loss conditions that initiate a Request for Action (RFA) submission.

3. With regards to pack rust, state the criteria for initiating a Request for Action (RFA) submission.

4. Repair methods implemented for various steel beam end conditions are shown below.

<table>
<tr><th>Beam end condition</th><th colspan="3">Repair method(s)</th></tr>
<tr><td>  </td><td>  </td><td colspan="2"> 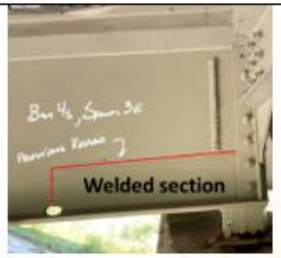
</td></tr>
<tr><td>Beam ends with a crack</td><td colspan="2">Crack arrest hole</td><td>Welded repair</td></tr>
<tr><td>  </td><td>  </td><td> 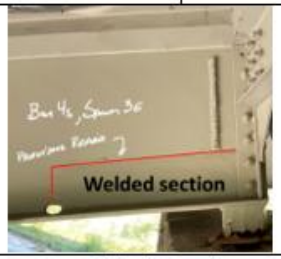
</td><td> 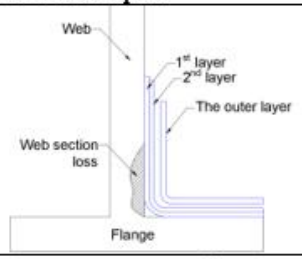
</td></tr>
<tr><td>Section loss due to corrosion</td><td>Bolted repair</td><td>Welded repair</td><td>CFRP repair</td></tr>
<tr><td>  </td><td>  </td><td> 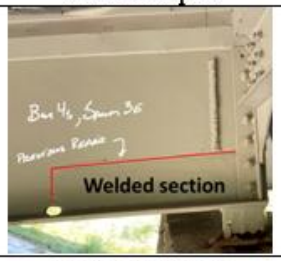
</td><td> 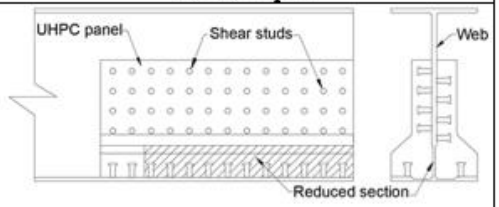
</td></tr>
<tr><td>Section loss with holes</td><td>Bolted repair</td><td>Welded repair</td><td>UHPC repair</td></tr>
</table>

Please describe the performance of the following steel beam end repair methods.

Bolted repair	
Welded repair	
Section replacement	
Crack arrest holes	
UHPC repair	
CFRP repair	
Cleaning and protection	
Other (specify the repair method)	

The following are possible options for bolted repairs.

5. Please list the types of bolts, washers, and nuts used in bolted repairs at beam ends and describe the performance.

Please provide access to additional resources regarding bolted repairs.

Steel beam ends are embedded into backwalls over the abutments and end diaphragms over the piers.

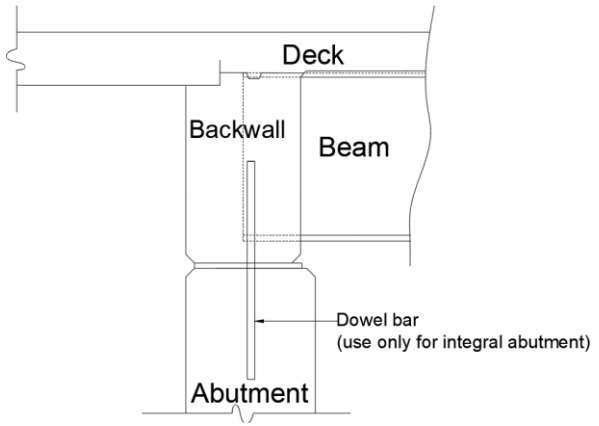

Integral and semi-integral abutment detail
(beam end embedded into the backwall)

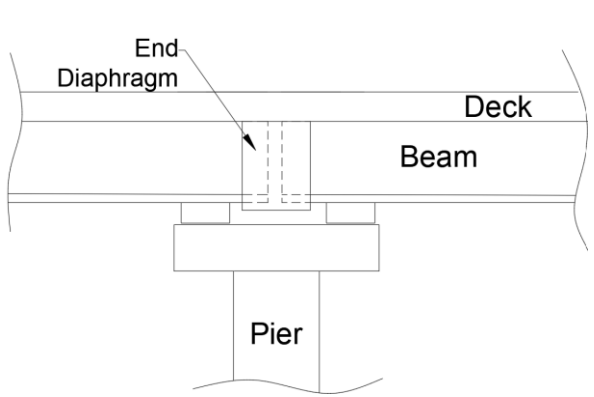

Continuous for live load detail over pier
(beam end embedded into the end diaphragm)

The following picture shows the loss of section of an embedded steel beam end due to corrosion.

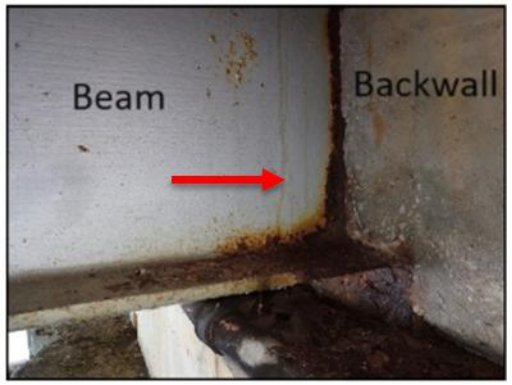

6. What is your approach for assessing the condition of a concealed beam end?

Please share your experience related to the implementation success, performance, and challenges of embedded beam end repairs.

	Indicate the repair method(s) suitable for embedded beam end	**Implementation success**	**Performance**	**Challenges**
Bolted repair				
Welded repair				
Section replacement				
UHPC repair				
CFRP repair				
Cleaning and protection				
Other, specify				

Please clarify any responses to this survey and/or provide additional information related to steel beam end inspection and repair performance.

A.2.2 Construction and Field Services

1. Please share your experience with the section loss assessment. *Select all that apply*.

1(a) Thickness is measured using	Ultrasonic thickness gauge
	Calipers
	Other, specify
1(b). Web thickness loss is measured	Over the entire section loss area
	Only within a 4-in. strip from the bottom flange
	On a grid and reported as the average
	Randomly at several discrete points and reported as the average
	Other, specify

2. Repair methods implemented for various steel beam end conditions are shown below.

Beam end condition	Repair method(s)		
		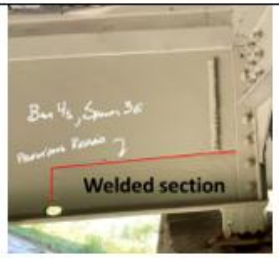	
Beam ends with a crack	Crack arrest hole	Welded repair	
		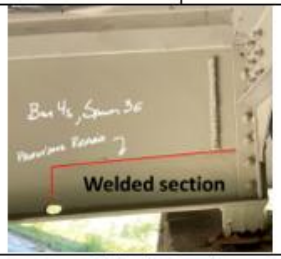	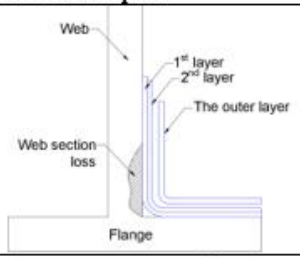
Section loss due to corrosion	Bolted repair	Welded repair	CFRP repair
		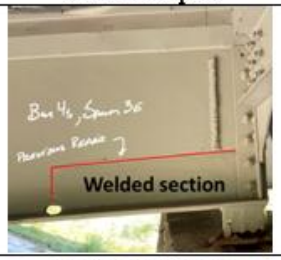	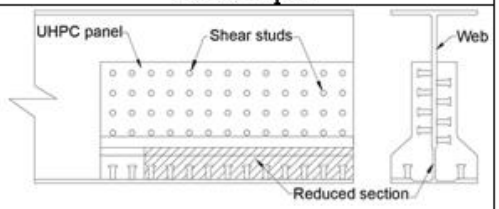
Section loss with holes	Bolted repair	Welded repair	UHPC repair

Please share your experience with the following repair methods and associated conditions.

	Crack(s) without section loss	**Crack(s) with section loss**	**Section loss**	**Section loss with holes**	**Other beam end conditions, specify**
Crack arrest holes					
Bolted repair					
Welded repair					
Beam end section replacement					
UHPC repair					
CFRP repair					
Cleaning and protection					
Other, specify					

Most preferred repair method(s)	
Reasons	

3. Even in the same bridge, different repair methods are implemented. For example, welded and bolted repairs are used on adjacent beam ends as shown in the following figure. Please share your experience with the following repair methods.

Repair method	Factors considered for selecting the repair method	Repair performance (expected service life, etc.)
Crack arrest holes		
Bolted repair		
Welded repair		
Section replacement		
UHPC repair		
CFRP repair		
Cleaning and protection		
Other, specify		

4. Please share your experience with welded repairs of steel beams/steel beam ends.

		Implementation challenges	Performance concerns	Reasons, if the method is NOT selected.
Shielded Metal Arc Welding (SMAW) is used in the field for	steel beam repair			
	steel beam end repair			
Gas Metal Arc Welding (GMAW) is used in the field for	steel beam repair			
	steel beam end repair			
Flux-Cored Arc Welding (FCAW) is used in the filed for	steel beam repair			
	steel beam end repair			
Laser Welding is used in the field for	steel beam repair			
	steel beam end repair			

Please list any other welding method(s) suitable for field welding of steel beam ends, implementation challenges, and performance concerns.

Please provide access to additional resources regarding welded repairs.

5. Please share you experience with bolted repairs at steel beam ends.

5(a). Are loose bolts or the loss of bolts and/or nuts a common problem?

Yes No

If Yes, state the precautions taken to minimize this problem:

5(b). The bolt tightening/pre-tensioning requirements:

(i) Snug-tight	Yes
	No

If Yes, do you verify the tension with a Calibrated Torque wrench	Yes	Required limits	
	No	Reasons:	

(ii)Pretensioned	Yes	If Yes, required pretension:	
	No		
(iii) Other, please describe			

5(c). Is there a preference for bolted repairs over welded repairs? Yes No

If *Yes*, please describe the reasons

The following are possible options for bolted repairs. *Eccentric nuts* and *Anaerobic adhesives* have outperformed the other methods when evaluated for retaining pretension under vibration.

Regular bolt and nut with a washer(s)

Double nuts

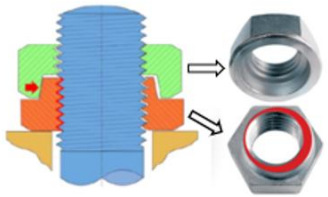

Eccentric nuts

Hexagon nut with flange

Nylon insert nut

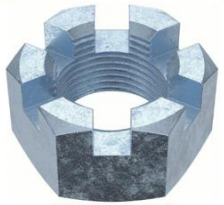

Slotted nut

Steel plate insert nut

Spring washer

Toothed washer

Wedge-locking washer

Anaerobic adhesive
(Threadlockers)

6. Please share your experience with the use of following techniques for steel beam repair.

	Regular bolt and nut	Regular bolt and nut with a washer	Anaerobic adhesive	Double nuts	Eccentric nuts	Hexagon nut with flange	Nylon insert nut	Slotted nut
(i) Snug-tight without tension verification								
(ii) Snug-tight with tension verification								
(iii) Pretension								

	Spring washer	Steel plate insert nut	Toothed washer	Wedge locking washers
Snug-tight with tension verification				
Snug-tight without tension verification				
Pretension				

(iv) Preferred methods	
Reasons	

Please provide access to additional resources regarding bolted repairs.

Steel beam ends are embedded into backwalls over the abutments and end diaphragms over the piers.

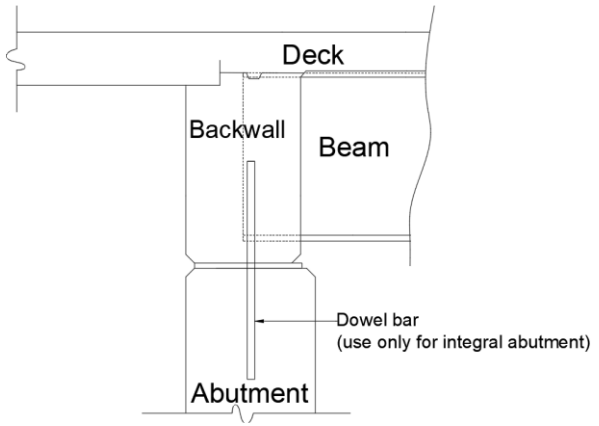

Integral and semi-integral abutment detail
(beam end embedded into the backwall)

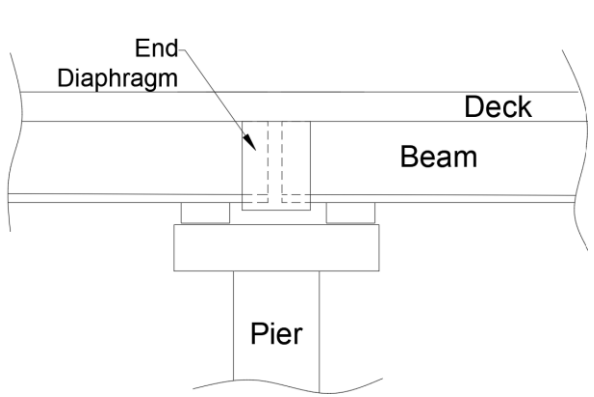

Continuous for live load detail over pier
(beam end embedded into the end diaphragm)

The following picture shows the loss of section of an embedded steel beam end due to corrosion.

7. What is your approach for assessing the condition of a concealed beam end?

8. Please share your experience related to the implementation successes, performance, and challenges of embedded beam end repairs.

	Indicate the repair method(s) suitable for embedded beam end	**Implementation successes**	**Performance**	**Challenges**
Bolted repair				
Welded repair				
Section replacement				
UHPC repair				
CFRP repair				
Cleaning and protection				
Other, specify				

Please clarify any responses to this survey and/or provide additional information related to steel beam end assessment, repair, and performance.

A.1.1 Design and Load Rating

Even in the same bridge, different repair methods are implemented. For example, welded and bolted repairs are used on adjacent beam ends as shown in the following figure.

1. Please state the factors that you would consider for selecting a specific repair method.

Repair method	Factors considered for selecting the repair method
(i) Bolted repair	
(ii) Welded repair	
(iii) Section replacement	
(iv) UHPC repair	
(v) CFRP repair	
(vi) Cleaning and protection	
(vii) Other, specify	

Steel beam ends are embedded into backwalls over the abutments and end diaphragms over the piers.

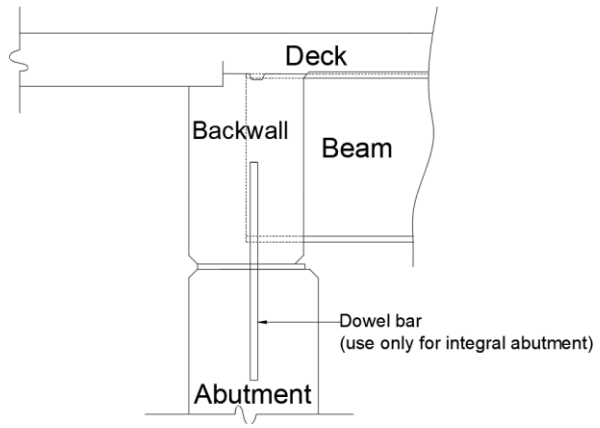

Integral and semi-integral abutment detail
(beam end embedded into the backwall)

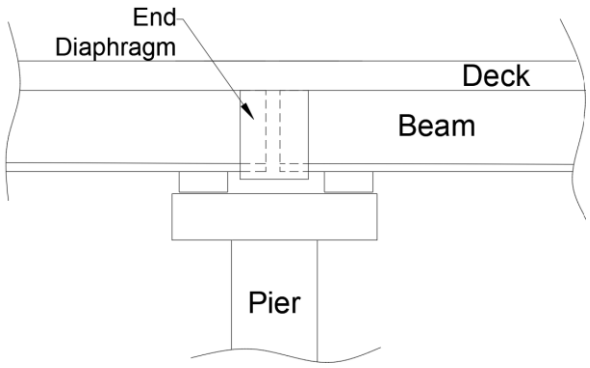

Continuous for live load detail over pier
(beam end embedded into the end diaphragm)

The following picture shows the loss of section of an embedded steel beam end due to corrosion.

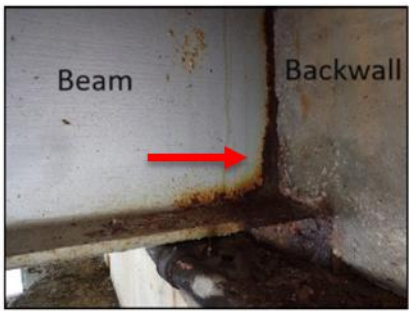

2. Do you consider the influence of end diaphragm or backwall for capacity assessment?

Yes No

If *Yes*, please describe the procedures or provide directions to access relevant information

3. The web thickness selected for capacity calculation *(select all that apply)*

Average thickness of the web

Average thickness of the section loss area

Average thickness within a 4-in. strip from the bottom flange

Other, specify

4. Select the specifications/guides/references that you use to calculate the capacity of deteriorated steel beam ends. Please state the resources used to introduce modifications to the process in the primary reference(s), if applicable.

Primary reference	Beam end condition	Resources used for additional modifications
AASHTO LRFD Bridge Design Specifications, 9th Edition	Beam ends with section loss	
	Beam ends with holes	
The AISC Steel Construction Manual, (Edition)	Beam ends with section loss	
	Beam ends with holes	
Massachusetts Department of Transportation Bridge Manual - Part I (Hundredth Anniversary Edition)	Beam ends with section loss	
	Beam ends with holes	
Agency developed manuals/guides/calculation sheets (please specify and share links to access such publications)		
Other (please specify and share links to access such publications)		

Please clarify any responses to this survey or provide additional information related to steel beam end condition/capacity assessment with/without repairs.

APPENDIX B: Survey responses

Survey Responses

A survey was conducted to document the assessment of steel beam and PSC I-beam end conditions, repair methods, repair designs, repair performance, and load rating experiences. Three sets of survey questionnaires were developed for each beam type, targeting inspection engineers, construction and field services engineers, and design and load rating engineers. The survey questionnaires are provided in Appendix A. The following sections describe the findings.

B.1 PSC I-BEAM END SURVEY RESPONSES

B.1.1 PSC I-Beam End Condition Assessment

1(a) Do you have established procedures to estimate the depth of delaminated area in PSC beams?

Response 1: No. Primarily visual inspection, sounding.

Response 2: No.

Response 3: No. We will sound the beam ends to find delaminated concrete, but if it doesn't spall off when sounding then we don't know how deep the delamination goes.

Response 4: No. Generally, delamination is assumed to exist at the first plane of rebar/strands

Response 5: No.

Response 6: No. Primarily visual inspection, sounding.

Response 7: No.

Response 8: No. Coring has been done in the past but is not a standard procedure. It is generally assumed that a delamination will form at the level of the reinforcement closest to the surface of the element.

Response 9: No. We generally only know if the concrete chips off when sounding the delaminated spot. However, I would defer to our inspection unit's response for more detail.

Response 10: No.

Response 11: No.

Response 12: No.

Response 13: No. No set procedures. We will hammer on the delaminated areas to ensure the concrete is not in danger of falling.

Response 14: No. Primarily visual inspection, sounding.

Response 15: No.

Response 16: Yes. IL DOT's estimation of corroded/ineffective strands for 1 (b) requires inspector(s) to determine depth of deteriorated concrete.

Response 17: No.

Response 18: No.

Response 19: No.

1(b) Do you have established procedures to estimate the number of corroded/ineffective strands?

Response 1: No. Primarily visual inspection.

Response 2: Yes. MassDOT uses a procedure based on IDOT's procedures for estimating corroded/ineffective strands. We modified this approach based on our own recent research. Estimates are made based on the results of visual inspection. Link to our Bridge Manual, Chapter 7 for Load Ratings which outlines the procedure: https://massdot.docs.mass.gov/hwy-bridge-manual/part-1/ch7-bridge-load-rating-guidelines.pdf

Response 3: Yes. Visually inspect them.

Response 4: No. Exposed strands are considered ineffective.

Response 5: No.

Response 6: No. Primarily visual inspection.

Response 7: Yes. MassDOT uses a procedure based on IDOT's procedures for estimating corroded/ineffective strands. We modified this approach based on our own recent research. Estimates are made based on the results of visual inspection. Link to our Bridge Manual, Chapter 7 for Load Ratings which outlines the procedure: https://massdot.docs.mass.gov/hwy-bridge-manual/part-1/ch7-bridge-load-rating-guidelines.pdf

Response 8: No. If the strands are not visible during an inspection it is typically not known.

Response 9: Yes. See Section 4.3.4.2.3, Section 4.3.4.2.4, and Appendix A-10 of the IDOT Structural Services Manual. (https://idot.illinois.gov/content/dam/soi/en/web/idot/documents/doing-business/manuals-guides-and-handbooks/highways/bridges/inspection/structural-services-manual.pdf)

Response 10: No.

Response 11: No.

Response 12: No.

Response 13: No set procedures. If delaminated concrete is taken off due to safety concerns and strands are exposed then an exact number can be had. If not but there is rusting, coming through the cracking then the plans can be referenced where the strands are and we can estimate.

Response 14: No. Primarily visual inspection

Response 15: No.

Response 16: Yes. See Page 7-111 of the attached link. https://public.powerdms.com/IDOT/documents/2084747/Structural%20Services%20Manua

Response 17: Yes. If exposed, it's broke.

Response 18: Yes. MassDOT uses a procedure based on IDOT's procedures for estimating corroded/ineffective strands. We modified this approach based on our own recent research. Estimates are made based on the results of visual inspection. Link to our Bridge Manual, Chapter 7 for Load Ratings which outlines the procedure: https://massdot.docs.mass.gov/hwy-bridge-manual/part-1/ch7-bridge-load-rating-guidelines.pdf

Response 19: No.

1(c) Do you have established procedures to estimate the number of corroded/ineffective stirrups?

Response 1: No. Primarily visual inspection.

Response 2: No.

Response 3: No. We will do a visual inspection and also use small hand tools during the inspection process and will note the condition of any stirrups that are exposed.

Response 4: No.

Response 5: No.

Response 6: No. Primarily visual inspection.

Response 7: No.

Response 8: No. A visual inspection is the only standard means to determine the number of stirrups impacted by corrosion and the extent of any deterioration. Miscellaneous quantities of reinforcement are typically included in projects to account for any deterioration.

Response 9: Yes. This is based on visual inspection and measurement of bar section loss. Stirrups are generally deemed fully ineffective if the majority of concrete beneath them is unsound. Stirrups are considered partially effective if broken on the underside with satisfactory cover and anchorage on the web portion.

Response 10: No.

Response 11: No.

Response 12: No.

Response 13: No. No set procedures, see (b).

Response 14: No. Primarily visual inspection.

Response 15: No.

Response 16: Yes. Goes hand-in-hand with procedure in 1 (b).

Response 17: No.

Response 18: No.

Response 19: No.

B.1.2 PSC I-Beam End Repair

2(a). Do you protect beam ends after patching using any of the following methods for enhanced durability?

Response 1: Yes. For concrete surface coating, most commonly used product(s) Saturating epoxy (e.g. Sikadur 300) used for CFRP application plus UV protective coating (e.g. Sikagard 550W). Performance - none of the repairs carried out within the last 12 years have had any issues.

Response 2: No. We generally do not perform precast repairs. Those that have been done are generally discounted for effectiveness and acknowledged to be surficial only.

Response 3: Yes. You'll have to get information from bridge design on the different products that we use to coat the beam ends. I prefer sealants over concrete surface coating, because I want the beam ends to be protected.

Response 4: Yes. Penetrating sealants, Implementation challenges: Access. Performance: useful life estimated at 5 years. Additional comments: Sealant coatings have become widely used at MDOT.

Concrete surface coating: Yes. Implementation challenges: Access, Additional comments: coatings were common, but now sealant is used more.

Response 5: No.

2(b) Do you apply bonding agents on the prepared concrete surface before patching?

Response 1: Yes, Sika Armatec.

Response 2: Yes.

Response 4: No.

Response 5: No.

3(a) Do you protect beam ends with overcasting using any of the following methods for enhanced durability?

Response 2: No.

Response 3: Yes.

Response 4: Yes. Penetrating sealants, Implementation challenges: Access. Performance: useful life estimated at 5 years. Additional comments: Sealant coatings have become widely used at MDOT.

Concrete surface coating: Yes. Implementation challenges: Access, Additional comments: coatings were common, but now sealant is used more.

Response 5: No.

3(b) Do you apply bonding agents on the prepared concrete surface before overcasting?

Response 2: No.

Response 4: No.

Response 5: No.

4. Various strategies can be implemented to protect exposed steel (strands/reinforcement) at damaged/deteriorated PSC I-beam ends. A few approaches are described below. Please share your experience with such approaches.

Response 1: Applying coating(s) for corrosion protection before patching/overcasting. Uses Sika Armatec, FX-406. Implementation challenges: if using Sika Armatec, it is also a bonding agent, so the patching needs to be carried out immediately after application. Performance: none of the repairs carried out within the last 12 years have had any issues.

Response 3: you'll have to get info from bridge design on this. We do coat beam ends and leave some if the deterioration is not significant. I'm not sure of the exact product we use.

Response 4: (i): Not frequent; Would be preventive maintenance; I have seen primer coat for exposed rebar.

(ii): Not common

(iii): Yes; Implementation challenges: Manufacturers have different spacings; Performance: good

(iv): Coating beam ends with epoxy mastic has been proposed several times, but I'm not sure it's been implemented.

Response 5: (iii): Galvanizing coating; Implementation challenges: tight access; Performance: good.

5. After chipping out and cleaning a deteriorated beam end, the cleaned concrete surface can be protected with penetrating sealants, concrete surface coatings, patching, or overcasting. Please share your experience with such approaches.

Response 3: So far, I think it has gone okay to just clean and coat the beam ends to protect them.

Response 4: No.

6(a). Please share your field implementation experience with the following repair materials and construction methods.

Response 1: Carbon fiber reinforced polymer (CFRP) sheets/strips. Implementation challenges: wrapping near/around the bearing/seat of the beams can be difficult. May need jacking if damage extends to areas over the bearing pads. Performance: None of the repairs carried out within the last 12 years have had any issues.

Response 3: Near surface mounted (NMS) FRP bars/strips : I think that FRP has worked well in University Region overall. We are still in the beginning stages of using it, so we don't have a significant amount of data.

Response 4: CFRP: Used commonly. Good performance

GFRP: advantages over CFRP are not clear.

NMS: full carbon wrap would be a more typical use at MDOT

UHPC: Use cases where latex modified concrete would not be effective is rare. Used occasionally. Good performance.

HESC: Used occasionally. Good performance.

6(b). Construction method.

Response 1: Cast-in-place concrete patching. Implementation challenges: forming and placing concrete near/around the bearing/seat of the beams can be difficult. Performance: None of the repairs carried out within the last 12 years have had any issues.

Response 3: Cast-in-place concrete. Patching: Need to get behind the rebar when these are patched, so the concrete has something to bond to and won't just fall off over time. Overcasting: Need to get behind the rebar when these are patched, so the concrete has something to bond to and won't just fall off over time.

Response 4: Shotcrete: Patching and Overcasting: Contractor equipment capital expense, can be difficult to apply. Not commonly used.

Cast-in-place concrete: Patching and Overcasting: Used commonly. Good performance.

7. Please share your experience related to the repair of PSC I-beam ends embedded into backwalls or end diaphragms.

Response 1: N/A. All repair received by KTC have been at 'free' ends next to the abutment.

Response 4: Integral and semi-integral abutment: hand chip backwall and repair beam; Requires additional chipping, forming challenges. Good. This type of repair is rare.

Continuous for live load over pier: hand chip backwall and repair beam; Requires additional chipping, forming challenges. Good. This type of repair is rare.

Response 13: Integral and semi-integral abutment: Patching and End Blocks: Patching: Usually cracking in the patch within 2-3 inspection cycles. (4-6 years), End block: Usually cracking and sometimes delam in the end blocks within 4-5 inspection cycles. (8-10 years)

Continuous for live load over pier: Patching and End Blocks: Patching: Usually cracking in the patch within 2-3 inspection cycles. (4-6 years), End block: Usually cracking and sometimes delam in the end blocks within 4-5 inspection cycles. (8-10 years)

Response 14: N/A. All repair received by KTC have been at 'free' ends next to the abutment.

Response 15: Continuous for live load over pier: The locations are constantly cracking however we have not attempted repairing this cracking as it is almost always occurring in the diaphragms and not the girders.

Response 16: N/A. IL DOT has not needed to repair any PSC Beam ends on bridges with integral abutments.

Response 17: Integral and semi-integral abutment: We don't see much issues here

Continuous for live load over pier: Used to have a detail of a dowel rod that went from the beam into the diaphragm and the concrete would always pop off; stopped using the detail, but spall was in diaphragm and hardly ever penetrates beam ends

Response 18: No experience.

Response 19: Breakout and patch concrete. Fair - There is usually excessive movement and concrete cracks or spalls.

8. Please share your experience with the following PSC I-beam end repair materials.

(a) Proprietary ultra-high performance concrete (UHPC)

Response 7: We don't repair precast beam ends.

Response 8: Has not been used to repair PSC beam ends

Response 9: Defer to Construction and Field Services response.

8(b) Non-proprietary ultra-high performance concrete (UHPC)

Response 7: We don't repair precast beam ends.

Response 8: Has not been used to repair PSC beam ends. Has been used to address the deterioration of the ends of steel girders on one project as a trial.

Response 9: Defer to Construction & Field Services ' response.

8(c) High early strength concrete (HESC)

Response 6: Patching. Meet or exceed existing concrete strength.

Response 7: We don't repair precast beam ends.

Response 8: Has not been used to repair PSC beam ends

Response 9: Defer to Construction & Field Services ' response.

Response 11: No experience.

8(d) Other repair materials

Response 7: We don't repair precast beam ends.

Response 8: Latex Modified Concrete: Standard details were proposed in MDOT Research Report R-1380.

Response 9: Defer to Construction & Field Services ' response.

Response 10: Dry-mix shotcrete from the approved products list. Meet or exceed the original beam end shear capacity

Response 11: Concrete patching with galvanic coating. Should be adequate.

Response 12: Conventional Repair grouts. Not commonly required repair at beam ends.

9. Concrete *patching* is a PSC I-beam end repair method. Sealants and/or coatings protect the repaired ends. Please comment on the *long-term performance* of the following implementations.

Response 13: Concrete patching without additional protection: Usually, cracking in the patch occurs within 2-3 inspection cycles. (4-6 years)

Concrete patching protected with penetrating sealants: Usually, cracking in the patch occurs within 2-3 inspection cycles. (4-6 years)

Concrete patching protected with surface coating: Usually, cracking in the patch occurs within 2-3 inspection cycles. (4-6 years)

Concrete patching protected with penetrating sealants and concrete surface coatings (hybrid systems): Not sure if we have used hybrid systems.

Response 14: Concrete patching without additional protection. This has been typically done only on small sections (<1 cu. ft.) behind the bearing region of the beams. The oldest such repair is about 12 years ago, and no defects have been detected so far.

Concrete patching protected with other techniques: Damages that extend beyond the bearing area into the span of the beam are patched and strengthened with CFRP fabric. The saturating epoxy is used as a sealant (moisture barrier) and the final repair is coated with a UV coating that is resistant to weathering, frost, and deicing salts.

Response 16: Patching of PSC Box/I-Beam ends due to deterioration is discouraged in IL. Patching of PSC Box/I-Beams while still at the fabrication plant or while being erected in the field has proven to be very effective if done per specification.

Response 17: Concrete patching without additional protection: mixed results.

Concrete patching protected with other techniques: CAT Strong (FRP wrap developed by University of KY); good results

Response 18: Concrete patching without additional protection: Some MassDOT Districts do this. Long-term performance is not good, which is one of the reasons we don't do precast repair.

Concrete patching protected with surface coating: One MassDOT District is known to use an elastomeric coating over patches. Long-term performance is not good, which is one of the reasons we don't do precast repair.

Response 19: Concrete patching protected with other techniques: Concrete patching with a galvanic coating system. Performing well.

10. Overcasting (or the use of end blocks) is a PSC I-beam end repair method. Please comment on the *long-term performance* of the following implementations.

Response 13: End blocks without additional protection: Usually cracking and sometimes delamination in the end blocks within 4-5 inspection cycles. (8-10 years)

End blocks protected with penetrating sealants: Usually cracking and sometimes delamination in the end blocks within 4-5 inspection cycles. (8-10 years)

End blocks protected with surface coating: Usually cracking and sometimes delamination in the end blocks within 4-5 inspection cycles. (8-10 years)

End blocks protected with penetrating sealants and concrete surface coatings (hybrid systems): Not sure if we have used hybrid systems.

Response 14: N/A.

Response 16: Use of end blocks for deteriorated PSC I-Beam end repair has proven to be effective if done per plans & specifications.

Response 17: N/A.

Response 18: MassDOT does not overcast/use end blocks.

Response 19: End blocks without additional protection: Did once and seemed to work. The repair only had to last until bridge replacement.

11. Please select the FRP repair methods with different anchorage systems for PSC I-beam ends that you are familiar with and provide information.

Response 1: FRP side-bonding. FRP U-wrap. Anchorage systems: FRP strip. Implementation challenges: Wrapping near/around the bearing/seat of the beams can be difficult. Performance: None

of the repairs carried out within the last 12 years have had any issues.

Response 2: MassDOT does not perform structural precast repairs. I worked on repair details when I was a consultant, but was not involved in the construction phase services to the extent to be exposed to any challenges. I don't know how they have performed.

Response 4: FRP side-bonding. FRP U-wrap. Good performance

Response 5: No experience with FRP at beam ends.

Response 6: FRP side-bonding. FRP U-wrap: In AASHTO I-beams where the damage is limited to the soffit area, the U wrap would only cover the bottom flange.

FRP strip: Typical repair. All the repairs carried out by KTC have been on beams with less than 10% section loss that extend less than 4 ft from the bearing area.

Response 7: The option to use a full U-wrap would be affected by how far back towards the beam end the repairs are needed. Can't U-wrap the bearing unless the beam is jacked and the bearing replaced.

As mentioned in prior responses, MassDOT does not perform precast repairs. My personal experience with other DOTs locally is that U-wraps are generally used due to local contractor experience with the application.

Response 8: None: This is the most common for MDOT applications. The reduced usable strain from non-anchored strips lowers the effective strengthening, but so far, we've been able to use it for the strengthening needed.

FRP strip: The design accounts for the reduced capacity of non-anchored FRP (max strain is limited to the debonding strain of FRP). Typically, the strengthening needed is within this reduced capacity of FRP. Anchor strips are used in cases where we need more capacity than the unbonded strips provide.

Response 9: Defer to Construction & Field Services ' response.

Response 10: FRP U-wrap: None: MnDOT has limited experience in PS beam FRP wraps. The few locations currently in service are not anchored other than U-wrap with the full height of the web

Response 11: No experience with these systems.

Response 13: No experience with these systems.

Response 14: FRP side-bonding. FRP U-wrap, FRP strip: None of the repairs carried out within the last 12 years have had any issues. Typically, all our repairs have FRP on the beam soffit as well.

Response 15: FRP U-wrap: None: The wraps were placed on the cross section of the bottom flanges where cracking had developed due to an issue with the temperature gradient at the end diaphragms over interior piers. The wraps have been in place for 30 years or so and seem to be functioning well.

Response 16: FRP U-wrap: None. Use of FRP wrapping has proven to be effective if done per plans & specifications and is done by qualified personnel.

Response 17: FRP side-bonding. FRP U-wrap, FRP strip at a 45° angle, FRP strip: We had good results with the UK's Cat Strong product

Response 18: FRP side-bonding. FRP U-wrap, FRP strip at a 45° angle, none: The option to use a full U-wrap would be affected by how far back towards the beam end the repairs are needed. Can't U-wrap the bearing unless the beam is jacked and the bearing replaced.

Response 19: We haven't used any of the above techniques

B.1.3 PSC I-Beam End Capacity Calculation

12. Select the specifications/guides/references that you use for the design/capacity assessment of FRP repairs using Carbon Fiber Reinforced Polymer (CFRP), Glass Fiber Reinforced Polymer (GFRP), and Near-Surface Mounted (NSM) FRP bars.

Response 6: AASHTO: CFRP: No GFRP or NSM field applications carried out by KTC.

ACI 440R.2-17: CFRP: No GFRP or NSM field applications carried out by KTC.

ICRI Guideline No. 330.2 is for installation and quality control and does not have guidance on design/capacity assessment.

Response 7: AASHTO: CFRP, GFRP, NSM

ACI 440R.2-17: CFRP, GFRP, NSM: We would most likely use this only as a concurrent reference to the AASHTO document, possibly to find additional clarification on some calculation or requirement.

ICRI Guideline No. 330.2: We wouldn't use this because our procurement rules would probably prevent us from buying it.

Response 9: Defer to Construction & Field Services ' response.

Response 10: AASHTO: CFRP: Currently, MNDOT uses the AASHTO Guide.

ACI 440R.2-17: CFRP: Earlier projects used ACI as the design specs.

Response 11: No experience with these systems.

13. Please select the method(s) used for calculating the shear and bearing capacities of deteriorated PSC I-beam ends.

Response 6: Other: When shear stirrups were damaged (corroded), these were primarily behind the bearing region. When there was corroded shear stirrups in front of the bearing region (within clear span), they were never sufficiently corroded to consider additional shear strengthening.

Response 7: In-house calculation tools based on the AASHTO Sectional Design Method: These would be "hand" calcs done internally and not posted online. AASHTOWare

Response 8: In-house calculation tools based on the AASHTO Sectional Design Method

Structural analysis software: LEAP Concrete

Response 9: AASHTOWare: Remove ineffective stirrups from the model. De-bond ineffective strands out to the point within the span where the concrete is sound again.

We occasionally apply some type of reduction factor to stirrup capacity if they are broken at the bottom flange with suitable anchorage elsewhere. This is based on judgment and incorporated by reducing the bar size/number of legs in the model.

Response 10: In-house calculation tools based on the AASHTO Sectional Design Method

Response 11: AASHTOWare:

Response 12: In-house calculation tools based on the AASHTO Sectional Design Method. In-house calculation tools based on the Strut-and-Tie Method. Structural analysis software.

14. Please clarify any responses to this survey and/or provide additional information related to PSC beam end condition/capacity assessment with/without repairs.

Response 3: We have had issues with concrete beam end repairs in the past (not having concrete bonded to steel or anything else), and the repairs fell off, then we had our maintenance crews chip them off, so they wouldn't fall on traffic/pedestrians.

Response 6: All PC beam end repairs carried out by KTC have been prior to a significant loss of section (< 10%) from the tendons or the shear stirrups within the clear span of the beams.

Response 10: MNDOT is in the process of establishing PCB beam end repair using FRP. We are interested in the anchorage details, such as the FRP plate anchor and/or the FRP strip. If you have detailed information and are able to provide it, it will be greatly appreciated. Thanks.

Response 12: For new designs, Alaska almost exclusively uses semi-integral abutments with full width full depth CIP end diaphragms, so the girder ends are not exposed to moisture and corrosive elements. Similarly, Alaska designs our PSC girders to a zero tension limit under the service III load combination so cracking in any portions of our girders is unexpected. Primarily, we would deal with girder repairs due to over-height strikes where strands and/or stirrups have been severed. We perform these repairs while preloading the girders from above using loaded dump trucks such that any patches are put back into compression when the preload is removed. Obviously, this is more applicable near the midspan of beams and not near the ends.

Response 13: There are several other factors that might go into longevity of repairs, such as correct/approved construction methods of the repaired area, joints above the beam ends

Response 17: Dr. Issam Harik is our contact at the UK for the Cat Strong product.

B.2 STEEL BEAM END SURVEY RESPONSES

B.2.1 Inspection

Q1(a): Thickness is measured using

Response 1: Ultrasonic thickness gauge and calipers
Response 2: Ultrasonic thickness gauge and calipers
Response 3: Ultrasonic thickness gauge
Response 4: Ultrasonic thickness gauge and calipers
Response 5: Ultrasonic thickness gauge and calipers

Q1(b): Web thickness loss is measured

Response 1: Over the entire section loss area, usually, the maximum loss is reported
Response 2: Over the entire section loss area
Response 3: Over the entire section loss area, measured on a grid and reported as the average.
Response 4: Over the entire section loss area, measured randomly at several discrete points and reported as the average.

Response 5: Over the entire section loss area, measured on a grid and reported as the average, measured randomly at several discrete points and reported as the average.

Q2: The section loss conditions that initiate a Request for Action (RFA)

Response 1: Usually 30% or greater

Response 2: When a detailed inspection is performed and section loss measurements are taken, usually an RFA is submitted for load analysis to reflect current field conditions.

Response 3: CS4

Response 4: 1/8" loss or more. Less than that would typically be in the negligible range.

Response 5: Identification of defects warranting repairs results in inspectors creating a recommendation for repairs as part of the bridge inspection.

Q3: The pack rust condition that initiates a Request for Action (RFA)

Response 1: Usually, when section loss is noted or when pack rust is deforming the base metal

Response 2: Pack rust that is causing distortion/distress in the connected members.

Response 3: Treat the pack rust the same as the section loss because the presence of pack rust indicates that section loss is present.

Response 4: All pack rust must be removed to take accurate measurements.

Response 5: Identification of defects warranting repairs results in inspectors creating a recommendation for repairs as part of the bridge inspection.

#881: Steel Section Loss (1 Each)

This element applies to bridges with primary steel members with section loss due to corrosion. This typically refers to steel superstructure members but could also apply to steel substructure members (such as pilings) that serve as primary supports. Section loss is typically expressed as a percentage of the total cross-section area of the member (the percentages listed below are intended to be general guidelines).

- The presence of flaking rust or pack rust indicates that at least some section loss is present.
- This element should not be used for culvert structures.

Structural Member	Defect Element Condition States			
	1 Good	2 Fair	3 Poor	4 Severe
Flanges or tension members	Less than 2% section loss of the flange cross-section area.	2% to 5% section loss of the flange cross-section area.	5% to 10% section loss of the flange cross-section area.	More than 10% section loss of the effective flange cross-section.
Webs or compression members	Less than 2% section loss (average over the full height of the web). No through corrosion.	2% to 5% section loss (average over the full height of the web). No through corrosion.	5% to 10% section loss (average over the full height of the web). Isolated through corrosion.	More than 10% section loss (average over full height of the web). Significant through corrosion.
Stiffeners, Lacing, or Batten Plates	Moderate section loss.	Extensive section loss. Isolated through corrosion.	Severe section loss. Significant through corrosion.	NA

Figure B- 1. Element condition states given in the MNDOT Bridge Inspection Field Manual (2016)

Q4: The performance of steel beam end repair methods.

Bolted repair	Response 1: Adequate performance Response 2: Most bolted repairs are high-performing. Surface preparation and sealing the perimeter of the repair is important. Response 4: Good repair, versatility in its application. Response 5: Fewer examples than welded
Welded repair	Response 1: Have not tried this repair type yet Response 2: High performing with little to no concerns with long-term performance. Response 4: Not as good, fatigue, and weld quality concerns Response 5: Many examples, performing well when the reverse side of the plate is seal-welded to prevent ingress of moisture
Section replacement	Response 1: Have not tried this repair type yet Response 2: No experience with this type of repair. Response 4: The best repair is achieved when full-penetration welds are used. Response 5: Has not been performed for the beam ends
Crack arrest holes	Response 1: Have not tried this repair type yet Response 2: Effective if the hole is captured, but requires checking during routine inspections to make sure the crack hasn't reestablished. Response 4: Good repair and cheap as long as the crack tip can be captured Response 5: Performance is dependent on properly capturing the crack tip
UHPC repair	Response 1: Have not tried this repair type yet Response 2: No experience with this type of repair. Response 4: Shows promise based on research Response 5: Only one known project, performing well
CFRP repair	Response 1: Have not tried this repair type yet Response 2: No experience with this type of repair. Response 4: Not used. Response 5: Have not used CFRP on steel
Cleaning and protection	Response 1: Best performance for preventing additional damage Response 2: Effective if capacity isn't affected by loss. Response 4: Good when only minor loss or scrapes Response 5: Many examples, performing well
Other	Response 1: Encasing steel ends in concrete; adequate performance

Q5: Types of bolts, washers, and nuts used in bolted repairs at beam ends and their performance.

Response 1: Just using regular bolts and nuts with washers, with adequate performance.

Response 2: High-strength bolts.

Response 3: Structural bolts, washers, and nuts for the required strength.

Response 4: Regular bolts and nuts w/wo washers. Lock washers are used occasionally—tried and true performance.

Response 5: Typically, regular bolts and nuts with washers - no known performance issues.

Q6: What is your approach for assessing the condition of a concealed beam end?

Response 1: We haven't encountered this issue yet, as we haven't encased many steel girders during initial construction or repaired them.
Response 2: Measure the loss and verify the load capacity.
Response 4: Can only inspect what is visible.
Response 5: Evaluate the concrete condition and the section loss of the beam end.

Q7: The implementation success, performance, and challenges of embedded beam end repairs.

Response 2: Have used bolted repair. Implementations are very successful. The performance is very high. Challenges in implementing skewed beams.
Response 5: Cleaning and protection - many examples, performing as well as any other beam.

B.2.2 Construction and Field Services

Q1(a): Thickness is measured using

Response 1: Ultrasonic thickness gauge and calipers
Response 2: Straight edge and rule
Response 3: Ultrasonic thickness gauge and calipers
Response 4: Ultrasonic thickness gauge and calipers
Response 5: Ultrasonic thickness gauge
Response 6: Ultrasonic thickness gauge and calipers
Response 7: Ultrasonic thickness gauge and calipers

Q1(b): Web thickness loss is measured

Response 1: Over the entire section loss area; usually, the maximum loss is reported
Response 2: Over the entire section loss area
Response 3: Over the entire section loss area
Response 4: Over the entire section loss area, we pick the areas with the greatest amount of loss and report that. May have to take measurements at several different points.
Response 5: On a grid and reported as the average
Response 6: Over the entire section loss area, randomly at several discrete points, and reported as the average
Response 7: Over the entire section loss area, on a grid and reported as the average, randomly at several discrete points and reported as the average

Q2: Experience with the repair methods and associated conditions

Response 1: Crack arrest holes have not been tried often.
Bolted repair for section loss and section loss with holes seems to work and match.
Cleaning and protection of the section loss area successfully arrest or slow down additional corrosion.
Response 2: Crack arrest holes are used for cracks with and without section loss

Bolted repairs are used for cracks with and without section loss

Cleaning and protection are used for section loss

Response 3: Crack arrest holes are used for cracks with and without section loss

Bolted repairs are used for cracks with and without section loss, as well as section loss with holes.

Welded repairs are used for cracks with and without section loss, as well as section loss with holes.

Beam end section replacement is an option for section loss and section loss with holes.

Response 4: Crack arrest holes are used for cracks with and without section loss.

Bolted repairs are used for section loss.

Welded repairs are used for section loss with holes.

Beam end section replacement is used for section loss with holes.

Cleaning and protection are used for section loss and section loss with holes. Would have to clarify with the design and SP's on paint standards and materials.

Response 5: Crack arrest holes are used for cracks with and without section loss.

Bolted repairs are used for cracks with section loss, and section loss with holes.

Beam end section replacement is used for cracks with section loss and section loss with holes.

Cleaning and protection are used for cracks with and without section loss, as well as for section loss with holes.

Response 6: Crack arrest holes are used for cracks without section loss.

Bolted repairs are used for cracks with and without section loss, as well as section loss with holes.

Welded repairs are used for section loss and section loss with holes. Some experience with maintenance, not recommended for a planned repair strategy.

Beam end section replacement is used for section loss and section loss with holes. Full penetration welds are required.

UHPC repair was conducted as a research project, but there is currently no implementation.

Concrete encasement is used for section loss.

Response 7: Crack arrest holes are used for cracks with and without section loss.

Bolted repairs are used for section loss and section loss with holes.

Termarust is used to protect steel sections with section loss and section loss with holes.

Q2: The most preferred beam end repair method and reasons for selection

Response 1: Bolted repair along with cleaning and protection
Maintenance can usually do a bolted repair, and cleaning and protection will arrest or slow additional corrosion.

Response 3: Bolted repairs are always preferred if possible. Welded repairs can be used if there is distortion in the beams that prevents the use of bolted repairs.
Bolted repairs are faster and require less skill by the contractor. Testing requirements are also reduced.

Response 4: Bolted and welded repairs and crack arrest holes. The preferred method of repair varies based on the condition of the beam end. Not all repair types would apply to every situation.

Response 5: Crack arrest holes if properly installed and bolted repairs. Crack arrest holes are easier to implement. Bolted repairs are also easier for field construction.

Response 6: Crack arrest holes if the crack end can be accurately located. Bolted repair is preferred because it can be easily scaled to different connection types and conditions.

Response 7: Bolted or welded, and crack arrest holes. Easy to perform by in-house maintenance staff or most contractors.

Q3: Please share your experience with the following repair methods.

Repair Method	Factors Considered for Selecting the Repair Method	Repair Performance (expected service life, etc.)
Crack arrest holes	Response 1: access, maintenance capabilities Response 2: Simple to perform. Usually effective. Response 3: All cracks should have crack arrest holes. Response 4: Type of cracks, length of cracks, and need buy-in from Christopher Idusuyi to say, drill a hole to arrest the crack. Response 5: No section loss present; proper usage Response 6: No section loss present. Easily drilled and monitored for performance. Response 7: Location and cause of the crack, access	Response 1: 10-30 years Response 2: Depends. Should be monitored. Response 3: Good as long as the crack tip is identified correctly. Response 4: The size of the hole plays a role. If the hole is too small, a crack could extend beyond the drilled hole. If it works, then the service life could be significant. Response 5: Stopped continuing cracks; didn't affect service life. Response 6: Expected life is equal to the bridge if the crack tip is captured, else reinspected at regularly defined NBIS intervals. Response 7: The Expected life is equal to the bridge.

Repair Method	Factors Considered for Selecting the Repair Method	Repair Performance (expected service life, etc.)
Bolted repair	Response 1: access, maintenance capabilities Response 2: Needs to be an adequate section remaining to bolt. Response 3: Use bolted repair unless a large loss of section is found or the beam has buckled. Response 4: The Amount of section loss and location of the section loss will determine if a bolted repair fits where it needs to go. Response 5: When section loss presents Response 6: Most versatile repair type. Must have sufficient remaining section and section loss abated, i.e., blasted and painted. Response 7: Most of the beam end repairs we perform are welded, as most contractors have access to a welder. Welded repairs are also easily performed in-house (TxDOT).	Response 1: 10-30 years Response 2: Ok, but it will remain an area of accelerated corrosion. Response 3: Good performance Response 4: These seem to work very well. They can significantly extend the service life. Response 5: performs well when maintenance is kept up. Response 6: The Expected life is equal to the bridge. Response 7: The Expected life is equal to the bridge.
Welded repair	Response 1: access, maintenance capabilities Response 2: Not done for field repair Response 3: Use when bolted repair is not possible. Response 4: The Amount of section loss is at the beam end. Are there any holes in the beam end? Response 6: In a maintenance application, or where a bolted repair is not feasible. Response 7: Most of the beam end repairs we perform are welded, as most contractors have access to a welder. Welded repairs are also easily performed in-house (TxDOT).	Response 1: 10-30 years Response 3: Good performance Response 4: Welded repairs work well. Certified welder required, weld testing required, to ensure it's a good quality weld Response 6: short-term repair, fatigue life issues Response 7: The Expected life is equal to the bridge.
Section replacement	Response 1: access, maintenance capabilities Response 2: When not an adequate section remaining to repair. Response 3: Unclear how this differs from the welded repair. Replacing the entire beam section would require removing the deck. The need for this is not common, but uses are at pin-and-hanger connections when pin plates are severely corroded. Response 4: amount of section loss - any holes? Any damage, out of alignment, etc. Response 5: only used for the special case, such as at hinge locations Response 6: Needed when the section loss is too advanced for just a bolted repair. Response 7: Has been performed at mid-span for overheight impacts, not at beam ends (TxDOT).	Response 1: 10-30 years Response 4: As long as it's done according to specification and properly, it can perform well for a long time. Response 5: costly and so far performs well Response 6: The Expected life is equal to the bridge. Response 7: Expected life is equal to the bridge (or until the next impact).

Repair Method	Factors Considered for Selecting the Repair Method	Repair Performance (expected service life, etc.)
UHPC repair	Response 1: Not tried Response 3: Not typical Response 5: considered but have not used because of the constructability and future inspection Response 7: Only done once for an extreme case (TxDOT).	Response 3: MDOT has tried this, but only recently, and performance is not known. Response 7: Expected life is equal to the bridge (being replaced soon).
CFRP repair	Response 1: Not tried Response 3: Not typical Response 7: Have not done (TxDOT).	Response 3: MDOT doesn't typically use CFRP on steel.
Cleaning and protection	Response 1: access, maintenance capabilities, adequacy of members with current corrosion losses Response 2: Full removal and moisture-cured urethane 3-coat system. All crevices are caulked. Steel bearings are greased. Response 3: Not a repair method, cleaning and coating are preventative maintenance. Response 4: The amount of corrosion on the beam Response 5: All repairs require cleaning and protection Response 6: Only minor section loss and not governing the load ratings Response 7: Extent of section loss, condition of bearings (TxDOT). Use **Termarust**.	Response 1: 10-20 years Response 2: 20-30 years. Response 3: Good performance. Response 4: Works very well. Highly recommended. Refer to the bridge paint matrix for the expected service life. Response 5: A couple of protective materials have been used for protection Response 6: The Expected life is equal to the bridge if properly cleaned, ground, and painted. Response 7: 10-15 years.
Other	Response 1: encasing beam ends; ability to "lock up" the bridge and remove joints Response 2: The perimeter of all faying surfaces shall be sealed with a paintable caulk as directed in DelDOT Section 616 or the manufacturer's recommendations. Faying surfaces are described as "crevices ½ inch or less, rivets, bolts, nuts, between built-up members, interface of steel and concrete surfaces, and/or where pack rust occurs." ***Areas that exhibit pack rust, as directed by the engineer, shall be treated with a 100% solids penetrating sealer before being sealed using a paintable caulk as directed by the manufacturer's recommendations and requirement***s. The caulk material to be used shall be compatible with the proposed paint system and submitted for approval. Caulk shall be applied to mid-coat immediately prior to topcoat application and shall be fully cured prior to the application of topcoat. The minimum time on Caulk PDS is 48 hours.	Response 1: 20-30 years

Q4: Please share your experience with welded repairs of steel beams/steel beam ends.

		Implementation challenges	Performance concerns	Reasons, if the Method is NOT selected.
Shielded Metal Arc Welding (SMAW) is used in the field for steel	beam repair	Response 1: maintenance capabilities Response 3: None Response 6: length of repair, start, and stop of welding.	Response 3: None Response 6: quality of weld and fatigue resistance	
	beam end repair	Response 1: maintenance capabilities Response 3: None Response 6: length of repair, start, and stop of welding.	Response 3: None Response 6: quality of weld and fatigue resistance	
Gas Metal Arc Welding (GMAW) is used in the field for steel	beam repair	Response 1: maintenance capabilities Response 3: Must not be allowed.	Response 3: Yes	Response 3: The Field is an unpredictable and uncontrolled environment. The risk is too significant to allow GMAW for field bridge welding. Response 6: Used in the shop only
	beam end repair	Response 1: maintenance capabilities Response 3: Must not be allowed.	Response 3: Yes	Response 3: The Field is an unpredictable and uncontrolled environment. The risk is too significant to allow GMAW for field bridge welding. Response 6: Used in the shop only
Flux-Cored Arc Welding (FCAW) is used in the field for steel	beam repair	Response 1: maintenance capabilities Response 3: Not currently allowed.	Response 3: Not currently allowed.	Response 3: Lack of contractor knowledge and internal technical support for their welders. The same applies to the MDOT field inspector side. Response 6: Used in the shop only
	beam end repair	Response 1: maintenance capabilities Response 3: Not currently allowed.	Response 3: Not currently allowed.	Response 3: Lack of contractor knowledge and internal technical support for their welders. The same applies to the MDOT field inspector side. Response 6: Used in the shop only

Laser Welding is used in the field for steel	beam repair	Response 3: Not currently allowed.	Response 3: Not currently allowed.	Response 3: MDOT does not have field experience with this. We have AISC-certified shops that are using laser welding. The field lacks the expertise, knowledge, and quality control necessary to implement. Challenges would be with both the Contractor and the MDOT field inspector sides. Response 6: Used in the shop only
	beam end repair	Response 3: Not currently allowed.	Response 3: Not currently allowed.	Response 3: MDOT does not have field experience with this. We have AISC-certified shops that are using laser welding. The field lacks the expertise, knowledge, and quality control necessary to implement. Challenges would be with both the Contractor and the MDOT field inspector sides. Response 6: Used in the shop only

Response 6: SMAW is the primary method for field welds

Response 7: All our welded repairs are to be performed per TxDOT Standard Specifications Item 448

Q5(a): Are loose bolts or the loss of bolts and/or nuts a common problem?

Response 1: No
Response 2: No
Response 3: No
Response 4: No, bolts must be installed using the turn of the nut method. See MDOT specs for this method.
Response 5: No
Response 6: No
Response 7: No

Q5(b): The bolt tightening/pre-tensioning requirements

(i) Snug tight:

Response 1: No
Response 2: Yes, verify the tension with a Calibrated Torque wrench
Response 3: No

Response 5: Yes, verify the tension with a Calibrated Torque wrench
Response 6: Yes, a Calibrated Torque wrench is not used. A turn of nut + ¼ is used.
Response 7: Yes, verify the tension with a Calibrated Torque wrench, see TxDOT Item 447

(ii) Pretensioned:
Response 1: Yes, usually turn-of-the-nut method.
Response 3: Yes, turn-of-the-nut method.
Response 5: No
Response 6: Yes
Response 7: Yes, see TxDOT Item 447 for required pretension

Q5(c): Is there a preference for bolted repairs over welded repairs?
Response 1: Yes, the capability of maintenance forces
Response 3: Yes
Response 4: If there aren't any holes, bolted repairs are preferred. We typically don't want to weld on bridges. But if we do weld, there are very specific and strict requirements to ensure a quality weld.
Response 5: Yes
Response 6: Yes, bolted repairs have much higher fatigue resistance.
Response 7: No (TxDOT)

Q6: Experience with the use of the following techniques for steel beam repair.
(i) Snug-tight without tension verification
Response 1: Regular bolt and nut, regular bolt and nut with a washer
Response 3: Regular bolt and nut
Response 6: Regular bolt and nut, regular bolt and nut with a washer, and double nuts
Response 7: Regular bolt and nut, regular bolt and nut with a washer, and double nuts

(ii) Snug-tight with tension verification
Response 1: Regular bolt and nut, regular bolt and nut with a washer
Response 2: Regular bolt and nut with a washer
Response 6: Regular bolt and nut, regular bolt and nut with a washer, and double nuts
Response 7: Regular bolt and nut, regular bolt and nut with a washer, and double nuts

(iii) Pretension
Response 1: Regular bolt and nut, regular bolt and nut with a washer
Response 1: Regular bolt and nut

Response 6: Regular bolt and nut, regular bolt and nut with a washer, and double nuts
Response 7: Regular bolt and nut, regular bolt and nut with a washer, and double nuts

(iv) Preferred method and reason(s)
Response 1: Regular bolt & nut; maintenance capabilities and ease of installation
Response 3: Regular bolt and nut; when the turn-of-the-nut process is done properly, the bolts should not come loose. All connections are assumed to be slip-critical.
Response 4: Turn of the Nut Method - refer to MDOT specifications for details. Bolts should not be able to come loose if they are tightened properly, per our standards.
Response 5: MN only uses structural bolts and nuts *because of the strength requirements*.
Response 6: Regular nut and bolt with or without washers; proven performance
Response 7: Bolt and nut with washer. Simple, time-tested, reliable. TxDOT Item 447 covers requirements for bolting

Q7: Approach for assessing the condition of a concealed beam end(s)
Response 1: Don't really have a problem yet for these conditions, usually a repair method.
Response 3: Generally, the concealed end is assumed to be fully braced by the concrete, and the controlling section would be at the face of the concrete.
Response 4: You can't tell what condition the concealed beam end is in without chipping out the backwall.
Response 5: Assessing the visible beam sections next to the concrete back walls
Response 6: Only inspect what is visible.
Response 7: Examine the concrete condition and section loss at the beam end. Destructive testing is not performed.

Q8: The repair method(s) suitable for embedded beam end
Response 2: Cleaning and protection, epoxy mastic grout placed around the steel to the concrete surface.
Response 3: Bolted repair: Implementation success – good, performance – good, challenges - requires hand chipping backwall
Welded repair: Implementation success – good, performance – good, challenges - requires hand chipping backwall
Cleaning and protection: Implementation success – good, performance – good, challenges - use if section loss is acceptable.
Response 5: Bolted repair

Cleaning and protection

Response 7: Cleaning and protection, since it is simple to paint. The performance is the same as any other beam end coating.

Additional responses:

Response 3: Concrete encasement could work if removing the deck above is acceptable. Probably could use a typical concrete mix instead of UHPC.

Response 5: The Challenge is no access to the end diaphragm/backwall concrete

B.2.3 Design and Load Rating

Q1: State the factors that you would consider for selecting a specific repair method

(i) Bolted repair

Response 1: access, ease of installation, and capability of maintenance works, installing the repair

Response 3: The Remaining section, presence of holes

Response 4: MN typically uses bolted repair

(ii) Welded repair

Response 1: access, ease of installation, and capability of maintenance works installing the repair

Response 3: Location (avoid creating NSTM), remaining section

Response 4: Field welding is hard to control. Cleaning the section with corrosion may not meet the welding requirements.

(iii) Section replacement

Response 1: access, ease of installation, and capability of maintenance works for installing the repair

Response 3: Remaining section, accessibility for repair, and inability to use the bolted or welded approach

Response 4: May be considered if unrepairable for the bolted option

(iv) UHPC repair

Response 1: access, ease of installation, and capability of maintenance works installing the repair

Response 3: Not currently used

Response 4: MN has not used because of the difficulty of construction and future inspection

(v) CFRP repair

Response 1: access, ease of installation, and capability of maintenance works for installing the repair

Response 3: Not currently used for steel repair

Response 4: Not used

(vi) Cleaning and protection

Response 1: access, ease of installation, and capability of maintenance works for installing the repair. Structural adequacy of the member without any repairs

Response 3: Only if sufficient capacity remains for loading without other repair approaches

Response 4: required for all repairs, using such as **ZRC**

(vii) Other methods

Response 1: Encasing ends of girders in the diaphragm. Can the bridge be "locked up" by encasing girders and eliminating joints

Q2: Do you consider the influence of the end diaphragm or the backwall for capacity assessment?

Response 1: No, I have not run into this situation yet.

Response 2: Yes, we rarely, if ever, embed steel beam ends in concrete. If encountered, the influence would primarily be to eliminate buckling as a failure limit state in the beam end. (ILDOT)

Response 3: No

Response 4: Yes/No; we started not including the end diaphragm/backwall. If more capacity is required, we will do a refined analysis with the end diaphragm/backwall.

Q3: The web thickness selected for capacity calculation.

Response 1: Average thickness of the section loss area.

Response 2: If checking the web above a bearing, the average thickness is taken over the length of the bearing at the base of the web and checked for steel bearing, crippling, yielding, shear, and local buckling. If SL runs the full height of the web, the average thickness over that full height is taken and checked for shear and global buckling.

Response 3: Average thickness within a 4-in. strip from the bottom flange (MassDOT)

Response 4: Average thickness of the section loss area.

Q4: The specifications/guides/references that you use to calculate the capacity of deteriorated steel beam ends.

Response 1: Beam ends with section loss – AASHTO LRFD Bridge Design Specifications, 9th Edition
Beam ends with holes – AASHTO LRFD Bridge Design Specifications, 9th Edition.

Response 2: Beam ends with section loss – AASHTO LRFD Bridge Design Specifications, 9th Edition; the AISC Steel Construction Manual, 9th Edition
Beam ends with holes – AASHTO LRFD Bridge Design Specifications, 9th Edition; the AISC Steel Construction Manual, 9th Edition.

Other sources: AASHTO Standard Specifications; ASCE Journal of Structural Engineering – Kayser and Nowak (1989) Capacity loss due to corrosion in steel girder bridges, Vol. 115, No. 6.

We account for holes by taking a weighted average of the web in the region where the limit state applies. In the case of bearing checks, it's a weighted average over the calculated length of the web with bearing load. For a shear or buckling check, it's the weighted average over the full height of the web.

For bridges designed LFD, we still load rate with LFR. In these cases, we use AISC App. B5 for an additional local buckling check and AISC K1.3 and K1.4 for web local yielding and crippling. For LRFR ratings, all checks are encompassed by the AASHTO LRFD code. For both LFR and LRFR, we also include an additional bearing check for unstiffened beam ends per the referenced ASCE journal.

Response 3: Beam ends with section loss – Massachusetts Department of Transportation Bridge Manual - Part I (Hundredth Anniversary Edition); additional resources: AASHTO and AISC

Beam ends with holes – Massachusetts Department of Transportation, Bridge Manual - Part I (Hundredth Anniversary Edition); additional resources: AASHTO and AISC

Note that the MassDOT Bridge Manual is known to have typographical errors. It will be updated this year to fix them.

Response 4: Beam ends with section loss – AASHTO LRFD Bridge Design Specifications, 9th Edition

Beam ends with holes – AASHTO LRFD Bridge Design Specifications, 9th Edition.

APPENDIX C: Inventory data request

C.1 INVENTORY DATA

#	**Item**
8	Structure Number
6	Features Intersected
7	Facility Carried
22	Owner
21	Maintenance Responsibility
27	Year Built
29	Average Daily Traffic
30	Year of Average Daily Traffic
31	Design Load
34	Skew
41	Structure Open, Posted, or Closed to Traffic
43	Structure Type, Main
44	Structure Type, Approach Spans
45	Number of Spans in Main Unit
46	Number of Approach Spans
48	Length of Maximum Span
49	Structure Length
51	Bridge Roadway Width, Curb-to-Curb
52	Deck Width
58	Deck Condition Rating
59	Superstructure Condition Rating
63	Method Used to Determine Operating Rating
64	Operating Rating
65	Method Used to Determine Inventory Rating
66	Inventory Rating
70	Bridge Posting
75	Type of Work
76	Length of Structure Improvement
90	Inspection Date
91	Designated Inspection Frequency
106	Year Reconstructed
109	Average Daily Truck Traffic

Note: Inventory items 41, 51, and 91 are added because.

41- could be helpful to narrow down the bridges having reduced capacity

51- is useful for load rating to determine the area with live load

91- the increased inspection frequency could show where regions are more concerned about the structure

C.2 ELEMENT LEVEL INSPECTION DATA

107 Steel Open Girder/Beam
Structure Number
826 Beam end deterioration (CS TABLE 9 defects with condition states)
CS TABLE 3 defects with condition states
845 Short Height Beam End Temporary Support (CS TABLE 9 defects with condition states)
846 Full Height Beam End Temporary Support (CS TABLE 9 defects with condition states)
899 Fiber Reinforced Polymer
Bearings (# 310 to 316) (CS TABLE 11 defects with condition states)

109 Prestressed Concrete Open Girder/Beam
Structure Number
826 Beam end deterioration (CS TABLE 9 defects with condition states)
CS TABLE 2 defects with condition states
845 Short Height Beam End Temporary Support (CS TABLE 9 defects with condition states)
846 Full Height Beam End Temporary Support (CS TABLE 9 defects with condition states)
899 Fiber Reinforced Polymer
Bearings (# 310 to 316) (CS TABLE 11 defects with condition states)

C.3 OTHER INFORMATION

- A list of open RFAs to identify the RFAs related to the beam end condition/deterioration. Since the RFA Committee meets every month to discuss open RFAs, this list provides up-to-date information.
- A list of "other special inspections" to identify any bridges that the regions are concerned about beam end condition and have scheduled reviews on an increased frequency.
- A list of programmed projects from JobNet showing structure numbers and the work planned (ex., beam end repairs) to determine the structures with beam end deterioration that are in the program for repairs. The list also typically includes past projects where work has already been completed.
- Repair details, original plans, scoping reports, pictures showing beam end conditions before and after repair, and other resources related to beam end repair.

APPENDIX D: PSC I-beam end repair performance

D.1 PERFORMANCE EVALUATION OF OVERCAST REPAIRS

D.1.1 STR 1413

The bridge (STR 1413) that carries M-37 (Bedford Road) over Kalamazoo River has five spans and is located in the City of Battle Creek, Calhoun County, Michigan (Figure D-1). The total length of the bridge is 333.4 ft and the width is 64.3 ft. It was originally constructed in 1973. Each span has ten prestressed AASHTO Type III beams.

(a) Elevation

(b) Deck surface

Figure D-1 M-37 bridge over Kalamazoo River.

During the routine inspection on 12/05/2005, the stringer (SIA-59) received a condition rating of 3 (serious) due to heavy spalling near beam ends at bearing areas of all piers and abutments. The spalling had exposed rusting rebars at several beam ends. The bridge was then repaired in 2006. The associated Request for Action (RFA) or scoping report for this repair is not available in the MiBRIDGE database. The repair plan dated 7/11/2005 under Job Number (JN) 60489 specified full-depth overcast beam end repairs for 22 beam ends at the piers and one beam end at the north abutment. The details of the full-depth overcast repair for both interior and exterior beam ends are shown in Figure D-2.

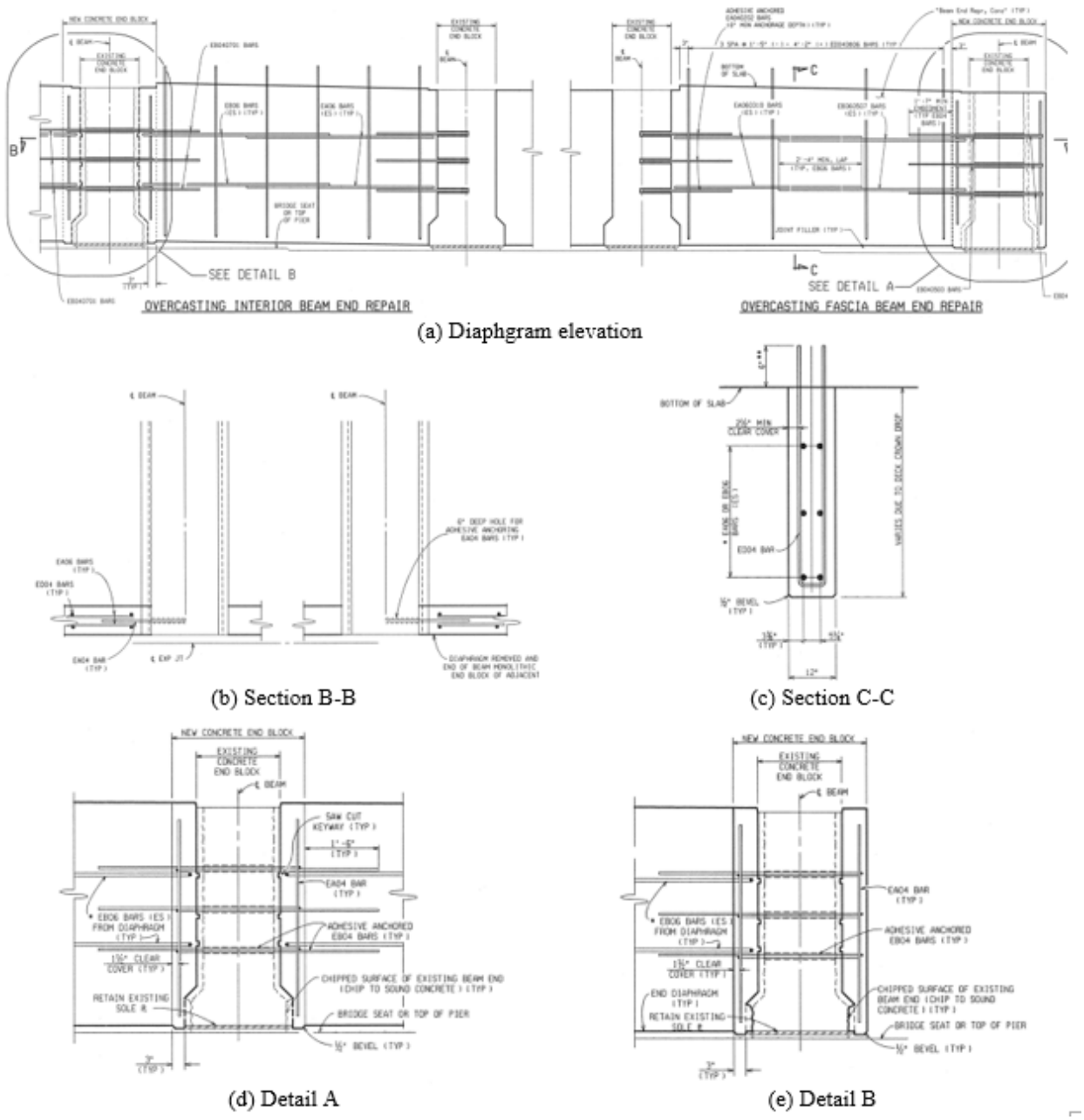

Figure D-2. Beam end full-depth overcast details.

Following the repair, the stringer was assigned a condition rating of 7 (good) during the routine inspection on 07/20/2007. The following conditions were documented during subsequent routine inspections:

07/16/2009: cracking at most of the repaired beam ends

07/09/2013: cracking at most of the repaired beam ends; a shear crack in the repaired area of beam 10W in span 3S over pier 3S

07/16/2019: most of the encased beam ends are cracked, and several have incipient spalls; a shear crack in the repaired area of beam 10W in span 3S over pier 3S.

The latest routine inspection, conducted on 07/05/2023, assigned a condition rating of 5 (fair). Even though the full-depth overcast repairs have been in service for 17 years by 2023, cracking was reported in the repairs within 2 years. The close-up photos of the repaired beam ends are not available in the MiBRIDGE database. The element inspection on 07/05/2023 assigned CS 2 (fair condition) to 36 beam ends and CS 3 (poor condition) to 55 beam ends. Since none of the beam ends received CS 1, it can be postulated that none of the repaired beam ends are in good condition.

D.1.2 STR 2538

The bridge (STR 2538) that carries I-69 EB over Linden Road has three spans and is located two miles southwest of Flint in Genesee County, Michigan (Figure D-3). The total length of the bridge is 136.8 ft and the width is 48.1 ft. The bridge was originally constructed in 1968. Each span has eight prestressed concrete I-beams. The exterior beams in Spans 1 and 3 and all the beams in Span 2 are AASHTO Type III. The interior beams in Spans 1 and 3 are AASHTO Type I.

(a) Elevation

(b) Deck surface

Figure D-3. I-69 Bridge over Linden Road.

Beam ends were repaired in 2008 and protected with concrete surface coating. The last inspection, prior to the repair on 10/29/2007, assigned a condition rating of 4 (poor) to the stringers. The repair plan, dated 6/30/2006 (JN 86879), specified full-depth overcast for the eight exterior beam ends at the piers, along with the replacement of the adjacent end diaphragms. The repair details are shown in Figure D-4. Following the repair, the routine inspection on 10/04/2008 assigned a condition rating of 7 (good) to the stringers. From 2014 to 2022, the 4 and 5 beam ends were assigned element level condition states of 2 and 3, respectively. Unfortunately, none of the available documents indicate the specific beam ends receiving such condition states.

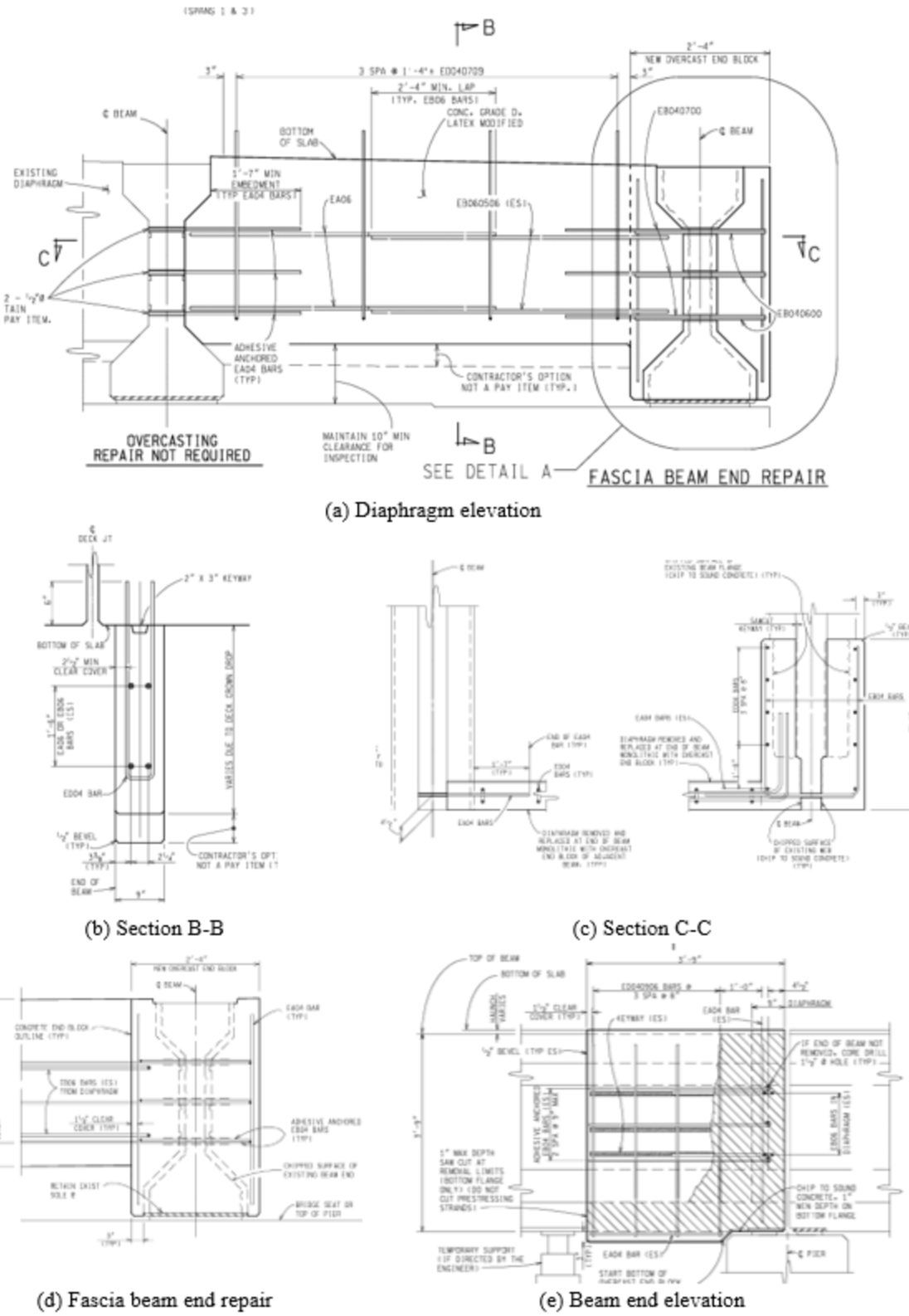

(a) Diaphragm elevation

(b) Section B-B

(c) Section C-C

(d) Fascia beam end repair

(e) Beam end elevation

Figure D-4. Details of the 2007 full-depth overcast repair.

During the routine inspection on 5/20/2019, the stringer received a condition rating of 4 (poor). Because of the observed beam end conditions, an RFA was submitted on 5/30/2019. The scoping report, dated 08/19/2019, provides details of the deterioration at ten interior beam ends at the piers. The documented beam end conditions included section loss at the bottom flange, loss of bearing (LOB) area, and exposed rebars and strands. Figure D-5 illustrates the condition of a few beam ends. The 08/19/2019 scoping inspection report cracking in 6 of the 8 fascia beam overcasts completed in 2008. The recommended repairs include replacing overcasts and bearing replacements. As of 2019, these overcast beam end repairs have been in service for 11 years.

(a) Beam 7s in span 2w at pier 1w - spall on the south side of beam

(b) Beam 5s in span 1w at pier 1w - spall with exposed steel/LOB

(c) Beam 3s in span 3w at pier 2w– spall with exposed steel/LOB

Figure D-5 Beam end condition as of 08/19/2019.

D.1.3 STR 3810 and 3811

Two bridges, STR 3810 and 3811, carry I-96 EB and WB over Sycamore Creek, respectively. Each bridge has two spans and is located in the city of Lansing, Ingham County, Michigan (Figure D-6). The total length of the bridges is 128 ft and the width is 43.7 ft. They are originally constructed in 1962. Each span has seven AASHTO Type III beams.

(a) Elevation of STR 3810

(b) Deck surface of STR 3810

(c) Elevation of STR 3811

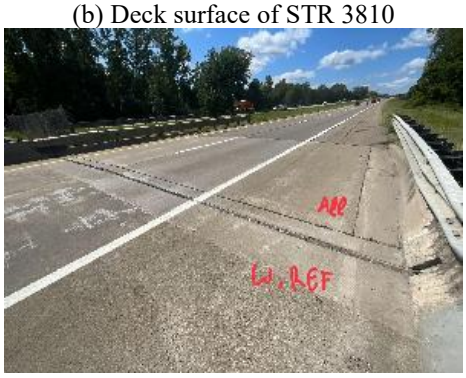

(d) Deck surface of STR 3811

Figure D-6. I-69 EB (STR 3810) and WB (STR 3811) bridges over Sycamore Creek.

The routine inspection on 08/25/2014 reported that both bridges had heavily corroded bearing plates and cracked neoprene pads, as well as cracks, shallow spalls, rust stains, and delamination at beam ends near the bearings. As a result, the bearings received a condition rating of 4 (poor). A repair was completed in 2016. The repair work included replacing bearings, patching diaphragms, and applying concrete surface coatings to all beam ends. Although the MiBRIDGE database includes a set of repair plans dated 06/07/2011 (JN 112712), it does not include overcast beam end repair details. However, the photos taken by the bridge inspectors showed full-depth overcasts at all beam ends at the abutments and piers (Figure D-7). The following construction quality and durability performance concerns related to the full-depth overcast repairs are documented in the inspection reports:

- Large gaps in several beam end repairs at bottom flanges (STR 3810, reported since 2016)
- Tight cracks in a few beam end repairs (reported since 2018)
- Peeling off of concrete surface coating at beam end repairs (reported since 2020)

According to these observations, cracks appeared within 2 years of the repair, and the concrete surface coating began to peel off within 4 years of the repair. During the most recent routine

inspection on 08/20/2024, the stringers of both bridges received a condition rating of 6 (fair). The bearings of STR 3810 received a condition rating of 7 (good), while the bearings of STR 3811 received a rating of 8 (good). All 28 beam ends in each bridge received an element condition rating of CS 1 (good condition). As of 2024, these beam end repairs have been in service for eight years.

(a) Beam end repair at the pier (STR 3810)

(b) Beam end repair at the west abutment (STR 3810)

(c) Beam end repair at the pier (STR 3811)

(d) Beam end repair at the east abutment (STR 3811)

Figure D-7. Beam end repairs at the abutments and piers.

D.1.4 STR 3832

The bridge (STR 3832) that carries Williamston Road over I-96 EB has six spans and is located in the city of Lansing in Ingham County, Michigan (Figure D-8). The total length of the bridge is 339.3 ft and the width is 34.9 ft. The bridge was originally constructed in 1962. Each span has six PSC I-beams. The exterior beams in Spans 1 and 6 and all the beams in Span 2 to 5 are AASHTO Type III. The interior beams in Spans 1 and 6 are AASHTO Type I.

(a) Elevation

(b) Deck surface

Figure D-8. Williamston Road bridge over I-96 EB.

During the routine inspection on 09/25/2014, both the stringer and the bearings received a condition rating of 2 (critical). It was reported that the elastomeric pads exhibited deformation, splitting, and misalignment. Beam end spalls exposed prestressing strands, and the loss of bearing (LOB) area at eight beam ends ranged from 23% to 47%. Figure D-9 shows the condition of a few beam ends and pier caps. As a result, an RFA was submitted on 11/05/2014, and temporary supports were installed.

(a) Beam 3w in span 6s at pier 5s – 45% LOB due to beam end spall

(b) Beam 4w in span 1s at pier 1s – 47% LOB due to bolster block spall

(c) Beam 5w in span 4s at pier 4s – 100% of bearing is on delaminated concrete

Figure D-9. Beam end deteriorations reported in the 2014 RFA.

A major repair (JN 130133) was carried out for this bridge in 2020. The repair included the replacement of 49 neoprene bearing pads, full-depth reinforced overcasts on 12 beam ends, and partial-depth unreinforced overcasts on 36 beam ends, all at the piers. Figure D-10 presents the beam end repair details in the plans dated 06/07/2019.

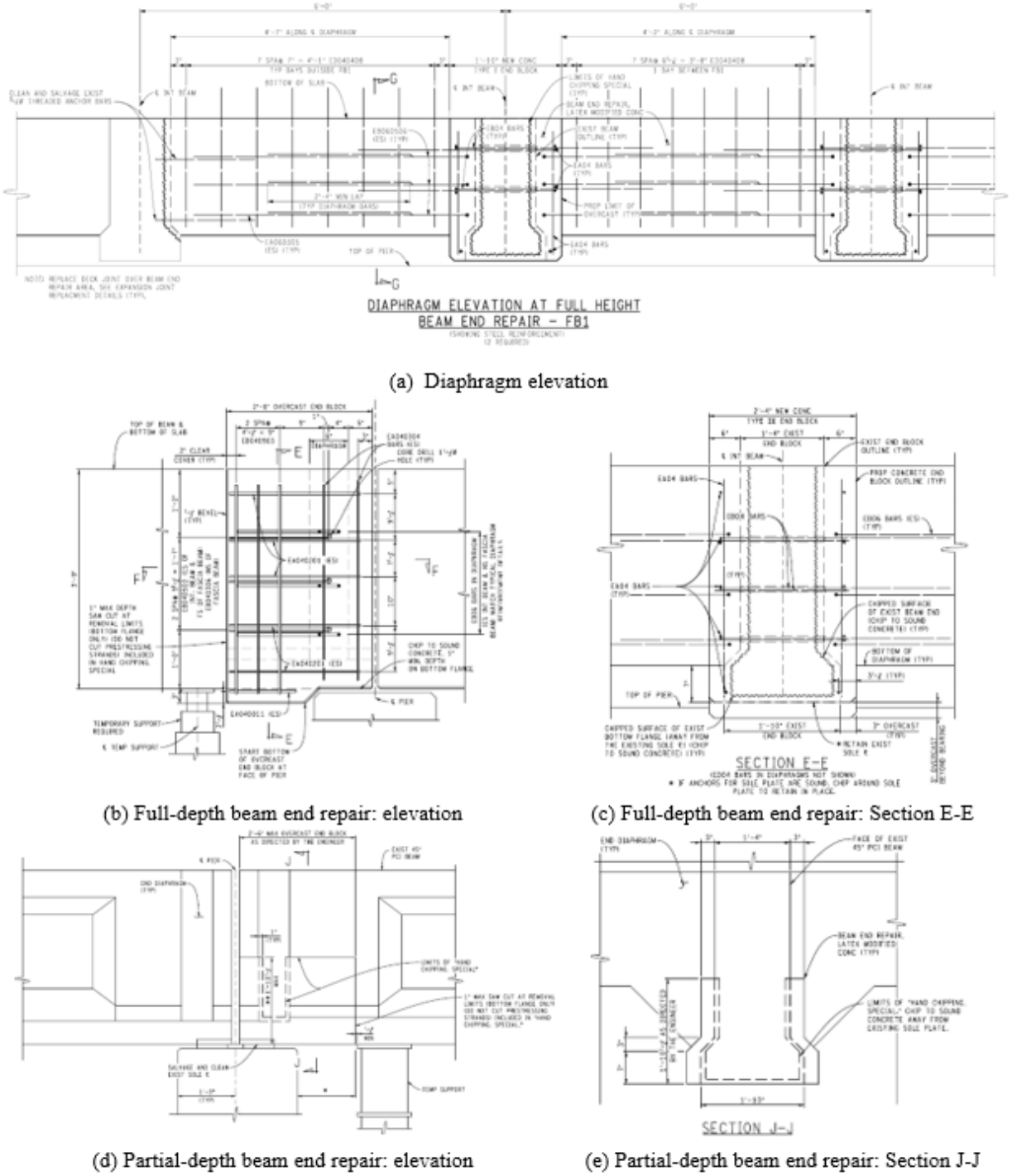

Figure D-10. Full-depth and partial-depth overcast beam end repair details.

The most recent routine inspection, conducted on 09/23/2024, assigned a condition rating of 6 (fair) for the stringers and bearings. The typical condition of repaired beam ends is shown in Figure D-11. Some of the beam end conditions reported in this inspection include horizontal cracks, vertical hairline cracks, small areas of shallow delamination, and STS in a few beam ends

near the bearing plates. However, the location of these conditions is not explicitly noted in the inspection report. In addition, a tight crack was recorded at the repaired beam (6w) end at pier 4s (Figure D-11(b)). The element inspection showed that 48 beam ends are in CS 1 (good condition) and 15 beam ends are in CS 2 (fair condition). As of 2024, the beam end repairs have been in service for four years and are postulated to be in good condition since 48 beam ends are in CS 1.

(a) Typical beam end repairs at the piers

(b) Beam 6w in span 5s at pier 4s – tight crack

Figure D-11. The condition of beam end repair recorded during 2024 inspection.

D.1.5 STR 3830

The bridge (STR 3830) that carries Zimmer Road over I-96 EB has three spans and is located in the city of Lansing, Ingham County, Michigan (Figure D-12). The total length of the bridge is 133.3 ft and the width is 30.9 ft. The bridge was originally constructed in 1962. Each span has six PSC I-beams. The exterior beams in Spans 1 and 3 and all the beams in Span 2 are AASHTO Type II. The interior beams in Spans 1 and 3 are AASHTO Type I.

(a) Elevation

(b) Deck surface

Figure D-12. Zimmer Road bridge over I-96 EB.

During the routine inspections on 09/13/2012 and 09/17/2013, stringers and bearings received condition ratings of 5 (fair) and 4 (poor), respectively. STS and delaminations were documented at several beam ends at the piers. An RFA was submitted on 9/20/2012 due to open cracks and spalls observed at the pier cap at bearing 3w and bearing 5w in span 3s at pier 2s, resulting in 56%

and 63% LOB, respectively. As a result, full-height temporary supports were added at the two beam ends in December 2012.

During the routine inspection on 09/18/2014, both stringers and bearings received condition ratings of 2 (critical). Multiple beam ends at the piers had LOB ranging from 13% to 24%. Shallow spalls, STS, and delaminations were documented at several beam ends. As a result, an RFA was submitted on 11/12/2014. Nine temporary supports were installed in December 2014. Later, during routine inspections performed on 9/28/2015, 09/14/2016, and 09/09/2018, both stringers and bearings received a condition rating of 3 (serious) because of similar conditions reported in 2014. An RFA was submitted on 10/17/2019 due to STS in beam 6w in span 1s over pier 1s with 48% LOB and two exposed prestressing strands, as shown in Figure D-13.

Figure D-13. The condition of beam 6w in span 1s over pier 1s with 48% LOB.

A repair was completed in 2020. The details from the repair plan dated 06/07/2019 are shown in Figure D-14. The repair of beam ends at piers included the replacement of all elastomeric bearing pads over the piers, two full-depth reinforced overcasts with the replacement of adjacent end diaphragms, and 15 partial-depth unreinforced overcasts, all at the piers.

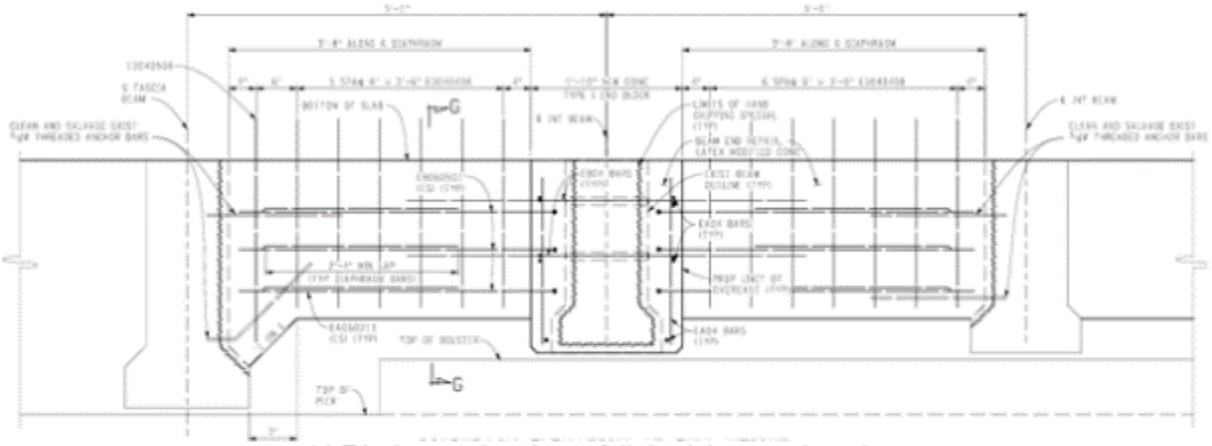

(a) Diaphragm elevation at full-depth beam end repair

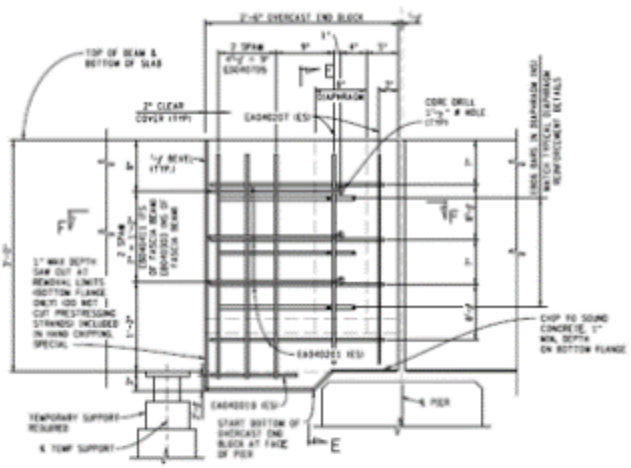

(b) Full-depth beam end repair: elevation

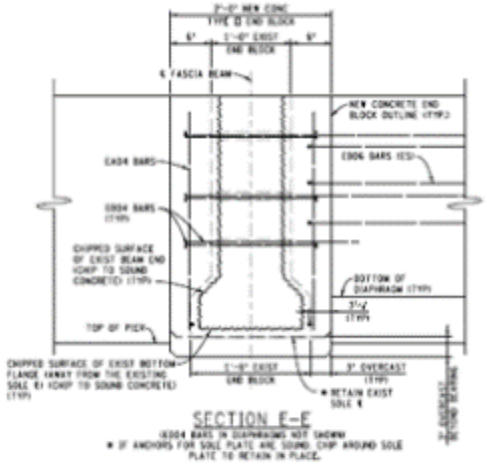

(c) Full-depth beam end repair: Section E-E

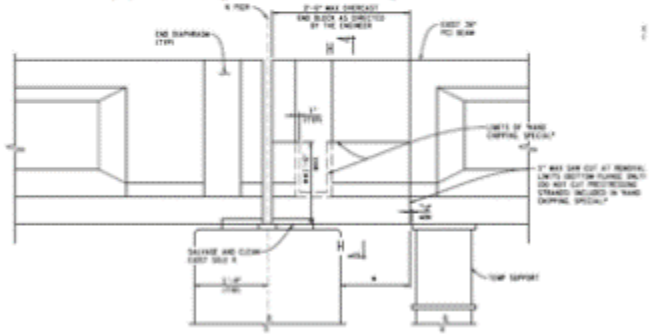

(d) Partial-depth beam end repair: elevation

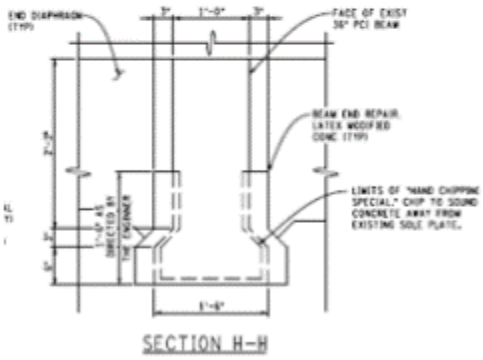

(e) Partial-depth beam end repair: Section H-H

Figure D-14. Full-depth reinforced overcast and partial-depth unreinforced overcast repair details.

During the most recent routine inspection on 09/20/2024, both stringers and bearings received condition ratings of 6 (fair). The element inspection reported CS 1 (good condition) and CS 2 (fair condition) for 23 and seven beam ends, respectively. Since 23 beam ends are in CS 1, it can be postulated that all the repairs, except the repair at one end, are in good condition. As of 2024, the beam end repairs have been in service for four years. The typical conditions of the repaired beam

ends are shown in Figure D-15(a). Beam end conditions reported subsequent to 2020 repair include:

- A minor crack in beam 1w partial-depth repair in span 3S over pier 2S (reported in 2022).
- An open crack in beam 1w partial-depth repair in span 3S over pier 2S (reported in 2024; Figure D-15(b))
-

(a) Typical beam end repair at the piers

(b) Beam 1w in span 3s over pier 2s – open crack

Figure D-15. Full-depth overcast repair and the condition of partial-depth repair.

D.1.6 STR 8012

The bridge (STR 8012) that carries Giddings Road over I-75 has four spans and is located in the city of Auburn Hills in Oakland County, Michigan (Figure D-16). The total length of the bridge is 265.8 ft and the width is 30.5 ft. The bridge was originally constructed in 1962. Each span has five PSC I-beams. The exterior beams in Span 1 and all the beams in the other three spans are AASHTO Type III. The interior beams in Span 1 are AASHTO Type II.

(a) Elevation

(b) Deck surface

Figure D-16. Giddings Road bridge over I-75.

During the routine inspection on 03/08/19, the stringer received a condition rating of 6 (fair). Shallow spalls were observed at the bottom flanges of the beam ends at all piers and abutments. The bearings received a condition rating of 4 (poor). Large spalls were reported under bearing

areas at pier 1s. STS was documented at three beam ends. All the bearings at pier 1s were undermined up to 2.5 inches and had up to 24% LOB area. The inspection referenced a 2018 scoping report under JN 133119; however, it is not available in the MiBRIDGE database. Figure D-17 shows beam end and pier cap conditions recorded during the 2019 inspection. An RFA was submitted following the inspection. The repairs under JN 130002 included epoxy overlay, full-depth deck patching, partial deck replacement, beam end repairs, diaphragm patching, partial pier cap replacement, substructure patching, and concrete surface coating. The associated repair plan dated 02/20/2019 included reinforced overcast repairs of 25 beam ends and three neoprene bearing pad replacements over the piers. Figure D-18 to Figure D-20 show the details of the beam end repair. The repair was completed in 2021.

(a) Beam 3w in span 1s - undermining (b) Beams 2w, 3w, 4w in span 1s

Figure D-17. Deterioration of beam ends and bent cap at pier 1s during the 2019 inspection.

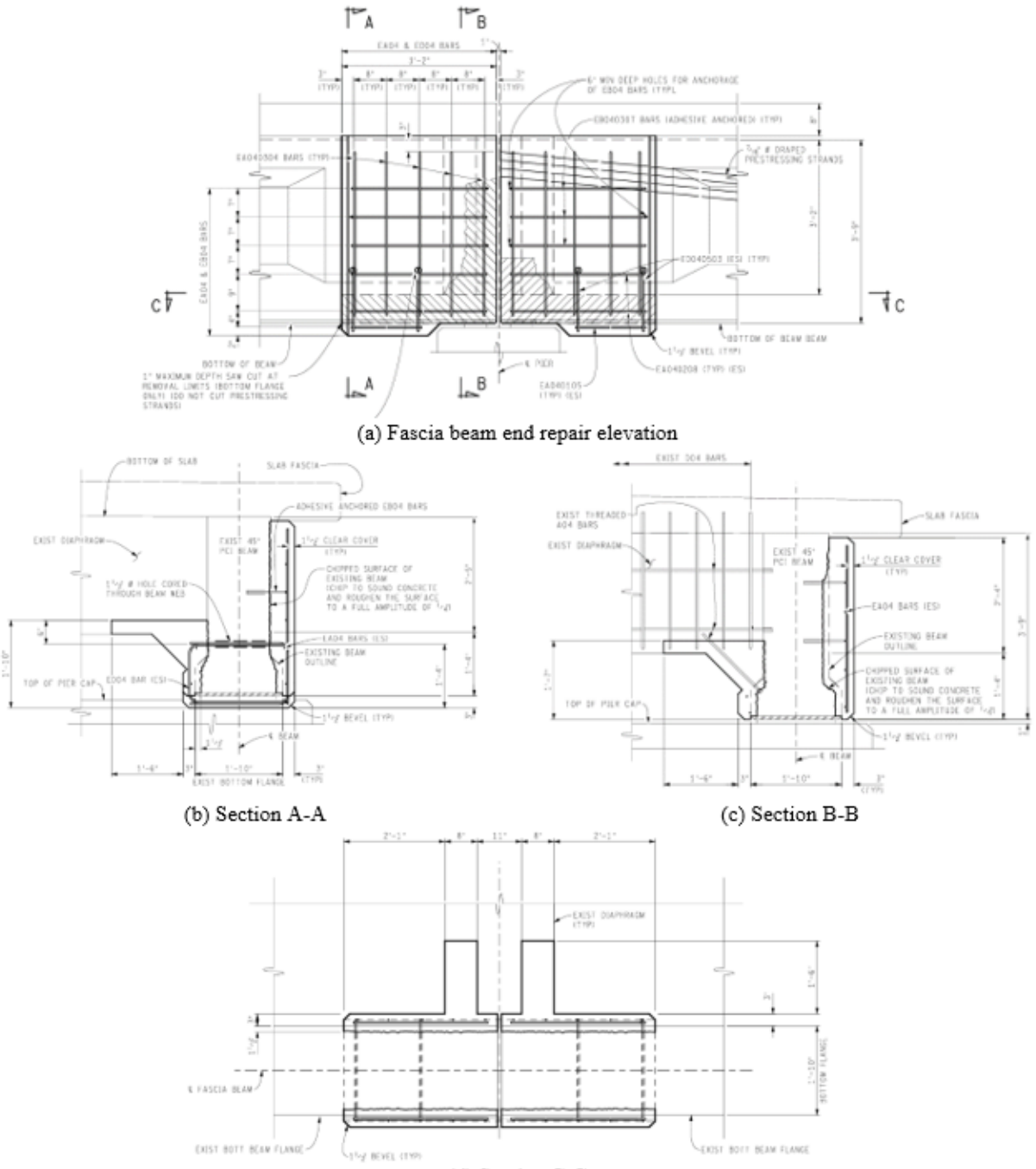

Figure D-18. Overcast repair at the fascia beam ends at all piers.

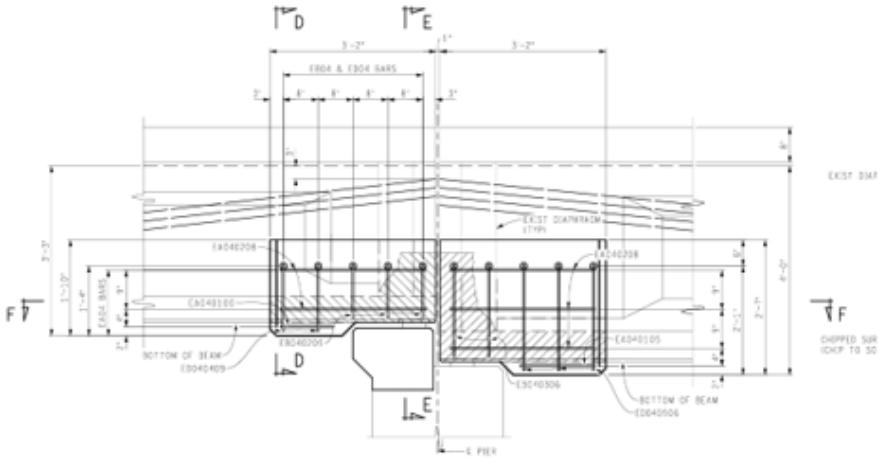

(a) Interior beam end repair elevation

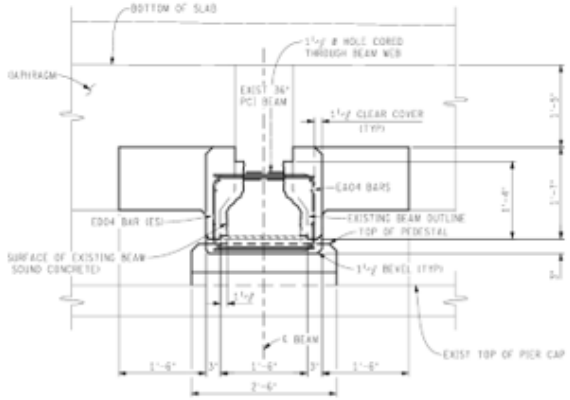

(b) Section D-D

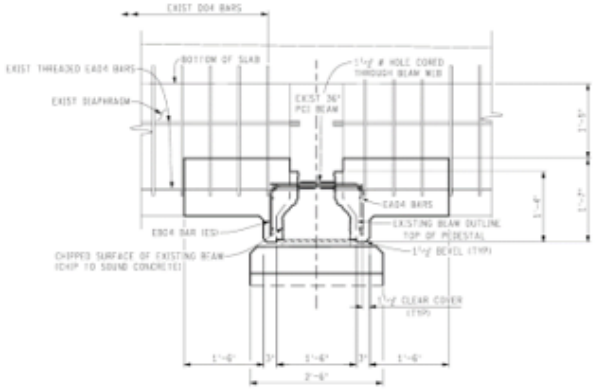

(c) Section E-E

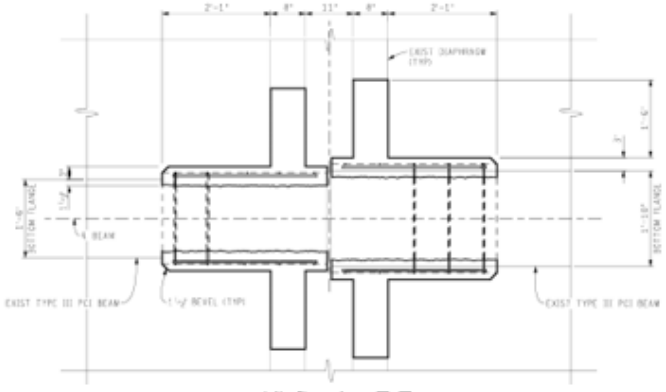

(d) Section F-F

Figure D-19. Partial-depth reinforced overcast repair at the interior beam ends at pier 1.

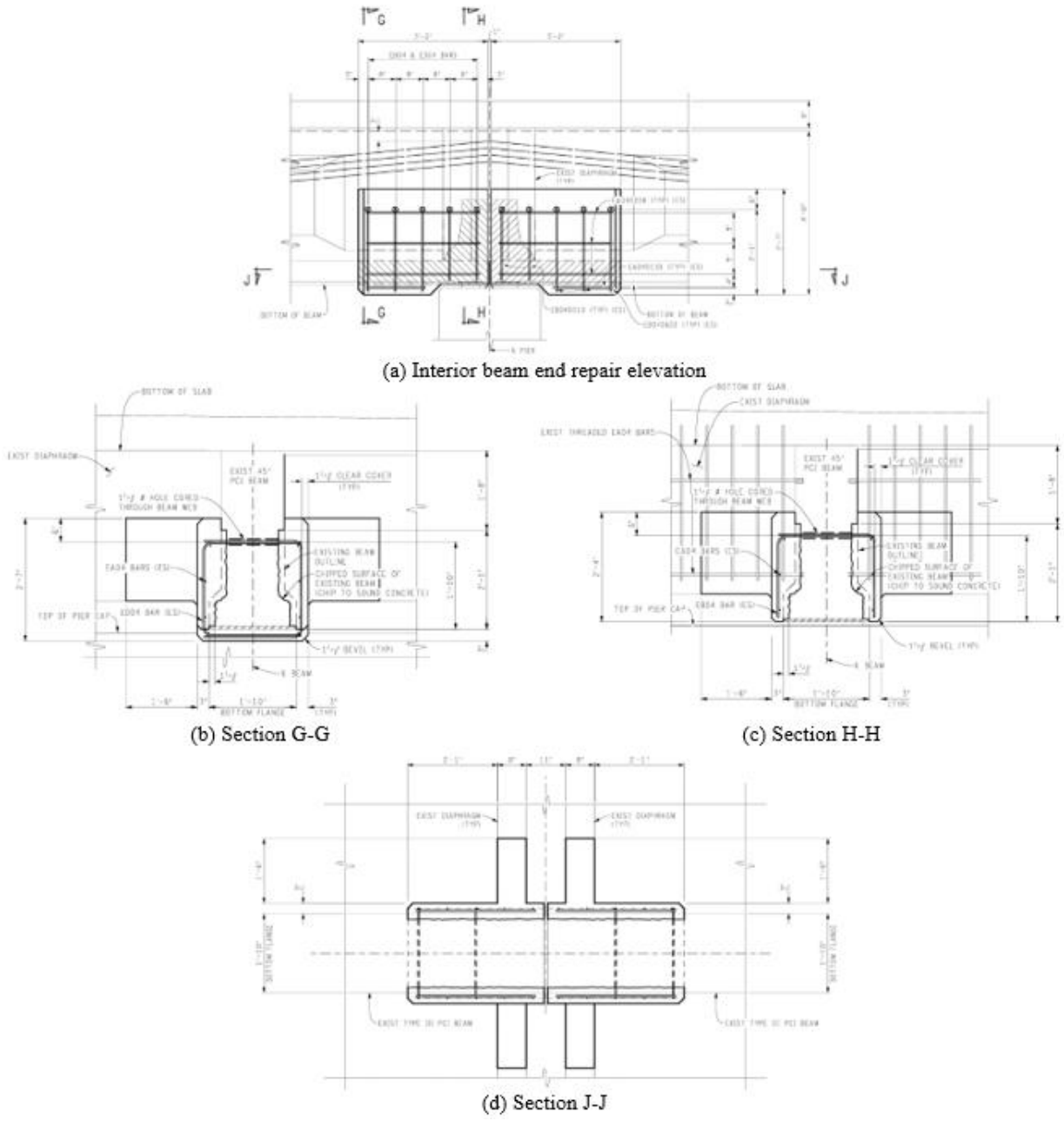

Figure D-20. Partial-depth reinforced overcast repair at the interior beam ends at pier 2 and 3.

During the routine inspection on 03/08/2023, stringers and bearings received condition ratings of 7 (good) and 6 (fair), respectively. Beam end conditions reported in this inspection included bottom flange shallow spall and delamination at sole plates for beams 2s to 5s at the west abutment and beams 2s and 3s at the east abutment, as shown in Figure D-21. The element inspection reported CS 1 (good condition) and CS 2 (fair condition) for 25 and six beam ends, respectively.

As of 2023, all 25 beam end repairs have been in service for two years and are postulated to be in good condition since 25 beam ends are in CS 1.

(a) Shallow delamination/spall at the beam end bottom flanges over the west abutment

(b) Shallow delamination/spall at the beam end bottom flanges over the east abutment

Figure D-21. Shallow delamination/spall at sole plates over the abutments.

D.1.7 STR 5753

The bridge (STR 5753) that carries US-23 NB over Center Road has three spans and is located in Livingston County, Michigan (Figure D-22). The total length of the bridge is 108 ft and the width is 47.2 ft. It was originally constructed in 1961. Each span has eight PSC I-beams. The exterior beams in Spans 1 and 3 and all the beams in Span 2 are AASHTO Type II. The interior beams in Spans 1 and 3 are AASHTO Type I.

(a) Elevation

(b) Deck surface

Figure D-22. US-23 NB bridge over Center Road.

Based on the historical routine inspection reports, it appears that a major repair of the bridge was completed in 1999. The repair details in the plans dated 10/13/1998 are shown in Figure D-23. The scope of repair included (i) full-depth overcast and the replacement of elastomeric bearing pads at 24 beam ends at the piers, and (ii) the replacement of a few end diaphragms at the piers. The subsequent inspections reported cracking, delamination, and spall within 10 years of repair, as listed below:

- The full-depth overcasts have cracking and small spalls with areas of delamination (2009 inspection).
- Most of the full-depth overcasts have cracking and spalling (2015 inspection).

During the routine inspection on 05/13/2013, the stringer received a condition rating of 5 (fair). The beam end conditions reported in this inspection included several beam ends having spalls and LOB areas ranging from 14% to 19%, as well as cracking, small spalls, and delamination in the repaired areas. An RFA was submitted on 05/16/2013 due to conditions at four beam ends shown in Figure D-24. Out of four beam ends, beams 3w and 4w in span 3s at pier 2s, shown in Figure D-24 (a) and (b), were repaired in 1999. As of 2013, the 1999 repairs were in service for 14 years.

The scope of repair performed in 2016 under JN 128409 to address the 2013 RFA included partial-depth beam end overcasts at the four beam ends, pier repair, and concrete surface coating. The details of the beam end repair as per the plan dated 06/06/2016 are shown in Figure D-25.

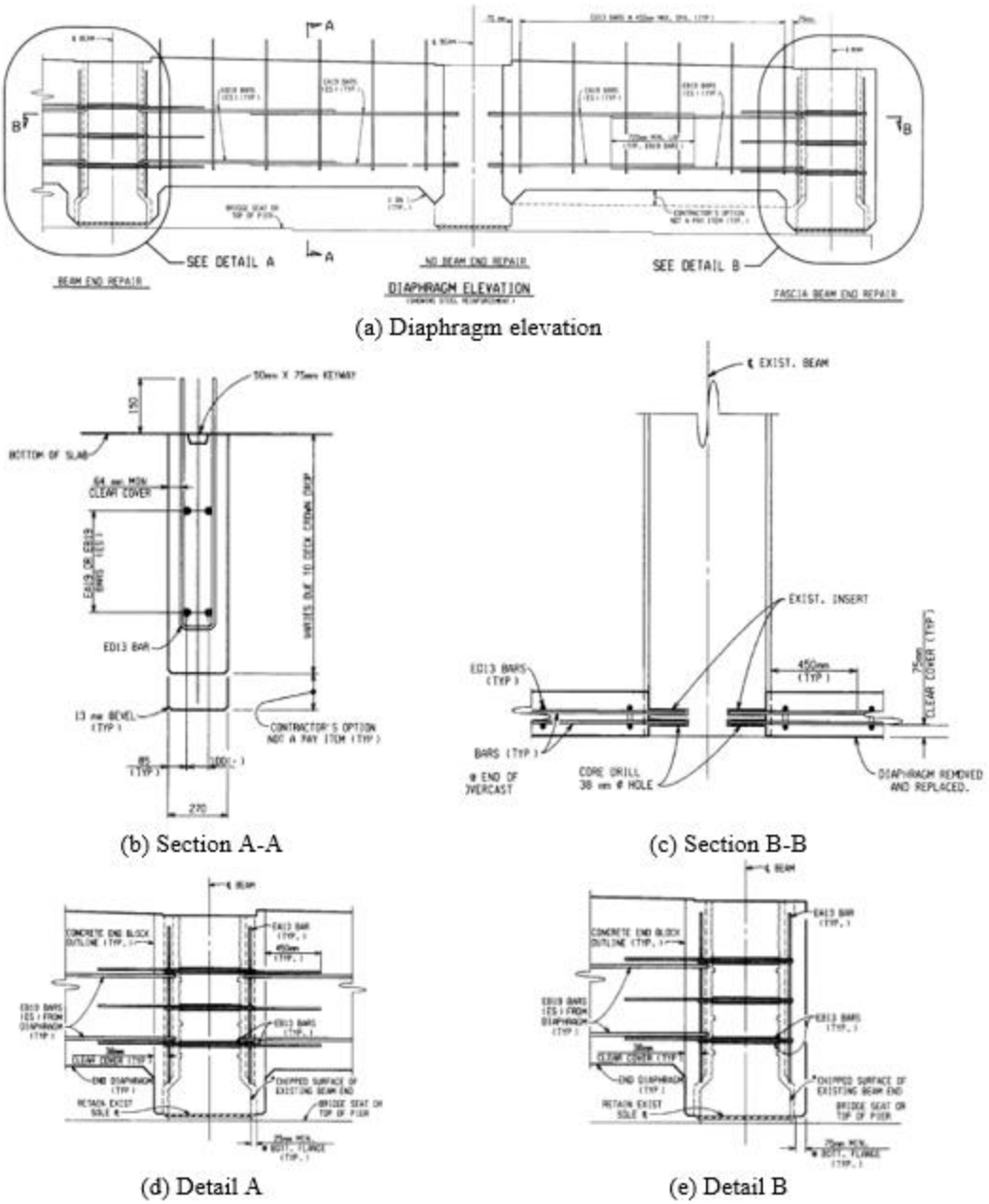

Figure D-23. Full-depth overcast repair details in the 1998 planset.

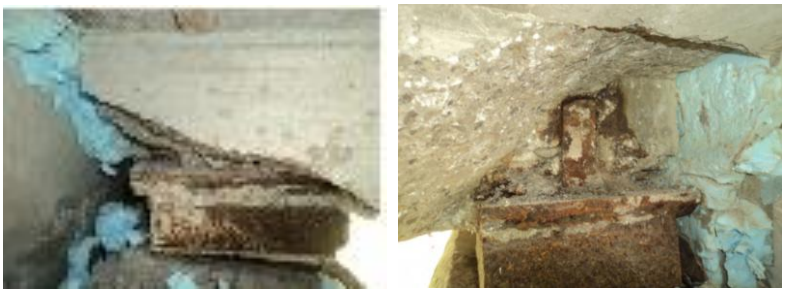

(a) Beam 3w in span 3s at pier 2s - spall with 18% loss of bearing

(b) Beam 4w in span 3s at pier 2s - spall with 19% loss of bearing

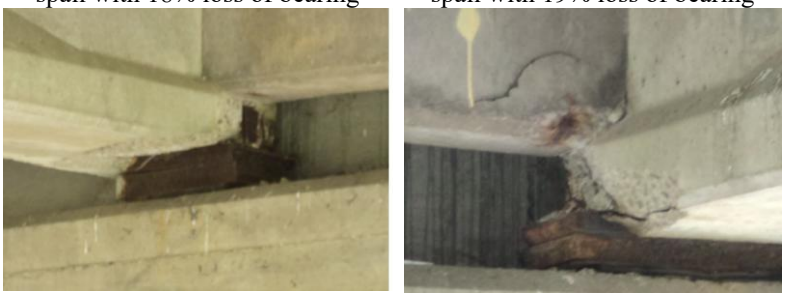

(c) Beam 5w in span 1s at pier 1s - spall with 16% loss of bearing

(d) Beam 6w in span 1s at pier 1s - spall with 14% loss of bearing

Figure D-24. Beam end deterioration documented in the 2013 RFA.

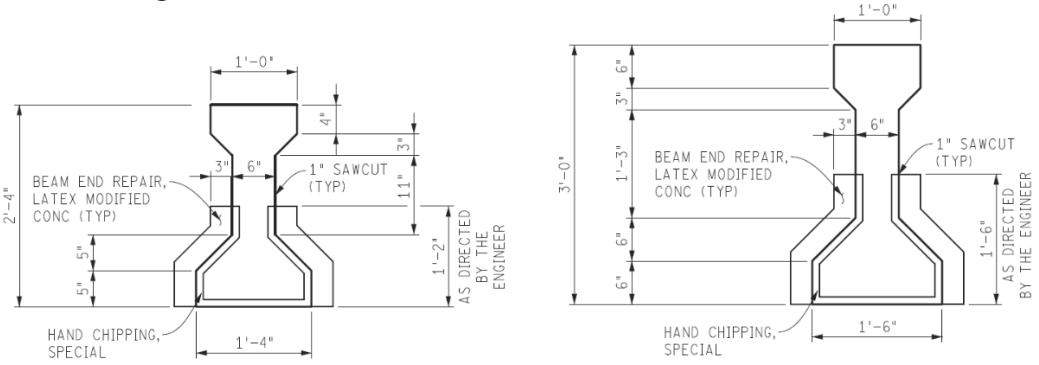

(a) Type I beam end repair

(b) Type II beam end repair

Figure D-25. Partial-depth unreinforced beam end repair details used in 2016.

During the most recent routine inspection on 08/09/2024, both stringers and bearings received a condition rating of 6 (fair). The element inspection reported CS 1 (good condition) and CS 2 (fair condition) for 26 and six beam ends, respectively. The total number of repaired beam ends from 1999 to 2016 is 26 (i.e., 24 repairs in 1999 and 4 repairs in 2016, with 2 re-repairs of the 1999 repaired ends); thus, it can be postulated that all repaired beam ends are in good condition. As of 2024, the beam end repairs completed in 1999 have been in service for 25 years, and the beam end repairs completed in 2016 have been in service for 8 years.

D.1.8 STR 5754

The bridge (STR 5754) that carries US-23 SB over Center Road has three spans and is located in Livingston County, Michigan (Figure D-26). The total length of the bridge is 108 ft and the width is 47.2 ft. It was originally constructed in 1961. Each span has eight PSC I-beams. The exterior beams in Spans 1 and 3 and all the beams in Span 2 are AASHTO Type II. The interior beams in Spans 1 and 3 are AASHTO Type I.

(a) Elevation (b) Deck surface

Figure D-26. US-23 SB bridge over Center Road.

Based on the historical routine inspection reports, it appears that a major repair of the bridge was completed in 1999. The repair details in the plans dated 09/01/1998 (JN 34120A) are shown in Figure D-27. The repair work included providing 31 full-depth overcasts over the piers and replacing all the elastomeric bearing pads at the piers, as well as replacing most of the end diaphragms at the piers. The beam end 2W in span 3S over pier 2S was the only one that was not repaired in 1999. The subsequent inspection reported the following conditions:

- Most beam ends have small cracks in the bottom flange at the piers (2003 inspection).
- Beam 6w in span 2s has a diagonal crack near the pier bearing (2011 inspection).
- Beam 1w in span 3s has a diagonal crack with delamination near the pier bearing (2011 inspection).
- Most beam ends at the piers have cracks, small spalls, and delamination in the bottom flanges with minor loss of bearing area and exposed prestressing strands (2013 inspection).
- Span 1: Patched beam ends at all beams over the pier. Map cracking in full-depth overcasts. Span 2: Map cracking in full-depth overcasts. (2014 inspection)

- Overcasting has map cracks and a few spalls. The most significant spalls are at beam 8w in span 2s over pier 1s, beam 4w in span 2s over pier 2, and beam 1w in span 3s over pier 2s. (2015 inspection)
- Minor cracking in overcasting at beam ends over piers. Few small areas of delamination in the bottom flange of beams 1w and 2w in span 2s over pier 1s. (2017 to 2024 inspections)

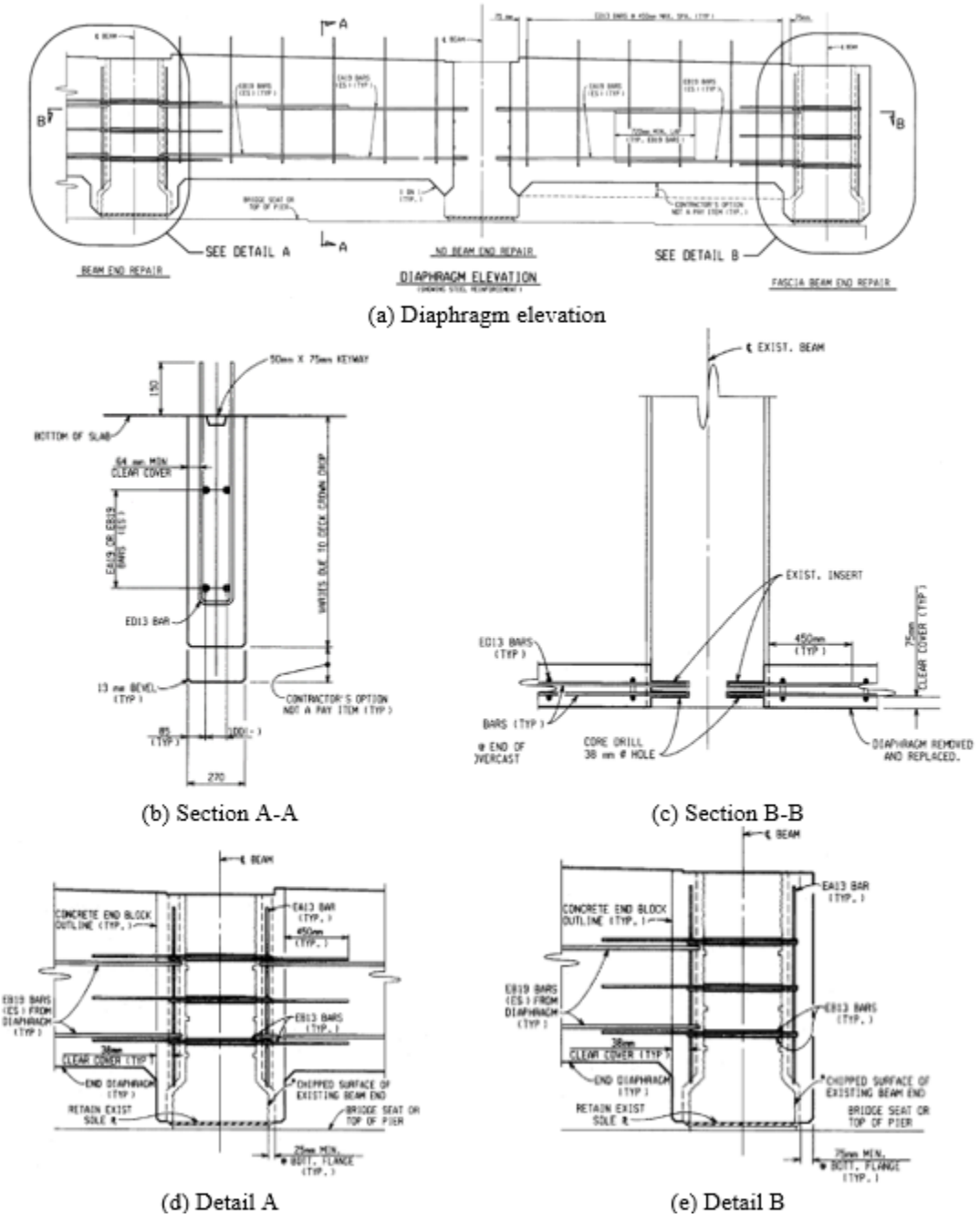

Figure D-27. Full-depth overcast repair details in the 1998 planset.

During the routine inspection on 05/13/2013, both stringers and bearings received a condition rating of 5 (fair). It was reported that most beam ends had cracks, small spalls, and delamination in the bottom flanges with minor loss of bearing and prestress strands exposed at the piers. An RFA was submitted on 05/16/2013 due to significant spalls noted at two fascia beam ends, as shown in Figure D-28. These two beam ends were previously repaired in 1999. As of 2013, the 1999 repairs were in service for 14 years.

(a) Beam 1w in span 3s at pier 2s - spall with 14% LOB

(b) Beam 8w in span 2s at pier 1s - spall with 13% LOB

Figure D-28. Beam end deterioration documented in the 2013 RFA.

A repair under JN 128409 was carried out in 2016 to address the concerns that resulted in the RFA and the conditions reported during a subsequent scoping inspection. The repair work included partial-depth unreinforced overcasts for nine beam ends that were repaired in 1999, pier repair, and concrete surface coating. The partial-depth beam end repair details used in 2016 are similar to those used in STR 5753 (Figure D-25).

During the most recent routine inspection on 08/09/2024, stringers and bearings received condition ratings of 6 (fair) and 5 (fair), respectively. The element inspection reported CS 1 (good condition) and CS 2 (fair condition) for 28 and four beam ends, respectively. However, it is unclear which specific beam ends correspond to CS 1 or CS 2. It is important to note that the element level inspection on 08/10/2017 reported CS 1 for 32 beam ends, and the element level inspections from 2018 to 2024 reported CS 1 and CS 2 for 28 and four beam ends, respectively. As of 2024, the beam end repairs completed in 1999 have been in service for 25 years, and the beam end repairs completed in 2016 have been in service for 8 years.

D.1.9 STR 10914

D.1.9.1 Overview

The bridge (STR 10914) that carries M-14 EB over the Earhart Road has three spans and is located in Washtenaw County, Michigan (Figure D-29). The bridge has a width of 58.9 ft and a total length of 109 ft. The bridge was built in 1964. Each span has eight AASHTO Type II beams.

(a) Aerial view of the bridge (b) South elevation

Figure D-29 M-14 EB bridge over Earhart Road (a) aerial view and (b) south elevation (Source: Google.com).

After the bridge was in service for 52 years, the stringer (SIA-59) received a condition rating of 5 (fair) on 09/13/2016 due to the following reasons:

- High load hit scrapes on the bottom flanges of beams 1 and 2s in span 2w.
- Several beam ends having cracks and spalling-to-steel (STS) around the bearing area.
- Beam 1s span1w having vertical cracks with minor spall and delamination at the web.
- Beam 1s in span 2w having a 2 ft^2 delaminated area at beam end and web.
- Several diaphragms having cracks, STS, and rust staining.

Additionally, the inspection reported corroded sole plates and deformed pads at the piers. Fascia bearings at abutments also had moderate corrosion.

A Request for Action (RFA) was submitted on 09/14/2016 for this bridge because spans 1 and 2w over pier 1w and spans 2 and 3w over pier 2w had several spalls, STS, and delamination over bearings at the beam ends. Figure D-30 shows the condition of a few beam ends that required issuing an RFA.

The Statewide Bridge Crew (SBC) inspected the bridge and installed short-height temporary supports on top of the pier cap by 01/26/2017 to support several beams due to concrete spall at the beam ends.

(a) Corroded sole and bearing plates and delamination in front of the sole plate

(b) Corroded sole and bearing plates, delamination and spall front of the sole plate, STS at beam ends and over the bearing, and corroded stirrups and strands

(c) STS along the vertical edge of the web and corroded stirrups

(d) STS in front of the sole plate and corroded stirrups and strands

Figure D-30 Beam end conditions as of 09/14/2016.

The JN 201081A - 07-13-2018 letting documents included partial-depth unreinforced concrete overcasts for the south fascia beam ends at pier 1w and 2w. As shown in Figure D-31, a latex modified concrete mix was used for the overcasts. The length of the overcast and the height on the fascia side were decided in consultation with the engineer. The letting documents required the application of a concrete surface coating to the entire perimeter of the repaired beam ends, extending 5 ft from the face of the pier. Beam ends were not repaired until 09/04/2018, as per the Bridge Safety Inspection Report (BSIR). However, the BSIR dated 09/15/2020 noted cracking and spalling of the partial-depth overcasts, as shown in Figure D-32, indicating a service life of less than 2 years.

Even though the letting documents included partial depth overcasts for the south fascia beam ends over pier 1w and 2w, the BSIR dated 09/15/2022 indicated that almost all the beam ends at pier 1 and 2w having partial depth overcasts.

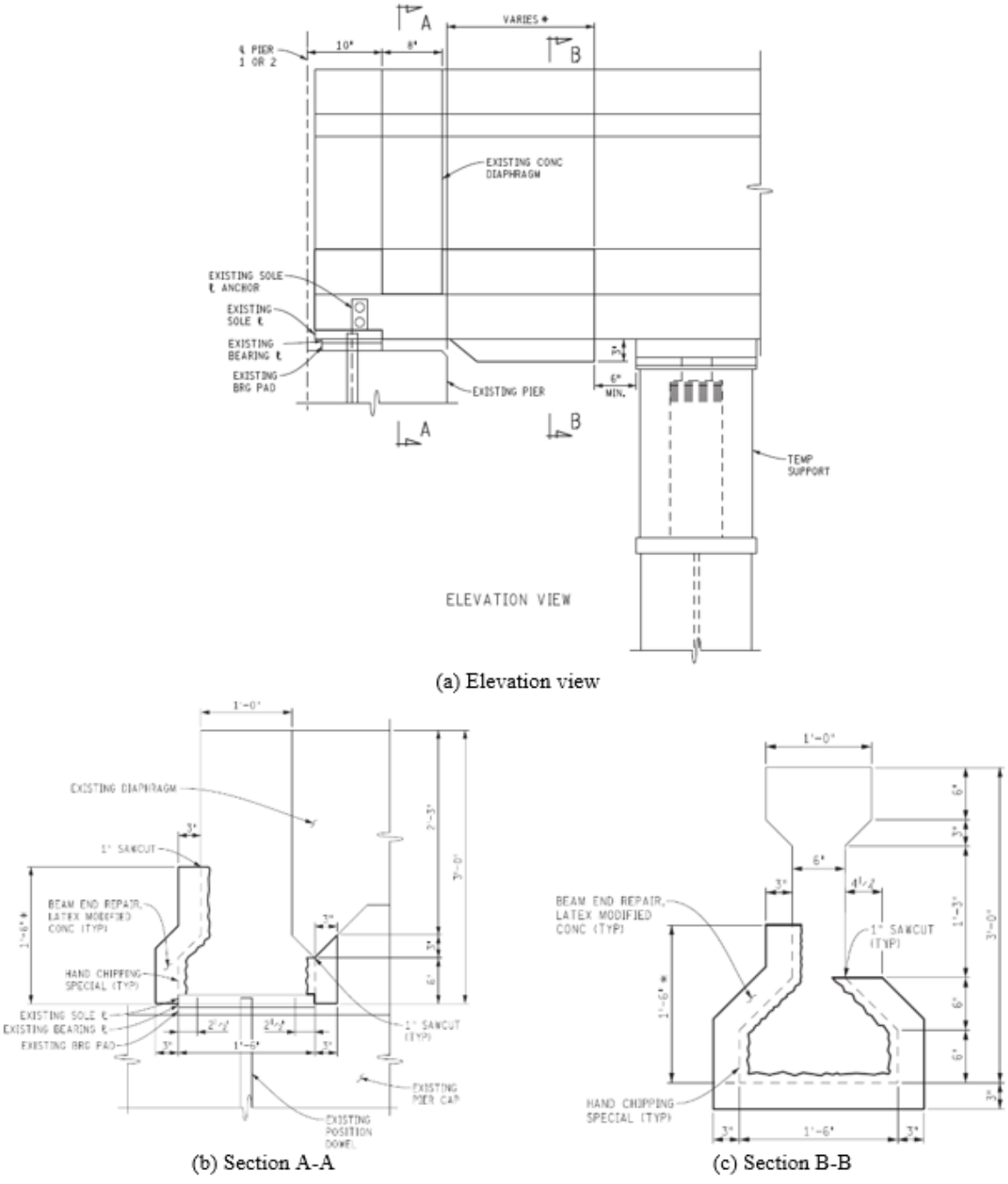

Figure D-31 Typical Type II beam end repair.

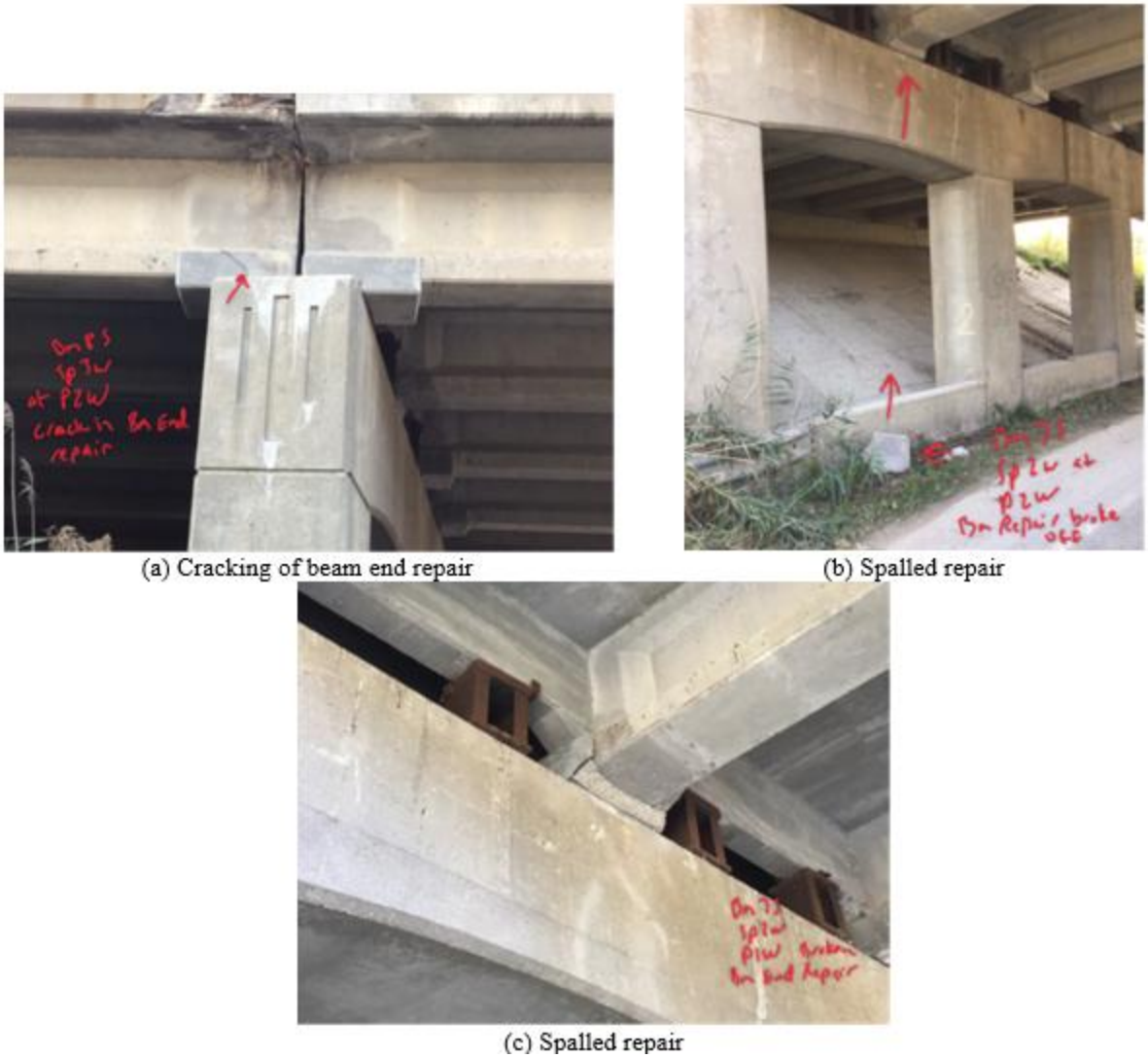

(a) Cracking of beam end repair

(b) Spalled repair

(c) Spalled repair

Figure D-32 Condition of partial depth beam end overcasts as of 09/15/2020.

D.1.9.2 Inspection of Repaired Beam Ends

Beam ends were inspected on October 04, 2024. Beam end repairs included (a) partial depth overcasts and (b) chipping and removal of cracked and delaminated overcasts due to the safety of vehicles, pedestrians, and cyclists on the Earhart Road.

Even though the south fascia beam end repairs over pier 1w were about 4 years old and consistently exposed to elements, they were in good condition with a couple of hairline cracks (Figure D-33). However, a majority of the repairs did not perform well. A few examples are shown in Figure D-33.

(a) South fascia beam end repairs at pier 1W

(b) Cracking on the overcast

(c) South fascia beam end repairs at pier 2W

Figure D-33. The condition of the south fascia beam repairs at pier 1w and 2w.

D.1.9.3 Summary

In general, the partial depth overcast did not perform well. Most of them delaminated and spalled. Considering safety, several of them were either entirely or partially removed by chipping out the delaminated sections. A few of these overcasts had hairline cracks, indicating a potential for accelerated deterioration with subsequent exposure to moisture. The use of these unreinforced overcasts with uncertain interface bond performance is not a viable option for promoting durability and adding strength to the beam ends. Further, none of the beam ends had received a concrete surface coating as noted in the letting documents.

D.1.10 STR 10919

D.1.10.1 Overview

The bridge (STR 10919) that carries M-14 WB over the Earhart Road has three spans and is located in Washtenaw County, Michigan (Figure D-34). The bridge has a width of 55.5 ft and a total length of 109 ft. The bridge was built in 1964. Each span has eight AASHTO Type II beams.

(a) Aerial view of the bridge

(b) South elevation

Figure D-34. M-14 WB bridge over Earhart Road (a) aerial view and (b) south elevation (Source: Google.com).

After the bridge was in service for 52 years, the stringer (SIA-59) received a condition rating of 5 (fair) on 09/13/2016 due to the following reasons:

- Several beam ends having delamination and spalling-to-steel (STS).
- Beam 1S in span 2W having a 2 ft^2 delaminated area at beam end and web.
- Several diaphragms having spalls, STS, and rust staining.

Additionally, the inspection reported corroded sole plates and deformed pads at the piers. Fascia bearings at abutments also had moderate corrosion. A Request for Action (RFA) was submitted on 09/14/2016 for this bridge because spans 1 and 2w over pier 1w and spans 2 and 3w over pier 2w had several spalls, STS, and delamination over bearings at the beam ends.

The Statewide Bridge Crew (SBC) inspected the bridge and provided the following temporary supports for beams by 01/26/2017:

(a) short-height temporary supports to south fascia beam over span 2w at pier 1 and 2w

(b) full-height temporary support to beam 4s at the east abutment due to spall at the bearing area.

The JN 201081A - 07-13-2018 letting documents included partial-depth unreinforced concrete overcasts for the south fascia beam ends at pier 1w and 2w. As shown in Figure D-35, a latex modified concrete mix was used for the overcasts. The length of the overcast and the height on the fascia side were decided in consultation with the engineer. The letting documents required

the application of a concrete surface coating to the entire perimeter of the repaired beam ends, extending 5 ft from the face of the pier. Even though the letting documents included partial depth overcasts for the south fascia beam ends over pier 1w and 2w, the 2020 Bridge Safety Inspection Report (BSIR) listed repairs at pier 1w spans 1 and 2w beams 1-8s; pier 2w spans 2 and 3w beams 1-2 and 4-8s.

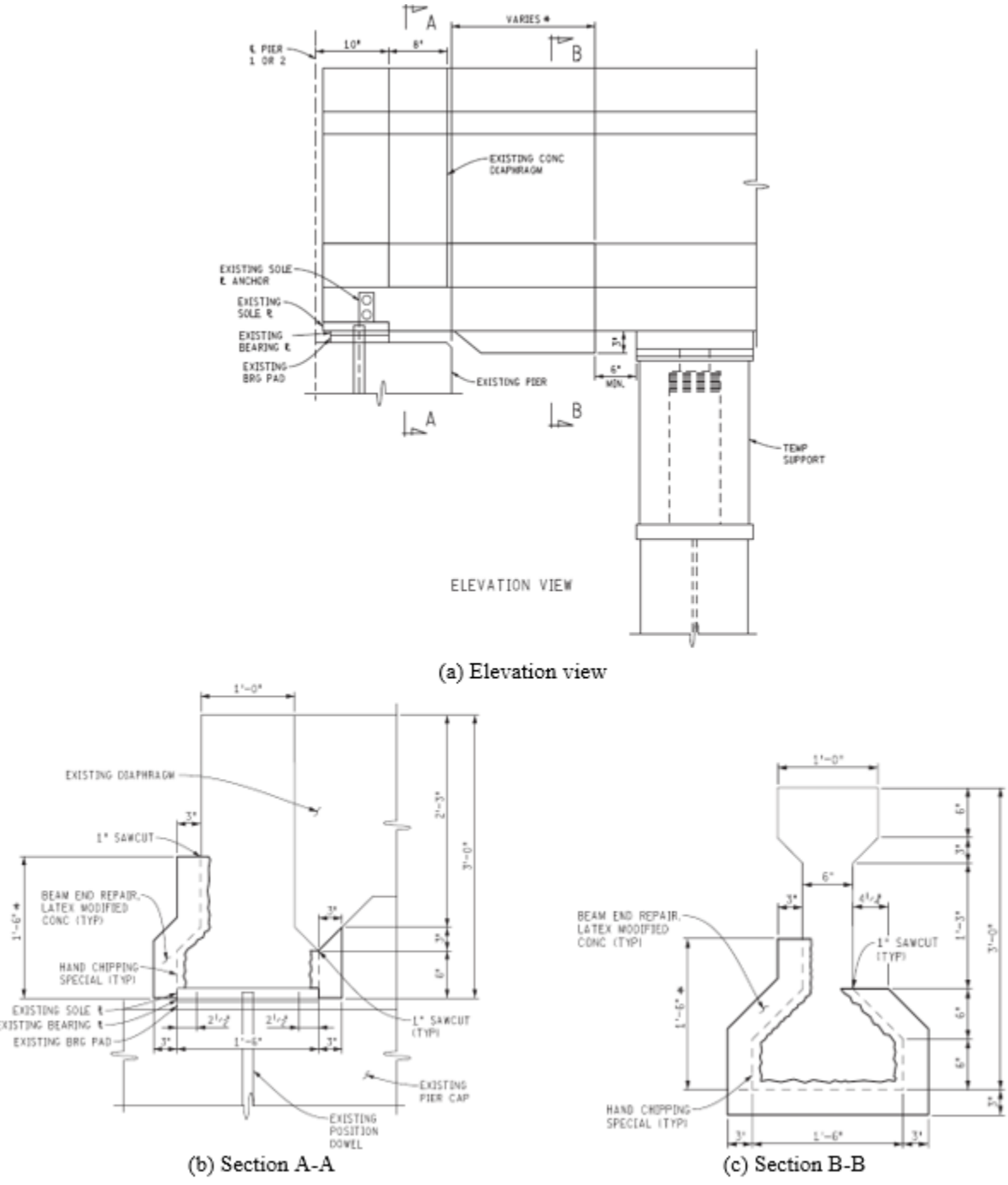

Figure D-35. Typical Type II beam end repair.

D.1.10.2 Inspection of Repaired Beam Ends

Beam ends were inspected on October 04, 2024. Beam end repairs included (a) partial depth overcasts and (b) chipping and removal of cracked and delaminated overcasts due to the safety of vehicles, pedestrians, and cyclists on the Earhart Road.

Even though the south fascia beam end repairs over pier 1w were about 4 years old and consistently exposed to elements, they were in good condition with a couple of hairline cracks (Figure D-36). However, a majority of the repairs did not perform well. A few examples are shown in Figure D-37.

(a) South fascia beam end repairs at pier 1w

(b) South fascia beam in span 1w at pier 1w

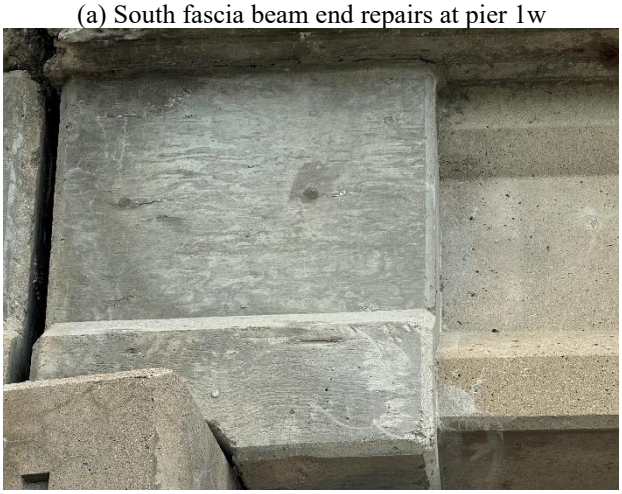

(c) South fascia beam in span 2w at pier 1w

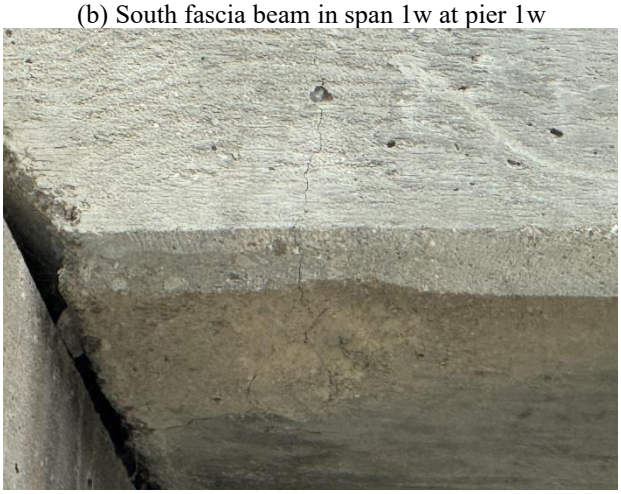

(d) South fascia beam in span 2w at pier 1w, overcast cracking

Figure D-36. The condition of the south fascia beam repairs at pier 1w.

(a) Completely removed overcast

(b) Delaminated and spalled overcast

(c) Delaminated and spalled overcast

(d) Overcast with map cracking and significant moisture exposure

Figure D-37. The condition of the repaired beam ends

D.1.10.3 Summary

In general, the partial-depth overcast did not perform well. Most of them delaminated and spalled. Considering safety, several of them were either entirely or partially removed by chipping out the delaminated sections. A few of these overcasts had hairline and map cracks, indicating a potential for accelerated deterioration with subsequent exposure to moisture. The use of these unreinforced overcasts with uncertain interface bond performance is not a viable option for promoting durability and adding strength to the beam ends. Further, none of the beam ends had received a concrete surface coating as noted in the letting documents.

D.2 PERFORMANCE EVALUATION OF REPAIR WITH FRP

D.2.1 STR 1213

D.2.1.1 Overview

The bridge (STR 1213) that carries I-69SB over St. Joseph River has three spans and is located in Calhoun County, Michigan (Figure D-38). The bridge has a width of 42.4 ft and a total length of 133 ft. The bridge was built in 1968. Each span has six prestressed concrete I-beams. The exterior beams in Spans 1 and 3 and all the beams in Span 2 are AASHTO Type III. The interior beams in Spans 1 and 3 are AASHTO Type II.

(a) General view of the bridge (b) East elevation

Figure D-38. I-69SB bridge over St. Joseph River (a) general view and (b) east elevation.

After 43 years of service life, the stringer (SIA-59) received a condition rating of 5 (fair) during the routine inspection on 10/04/2011 due to the following reasons:

- Fascia beam 6W in span 3S at pier 2S having cracks and delamination on the web
- Both fascia beams (1W and 6W) in span 2S at pier 1S having delamination, cracks, and rust stains
- Both fascia beams (1W and 6W) in spans 2S and 3S at pier 2S having spalls on the side of the bottom flange to the prestressing strands
- Both fascia beams (1W and 6W) in span 1S at pier 1S having spalls on the side of the bottom flange to the prestressing strands
- About 3 in. long exposed strand length
- Most interior beams at piers have cracks and discoloration
- Several diaphragms at piers have cracks and shallow spalls to rebar.

According to the 06/18/2019 inspection report, the stringer (SIA-59) condition rating has remained at 5 (fair) since 2011. The 2019 BSIR listed the following conditions in addition to what has already been noted in the 2011 BSIR:

- Beam end 5W at pier 1S in span 2S having an incipient spall.
- Most interior beam ends at piers have cracks, minor delamination, and discoloration
- Several diaphragms at piers have cracks, delamination, and shallow spalls to rebar.

Even though the 06/15/2021 inspection reported the stringer (SIA-59) condition rating of 5 (fair), which remained the same during the 10-year period since 2011, the 2021 BSIR report listed the following conditions in addition to what had already been noted in the previous reports:

- Beams 2, 4, and 5W in span 2S at pier 2S, having incipient spalls in the side of the bottom flange.
- Beam 6W in span 1S at pier 1S, having cracks and incipient spall on the web.

The research team was unable to locate a copy of the RFA to determine the recommended repairs and the exact schedule for their completion. Even though the 2017 Safety Inspection Report – AASHTO Elements listed 24 beam ends under the conditions state of two (CS 2), the 2017 scoping report called for the repair of only eight beam ends.

The 12/06/2022 inspection assigned a condition rating of 7 (good) for the stringer (SIA-59) and noted beam end repairs as follows:

- All beam ends over the piers have been repaired.
- The fascia beam ends at the piers and the beam end 5W at pier 2S in span 3S has been wrapped with FRP.

The 10/01/2021 letting (JN 200914A) included the repair details shown in Figure D-39 and Figure D-40. Eight fascia beam ends over piers received unreinforced, latex-modified concrete, partial-depth patch repairs, and FRP U-wraps (Figure D-39). Each beam end with partial-depth patch repair was wrapped using FRP sheets that extended a minimum of 6 in. beyond the end block patch. Cutouts were provided in the FRP sheeting for the sole plate and diaphragm on the interior face. Sole plates were salvaged and blast cleaned. Concrete surface coating (CSC) was applied along the full length of the fascia beam's outer surface, the bottom surface, and the inside surface of the bottom flange. Also, the entire area covered with FRP was protected with CSC.

Seven beam ends were cleaned and protected as shown in Figure D-40. The work included (i) removing loose material from the beam end, (ii) chipping a maximum of ½ in. as directed by the engineer, and (iii) cleaning and coating exposed bars using epoxy repair products from the

qualified product list. The details in the plans did not require patching with latex-modified concrete.

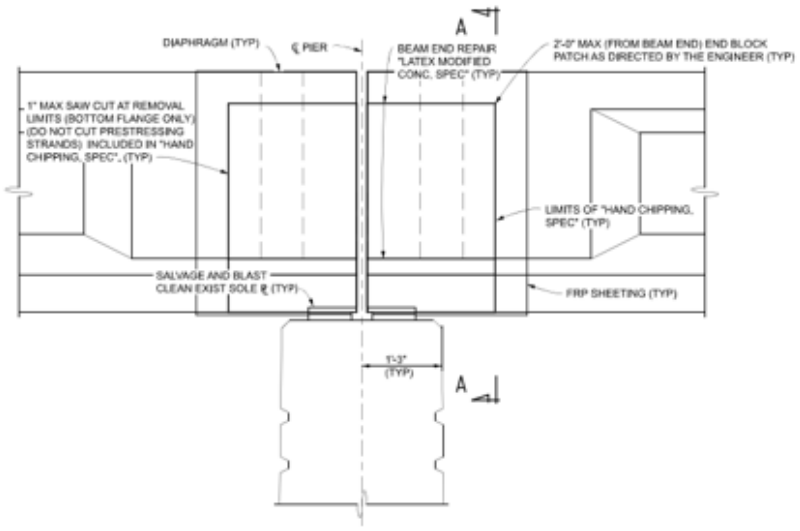

(a) Elevation

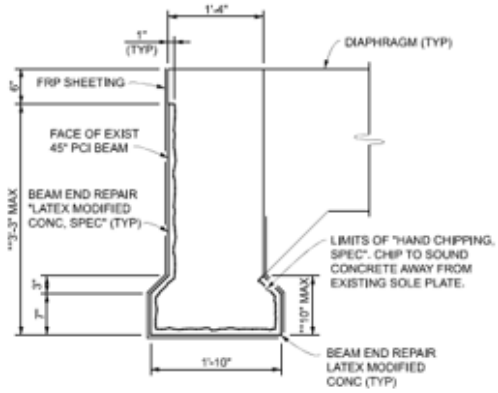

(b) Cross-section A-A

Figure D-39. Beam end partial-depth patch repair details.

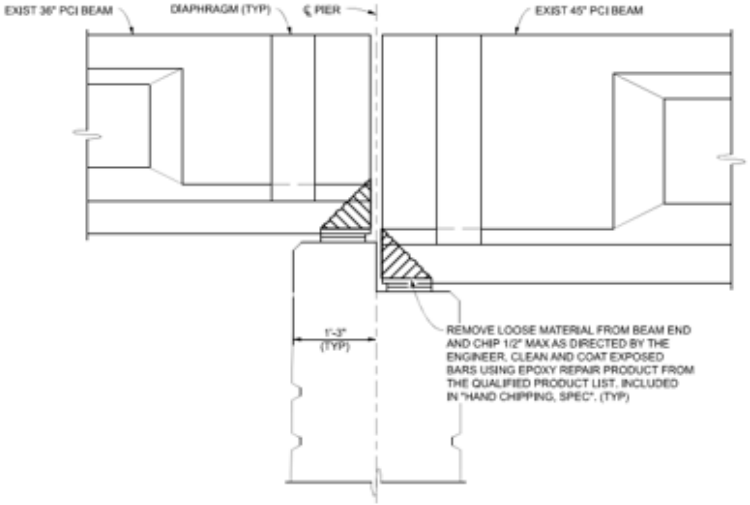

Figure D-39. Beam end partial-depth patch repair details.

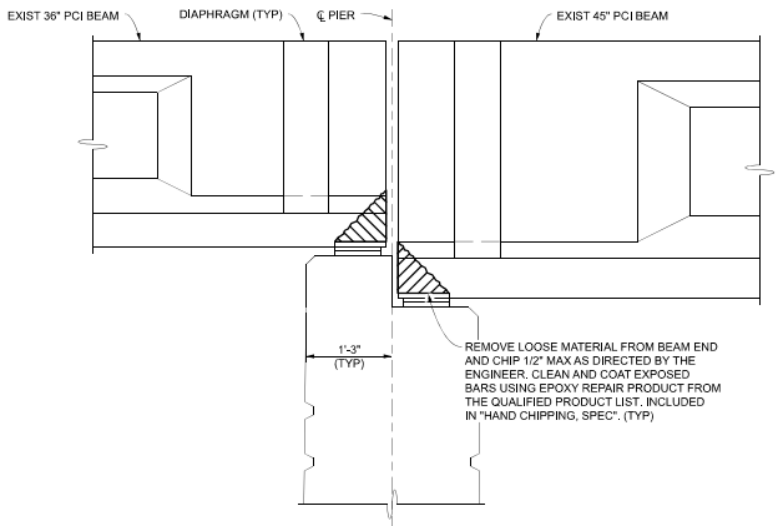

Figure D-40. Beam end elevation showing overcast details.

D.2.1.2 Inspection of Repaired Beam Ends

Beam ends were inspected on November 15, 2024, two years after the repairs were completed. The repair included (a) unreinforced latex-modified concrete partial-depth patch repairs and FRP U-wraps of fascia beam ends at the piers, (b) protecting the entire length and the overcasts of fascia beams with CSC, and (c) the repair of seven interior beam ends presumably using latex modified concrete. The following observations are reported during this inspection:

- Figure D-41: The two-year-old CSC on fascia beams and beam end repairs are in good condition.
- Figure D-42 (a) and (b): Corroded steel sole plate and bearing plate accelerate beam end deterioration and reduce the service life of repaired beam ends.
- Figure D-42 (c): Typical crack observed in overcast repairs without sole plate replacement.
- Figure D-42 (d): Pin holes in the adhesives used for FRP. Such conditions promote poor bonding of FRP layers.
- Figure D-42 (e): Inadequate FRP bond length at cross-section transitions promotes FRP delamination.
- Figure D-42 (f): Air voids in FRP repair.
- Figure D-43 (a) and (b): Latex modified concrete repair in good condition.
- Figure D-43 (b): An example of a properly formed, finished, and cleaned repair.
- Figure D-43 (c): An example of a poorly completed beam end repair leading to cracking and spall.

- Figure D-43 (d): An example of an inadequately cleaned and finished repair promoting cracking in the repair.
- Figure D-43 (e): Typical cracks in beam end repairs.
- Figure D-43 (f): An example of a repair performed without properly cleaning a beam end by removing all delaminated concrete.

The findings support the use of (i) CSC along the entire length of the fascia beams to protect the exterior surface and the bottom surface of the beam, (ii) FRP and CSC to minimize the impact of cracking and promote durability, and (iii) proper procedures and techniques for the preparation of beam ends for repair, formwork installation, and finishing.

(a) Fascia beam protected with CSC

(b) Repair with FRP U-wraps and CSC

(c) Overcast protected with CSC without FRP

(d) Beam end with partial-height repair, FRP, and CSC

(e) Beam end with partial-height repair, FRP, and CSC

Figure D-41. The condition of repaired fascia beams with FRP U-wraps and CSC.

(a) Corroded sole plate and bearing plate promoting deterioration

(b) Corroded sole plate and bearing plate promoting deterioration

(c) Typical cracking observed in overcasts without bearing replacement

(d) Adhesives with pin holes

(e) Inadequate bond length leading to delamination

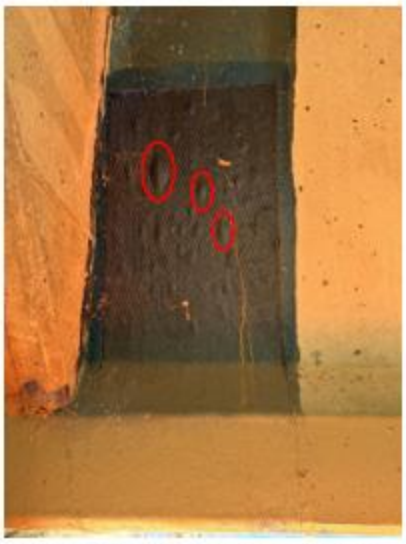

(f) Air voids due to poor bonding

Figure D-42. The condition of the FRP-repaired exterior beam ends at piers.

(a) Latex-modified concrete repair in good condition

(b) An example of a correctly completed beam end repair

(c) An example of a poorly completed beam end repair showing cracking and spalling

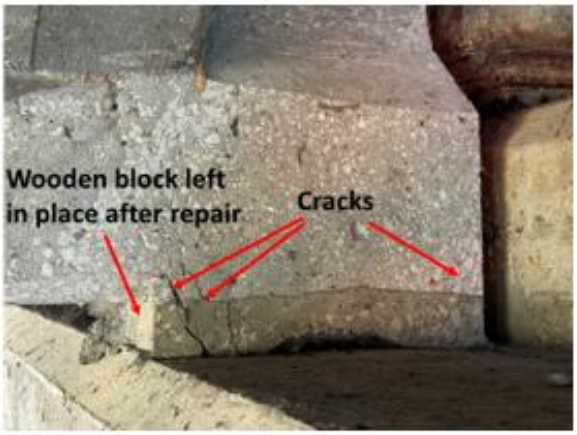

(d) Inadequately cleaned and finished repair with cracking

(e) Typical cracks in beam end repairs

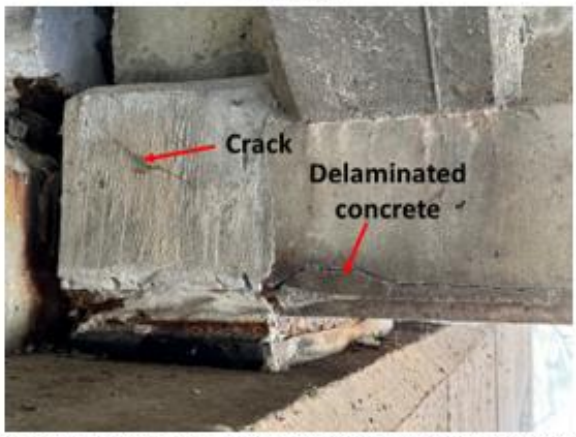

(f) An example of a repair performed without removing all delaminated concrete

Figure D-43. The condition of two-year-old latex-modified concrete beam end repairs.

D.2.2 STR 1215

D.2.2.1 Overview

The bridge (STR 1215) that carries I-69NB over St. Joseph River has three spans and is located in Calhoun County, Michigan (Figure D-44). The bridge has a width of 42.4 ft and a total length of 130.1 ft. The bridge was built in 1968. Each span has six prestressed concrete I-beams. The exterior beams in Spans 1 and 3 and all the beams in Span 2 are AASHTO Type III. The interior beams in Spans 1 and 3 are AASHTO Type II.

(a) General view of the bridge

(b) East elevation

Figure D-44. I-69NB bridge over St. Joseph River (a) general view and (b) east elevation.

After the bridge was in service for 43 years, the stringer (SIA-59) received a condition rating of 5 (fair) during the routine inspection on 10/04/2011 due to the following reasons:

- Fascia beams at both piers and beam 2W in span 2S at both piers having spalls to prestressing strands at the bottom flange
- Most interior beams at piers having cracks and discoloration
- Several diaphragms at piers having cracks and rust stains
- Backwalls having a few vertical leaching cracks.

The BSIRs dated 10/04/2011 and 06/18/2019 documented the same information. The BSIR dated 06/16/2021 documented the following in addition to the information presented in the previous reports.

- Beams 2, 4 and 5W at pier 1S having spalls to prestressing strands on the bottom flange
- Beams 4 and 5W in span 2S at pier 2S having incipient spalls.

The research team was unable to locate a copy of a Request for Action (RFA) to determine the recommended repairs and the exact schedule for their completion. The 12/06/2022 and 06/05/2023 inspections assigned a condition rating of 5 (fair) for the stringer (SIA-59) and noted beam end repairs and conditions as follows:

- All beam ends at the piers having patch repairs
- The fascia beam ends at each pier having patch repairs with FRP wrapping
- Both fascia beams having concrete surface coating (CSC) on the outside and bottom flange for the full length
- Beam 5W in span 1S at pier 1S having cracks
- Several diaphragms at the piers having cracks and rust stains
- Backwalls having a few vertical leaching cracks.

The 10/01/2021 letting (JN 200914A) included the repair details shown in Figure D-45 and Figure D-46. Eight fascia beam ends over piers were repaired using unreinforced, latex-modified concrete, partial-depth patch repairs, and FRP U-wraps (Figure D-45). Each beam end with partial-depth patch repair was wrapped using FRP sheets that extended a minimum of 6 in. beyond the end block patch. Cutouts were provided in the FRP sheeting for the sole plate and diaphragm on the interior face. Sole plates were salvaged and blast cleaned. CSC was applied along the full length of the fascia beam's outer and bottom surfaces as well as the inside surface of the bottom flange. Also, the entire area covered with FRP was protected with CSC.

Six beam ends were cleaned and protected as shown in Figure D-46. The type 1 detail shown in Figure D-46(a) was used at five beam ends, while the type 2 detail shown in Figure D-46(b) was used at only one end. The work included (i) removing loose material from beam ends, (ii) chipping a maximum of ½ in. as directed by the engineer, and (iii) cleaning and coating exposed bars using epoxy repair products from the qualified product list. The details in the plans did not require patching with latex-modified concrete.

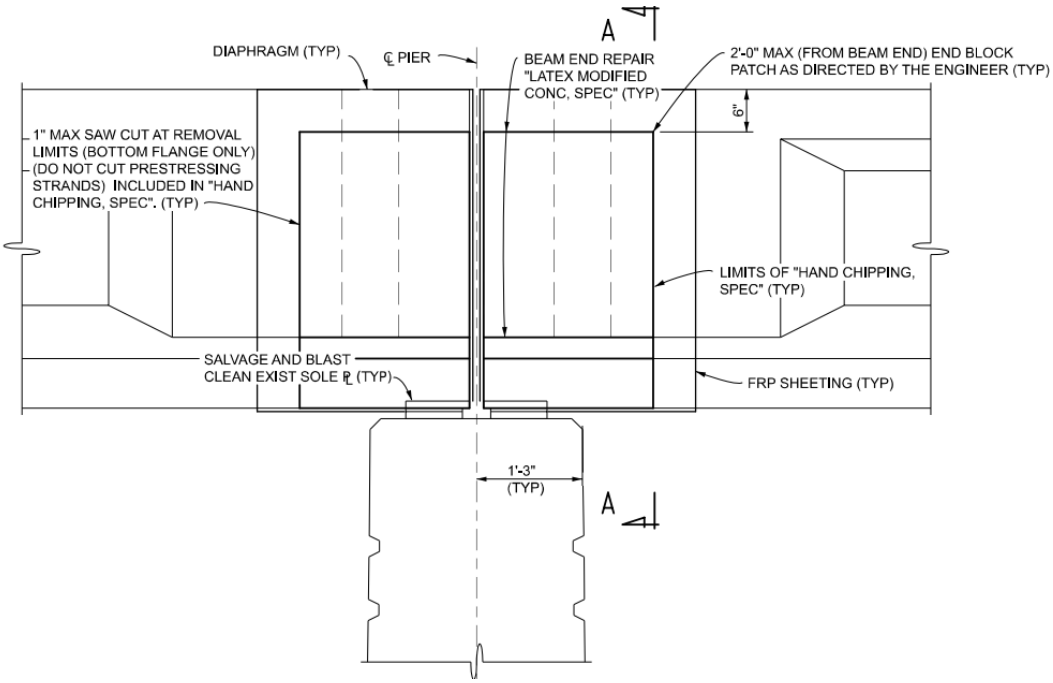

(a) Elevation

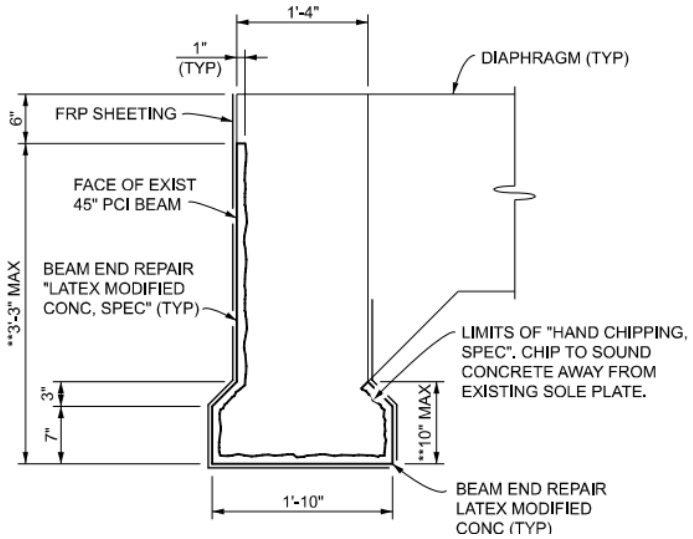

(b) Section A-A

Figure D-45. Beam end partial-depth patch repair details.

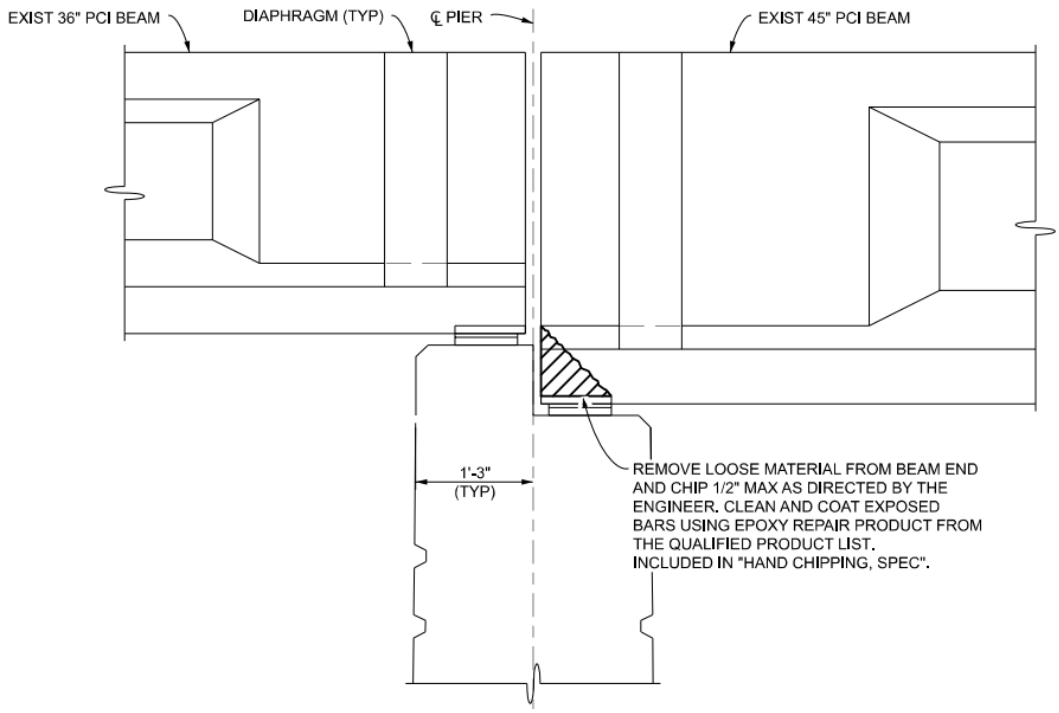

(a) Beam end repair type 1

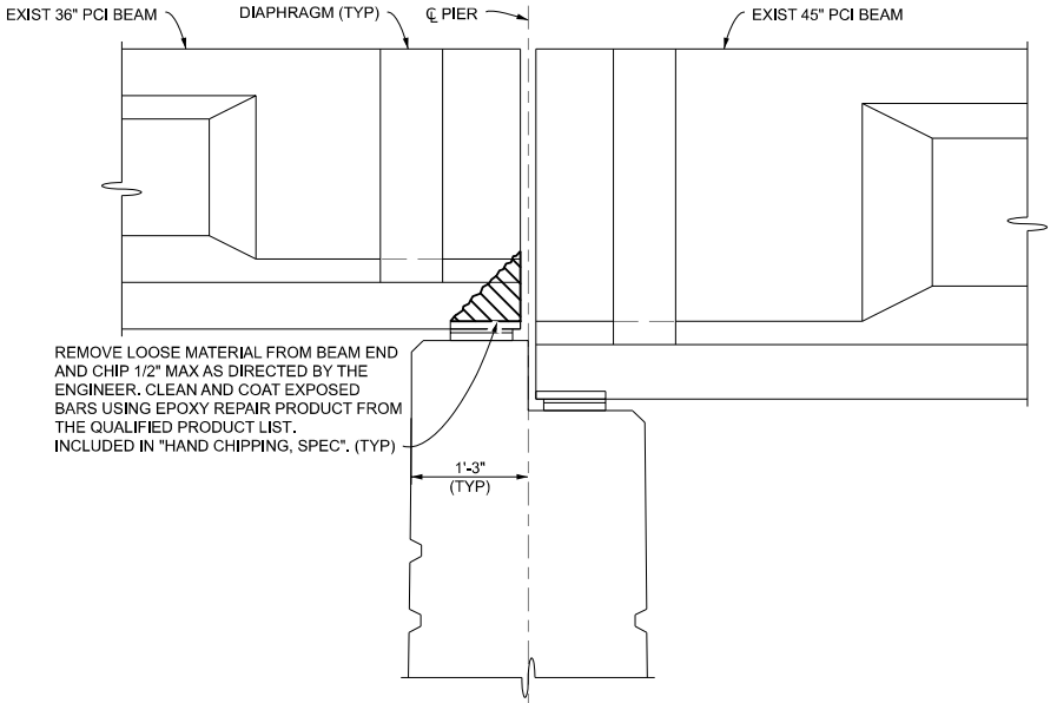

(b) Beam end repair type 2

Figure D-46. Beam end elevation showing repair details.

D.2.2.2 Inspection of Repaired Beam Ends

Beam ends were inspected on November 15, 2024, two years after the repairs were completed. The repair included (a) unreinforced, latex-modified concrete, partial-depth repairs and FRP U-wraps of fascia beam ends at the piers, (b) protecting the entire length and the repairs on fascia beams using CSC, and (c) the repair of six interior beam ends presumably using latex-modified concrete. Even though the repair plans did not include beam end overcasts, unreinforced concrete overcasts were provided at several interior beam ends over the piers. The following observations are reported during this inspection:

- Figure D-47: The two-year-old CSC on fascia beams and beam end repairs are in good condition.
- Figure D-48 (a): Latex modified concrete repair in good condition.
- Figure D-48 (b): Unreinforced latex-modified concrete overcast on an interior beam end.
- Figure D-48 (c): Typical cracking observed in an overcast.
- Figure D-48 (d): Through-thickness crack in the unreinforced latex-modified concrete overcast.

The findings support the use of (i) CSC along the entire length of the fascia beams protecting the exterior surface and the bottom surface of the beam and (ii) FRP and CSC to minimize the impact of cracking and promote durability. The use of unreinforced concrete overcasts is not encouraged due to cracking observed within two years of repair and the potential for delamination and spalling.

(a) Fascia beam protected with CSC

(b) Partial-height repair with FRP U-wraps and CSC

(c) Beam end with partial-height repair, FRP, and CSC

(d) Beam end with partial-height repair, FRP, and CSC

Figure D-47. The condition of repaired fascia beams with FRP U-wraps and concrete surface coating.

(a) Latex modified concrete repair in good condition

(b) Unreinforced concrete full-depth overcast

(c) Typical crack observed on unreinforced concrete overcasts

(d) Through-thickness crack in the unreinforced overcast

Figure D-48. The condition of two-year-old latex-modified concrete beam end repairs.

D.2.3 STR 7412

D.2.3.1 Overview

The bridge (STR 7412) that carries US-131SB and M-46SB over Tamarack Creek has three spans and is located in Montcalm County, Michigan (Figure D-49). The bridge has a width of 48.1 ft and a total length of 167 ft. The bridge was built in 1972. This bridge has eight AASHTO Type III beams in each span.

(a) General view of the bridge (b) East elevation

Figure D-49. US-131SB and M-46SB bridge over Tamarack Creek (a) general view and (b) east elevation.

After the bridge was in service for 38 years, the stringer (SIA-59) received a condition rating of 4 (poor) during the routine inspection on 03/24/2010 due to the following reasons:

- Large spalls and some vertical cracks in fascia beam ends over piers
- Some moderate cracking and spalling on interior beam ends over piers
- Spall-to-steel (STS) at several beam ends over piers
- Several hairline horizontal cracks in the lower flanges of fascia beams.

The research team was unable to locate a copy of a Request for Action (RFA) to determine the recommended repairs and the exact schedule for their completion. The subsequent inspections reported in Bridge Safety Inspection Reports (BSIRs) dated 03/24/2011 and 03/20/2012 stated the same conditions observed on 03/24/2010. As per the BSIR dated 10/26/2012, beam ends at piers 1s and 2s have been repaired, new full-depth diaphragms have been installed at both piers, and the cracking in fascia beams has been epoxy injected.

The repair details dated 04/13/2011 and shown in Figure D-50 through Figure D-52 include replacement of elastomeric bearing pads at the piers, reinforced concrete full-depth overcasts for all the beam ends at the piers, new diaphragms at the piers, fiber reinforced polymer (FRP) U-wraps for all the beam ends at piers and abutments, and concrete surface coatings for all the beam ends. A latex-modified concrete mix was used for the overcasts and the new end diaphragms at the piers.

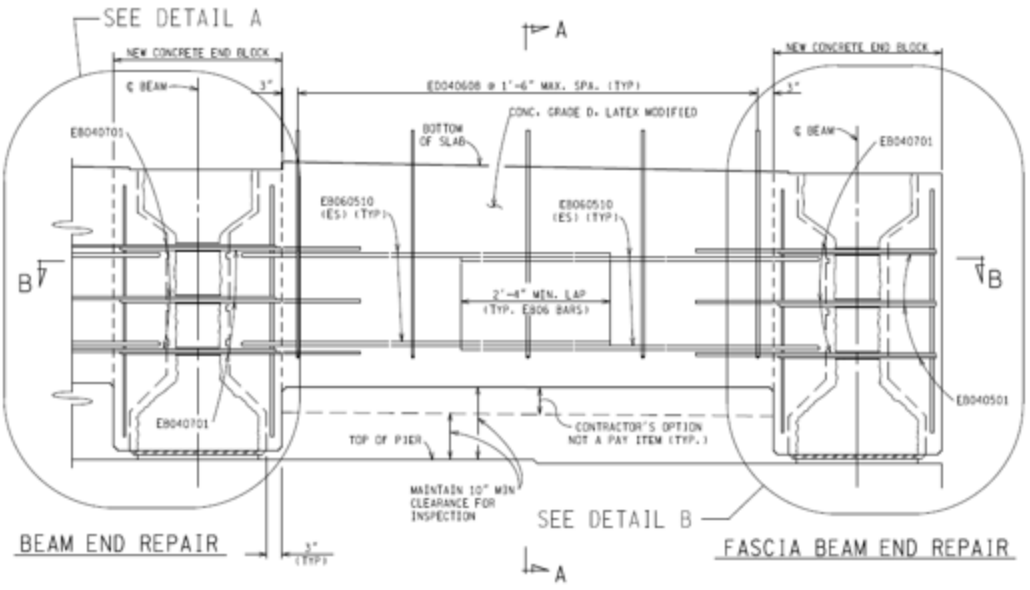

(a) Diaphragm elevation

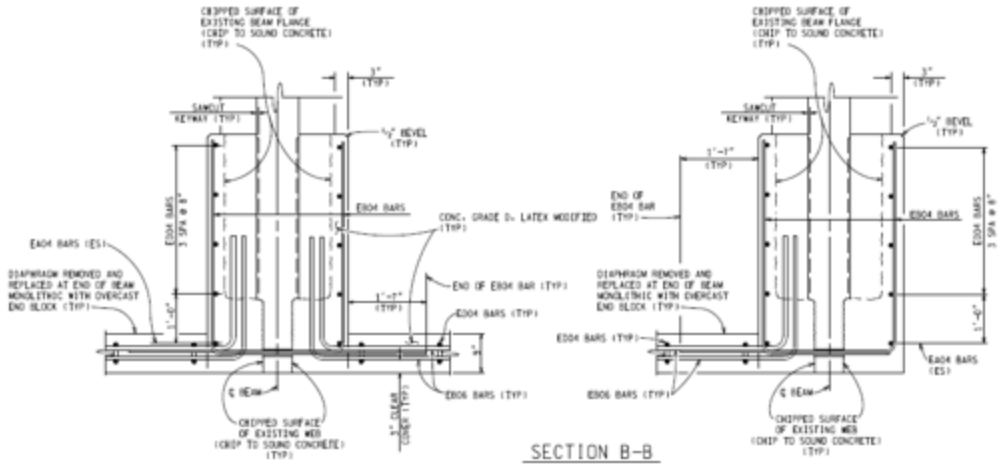

(b) Section B-B

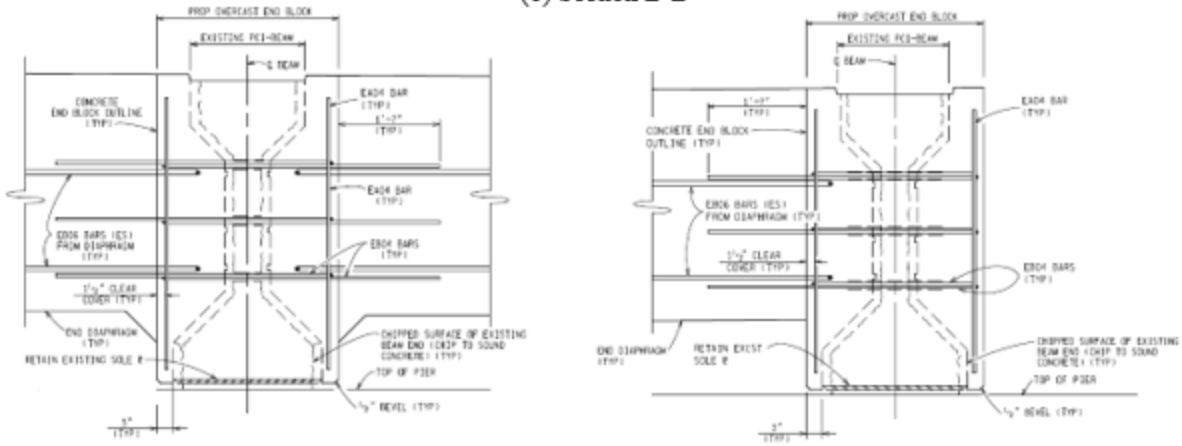

(c) Detail A

(d) Detail B

Figure D-50. Beam end overcast and new end diaphragm details.

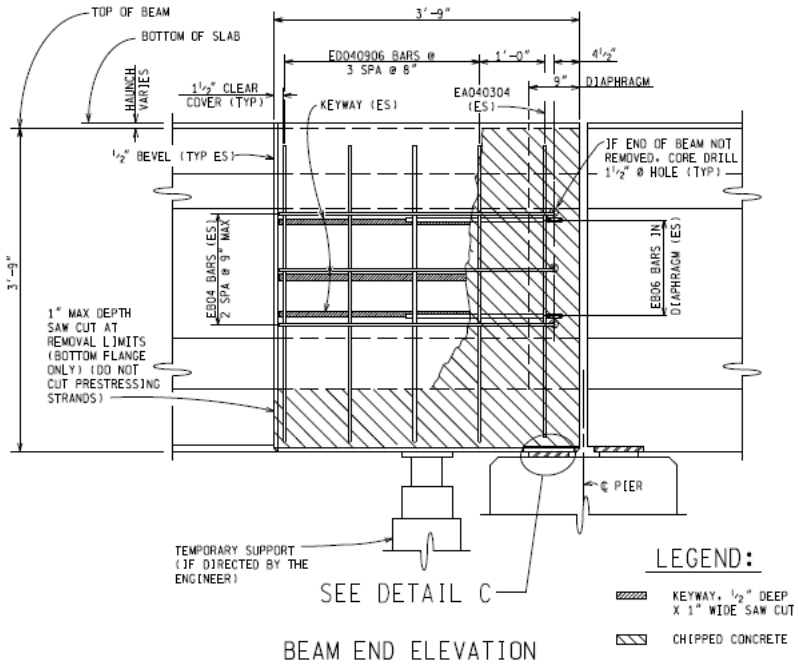

Figure D-51. Beam end elevation showing overcast details.

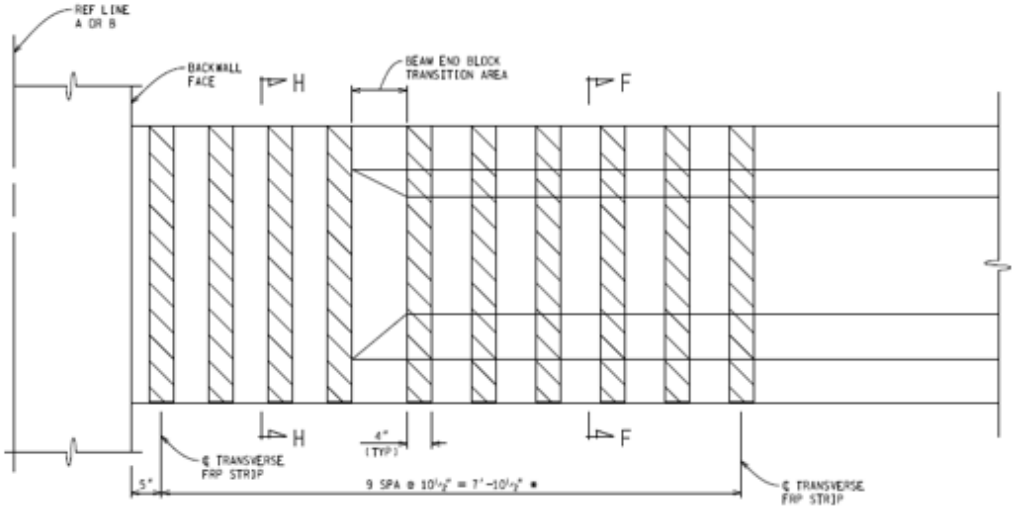

* Adjust spacing to gap out FRP stips in beam end block transition area.

(a) Elevation of FRP repair at abutment

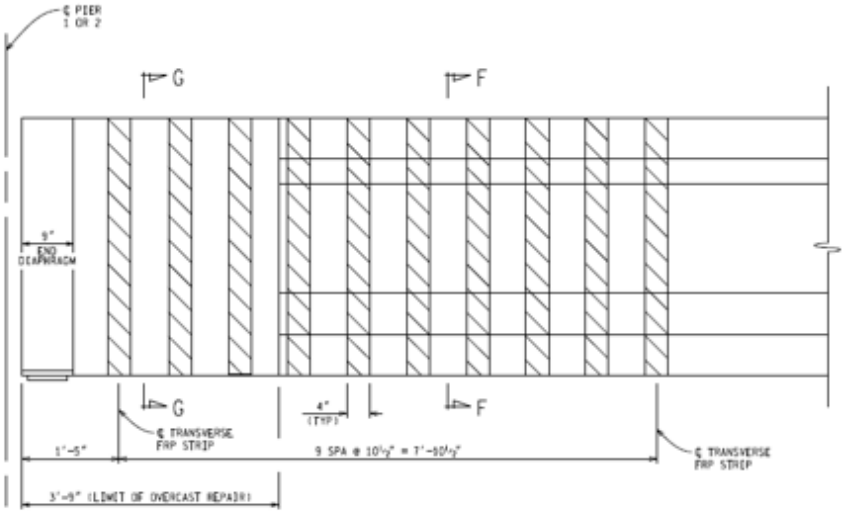

(b) Elevation of pier end FRP repair

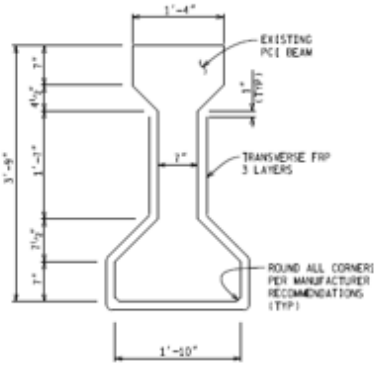

(c) Section F-F

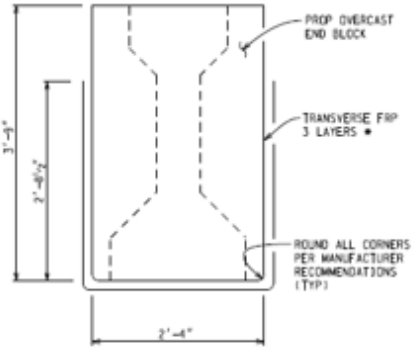

* FRP strips shall not be placed on new concrete less than 28 days of age.

(d) Section G-G

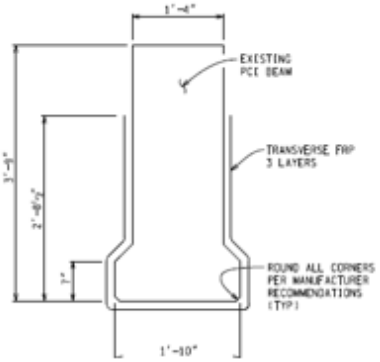

(e) Section H-H

Figure D-52. FRP repair details.

D.2.3.2 Inspection of Repaired Beam Ends

Beam ends were inspected on October 17, 2024. Repairs included (a) overcasting of beam ends at the piers with latex-modified concrete, (b) providing FRP U-wraps for beam ends at the piers and abutments, (c) epoxy injection of fascia beam cracks, and (d) protecting beam ends using concrete surface coating. As shown in Figure D-53 through Figure D-56, beam end repairs are in good condition. The following performance concerns are noted:

- Figure D-53 (d): Corroded steel plates at the beam end.
- Figure D-54 (b) and (c): Concrete deterioration along the uncoated exterior surface of the fascia beam bottom flange.
- Figure D-55 (b) and (c): Beam end exposure to moisture due to leaking deck and beam end bottom flange delamination due to corroding steel plates.
- Figure D-56: FRP U-wraps can control horizontal crack propagation in the latex-modified concrete overcasts.
- Figure D-57: Deteriorated expansion joints and clogged deck drains promote beam end exposure to moisture.
- Figure D-54 and Figure D-56: Cracking and efflorescence highlight the need for reapplication of concrete surface coating to extend the service life of these details. Although the reapplication frequency needs to be determined after evaluating the full-depth overcast and concrete surface coating performance using an adequately representative dataset, the performance of this bridge would support reapplication at least every 10 years.

D.2.3.3 Summary

Beam ends were repaired in 2012. The research team assessed that the repaired beam ends are in good condition after being in service for 12 years. The findings support the use of reinforced concrete, full-depth overcasts with latex-modified concrete for extending the service life for more than 12 years. The following maintenance activities are suggested to enhance the durability of repaired beam ends and the fascia beams:

- Application of a thin epoxy overlay to protect the bridge deck and prevent moisture ingress through the cold joint between the deck and the newly placed concrete along the repaired expansion joint.

- Regular power washing of the deck to prevent debris accumulation at the expansion joint and the deck drainage.
- Application of a concrete surface coating along the entire length of the fascia beam, protecting the exterior surface and the bottom surface of the beam.
- Reapplication of concrete surface coating at least every 10 years.

(a) Elevation view of an interior beam end

(b) A close-up view showing the effectiveness of concrete surface coating and the quality of FRP bonding

(c) Bottom surface of a beam end

(d) Bearing plate condition

Figure D-53. The condition of an FRP repaired interior beam end at the south abutment.

(a) Elevation view of an exterior beam end

(b) A close-up view showing the effectiveness of concrete surface coating and the quality of FRP bonding

(c) The condition of the exterior beam without surface coating

Figure D-54. The condition of an FRP repaired exterior beam end at an abutment.

a) General view of an interior beam end with an overcast

(b) Beam end with overcast exposed to moisture due to leaking bridge deck

(c) Delamination over the bearing plate

Figure D-55. The condition of an FRP-repaired exterior beam end with an overcast at a pier.

(a) A general view of the overcast

(b) A close-up view showing concrete cracking

(c) FRP strips controlling horizontal crack development

Figure D-56. The condition of an FRP-repaired exterior beam end with an overcast at a pier.

(a) An expansion joint over a pier filled with debris

(b) A close-up view of the expansion joint

(c) Partially clogged deck drains

Figure D-57. The condition of the expansion joint over a pier and the deck drains.

D.2.4 STR 10942

D.2.4.1 Overview

The bridge (STR 10942) that carries I-94 EB over the Dancer Road has three spans and is located in Washtenaw County, Michigan (Figure D-58). The bridge has a width of 47.4 ft and a total length of 112 ft. The bridge was built in 1961. This bridge has two AASHTO Type II fascia beams and six AASHTO Type I interior beams in Span 1, and eight AASHTO Type II beams in Span 2 and 3.

(a) General view of the bridge

(b) South elevation

Figure D-58. I-94 EB bridge over Dancer Road (a) general view and (b) south elevation.

After the bridge was in service for 55 years, the stringer (SIA-59) received a condition rating of 4 (poor) during the routine inspection conducted on 06/08/2016 due to the following reasons:

- Several beam ends having spalling and delamination.
- A few beam ends having exposed steel and prestressing strands with minor section losses.
- Several areas of fascia beams and beam ends at piers and abutments with damaged (peeling off of) concrete surface coating.

A Request for Action (RFA) was submitted on 06/09/2016 for this bridge because of the following beam end conditions:

- Several beam ends having delamination, spalling, and cracking, as shown in Figure D-59.
- The end of beam 3s located at the west abutment having spalling and delamination, as shown in Figure D-60.
- The end of beam 4s in span 1w located at pier 1w having spalling in the bottom flange with exposed steel and prestressing strands with loss of bearing area, as shown in Figure D-61.

- The end of beam 2s in span 2w located at pier 1w having spalling, cracking, and delamination, as shown in Figure D-62.

Even though providing temporary supports was considered as an alternative, beam ends with significant deterioration were repaired with partial-depth overcasts, as shown in Figure D-60, Figure D-61, and Figure D-62. For some reason, as shown in Figure D-62c, the beam end over the bearing was not repaired even though the section over the bearing was significantly deteriorated. This repair hinders the inspection of the beam ends over the bearing during routine inspections. Also, the top surface of the overcast had a rough horizontal surface, promoting the accumulation of nesting pigeons and pigeon waste.

(a) Concrete cracking and delamination in front of the bearing plate

(b) Shallow spall at the bottom flange soffit

Figure D-59. Typical beam end distress.

(a) Bottom flange soffit (b) North elevation

(c) Overcast after 2016 RFA

Figure D-60. The condition of beam 3s in span 1w at the west abutment as of 06/09/2016 and the subsequent repair of the beam end.

(a) General view (b) North elevation

(c) Bottom flange soffit (d) Overcast after 2016 RFA

Figure D-61. The condition of beam 4s in span 1w at pier 1w as of 06/09/2016 and the subsequent repair of the beam end.

Figure D-62. The condition of beam 2s in span 2w at pier 1w as of 06/09/2016 and the subsequent repair of the beam end.

Another RFA was submitted on 05/08/2020, primarily due to the condition of the end of beam 1s in span 2w located at pier 1w. As shown in Figure D-63, a spall-to-steel was noted in the RFA with a 4-in. deep spall that reduced the bearing contact area approximately by 22%. The initial recommendation was to have temporary supports to reduce the load at the beam end. This was subsequently changed, and it was decided to clean and coat the exposed concrete surface with a silane-based water repellent. However, the final decision was to provide partial depth overcasts for the two beam ends located over the pier (i.e. the ends of beam 1s in span 1w and 2w) and protect them with CFRP U-wraps as an experimental study, as shown in Figure D-64, since there were three partial depth overcasts already in the bridge. In addition, the overcasts provided as a result of the 2016 RFA were also protected with CFRP U-wraps, as shown in Figure D-65, Figure D-66, and Figure D-67. All remaining deteriorated ends were cleaned by removing delaminated concrete and protected with concrete surface coatings. This repair was completed in 2021.

Figure D-63. The condition of beam 1s in span 2w at pier 1w as of 05/08/2020.

(a) General view (b) South elevation

Figure D-64. The overcast with CFRP wrapping at beam 1s in span 1w and 2w at pier 1w as of 10/04/2024.

(a) South elevation (b) Bottom flange soffit

Figure D-65. The overcast with CFRP wrapping at beam 3s in span 1w at the west abutment as of 10/04/2024.

(a) South elevation (b) General view

Figure D-66. The overcast with CFRP wrapping at beam 4s in span 1w at the west abutment as of 10/04/2024.

(a) General view

(b) South elevation

Figure D-67. The overcast with CFRP wrapping at beam 4s in span 1w at pier 1w as of 10/04/2024.

D.2.4.2 Inspection of Repaired Beam Ends at Arm's Length

The beam ends were inspected on October 04, 2024. Beam end repairs included (a) removing delaminated concrete and cleaning and protecting with concrete surface coatings and (b) overcasting with CFRP wrapping.

Figure D-68 shows a beam end protected with a concrete surface coating after removing delaminated concrete in front of the bearing. This beam end was repaired in 2021. The beam end is in good condition except having mild rust on the bearing plate. Bearing plate corrosion is a typical durability concern at beam ends, leading to delamination and spalling of the concrete surrounding the end.

Since this bridge is not allowed to close for traffic for more than 8 hours, all the repairs were completed under live traffic conditions. This did not allow jacking up the beam end to replace the sole plate and provide extra space for the repair. Hence, most of the partial depth overcasting was not extended to cover the concrete over the bearing. As shown in Figure D-69 and Figure D-70, this particular repair conceals beam ends and the progress of deterioration during routine inspections.

Figure D-62 shows the condition of beam 2s in span 2w at pier 1w as of 06/09/2016 and the subsequent repair of the beam end. The overcast was further enhanced by providing CFRP wrapping in 2021. However, the deteriorated beam end over the bearing was not repaired. The inspection on 10/04/2024 shows further deterioration at that location, as shown in Figure D-71.

CFRP bonding is weak and fails to provide the necessary capacity when applied as small strips. As shown in Figure D-72, these strips can be easily removed.

The other observations include uneven thickness of overcast and the peeling off of the concrete surface coating (Figure D-73).

(a) Isometic view showing beam end, bearing, and end diaphragm

(b) Close-up of beam end showing bearing and a section with concrete removed from the bottom flange

(c) Bottom flange showing the area cleaned and protected with concrete surface coating

Figure D-68. The beam end bottom flange was cleaned and protected with concrete surface coating in 2021 and inspected in 2024.

(a) Isometric view showing beam end with overcast, bearing, and end diaphragm

(b) Close-up of beam end showing bearing and the section over bearing without overcast

(c) Heavily corroded bearing and the bottom flange over the bearing protected with a concrete surface coating

(d) Concrete spall between the overcast and the corroded bearing

Figure D-69. The condition of beam 3s in span 1w at the west abutment as of 10/04/2024.

(a) South elevation

(b) Beam end cracking over the corroded bearing

Figure D-70. The condition of the end of beam 4s in span 1w at pier 1w as of 10/04/2024.

(a) Beam end condition as of 06/09/2016

(b) Overcast after 2016 RFA

(c) Condition of beam end with CFRP wrapping as of 10/04/2024

(d) Deteriorated beam end over the bearing

Figure D-71. The condition of beam 2s in span 2w at pier 1w.

(a) North elevation

Figure D-72. Short CFRP strips used below the end diaphragms at the end of beam 1s in span 2w at the pier 1w as of 10/04/2024.

(a) Uneven thickness of the overcast and damaged concrete surface coating

Figure D-73. The condition of beam 4s in span 1w at the west abutment as of 10/04/2024.

D.2.4.3 Summary

The beam end clearing and protection is a promising maintenance approach for shallow delaminations and spalls since it allows easy access for the inspectors to document subsequent deteriorations and assess the condition more accurately.

A majority of the partial-depth overcasts were provided at locations that could have been cleaned and protected with minimal impact on load capacity. The partial-depth overcasts were not extended to protect the concrete over the bearing or enhance the load capacity. However, this approach conceals further deterioration from the inspectors doing the routine inspection. Figure D-74 and Figure D-75 show typical details of beam ends with overcast and CFRP repairs. Even

though the use of CRFP to prevent concrete cracking and spall seems promising, the contribution to load capacity is not guaranteed due to a lack of anchorage and confinement with the specific configurations used at these beam ends.

As shown in Figure D-74c, only one side of the overcast over the bearing is protected with a CFRP strip. However, this strip is not properly anchored and the expected performance is questionable.

Irrespective of the repair methods, one of the major concerns is the corrosion of the bearing plates. It is recommended to consider non-corrosive material for the bearing plates in future bridges or when replacing bearings. For existing bridges, the bearing plate corrosion mitigation strategies need to be developed.

(a) General view

(b) South elevation

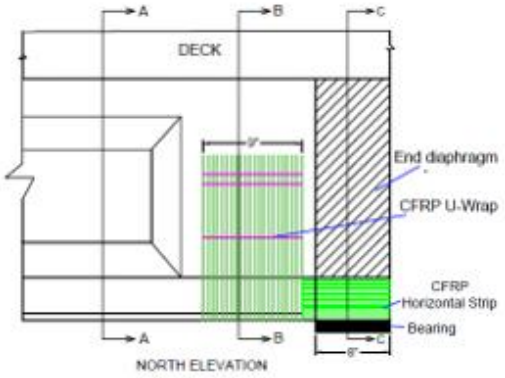

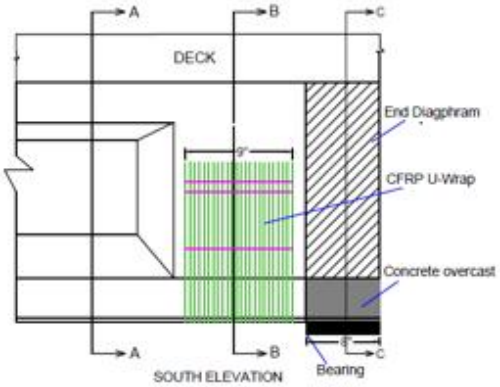

(c) Elevations

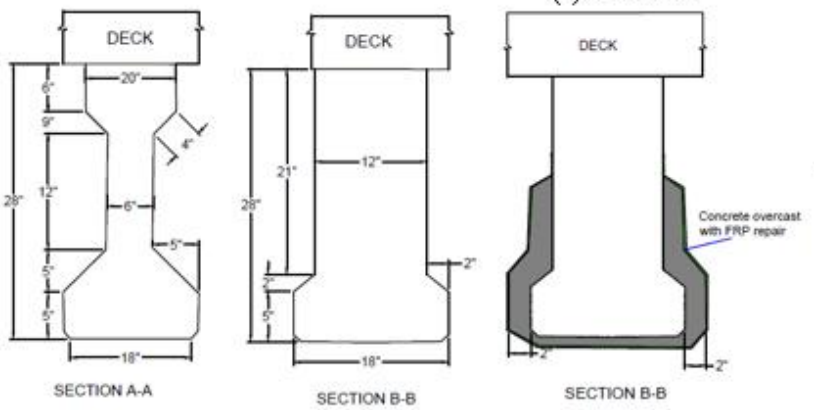

(d) Cross-sections of unrepaired beam

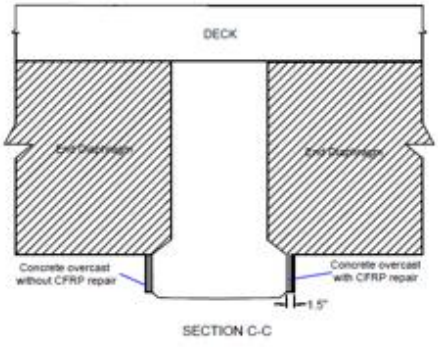

(e) Cross-sections showing overcast

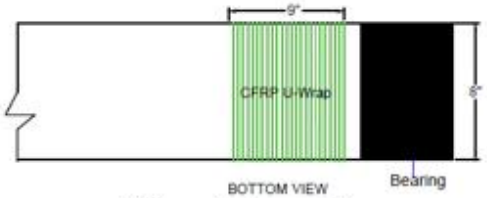

(f) Beam bottom surface

Figure D-74. Overcast and CRFP repair details at beam 4s in span 1w at the west abutment.

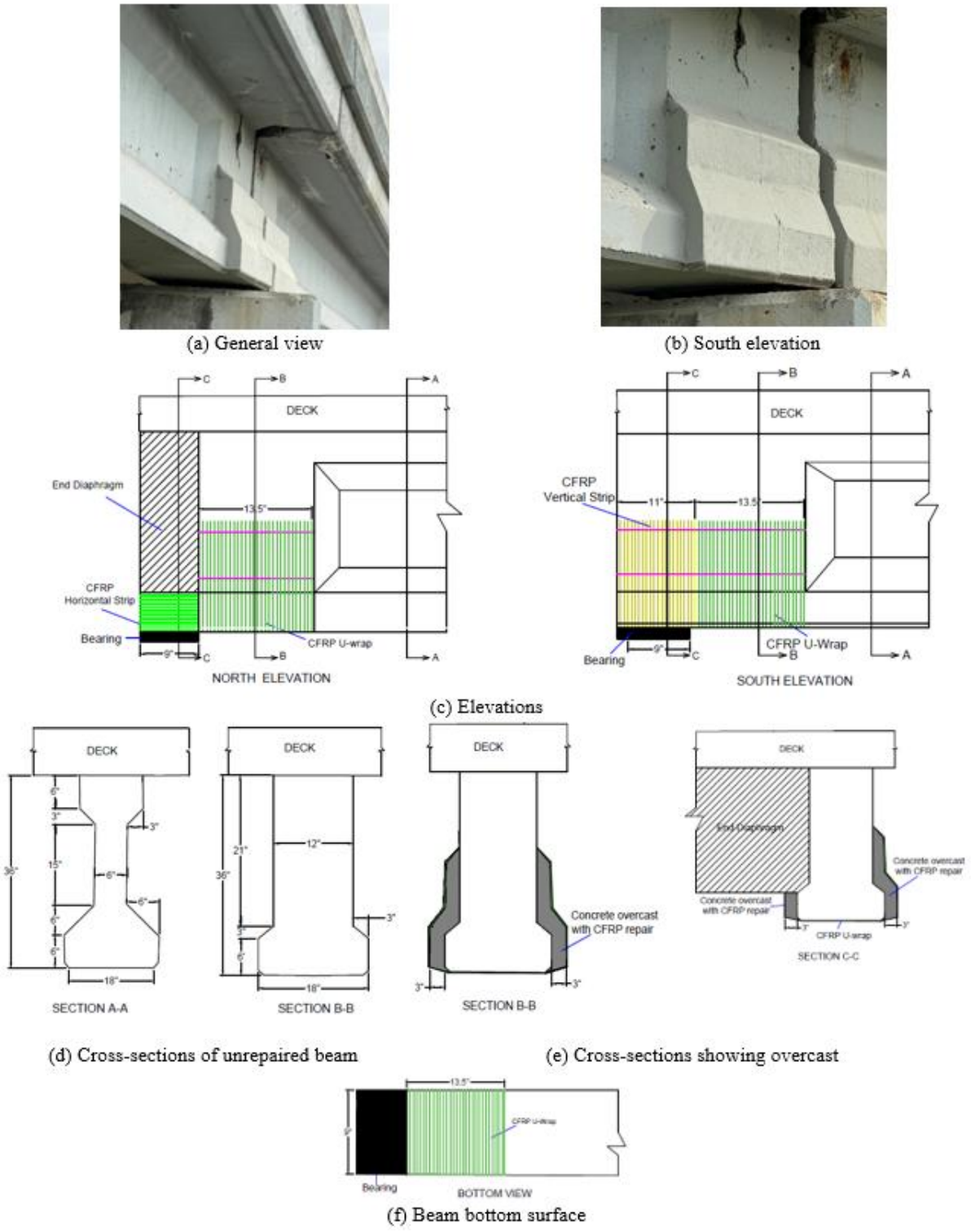

Figure D-75. Overcast and CRFP repair details at beam 1s in Span 1w at Pier 1.

APPENDIX E: PSC I-beam end capacity calculation – User manual

E.1 OVERVIEW

This document describes the content of the Mathcad calculation sheets shown in Figure E-1. The working folder must contain all the files to complete the calculations since the content is shared between these files to minimize the length of each calculation sheet. For example, the *0_Master_File_PSC_I-Beam_End_Capacity* file includes input data for the other files. Also, the *GirderSectionTable* Excel file contains beam cross-section properties.

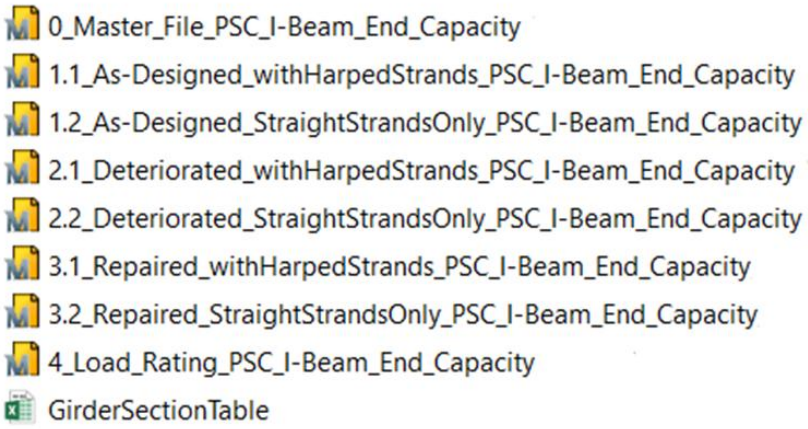

Figure E-1 The list of Mathcad calculation sheets and the section property table.

Figure E-2 shows the relationship between the Mathcad files and the Excel section property table. The "Master File" provides necessary data for all the capacity calculation cases, including as-designed, deteriorated, and repaired beams. Each capacity calculation case is separated for beam ends with (i) harped strands and (ii) straight strands. The sectional design model and the strut-and-tie method (STM) are used for as-designed and repaired cases. For the deteriorated cases, only STM is used. The load rating file provides shear load rating using LFR and LRFR methods. The load rating file can be used as an independent calculation sheet since it requires manually entering shear capacity and load factors.

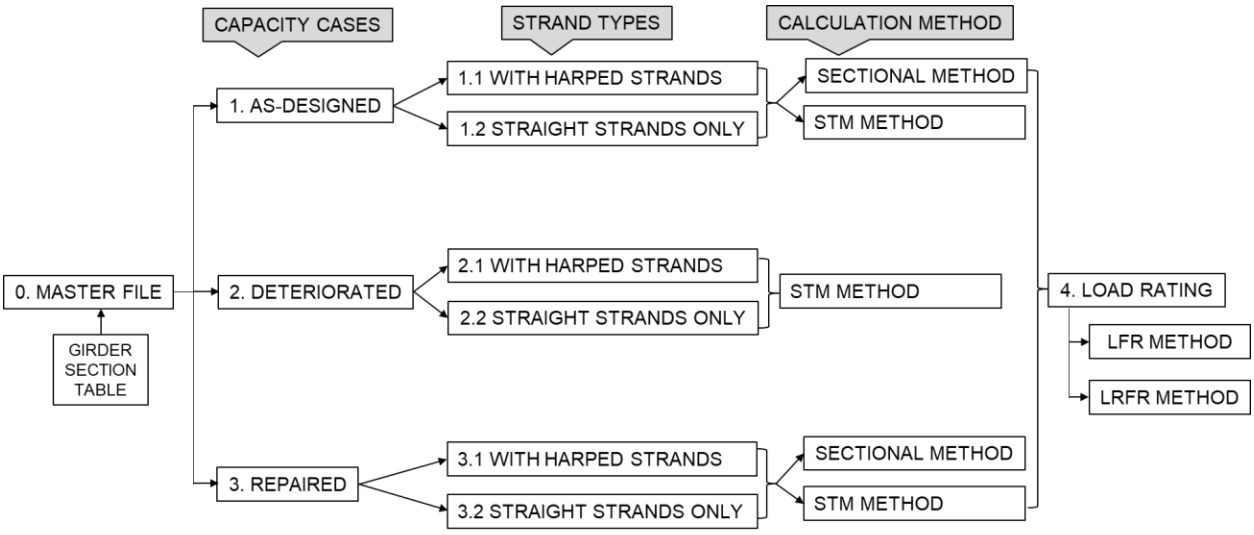

Figure E-2. Relationship between Mathcad files and the Excel sheet shown in Figure E-1.

Figure E-3 shows the primary data input and calculation steps in the Mathcad sheets. As required, sub-steps are further developed for as-designed, deteriorated, and repaired beam ends.

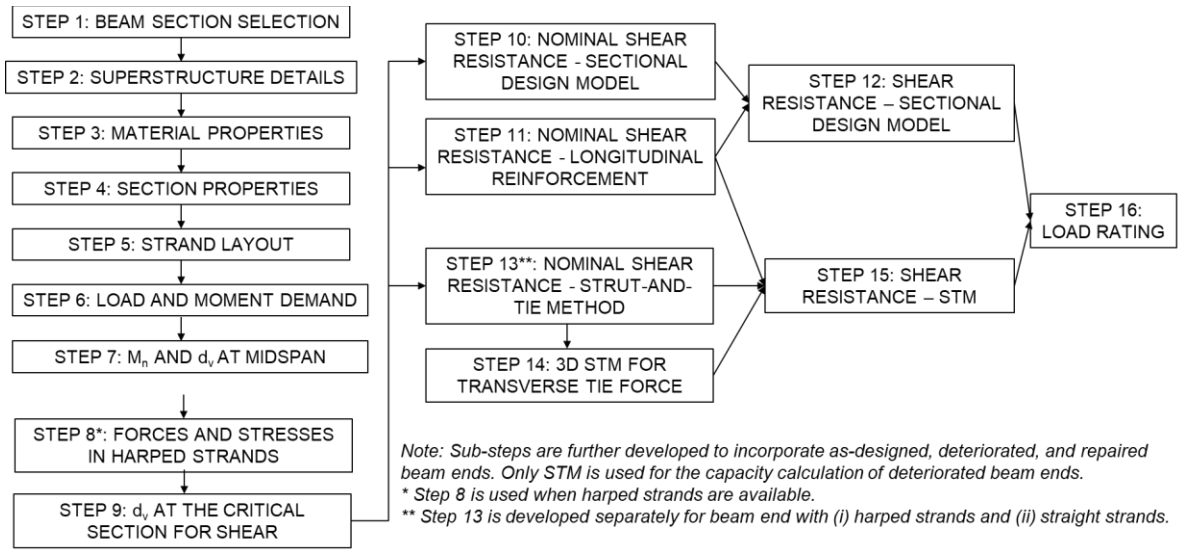

Figure E-3. The primary data input and calculation steps presented in the Mathcad sheets.

The user actions required to complete the calculations are explained using blue text. The gray highlighted text represents the primary data input and calculation steps.

LEGEND

Presents the format and color coding used in calculation sheets to identify *Commentary*, *Input Variables*, *References*, *Results and Checks* and *Special Notes*.

REFERENCES

Lists the primary references used to develop the calculation process.

ASSUMPTIONS AND LIMITATIONS

Lists the assumptions and limitations in the calculation process.

STEP 1: BEAM SECTION SELECTION

MDOT I-beam sections are defined and linked to the calculation sheet. The following image appears when the Excel file is properly linked to the Mathcad sheet. The pull-down menu allows selecting the desired beam section for capacity calculation and load rating. Section properties of the selected beam are automatically assigned to the variables defined in the Mathcad.

When the "*User defined*" option is selected from the pull-down menu, the section properties highlighted in pink need to be completed by the user.

Step 2: Superstructure Details

The user input is required only for the green highlighted cells.

Step 3: Materials Properties

The user input is required only for the green highlighted cells.

Step 4: Section Properties

STEP 4.1: NONCOMPOSITE BEAM SECTION PROPERTIES

Step 4.1.1: As-designed Noncomposite Beam Section Properties

The required data is automatically calculated based on the selected beam section or the input data provided in Step 1.

Step 4.1.2: Damage on Beam Soffit at Z3 (BTM)

The user needs to provide the dimensions shown in the following figure.

$S_D := 1.5in$ *Depth of spall/delamination*

$S_L := 6in$ *Length of spall/delamination*

$S_W := 8in$ *Width of spall/delamination*

$S_{LP} := 0in$ *Distance from sole plate to spall/delamination*

$S_{WE} := 12in$ *Distance from flange edge to spall/delamination*

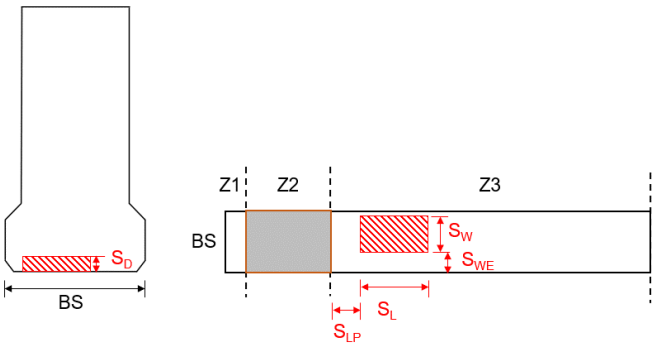

Based on the depth and location of spall/delamination, identify the number of exposed strands to be removed from the as-designed strand layout defined in Step 5. The spalled/delaminated area is assumed to be rectangular for calculation and reporting purposes.

Step 4.1.3: Damage on Beam Side

The user needs to provide the dimensions shown in the following figure.

$S_{HL} := 5.5in$

$S_{HLE} := 0in$

$S_{LEL} := 0in$

$S_{LL} := 6in$

$S_{WL} := 4in$

$S_{HR} := 5.5in$

$S_{HRE} := 0in$

$S_{LER} := 0in$

$S_{LR} := 6in$

$S_{WR} := 4in$

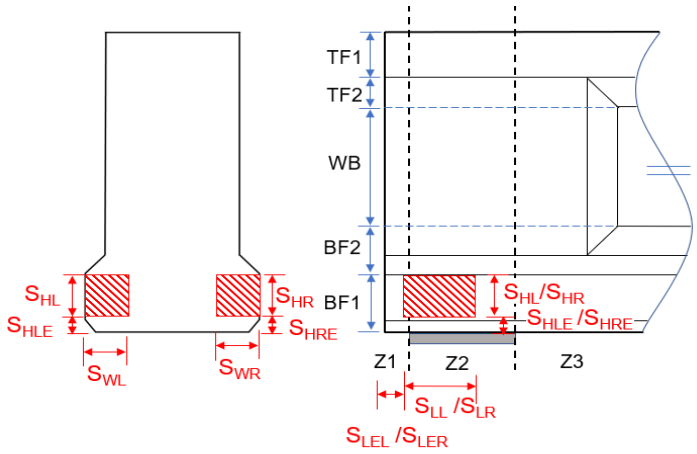

Based on the depth and location of spall/delamination, identify the number of exposed strands to be removed from the as-designed strand layout defined in Step 5. The spalled/delaminated area is assumed to be rectangular for calculation and reporting purposes.

Step 4.1.4: Damaged Noncomposite Beam Section Properties

The required data is automatically calculated based on the selected beam section or the input data provided in Step 1.

STEP 4.2: COMPOSITE BEAM SECTION PROPERTIES

Step 4.2.1: As-designed Composite Beam Section Properties

Composite section properties are automatically calculated.

Step 4.2.2: Damaged Composite Beam Section Properties

The user input is not required. The required data is automatically calculated.

Step 5: Strand Layout

STEP 5.1: DEFAULT PRESTRESSING STRAND LAYOUT

The following prestressing strand layout is selected to accommodate all possible strand patterns in MDOT I-, bulb-tee, and Michigan 1800 beams in the MDOT Bridge Design Guide

(BDG) as of **3/31/2025**. This layout is referred to as the default prestressing strand layout throughout this manual.

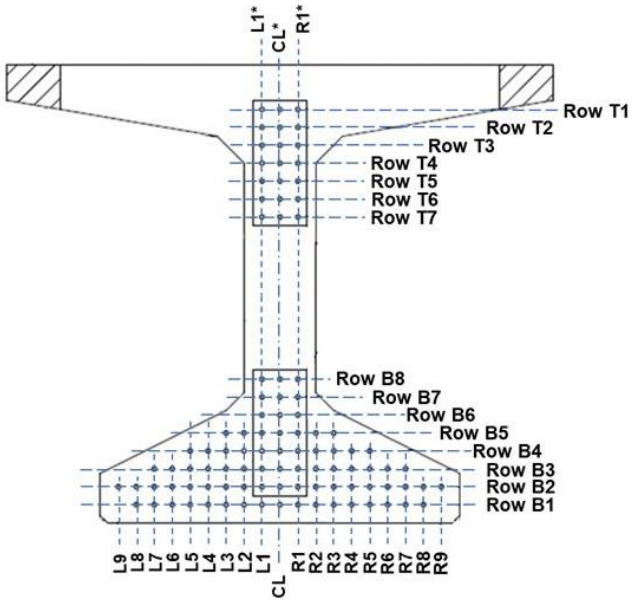

The layout includes 8 rows (Row B1 to Row B8) and 19 columns (L9, L8, …, CL, ..., R8, R9) in the bottom flange, and 7 rows (Row T1 to Row T7) and 3 columns (L1*, CL*, R1*) in the top flange. The center-to-center spacing between strands in each column and row is 2 in.

As shown in the following figure, the column 1 of the table *PS_Layout_Hor* represents the maximum number of strands that can be accommodated in each row. The column 2 represents the vertical distance to each row from the extreme bottom fiber or the top fiber of the section. The user shall not change the content of this table.

DO NOT change the content of the following table.

PS_Layout_Hor :=

	0	1	2
0	"Row B1"	17	2
1	"Row B2"	19	4
2	"Row B3"	15	6
3	"Row B4"	11	8
4	"Row B5"	7	10
5	"Row B6"	3	12
6	"Row B7"	3	14
7	"Row B8"	3	16
8	"Row T1"	3	3
9	"Row T2"	3	5
10	"Row T3"	3	7
11	"Row T4"	3	9
12	"Row T5"	3	11
13	"Row T6"	3	13
14	"Row T7"	3	15

Column 0: strand row label
Column 1: the maximum number of strands that can be accommodated in each row.
Column 2:
For Row B1 to Row B8: vertical distance from extreme bottom fiber to the center of strands in each row (in.)
For Row T1 to Row T7: vertical distance from beam extreme top fiber to the center of strands in each row (in.)

As shown in the following figure, the column 1 of the table *PS_Layout_Ver* represents the maximum number of strands that can be accommodated in each column. The column 2 represents the horizontal distance to each column from the centerline of the section. The user shall not change the content of this table.

DO NOT change the content of the following table.

PS_Layout_Ver :=

	0	1	2
0	"L9"	1	-18
1	"L8"	2	-16
2	"L7"	3	-14
3	"L6"	3	-12
4	"L5"	4	-10
5	"L4"	4	-8
6	"L3"	5	-6
7	"L2"	5	-4
8	"L1"	8	-2
9	"CL"	8	0
10	"R1"	8	2
11	"R2"	5	4
12	"R3"	5	6
13	"R4"	4	8
14	"R5"	4	10
15	"R6"	3	12
16	"R7"	3	14
17	"R8"	2	16
18	"R9"	1	18
19	"L1*"	7	-2
20	"CL*"	7	0
21	"R1*"	7	2

Column 0: strand column label
Column 1: the maximum number of strands that can be accommodated in each column.
Column 2:
*For L9 to R9 (including **L1*, CL*, and R1***): horizontal distance from beam vertical centerline (CL) to the center of each column (in.)*
L1*, CL*, and R1 *represent harped strands.*

STEP 5.2: AS-DESIGNED PRESTRESSING STRAND LAYOUT AT MIDSPAN

The number of prestressing strands in the as-designed beam section is defined with respect to the default layout presented in the "Default Prestressing Strand Layout" section. The following example demonstrates the procedure for defining prestressing strand layout for an as-designed beam.

Example 1: The following figure shows a 36 × 49 in. bulb-tee beam midspan section.

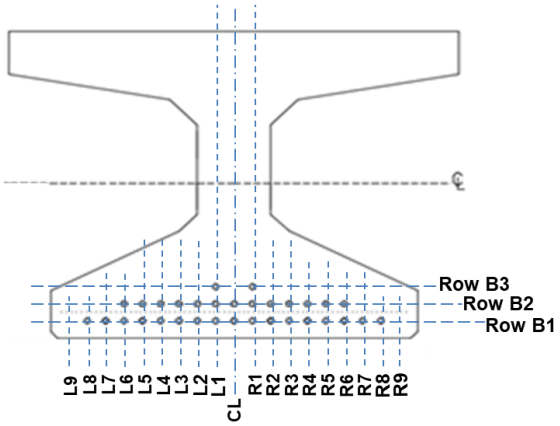

The following tables presents the procedure to identify the number of strands to be removed from the default layout to define the midspan strand layout of this 36 × 49 in. section.

Table 1. Number of Strands to be Removed from Each Row to Define the As-Designed Midspan Layout

Row no. (a)	No. of strands in the default layout (b)	No. of strands absent from the default layout (c)	No. of strands to be removed from the default layout (d) = (c)	No. of strands in the as-designed section (e) = (b) – (d)
B1	17	0	0	17
B2	19	6	6	13
B3	15	13	13	2
B4	11	11	11	0
B5	7	7	7	0
B6	3	3	3	0
B7	3	3	3	0

Row no. (a)	No. of strands in the default layout (b)	No. of strands absent from the default layout (c)	No. of strands to be removed from the default layout (d) = (c)	No. of strands in the as-designed section (e) = (b) – (d)
B8	3	3	3	0
T1	3	3	3	0
T2	3	3	3	0
T3	3	3	3	0
T4	3	3	3	0
T5	3	3	3	0
T6	3	3	3	0
T7	3	3	3	0

Table 2. Number of Strands to be Removed from Each Column to Define the As-Designed Midspan Layout

Column no. (a)	No. of strands in the default layout (b)	No. of strands absent from the default layout (c)	No. of strands to be removed from the default layout (d) = (c)	No. of strands in the as-designed section (e) = (b) – (d)
L9	1	1	1	0
L8	2	1	1	1
L7	3	2	2	1
L6	3	1	1	2
L5	4	2	2	2
L4	4	2	2	2
L3	5	3	3	2
L2	5	3	3	2

Column no. (a)	No. of strands in the default layout (b)	No. of strands absent from the default layout (c)	No. of strands to be removed from the default layout (d) = (c)	No. of strands in the as-designed section (e) = (b) – (d)
L1	8	5	5	3
CL	8	6	6	2
R1	8	5	5	3
R2	5	3	3	2
R3	5	3	3	2
R4	4	2	2	2
R5	4	2	2	2
R6	3	1	1	2
R7	3	2	2	1
R8	2	1	1	1
R9	1	1	1	0
L1*	7	7	7	0
CL*	7	7	7	0
R1*	7	7	7	0

As shown below, complete Column 1 of "AsD_PS_Mid_Layout_Hor" table using the numbers in column (d) of Table 1. The table "StrandLayout_Mid_Hor_AsD" represent the as-designed strand layout at the midspan.

AsD_PS_Mid_Layout_Hor :=

	0	1	2
0	"Row B1"	0	2
1	"Row B2"	6	4
2	"Row B3"	13	6
3	"Row B4"	11	8
4	"Row B5"	7	10
5	"Row B6"	3	12
6	"Row B7"	3	14
7	"Row B8"	3	16
8	"Row T1"	3	3
9	"Row T2"	3	5
10	"Row T3"	3	7
11	"Row T4"	3	9
12	"Row T5"	3	11
13	"Row T6"	3	13
14	"Row T7"	3	15

$StrandLayout\_Mid\_Hor\_AsD^{\langle 1 \rangle} := (PS\_Layout\_Hor^{\langle 1 \rangle}) - (AsD\_PS\_Mid\_Layout\_Hor^{\langle 1 \rangle})$

	0
0	17
1	13
2	2
3	0
4	0
5	0
6	0
7	0
8	0
9	0
10	0
11	0
12	0
13	0
14	0

As shown below complete Column 1 of "AsD_PS_Mid_Layout_Ver" table using the numbers in column (d) of Table 2. The table "StrandLayout_Mid_Ver_AsD" represent the as-designed strand layout at the midspan.

AsD_PS_Mid_Layout_Ver :=

	0	1	2
0	"L9"	1	-18
1	"L8"	1	-16
2	"L7"	2	-14
3	"L6"	1	-12
4	"L5"	2	-10
5	"L4"	2	-8
6	"L3"	3	-6
7	"L2"	3	-4
8	"L1"	5	-2
9	"CL"	6	0
10	"R1"	5	2
11	"R2"	3	4
12	"R3"	3	6
13	"R4"	2	8
14	"R5"	2	10
15	"R6"	1	12
16	"R7"	2	14
17	"R8"	1	16
18	"R9"	1	18
19	"L1"*	7	-2
20	"CL"*	7	0
21	"R1"*	7	2

$StrandLayout\_Mid\_Ver\_AsD^{\langle 1 \rangle} := (PS\_Layout\_Ver^{\langle 1 \rangle}) - (AsD\_PS\_Mid\_Layout\_Ver^{\langle 1 \rangle})$

	0
0	0
1	1
2	1
3	2
4	2
5	2
6	2
7	2
8	3
9	2
10	3
11	2
12	2
13	2
14	2
15	2
16	1
17	1
18	0
19	0
20	0
21	0

STEP 5.3: AS-DESIGNED PRESTRESSING STRAND LAYOUT AT BEAM END

The number of prestressing strands in the as-designed beam section is defined with respect to the default layout presented in the "Default Prestressing Strand Layout" section. The following example demonstrates the procedure for defining prestressing strand layout for an as-designed beam end section.

<u>Example 1</u>: The following figure shows a 36 × 49 in. bulb-tee beam end section

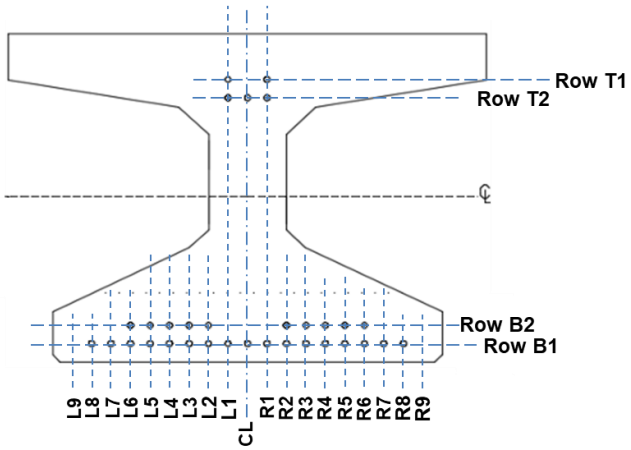

Table 3. Number of Strands to be Removed from Each Row to Define the As-Designed Beam End Layout

Row no. (a)	No. of strands in the default layout (b)	No. of strands absent from the default layout (c)	No. of strands to be removed from the default layout (d) = (c)	No. of strands in the as-designed section (e) = (b) – (d)
B1	17	0	0	17
B2	19	9	9	10
B3	15	15	15	0
B4	11	11	11	0
B5	7	7	7	0
B6	3	3	3	0
B7	3	3	3	0
B8	3	3	3	0
T1	3	1	1	2
T2	3	0	0	3
T3	3	3	3	0
T4	3	3	3	0
T5	3	3	3	0
T6	3	3	3	0
T7	3	3	3	0

Table 4. Number of Strands to be Removed from Each Column to Define the As-Designed Beam End Layout

Column no. (a)	No. of strands in the default layout (b)	No. of strands absent from the default layout (c)	No. of strands to be removed from the default layout (d) = (c)	No. of strands in the as-designed section (e) = (b) – (d)
L9	1	1	1	0
L8	2	1	1	1

Column no. (a)	No. of strands in the default layout (b)	No. of strands absent from the default layout (c)	No. of strands to be removed from the default layout (d) = (c)	No. of strands in the as-designed section (e) = (b) – (d)
L7	3	2	2	1
L6	3	1	1	2
L5	4	2	2	2
L4	4	2	2	2
L3	5	3	3	2
L2	5	3	3	2
L1	8	7	7	1
CL	8	7	7	1
R1	8	7	7	1
R2	5	3	3	2
R3	5	3	3	2
R4	4	2	2	2
R5	4	2	2	2
R6	3	1	1	2
R7	3	2	2	1
R8	2	1	1	1
R9	1	1	1	0
L1*	7	5	5	2
CL*	7	6	6	1
R1*	7	5	5	2

As shown below, complete Column 1 of "AsD_PS_End_Layout_Hor" table using the numbers in column (d) of Table 3. The table "StrandLayout_End_Hor_AsD" represent the as-designed strand layout at the end.

AsD_PS_End_Layout_Hor :=

	0	1	2
0	"Row B1"	0	2
1	"Row B2"	9	4
2	"Row B3"	15	6
3	"Row B4"	11	8
4	"Row B5"	7	10
5	"Row B6"	3	12
6	"Row B7"	3	14
7	"Row B8"	3	16
8	"Row T1"	1	3
9	"Row T2"	0	5
10	"Row T3"	3	7
11	"Row T4"	3	9
12	"Row T5"	3	11
13	"Row T6"	3	13
14	"Row T7"	3	15

$StrandLayout\_End\_Hor\_AsD^{\langle 1 \rangle} := \left(PS\_Layout\_Hor^{\langle 1 \rangle}\right) - \left(AsD\_PS\_End\_Layout\_Hor^{\langle 1 \rangle}\right)$

	0
0	17
1	10
2	0
3	0
4	0
5	0
6	0
7	0
8	2
9	3
10	0
11	0
12	0
13	0
14	0

As shown below complete Column 1 of "AsD_PS_End_Layout_Ver" table using the numbers in column (d) of Table 4. The table "StrandLayout_End_Ver_AsD" represents the as-designed strand layout at the end.

AsD_PS_End_Layout_Ver :=

	0	1	2
0	"L9"	1	-18
1	"L8"	1	-16
2	"L7"	2	-14
3	"L6"	1	-12
4	"L5"	2	-10
5	"L4"	2	-8
6	"L3"	3	-6
7	"L2"	3	-4
8	"L1"	7	-2
9	"CL"	7	0
10	"R1"	7	2
11	"R2"	3	4
12	"R3"	3	6
13	"R4"	2	8
14	"R5"	2	10
15	"R6"	1	12
16	"R7"	2	14
17	"R8"	1	16
18	"R9"	1	18
19	"L1""	5	-2
20	"CL""	6	0
21	"R1""	5	2

$StrandLayout\_End\_Ver\_AsD^{\langle 1 \rangle} := \left(PS\_Layout\_Ver^{\langle 1 \rangle}\right) - \left(AsD\_PS\_End\_Layout\_Ver^{\langle 1 \rangle}\right)$

	0
0	0
1	1
2	1
3	2
4	2
5	2
6	2
7	2
8	1
9	1
10	1
11	2
12	2
13	2
14	2
15	2
16	1
17	1
18	0
19	2
20	1
21	2

STEP 5.4: ELIMINATION OF DAMAGED STRANDS FROM THE DEFAULT BEAM END LAYOUT

Follow a similar process as described in Step 5.3 to remove damaged strands from the default layout.

Fill Column 1 of the table "D_PS_End_Layout_Hor" with the number of strands to be removed from each row (Row B1 to Row T7) representing the number of strands absent from the default layout.

Fill Column 1 of the table "D_PS_End_Layout_Ver" with the number of strands to be removed from each row (L9 to R1) representing the number of strands absent from the default layout.*

Step 6: LOAD AND MOMENT DEMAND

The user need to provide factored moment at midspan and factored moment, shear and axial force at the critical section for shear.

The effective shear depth, dv, at the critical section for shear is calculated in Step 9. The location of the critical section for shear is located at a d_V distance from the face of support on the span side.

Step 7: M_n and d_v AT MIDSPAN

The necessary steps for calculating nominal flexural strength, M_n, and the effective shear depth, d_v, at midspan are presented.

The user is NOT required to make any changes to the calculations presented in this section.

Step 8: Forces and Stresses IN Harped Strands

This step is used when harped strands are available.

The user is NOT required to make any changes to the calculations presented in this section.

Step 9: d_v AT the Critical Section for Shear

The necessary steps for calculating d_v at the critical section for shear are presented.

The user is NOT required to make any changes to the calculations presented in this section.

Step 10: Nominal Shear RESISTANCE – Sectional Design Model

The necessary steps for calculating V_n at the critical section for shear are presented.

The user is NOT required to make any changes to the calculations presented in this section.

Step 11: Nominal Shear RESISTANCE on Minimum Longitudinal Reinforcement Requirement

The necessary steps are presented.

The user is NOT required to make any changes to the calculations presented in this section.

Step 12: Shear RESISTANCE – Sectional Design Model

The necessary steps are presented.

The user is NOT required to make any changes to the calculations presented in this section.

Step 13: Nominal Shear RESISTANCE - Strut-And-Tie Method

STEP 13.1: STM FOR AS-DESIGNED SHEAR RESISTANCE WITH HARPED STRANDS

The necessary steps are presented.

The user is NOT required to make any changes to the calculations presented in this section.

Step 14: 3D STM for Transverse Tie Force

Enter the value of "i" to decide the number of bonded strands (n_f) in one side of the bottom flange outer portions of the web.

Similarly, enter the value of "i" to calculate the horizontal distance from the beam centerline to centroid of the number of bonded strands.

Example 1: The following figure shows the strand arrangement in a 36 × 49 in. bulb-tee beam end section.

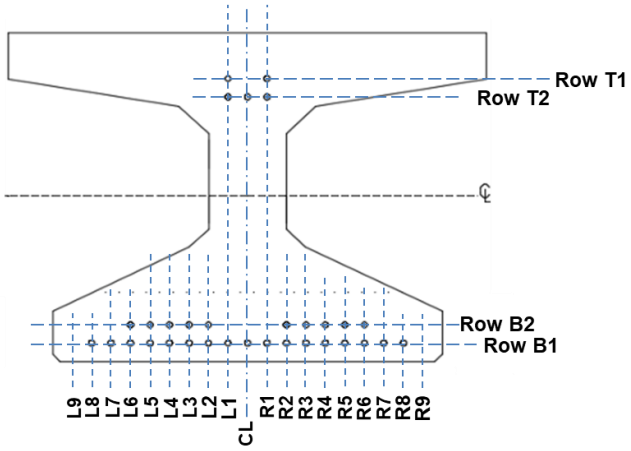

For example, R2 to R9 represent the prestressing strands in the right-side outer portion of the web. As shown below, the tables in Mathcad calculation sheet lists the row numbers corresponding each label and the number of strands. For example, "R2" is listed in row 11 with 2 strands. Similarly, "R9" is listed in row 18 with 0 strands.

StrandLayout_End_Ver_AsD⟨1⟩ :=

	0
0	0
1	1
2	1
3	2
4	2
5	2
6	2
7	2
8	1
9	1
10	1
11	2
12	2
13	2
14	2
15	2
16	1
17	1
18	0
19	2
20	1
21	2

	0
0	"L9"
1	"L8"
2	"L7"
3	"L6"
4	"L5"
5	"L4"
6	"L3"
7	"L2"
8	"L1"
9	"CL"
10	"R1"
11	"R2"
12	"R3"
13	"R4"
14	"R5"
15	"R6"
16	"R7"
17	"R8"
18	"R9"
19	"L1*"
20	"CL*"
21	"R1*"

To count the number of bonded strands in the right-side outer portion of the web, the user need enter 11 and 18 for the range, as shown below.

$$n_f := \sum_{i=11}^{18} \left(StrandLayout\_End\_Ver\_AsD_{i,1}\right) = 12$$

Number of bonded strands in one side of the bottom flange outer portions of the web

Similarly, the user need to enter11 and 18 for the range to calculate the horizontal distance from beam centerline to the centroid of the bonded strands in the right-side outer portion of the web.

$$x_p := \frac{\sum_{i=11}^{18} \left[StrandLayout\_End\_Ver\_AsD_{i,1} \cdot \left(AsD\_PS\_End\_Layout\_Ver_{i,2}\right)\right]}{n_f} \cdot in = 9.17\,in$$

Horizontal distance from the beam centerline to the centroid of the bonded strands in the selected bottom flange outer portion of web.

The vertical distance from beam soffit to the centroid of the bonded strands in the selected bottom flange outer portion of web need to be calculated.

As shown below, enter the number of bonded strands in each layer located in the selected bottom flange outer portion of web and the vertical distance from beam soffit to the centroid of each strand layer.

$$y_p := \frac{StrandArea \cdot [(7 \cdot 2) + (5 \cdot 4) + (0 \cdot 6) + (0 \cdot 8) + (0 \cdot 10)]in}{StrandArea \cdot n_f} = 2.83\,in$$

Vertical distance from beam soffit to the centroid of the bonded strands in the selected bottom flange outer portion of web.

As shown in Step 5, the default strand layout has five rows of strands in the bottom flange outer portion of the web, labeled as Row B1 to Row B5. However, the as-designed details of the 36 × 49 in. bulb-tee beam end section used in this example include bonded strands only in Row B1 and Row B2. The bottom flange outer portion of the web includes 5 bonded strands in Row B1 and 5 strands in Row B2. The vertical distance from beam soffit to the centerline of Row 1 is 2 in. The vertical distance between each row is 2 in., too. Hence, the following numbers are included in the above calculation.

$$(7 \cdot 2) + (5 \cdot 4) + (0 \cdot 6) + (0 \cdot 8) + (0 \cdot 10)$$

Input height of the bulb (h_b).

$$h_b := 12.5in$$

Height of the bulb

Input an average cross-section area of a stirrup and average spacing for the stirrups located within L_{t_force}.

$$L_{t\_force} := \left(\frac{h_c}{4}\right) + l_b = 19.75\,in$$

Beam length with transverse steel resisting the tie force

$$A_{st} := 0.11in^2$$

$$Spacing := 3in$$

Step 15: Shear RESISTANCE – STM

The necessary steps are presented.

The user is NOT required to make any changes to the calculations presented in this section.

Step 16: Load Rating

NOMINAL SHEAR RESISTANCE

User defines the n*ominal shear resistance of the damaged/repaired section.*

DEAD AND OTHER LOADS

User defines the shear due to dead and permanent loads.

- *total unfactored dead load shear acting on the noncomposite section, V_{dnc} (i.e. beam self-weight, diaphragm weight, slab weight, and haunch weight).*
- *total unfactored dead load shear acting on the composite section, V_{dc} (i.e. barrier weight) and M_{DW} (i.e. unfactored dead load moment due to wearing surface and utilities).*
- *unfactored shear due to permanent loads other than dead loads, V_P.*
- *unfactored shear due to secondary prestress forces, V_S.*

LIVE LOADS

User defines,

- *live load distribution factor for shear (LFR method), DF_{L_LFR}*
- *live load distribution factor for shear (LRFR method), DF_{L_LRFR}*
- *shear due to HS 20 truck, V_{LL_HS20}*

- *shear due to HL 93load, V_{LL_HL93}*
- *shear due to Michigan Operating Truck Loads: one-unit truck (V_{LL_M1}), two-unit truck (V_{LL_M2}), and three-unit truck (V_{LL_M3})*
- *shear due to permit loads, V_{LL_permit}.*

LOAD AND IMPACT FACTORS

User defines,

- *the LRFD load factor for wearing surface and utilities for strength I and II limit states ($\gamma_{DW\_strength}$).*
- *live load factor for strength I limit state for MI legal loads, $\gamma_{LL\_strengthI\_MIoper}$*
- *live load factor for strength II limit state for permit loads, $\gamma_{.LL\_strengthII\_permit}$*
- *length of beam between bearing centerlines, Beam_span*
- *dynamic load allowance (LRFR) for permit loads, IM_LRFR_permit.*

PRESTRESSED CONCRETE I-BEAM CROSS-SECTIONS WITH STRAND DETAILS

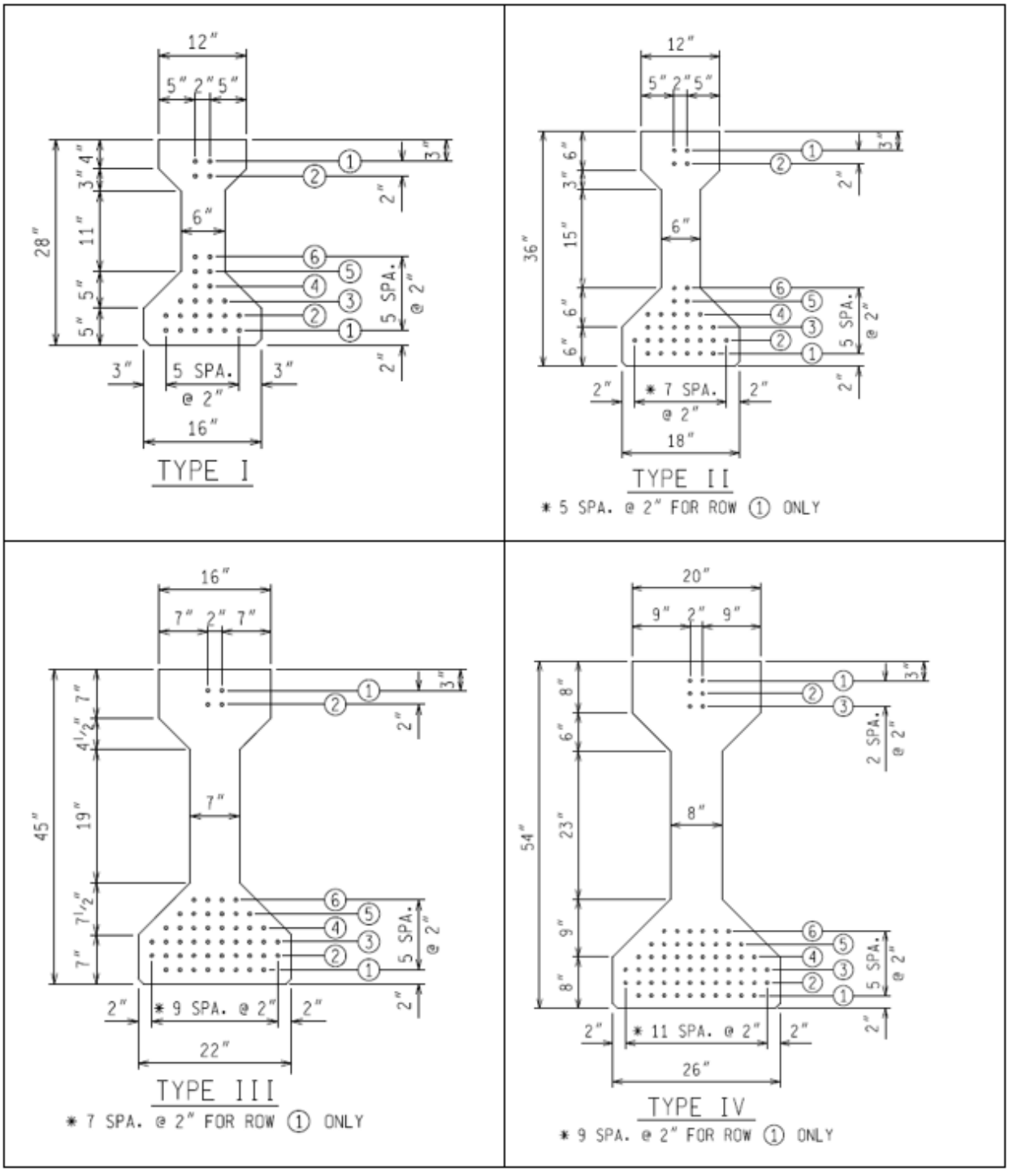

BEAM PROPERTIES					
TYPE	WEIGHT lbs/ft	AREA in^2	S_T in^3	S_B in^3	I in^4
I	288	276	1475	1805	22,800
II	384	369	2530	3220	51,000
III	583	560	5070	6190	125,000
IV	822	789	8910	10,550	261,000

BDG 6.60.01

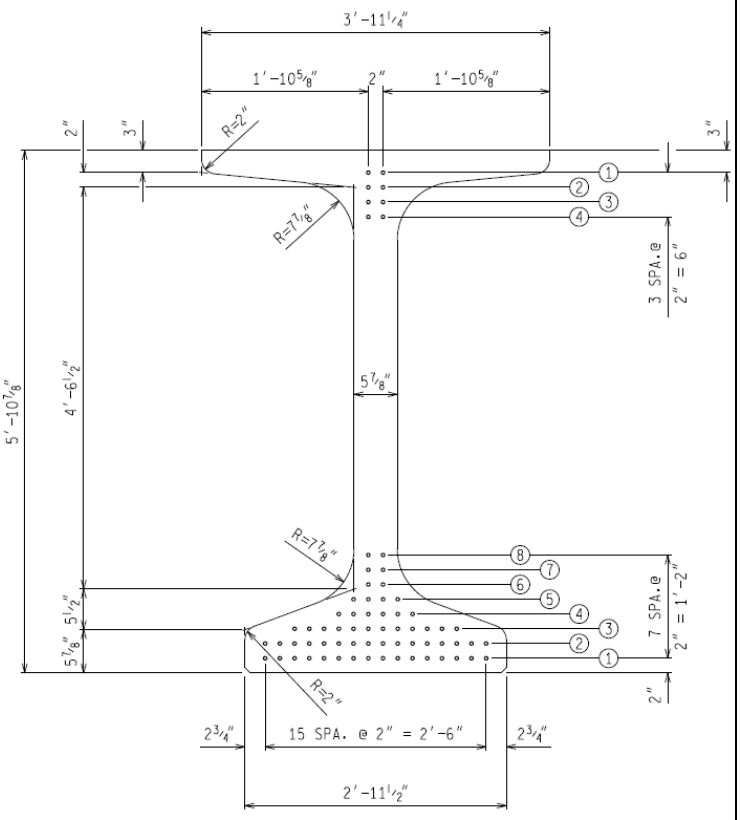

MICHIGAN 1800 GIRDER

BEAM PROPERTIES				
WEIGHT lbs/ft	AREA in^2	S_T in^3	S_B in^3	I in^4
910	875	16,600	18,800	624,700

BDG 6.60.02

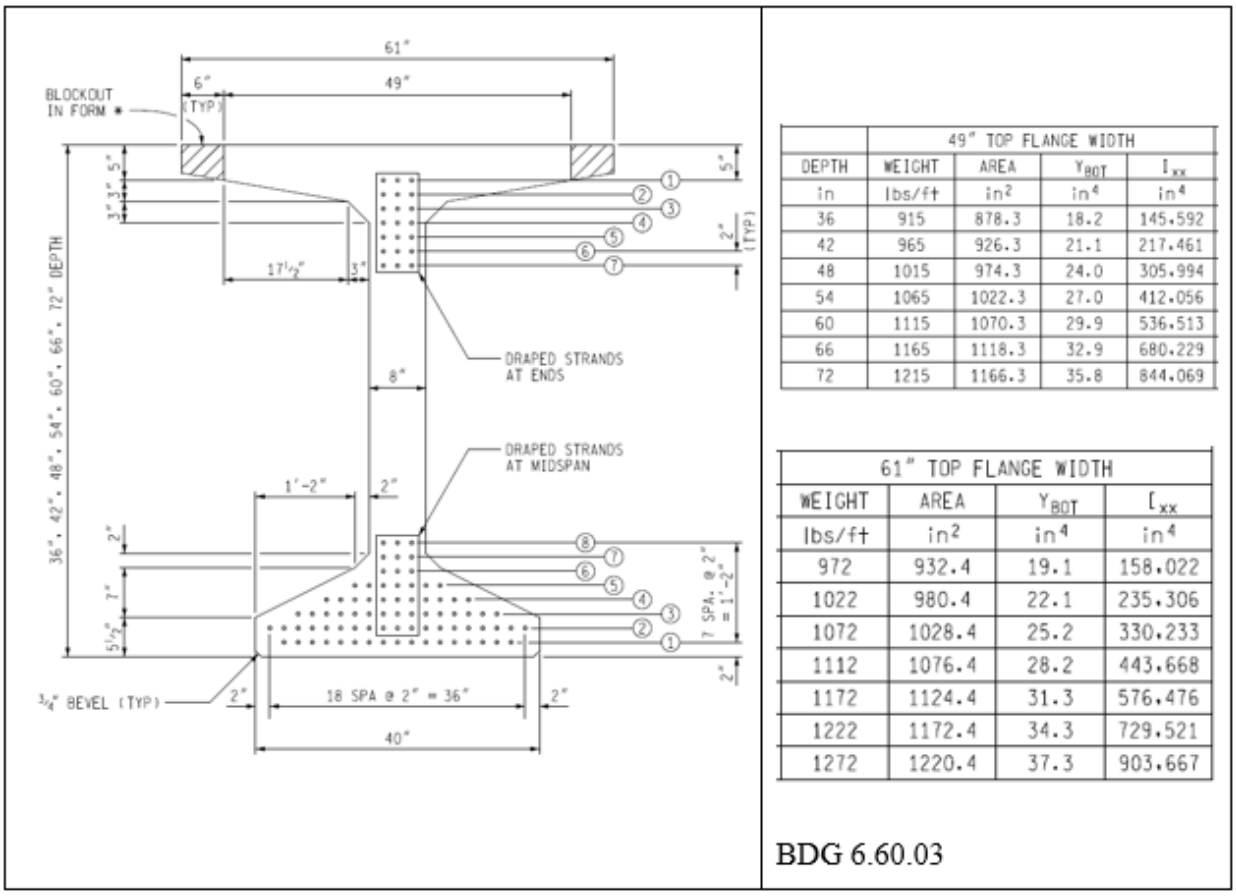

	49" TOP FLANGE WIDTH			
DEPTH	WEIGHT	AREA	Y_{BOT}	I_{xx}
in	lbs/ft	in^2	in^4	in^4
36	915	878.3	18.2	145,592
42	965	926.3	21.1	217,461
48	1015	974.3	24.0	305,994
54	1065	1022.3	27.0	412,056
60	1115	1070.3	29.9	536,513
66	1165	1118.3	32.9	680,229
72	1215	1166.3	35.8	844,069

61" TOP FLANGE WIDTH			
WEIGHT	AREA	Y_{BOT}	I_{xx}
lbs/ft	in^2	in^4	in^4
972	932.4	19.1	158,022
1022	980.4	22.1	235,306
1072	1028.4	25.2	330,233
1112	1076.4	28.2	443,668
1172	1124.4	31.3	576,476
1222	1172.4	34.3	729,521
1272	1220.4	37.3	903,667

BDG 6.60.03

The following figure shows the typical length of beam endblock.

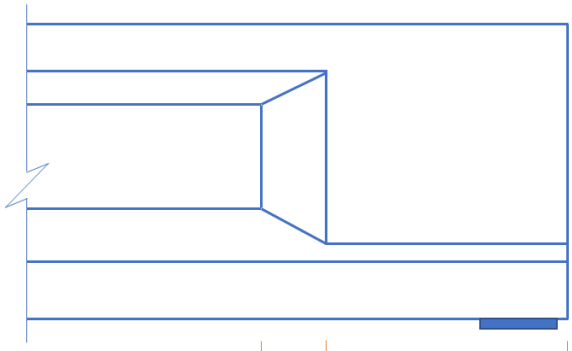

Type I or II:	6″	2′-0″ min.
Type III:	9″	3′-6″ min.
Type IV:	1′-0″	4′-6″ min.

Appendix F: Construction of full-depth overcast repair

F.1 OVERVIEW

The construction process of full-depth reinforced concrete overcasts at PSC I-beam ends is described. The bridge (STR 3805) that carries I-96 WB over Washington Avenue Road has three spans and is located in Ingham County, Michigan (Figure F-1). The bridge has a width of 46.58 ft and a total length of 107.92 ft. The bridge was built in 1962. Each span has seven AASHTO Type beams. The tail span fascia beams and all beams in span 2w are 36 in. deep. The interior beams along both tail spans are 28 in. deep.

(a) Aerial view of the bridge (b) South elevation

Figure F-1. I-96 WB bridge over Washington Avenue (a) aerial view and (b) south elevation.

The regular BSIR inspections of the bridge recorded the following condition ratings of the beams (item SIA-59): in 2000 and 2002, the bridge received a rating of 6 (fair); in 2004, the rating declined to 5 (fair). In 2006, following the diaphragm repair, the rating improved back to 6 (fair). The beams consistently received a rating of 6 until 2014, when it dropped to 5 (fair), and it was recommended that short temporary supports be provided. The inspection conducted on 08/12/2018—after 56 years in service— beams received a BSIR condition rating of 4 (poor) due to the following reasons:

- Beam ends over piers have cracks, spalls, and spalls with exposed steel.
- Short height temporary supports at: beams 1s-6s in span 1w at pier 1w; beams 1s, 4s, and 5s in span 2w at pier 1w; beam 1s in span 2w at pier 2w; beam 4s in span 3w at pier 2w.
- High load hit spalls along beams 6s and 7s in span 2w
- Few diaphragms with minor spalls and delaminated areas.

A scoping report was submitted on 06/12/2018 for this bridge. The report recommended a deep concrete overlay on the deck surface, PSC beam end repair, including temporary

supports, and cleaning and coating of sole plates. The JN 204942 - 08-29-2022 letting documents specified full-depth reinforced concrete overcasts for all the beam ends at pier 1w and 2w. Beam end overcast elevation and cross-section details are shown in Figure F-2 and Figure F-3, respectively. The repair plan also included deck patching, railing patching, expansion joint replacement, deep concrete overlay, removal and replacement of slope paving, application of concrete surface coating, and substructure patching.

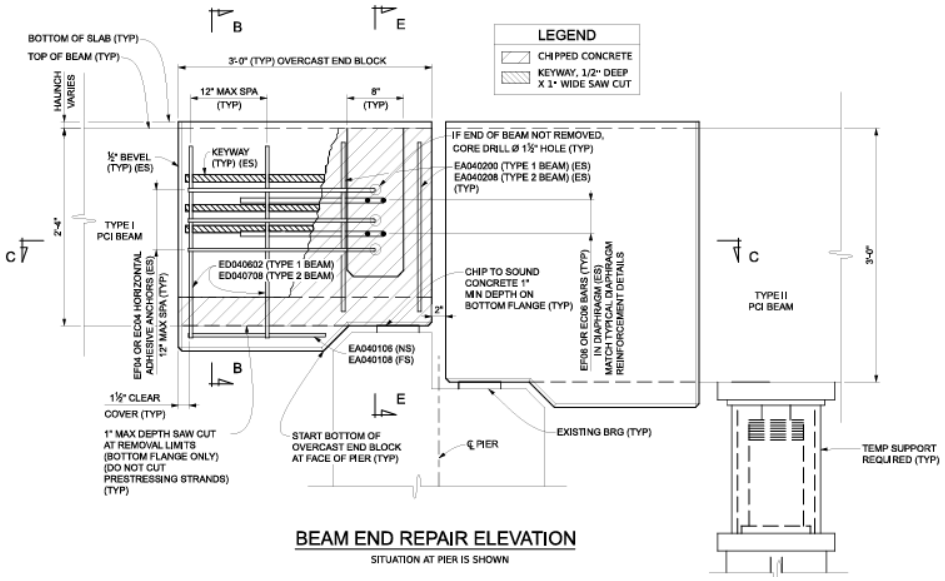

Figure F-2. Beam end elevation showing overcast details.

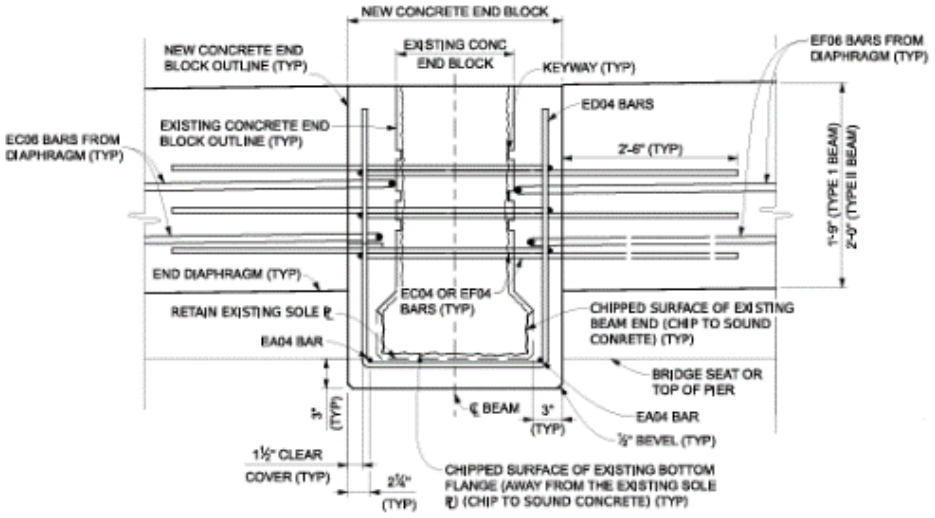

Figure F-3. Section B-B showing overcast details.

F.2 CONSTRUCTION PROCEDURE

F.2.1 Erection of Temporary Supports

The construction of a full-depth reinforced beam end overcast begins with the installation of temporary supports for the beam ends and working platforms to provide access to perform repair activities. Proper soil base preparation for a temporary support column is crucial to ensure stability and prevent the column from settling or tilting during construction. Moreover, a well-prepared soil base helps protect the existing roadway from damage. Figure F-4 shows the elevation details of a temporary support.

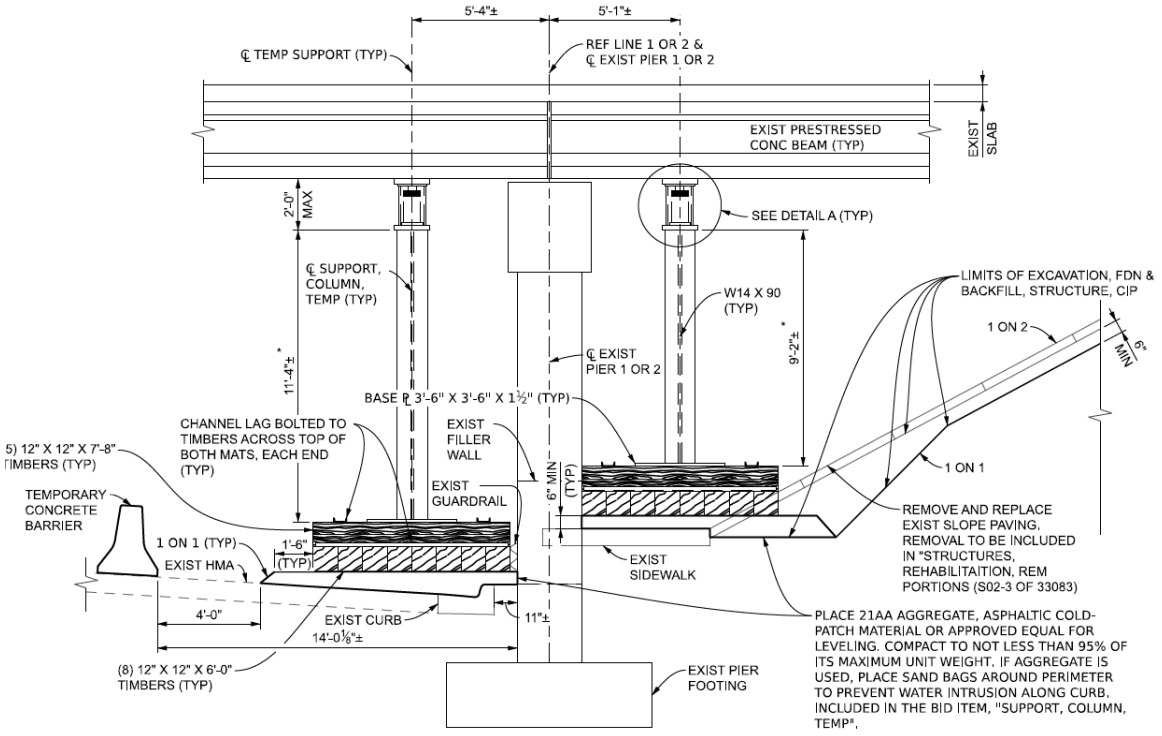

Figure F-4. Details of temporary supports at a pier.

Figure F-5 shows the preparation of a soil base over the road surface and the placement of a temporary support column. The temporary support installation process includes checking column alignment, welding base plates, and connecting multiple support columns to ensure structural stability, as shown in Figure F-6. After erecting the temporary support frame, a working platform is mounted to provide safe and efficient access for subsequent repair operations (Figure F-7).

(a) Soil base preparation

(b) Completed base support

Figure F-5. Preparing a temporary support base over the road surface.

(a) Column alignment check

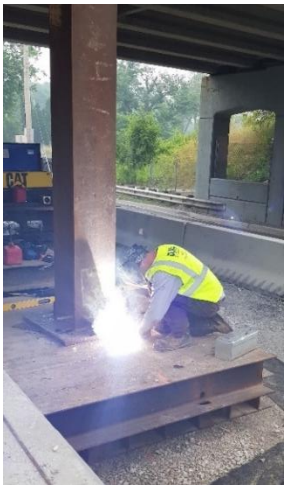

(b) Column base welding

(c) Framing up the support using horizontal members

Figure F-6. Erection of a temporary support.

Figure F-7. Temporary support system with a working platform.

F.2.2 Jacking and Lifting of Beam Ends

Figure F-8 illustrates the jacking and lifting process used to elevate PSC I-beam ends for repair. The detailed setup, including the hydraulic jack, base plate, shims, and the jack bearing plate, is shown in Figure F-8(a). As shown in Figure F-8(b), a manual hydraulic jack is placed on a steel support column to gradually lift a beam end. The beam end is carefully lifted approximately 1/4 in. to relieve the bearing pressure and allow for repair access. After reaching the desired elevation, steel shims are inserted to maintain the lifted position of the beam end, as shown in Figure F-8(c). Figure F-8(d) presents the beam end in its elevated state, clearly showing the gap created by this lifting operation.

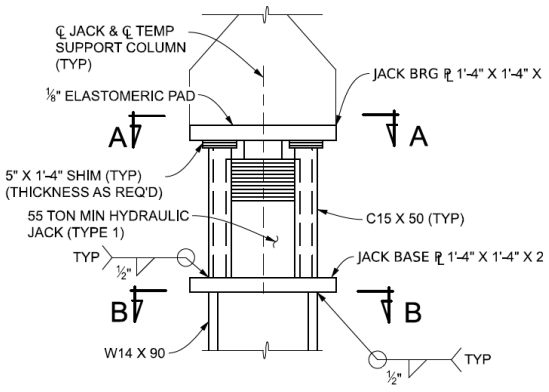

(a) Jacking details

(b) Hydraulic jack

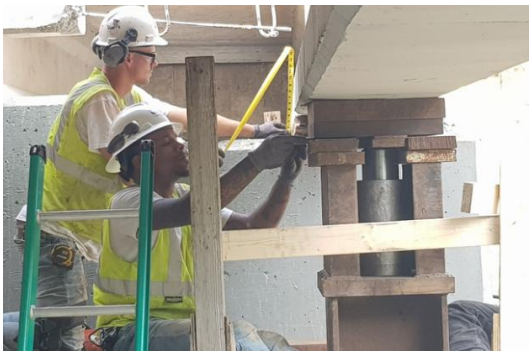

(c) Placing steel shims and measuring elevation

(d) The gap at the lifted beam end

Figure F-8. Jacking and lifting of beam ends.

F.2.3 Chipping and Cleaning of Beam Ends

Once the beam ends are lifted, the repair process begins with the removal of the concrete deck section over the beam end, as shown in Figure F-9. The deck rebar is preserved and not cut during this process to allow for proper integration during subsequent deck repairs. Removal of the deck section is necessary to expose the underlying structural components for access to repair.

(a) (b)

Figure F-9. Exposed beam ends after the removal of the deck at the expansion joint.

Beam end diaphragms are removed using a jackhammer following the deck removal to provide adequate access to the beam end, as shown in Figure F-10. At locations where adjacent beam ends are not repaired, only half of the diaphragm is removed to maintain structural continuity.

Figure F-10. Removal of an end diaphragm using a jackhammer.

Following the removal of end diaphragms, beam ends are carefully chipped out and cleaned to expose sound concrete and steel (Figure F-11). The entire beam end region designated for overcasting is chipped out, including areas with sound concrete to enhance bonding between the overcast and the beam end (Figure F-11c).

(a) Saw cutting

(b) Saw cut showing the section to be chipped out and cleaned

(c) Chipped out and cleaned beam ends

Figure F-11. Beam ends prepared for overcasting.

As shown in Figure F-3, three horizontal rebars are placed through the holes drilled at the beam ends and connected to the rebar cages prepared for the diaphragms. Figure F-12 shows the drilling of holes across the beam webs at the ends for three adhesive anchor rebars. According to the repair details, a 1.5-inch diameter drill is used for this purpose.

Figure F-12. Drilling holes at the beam end for adhesive anchors.

The existing rebars exposed during beam end preparation are thoroughly cleaned and embedded into the overcasts without the application of any coatings or corrosion protection measures. Additional epoxy-coated reinforcements are included at the beam ends to support the full-depth overcast repair. The completed reinforcement arrangement is shown in Figure F-13.

Figure F-13. Beam ends prepared for overcasts with additional reinforcement.

F.2.4 Formwork and Overcasting

Figure F-14 shows the formwork setup for full-depth overcasts and end diaphragms. The overcast and end diaphragm are cast monolithically to ensure structural continuity and durability. Latex Modified Concrete (LMC), mixture type C-L, is used as the repair material when the repair depth exceeds 1.5 inches, as shown in Figure F-15. Table 703-1 of the MDOT Construction Manual provides the mix proportions for LMC mixes. The concrete mix used in the specific bridges discussed in this document is highlighted.

The concrete is mixed on-site using a mobile volumetric concrete mixer truck, as shown in Figure F-16(a). Concrete field tests are conducted during the placement of LMC at the beam ends. Fresh concrete properties are recorded, as shown in Figure F-16(b), including slump, air temperature, concrete temperature, and air content. For example, the report includes a slump of 5 inches, an air temperature of 72°F, a concrete temperature of 79°F, and an air content of 5.9%. These field test results confirm that the delivered concrete meets the specified performance requirements for the beam end overcast repair, as outlined in the MDOT Construction Manual, Table 703-1.

Figure F-14. Formwork for an interior beam end overcast with an end diaphragm.

Table 703-1
Structures Patching Mixtures

Depth of Patch in	Aggregate Required	Mixture Type (g)	Mixture Proportions per cyd, dry weight					Air Content %
			Cement lb	Net Water (approx) lb	Latex Admixture lb (gal)	Fine Aggregate lb	Coarse Aggregate lb	
<1.5	2NS	F-L	752 (c)	(b)	235 (28.0)	2,450	N/A	6.0 ±2.0
1.5 – 4	2NS & 26A	M	799	358 (a)	N/A	1,260	1,260	7.5 ±1.5
≥1.5	2NS & 26A (d)	C-L	658 (c)	169 (b)	143 (17.0)	1,348 (e)	1,458 (e)	4.5 ±1.5
		C-L-HE	846 (c)	(b)	228 (27.0)	1,308 (e)	1,416 (e)	4.5 ±1.5
>4 (f)	2NS & 6AA	C	705	315 (a)	N/A	1,220	1,530	6.5 ±1.5
		C-HE	846	300 (a)	N/A	1,220	1,590	5.5 ±1.5

a. Control water to provide a stiff, workable mixture with 1 in to 2 in slump. During hot and windy weather, the Contractor may increase slump to 3 in to 4 in, as determined by the Engineer.
b. Add water, in addition to water in the latex admixture, to control slump to within 3 in to 5 in. Measure slump from 4 min to 5 min after discharge from the mixer. During this waiting period, deposit concrete on the deck and do not disturb. If placing mixtures on sections within super-elevated curves, the Contractor may need to use the lower allowable range of the slump requirement, as determined by the Engineer. Do not exceed water-cement ratio, by weight, of 0.30 including water contained in the latex emulsion.
c. Use only Type I cement in these mixtures.
d. Ensure the 26A absorption does not exceed 2.5%, in accordance with ASTM C 127.
e. The aggregate proportions are approximate; due to gradation changes, the Engineer may make adjustments. The Contractor may increase the fine aggregate quantity by no greater than 5% by weight of total aggregate if reducing coarse aggregate by an equivalent volume.
f. Substructure repairs.
g. F, M, and C indicate fine, medium, and coarse: L indicates latex modified; HE indicates high-early strength. Type F mixtures are mortars.

Figure F-15. Concrete mix proportions for patching.

(a) Mobile volumetric concrete mixer

CONCRETE FIELD TEST REPORT

CLIENT: Davis construction & Rohrscheib

D&A PROJECT NO.: 2340089.4A

DATE: 07/09/2024

PROJECT: I-96 over M-99, Washington St, Billwood Hwy & Grand River

INSPECTOR: Levi Jackson

CONTRACTOR: Davis Construction

CONTROL SECTION/MDOT JOB NO.: 33083 / 204907

CONCRETE SUPPLIER & CITY: Davis Construction / Lansing

PROJECT ENGINEER: Jim Stankiewicz - AECOM

WEATHER: Cloudy 72°F

TIME ARRIVED: 8:15am

SCHEDULED ARRIVAL TIME: 9:00 am

A.M. / P.M.

TIME LEFT SITE: 11:30am

AGGREGATE CORRECTION FACTOR: —

Pour Description: I-96 W over S Washington Ave Beam ends for bridge over S Washington Ave.

Mix Design: Latex6-L Quantity Placed (yd³): — Lot Number: — Sublot: —

Grade of Concrete: C-L Batch Quantity (yd³): Pour Start: 9:30 Pour End:

FIELD TEST RESULTS

Truck No.	Ticket #	Batch Time	Start	Empty	Slump (in)	Air Temp. (°F)	Conc. Temp. (°F)	Air Content (%)	Unit Wt. (pcf)	Yield	No. of Cylinders
410		9:30	9:30		5	72°	79°	5.9	—	—	4

(b) Concrete field test report

Figure F-16. Preparation of LMC mix in the field.

Once the formwork is in place, concrete is poured at the beam ends, as shown in Figure F-17(a). Vibrators are used during placement, as depicted in Figure F-17(b), to ensure proper consolidation and elimination of air pockets. This process is critical in achieving a high-quality repair with strong bonding to the existing beam and diaphragm surfaces.

(a) Pouring concrete

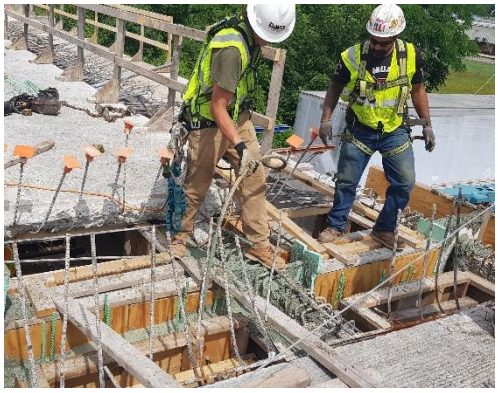

(b) Consolidation of concrete using a porker vibrator

Figure F-17. Pouring concrete over beam ends.

After concrete placement, the repaired area is immediately covered to ensure proper curing conditions, as shown in Figure F-18. Plastic sheeting is used to retain moisture and protect the freshly placed latex-modified concrete from direct sunlight, wind, and potential contamination. At the end of curing the formwork is removed. A properly completed job is expected deliver a smooth and well-integrated repair at the beam end, as illustrated in Figure F-19. The completed repair is expected to exhibit good quality, with no signs of initial cracking or distress, indicating proper bonding between the new overcast and the existing concrete surfaces.

Figure F-18. Covering the concrete after placement.

Figure F-19. Repaired beam ends after removing formwork.

F.3 TYPICAL OBSERVATIONS

The repair plan recommends removing only unsound concrete and limiting the chipping depth to 1 in., along with forming three shear keyways in sound concrete, as illustrated in Figure F-20(a). However, field observations revealed that the entire beam end region designated for overcasting is chipped out, including areas with sound concrete, as shown in Figure F-20(b). This excessive chipping resulted in the unintended exposure of additional prestressing strands in the beam soffit and some strands on the sides of the bottom flange. Consequently, a portion of the prestressing force is lost, and the capacity of the beam end is reduced.

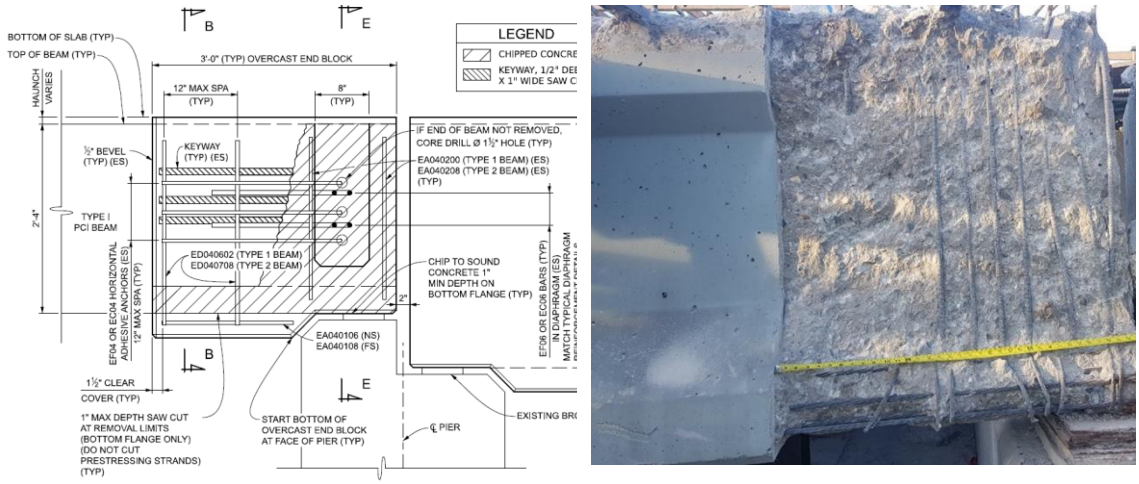

(a) Beam end repair details (b) Chipped out and cleaned area

Figure F-20. Chipped out and cleaned more area than recommended in the repair details.

Figure F-21 shows significant corrosion on the existing reinforcement at the beam end before concrete placement. Although the exposed rebar is cleaned after chipping, corrosion develops due to the delay of several weeks between cleaning and the start of concrete casting. Corrosion on existing reinforcement is a concern, as it compromises bond strength and accelerates future deterioration. This concern can be addressed by applying a protective coating to the exposed steel immediately after cleaning and before pouring concrete.

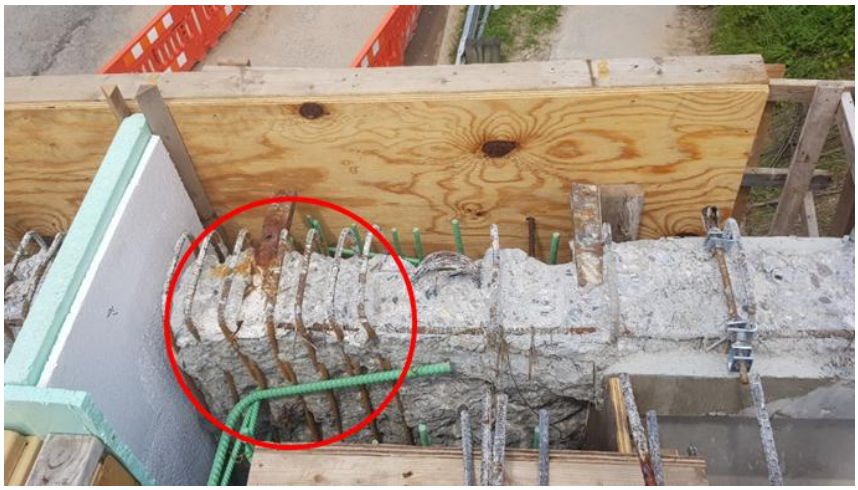

Figure F-21. Corrosion was observed on the existing reinforcement before pouring concrete.

Figure F-22 shows an inconsistency in the gap between adjacent beam ends observed during the repair process. The beam end repair details require a two-inch gap between the beam ends. However, as shown in Figure F-22 (a), the actual gap at one location is only

one inch, while the gap at another location is two inches, as shown in Figure F-22 (b). Maintaining the specified gap is necessary to allow for adequate spacing to accommodate thermal expansion.

(a) One (1) in. gap

(b) Two (2) in. gap

Figure F-22. Inconsistent spacing between beam ends.

Appendix G: Structured light 3D scanning technology for documenting prestressed concrete beam end conditions

G.1 INTRODUCTION

The degradation of in-service prestressed concrete (PSC) bridges has been a concern. One specific issue that significantly affects PSC bridges is the deterioration of the girders' end sections. This deterioration is mainly caused by the leakage of expansion joints, which allows water, deicing chemicals, and contaminants to penetrate the girder ends. Figure G-1 illustrates typical beam end conditions in PSC I-beam bridges. As a consequence of the deterioration, there is a loss of bearing area, corrosion of prestressed strands and transverse reinforcement, and a reduction in the effective concrete section, all of which negatively impact the load-carrying capacity of the beam.

(a) Spall and corroded bearing (b) Cracking, delamination, and spall (c) Spall behind the bearing

Figure G-1 Typical deteriorations at PSC beam ends.

The evaluation of a bridge's condition starts with biennial inspections. The FHWA Bridge Inspector's Reference Manual (1) stresses the significance of scrutinizing the bearing areas of PSC beams for delamination, spalls, or vertical cracks. Additionally, the inspection should encompass the examination of beam ends and sections above substructure units for transverse cracks on the bottom flange of I-beams and diagonal shear cracks in webs. In the AASHTO Manual for Bridge Element Inspection (2), PSC bridge elements are evaluated using a condition state scale ranging from 1 (good) to 4 (severe). These assessments take into account various factors, such as spalls, delamination, patch areas, exposed rebars, exposed prestressing, cracking, vehicle impact damage, and more. The manual designates spalls as fair when they are not deeper than 1 in., or not greater than 6 in. in diameter. However, it does not provide a quantitative explanation of how these spalls

specifically affect the bearing or shear capacity of the beam. The inspectors have the discretion to decide on condition states.

Currently, the primary approach for assessing deterioration in bridges relies on visual inspection. Inspectors commonly use tools like tape measures, rulers, calipers, and crack gauges to measure the extent of deterioration. However, the accuracy of these on-site measurements heavily depends on the inspector's ability to correctly identify the defects in the deteriorated area. With these traditional tools, inspectors are left with pictures and field notes to re-review the condition when there are ambiguities in the assessment. Therefore, there is a critical need for introducing innovative tools and techniques that can provide quantitative data and assessment of hard-to-reach details with traditional procedures.

In recent years, there has been notable progress in the development of reliable bridge inspection methods through the use of three-dimensional (3D) scanning and point cloud data. By employing 3D scanning technology, point cloud data is generated, representing the scanned objects' surfaces as 3D space coordinates and normal vectors. These methods serve various bridge inspection purposes, such as creating geometric models, measuring displacement and settlement, generating Bridge Information Models (BIM), and identifying surface defects. The application of 3D scanning in bridge engineering has become increasingly common, leading to several recent comprehensive review papers (3-7) in this field. These publications have showcased the widespread use of laser scanners, particularly terrestrial laser scanners, in bridge engineering, proving their effectiveness in various applications. However, the literature also highlights some limitations associated with this technology, including high costs and time-consuming processes. Despite these limitations, the advancements in 3D scanning and point cloud data analysis have shown great promise for enhancing bridge inspection practices.

Alternative 3D scanning techniques can address some of the limitations associated with traditional laser scanning. One such option is photogrammetry, which reconstructs 3D models by using multiple images taken from different angles. While photogrammetry is cost-effective, it typically offers lower accuracy compared to laser scanning. Another viable alternative is structured-light scanning (SLS). The structured light 3D scanners

adopt a striped light pattern with horizontal and vertical bands using an uncalibrated near IR dot, bars, or stripe projector which is captured by two cameras to reconstruct the object. Typically, structured light scanners can capture 20-30 frames per second, which allows to create a handheld device. Structured light scanners consist of a projector that projects a light pattern onto the surface and multiple cameras slightly offset from the projector to capture the shape of the projected light pattern and to calculate the distance of every point in the field of view. Compared to laser scanning, SLS offers several advantages, including enhanced safety, faster scanning speed, higher resolution, and generally lower cost. Despite the advantages of structured-light scanning, there have been relatively few studies reported in the literature regarding its implementation in bridge inspection. Some noteworthy examples include Hain et al. (8), who applied structured-light 3D scanning to create high-resolution representations of locally corroded steel girders. Wang et al. (9) used structured-light cameras to inspect the overall dimensions of precast concrete components. Franceschini et al. (10) utilized a structured-light 3D scanner to evaluate pitting corrosion damage of prestressed strands by extracting pit depth, mass loss, and wire section loss from the 3D scanning data.

SLS systems also have limitations. For instance, the coverage area may be insufficient for scanning larger areas, making it challenging to scan full-size bridges or bridge components. Nevertheless, this limitation is less of a problem when scanning smaller areas as beam ends. Another drawback is that the reconstruction quality of scanned objects can degrade under strong outdoor ambient light due to large amounts of infrared radiation, manually holding the scanner at the same location for prolonged periods to scan a specific area, and the higher post-processing hardware requirement to achieve a considerable result in real-time. One possible solution is to increase the power of the light source of the projector, but this may not always be feasible in outdoor settings, especially with low-cost hand-held projectors that are becoming increasingly popular. Providing proper shade during outdoor work could be an alternative solution, but this can add complications due to site constraints.

This paper presents an overview of structured-light 3D scanning technology and equipment, data collection procedure, post-processing of the data and preliminary results, and lessons learned from a field application. It is anticipated that the conclusions and

observations presented will provide support for the use of structured-light 3D scanning as a tool for bridge engineers to collect inspection data more accurately reflecting the state of the in-service bridges. The data will be crucial for bridge owners and engineers to make more informed decisions regarding the preservation and maintenance of bridges.

G.2 SCANNING TECHNOLOGY, DATA COLLECTION, AND DATA PROCESSING

G.2.1 An Overview of Available Scanners

Many different 3D scanners exist in the current market varying from portable to advanced systems where they have an extensive range of applications. For instance, it can be attempted to compare different perspectives which can be categorized as handheld, aerial, terrestrial, and metrological. Handheld scanners have advantages in portability which are required to have the ability to reach tight spaces and sufficient scanning accuracy (11). Also, handheld scanners should be lightweight; therefore, operators should not get tired of holding the scanner for a longer duration. The post-processing software that comes with the scanner is the most important part of the 3D scanning workflow where it eases the operator's work to generate a high-quality 3D model of the object (12).

The metrological 3D scanners are specialized hardware developed to scan the most demanding use scenarios like quality inspection of parts, and archeological object reconstruction with the highest accuracy corresponding to the reference physical object (13). Most metrological scanners can achieve an accuracy of at least 0.0008 in. (0.02mm) with combined laser and structured or standalone laser technologies. The measurement rates of metrological 3D scanners are significantly faster than any other scanner type according to the specifications. Moreover, in contrast to other 3D scanner types metrological and terrestrial 3D scanners are the most expensive scanner types in the commercial market (14). The terrestrial 3D scanners are a model of 3D scanners which deploy lasers to capture larger areas or objects at longer distances with precision. These scanners are typically mounted on a tripod and are widely used in surveying archeological sites, coastal projectors, and constructions (15). Due to the underlying applications, aerial 3D scanners are particularly used for 3D mapping purposes such as traffic monitoring, landslide activity analysis, and defense and military surveillance purposes (16).

Table G-1 shows the comparison of specifications of various 3D scanners available at present. The accuracy of the laser-type 3D scanners is comparatively higher than structured light-type scanners because the laser triangulation is more precise than pattern-based 3D reconstruction. In addition, handheld scanners are the most affordable 3D scanners with performance matching up to other high-end scanners. Overall, handheld scanners are the best tool that can be employed for structural condition assessment.

Table G-1. Comparison of Available 3D Scanners

Model	Technology	Accuracy, in. (mm)	Measurement Rate, points/s
Handheld			
Shining 3D Einstar	Structured	0.004 (0.102)	980,000
Shining 3D Einscan HX	Structured+ Laser	0.040 (1.016)	480,000
Revopoint pop 2	Structured	0.050 (1.270)	8,000
Metrological			
Creaform Handyscan BLACK Elite	Laser	0.025 (0.635)	1,300,000
Shining 3D FreeScan Combo	Laser +Structured	0.020 (0.508)	1,860,000
Scantech Simscan	Laser	0.020 (0.508)	2,020,000
Terrestrial			
Leica Geosystems Leica BLK360	Laser	4 (101.6)	680,000
Surphaser 100HSX	Laser	0.25 (6.35)	208,000
RIEGL VZ-400i	Laser	5 (127)	500,000
Aerial			
TOPODRONE Lidar HI-RES	Laser	30 (762)	300,000

A 3D structured-light handheld scanner was used in this study. Based on the study requirements and budget, the Shining 3D Einstar® 3D scanner was selected. The scanner is capable of capturing details of deteriorated PSC beam ends. Features like texture-based alignment, availability of IR (Infrared) dot projectors, and portable design preferably a better solution to scan the beams under outdoor conditions without having markers placed on the scanning surface. The RGB (Red, Green, Blue) color camera combines the color to the point clouds and acts as the grayscale viewfinder for the scanner in real-time (16). Figure G-2 shows the components of a Structured Light 3D scanner.

Figure G-2 Structured Light 3D scanner.

G.2.2 Data Collection Procedures

These scanners need a compatible laptop with the scanner manufacturer's software. The software is essential for configuring scanner parameters and saving the scanned data. Before commencing the scanning process, it is necessary to calibrate the scanner. During this calibration, the scanner parameters are recalculated. Following the calibration, a new project with a user-defined file name is created. The scanning parameters are selected based on the site conditions and object size. After configuring the scanner parameters, the scanning process is initiated using the preview option to track the starting location. During scanning, an operator moves the scanner around the object slowly while maintaining a relatively perpendicular orientation to the surface of interest. Tracking problems may arise due to excessive rotation or being out of the scanning distance range. When a track-lost warning occurs, it is necessary to return to the previously scanned area to reestablish the track. The scanner uses structured light to capture the surface geometry and texture of the object. During the scanning process, the laptop displays a live image of the scanned area, enabling the user to verify that the specific object geometry of interest has been successfully captured. The scanner operating system typically includes pause and restart features. If necessary, the scanning process can be paused to allow for a change in the user's position. After completing one side of the bridge beam scanning, the operator checks the

scan data before proceeding to the other side. In case any part of the selected object is incomplete or missing, the scanning operation can be resumed to capture the missing details. However, it's important to note that frequent pauses and restarts increase the size of the data file. Figure G-3 illustrates the basic steps to collect data under field conditions. Once the scanning is complete, it is recommended to save the file by generating point cloud data. However, this particular step can be quite time-consuming, and its duration largely relies on the processing speed of the computer being used. To save time during data collection and to minimize the time spent at the site, scanning operations can be aborted manually without generating a point cloud. The manufacturer's software by default stores the scanned data as a *.asc file. Later, this file can be opened to resume data collection or post-process data to generate the geometry. However, the inspectors need to be careful in handling the aborted data files since there is a possibility of accidentally adding unwanted data to the file.

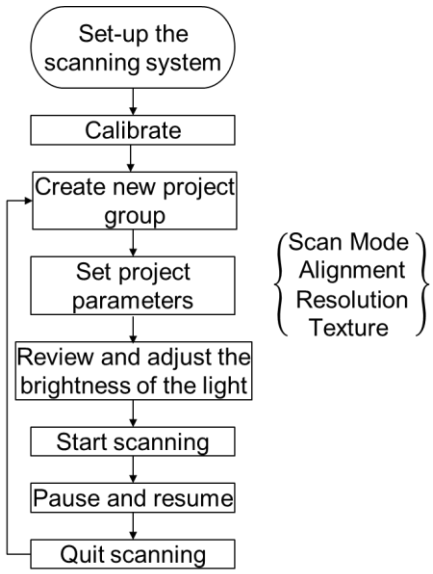

Figure G-3 Process for setting up and operating a scanner for data collection.

For this study, the scan data was collected on several PSC I-beam ends in an in-service bridge. The scanner and the laptop were powered using an inverter connected to the vehicle's battery. A portable power station served as a backup power source for the scanner. Figure G-4 (a) shows the scanning device, laptop, portable power source, and extension cables. Since it was required to connect the laptop placed at the ground level and the handheld scanner, two extension cables, each more than 20 ft long, were used to power the

scanner and establish a connection with the laptop. This setup allowed the operator to move around the beam end to capture the required data. Figure G-4 (b) shows an operator scanning a beam end while standing on a ladder. Figure 4 (c) shows another checking the data for completeness as the beam end is being scanned.

(a) (b) (c)

Figure G-4 (a) Scanner, laptop, and other accessories, (b) scanning a beam end, (c) checking data during scanning.

G.2.3 Post-processing and Analysis

Typically, a scanned dataset contains additional data (noises) from the surrounding surfaces. During post-processing, the dataset is cleaned by removing unwanted data using editing tools in the post-processing software. Figure G-5 shows the scanned image generated after cleaning the data file. The raw file in *.asc format is processed to generate a point cloud for further processing. This step takes at least 20 minutes per beam end and demands significant memory to process. The resulting working model consists of meticulously selected scanned locations specifically focusing on the sides of the beam end.

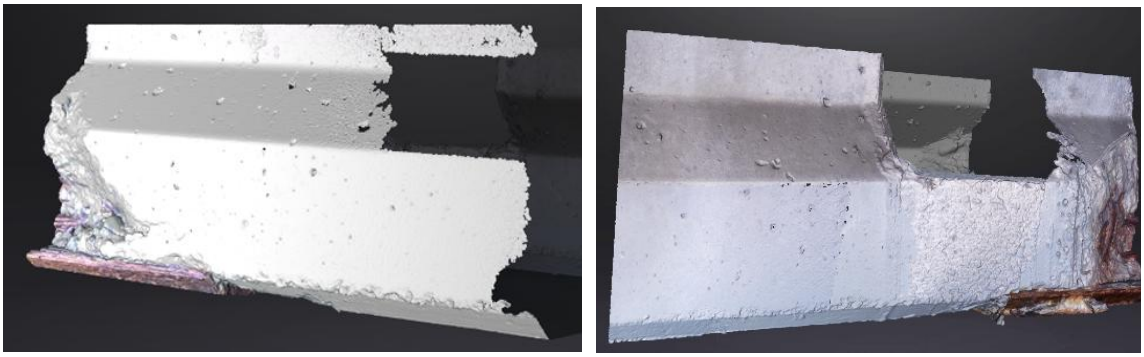

(a) (b)

Figure G-5 Scanned image after cleaning the data file: (a) left side and (b) right side views.

To create a mesh for the model, the "unwater tight" model option is selected. Further editing of the model, such as completing the model by filling in missing data, is possible with mesh editing tools. Subsequently, the model is saved using *.stl and *.asc formats. Before saving the model, alignment adjustments are made to ensure it is suitably positioned in the global coordinate system. Proper alignment significantly reduces post-processing time when using third-party software such as CATIA® (17). These post-processing steps ensure a refined and optimized dataset, leading to manageable file sizes and a model defined in the global coordinate system.

The converted *.stl file was used for further processing in CATIA® V5 modeling software. The Digitized Shape Editor (DSE) was used to import the file without scaling the mesh size. The imported scanned object is shown in Figure G-6, along with its statistical information from the analysis option. To maintain the highest mesh surface quality, mesh decimation was not performed during this stage.

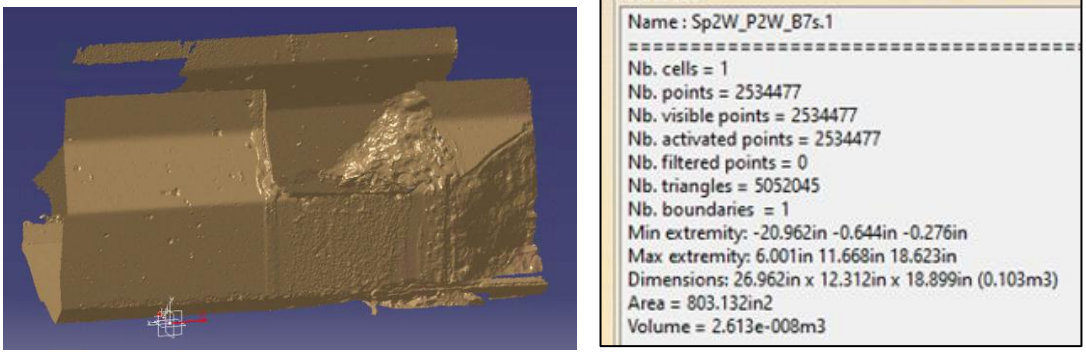

(a) (b)

Figure G-6 (a) Imported scanned object and (b) statistical information.

The editable plane was generated using the quick surface reconstruction (QSR) workbench. The "basic surface recognition" option was employed to create a new plane from the scanned object surface. Then the plane was extended to cover the desired area. Subsequently, the extended plane portion was removed using the trim command. In cases where the scanned object contained curved regions, the "planar sections" tools were used for selection. Then, either the "curve from scan" or "sketch from scan" option was used to draw the desired line shape before using the extrude command to develop the plane. For

rough and highly irregular surfaces in the scanned object, like the section loss area of the beam end, the "automatic surface" option provided a suitable solution. Once the basic shape was created, measuring tools were used to determine the section loss and other measurements. Figure G-7 showcases a model that closely resembles the scanned shape, highlighting the effectiveness of the post-processing steps.

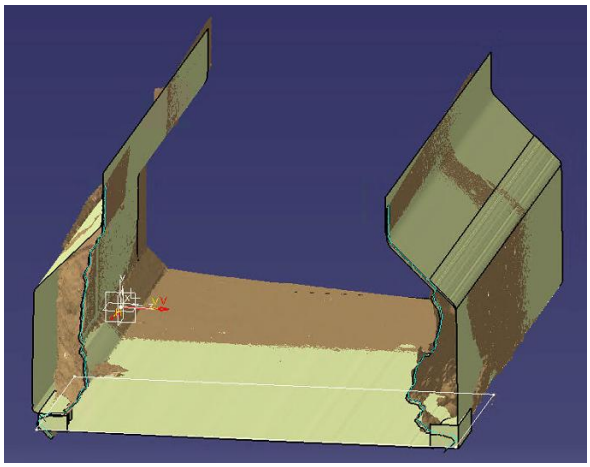

Figure G-7 Working model developed from the 3D scanned data.

G.3 DOCUMENTATION OF BEAM END CONDITION OF AN IN-SERVICE BRIDGE

Data was collected from the PSC I-beam bridge that carries I-96 Eastbound over Washington Avenue in Ingham County, Michigan. Built in 1962, this 5° skew bridge has three spans with a total length of 107 ft 11 in. and a width of 43 ft 7 in. Each span has 7 beams. Span 1 and 3 have AASHTO Type I interior beams and Type II fascia beams. Span 2 has Type II beams. The beam layout and north-side elevation view of the bridge are shown in Figure G-8.

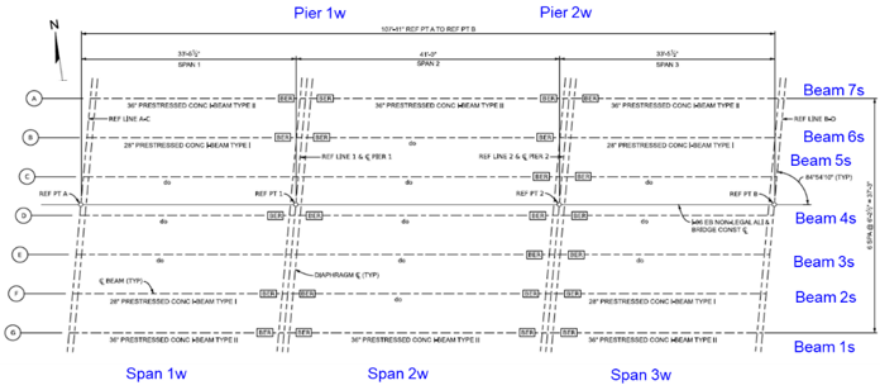

(a)

(b)

Figure G-8 (a) Beam layout and (b) north side elevation view

The beams are supported on expansion bearings at the piers and fixed bearings at the abutments. The bridge deck has expansion joints over the piers. The failure of these expansion joints exposed the beam ends to chloride-laden water from the deck. The latest inspection conducted in October 2022 reported that the beams are in fair condition. However, the latest scoping report rated the beams as in fair to poor condition.

G.3.1 Beam End Conditions

Figure G-9 and Figure G-10 show the condition of beam end 7s over pier 2W in span 2W before and after preparing for the repairs. The latest scoping report mentioned the spalls and delamination on the selected beam end but did not quantify the bearing area loss. Even though the photographs have higher resolution compared to the 3D scan images, the physical features can be extracted only from the 3D scans. When the image developed using scan data is rotated, the inspectors or load rating engineers can get a more comprehensive view with finer details that may not be easily visible in photographs or 2D representations. Also, the scan data offers enhanced measurement capabilities. It is possible

to identify exposed strands and rebars. By comparing the scanned models captured before and after cleaning for repairs, the loss of cross-section due to deterioration can be calculated. Indeed, 3D scanning can be more time-consuming compared to regular visual inspections, especially for relatively large objects like bridge beams. Scanning each beam end alone can take approximately 30 to 40 minutes, not accounting for other related activities during the process. In contrast, visual inspections are generally faster since inspectors can move around and visually examine multiple areas in a shorter amount of time. However, while visual inspections are faster, they may not capture every inch of the beam end with the same level of accuracy provided by 3D scanning.

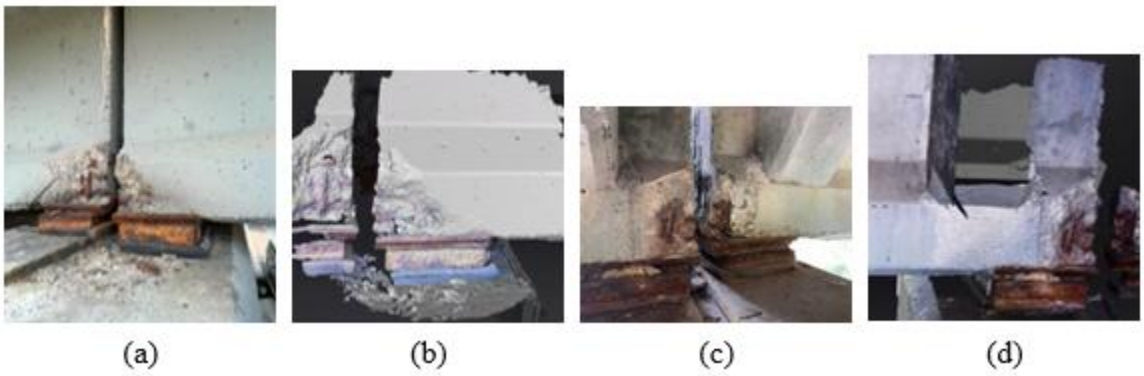

Figure G-9 Beam end condition before cleaning for repairs: (a) left side photograph, (b) left side scan, (c) right side photograph, and (d) right side scan.

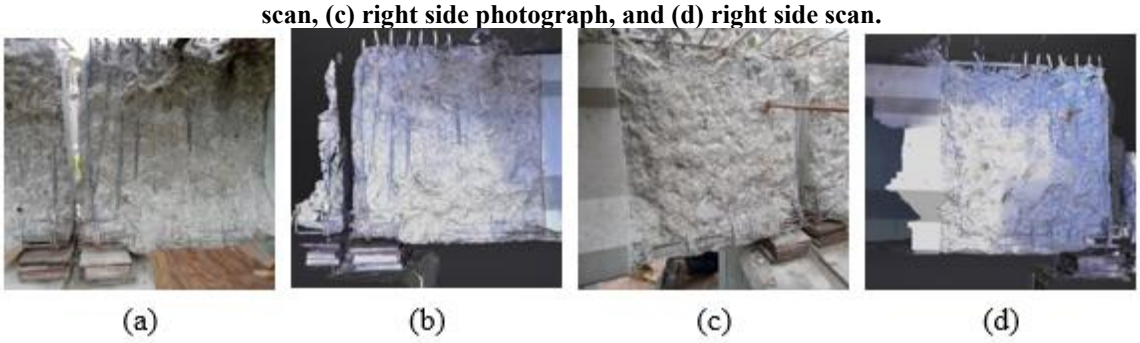

Figure G-10 Beam end condition after cleaning for repairs: (a) left side photograph, (b) left side scan, (c) right side photograph, (d) right side scan.

G.3.2 Calculation of Bearing Loss

The beam end has two spalls, on the left and right sides as shown in Figure G-11. The spalled areas over the bearing and on the right and left sides are 3.4 in.^{2} and 2.3 in.^{2}, respectively. The bearing sole plate area of 160.1 in.^{2} (17.925 in. × 8.929 in.) is also calculated from the model, as shown in Figure G-12. Bearing area loss due to spalls is less than 5% when compared to the bearing sole plate area.

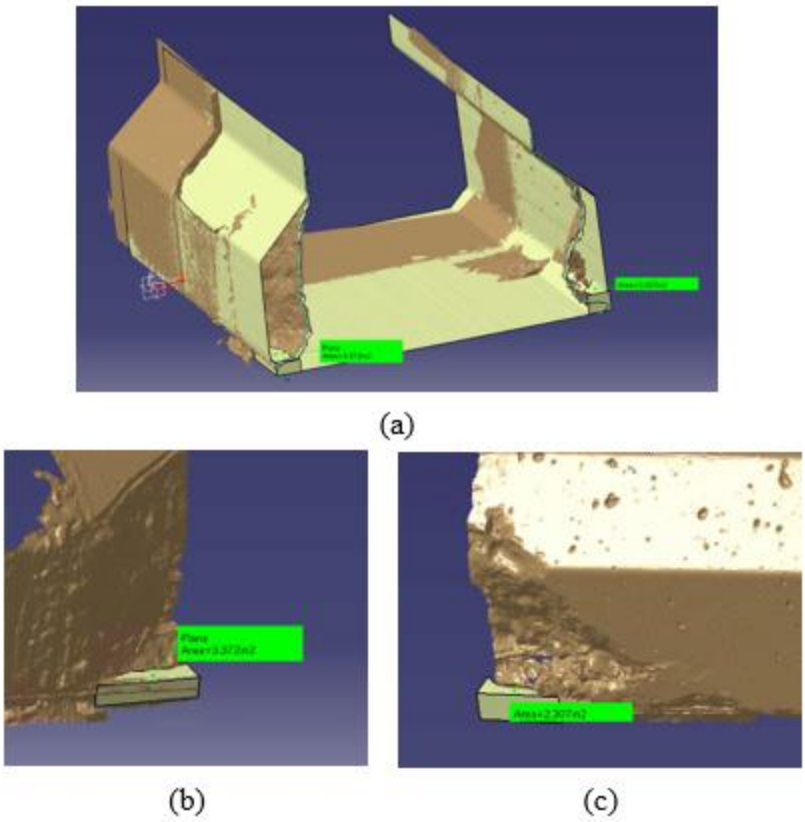

Figure G-11 (a) Model with the section losses, (b) right side spall, and (c) left side spall.

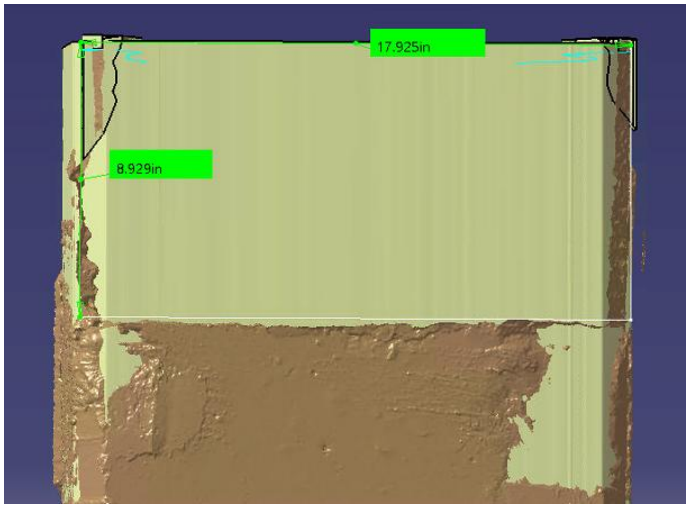

Figure G-12 Sole plate dimension from the scan.

G.4 LIMITATIONS AND CHALLENGES

Several limitations and challenges of this technology were identified during this study.

a) The scanner is not wireless. It requires power supply and data transfer cable connections. Connecting the scanner to the laptop can be challenging at times, particularly when dealing with tall piers or site constraints for parking. During this study, such challenges were overcome by connecting the scanner using a long extension cable to the operating device and the power supply. Users need to be careful about the scanner extension cable while scanning. When the user is unable to view the real-time scan output, it presents a challenge in resolving tracking issues. This challenge is amplified when there is a time delay in the real-time output caused by the processing capabilities of the laptop. Moreover, the computer may experience freezing or slow down when dealing with large scans. To tackle this issue, use a computer with a powerful graphics card and ample memory to surpass the scanner specification requirements. A robust graphics card and sufficient memory allow the computer to handle and process a substantial amount of data generated during scanning more efficiently.

b) Each beam end generates a significant amount of 3D scan data, including point cloud information and other backup data. Before post-processing, the size of a complete scan of one beam-end ranged from 25 to 35 gigabytes (GB). Storage space can indeed become a concern when dealing with many beam ends. If the anticipated data size is substantial, considering using external storage solutions such as external hard drives or network-attached storage (NAS) can be beneficial. Regularly archiving and backing up the data to free up space on the primary storage and safeguard against data loss is also recommended.

c) Maintaining the scanning distance range of approximately 6.3 to 24 inches suitable for medium to large-scale objects becomes a challenge in the presence of closely positioned temporary supports or diaphragm sections near the beam end, as shown in Figure G-13. When the scanner is out of the specified distance range the projected light pattern of the scanner might become distorted or less distinguishable, leading to less precise measurements.

d) Direct sunlight on the beam ends, especially on the fascia beams exposed to direct sunlight can interfere with the structured light patterns projected by the scanner. This is

often not a concern for scanning interior beam ends, as the deck or other structural elements typically shade them. During this study, the beam ends were scanned both in the presence of the deck and after the deck was removed over the beam ends. To mitigate the effects of sunlight, a temporary shade was provided on the removed deck section using a blue poly tarp, shown in Figure G-14.

Figure G-13 Temporary supports and end diaphragm over the pier

Figure G-14 (a) Exposure to ambient light through the removed deck section; (b)removed deck section; (c) tarp placed over the opening to block ambient light.

G.5 CONCLUSIONS

The possibility of using a structured-light handheld scanner for documenting bridge details was evaluated. The following conclusions are derived from this study:

- The structured-light scanner was selected for this study due to its acceptable accuracy and precision in capturing the required 3D data. This scanning technology proves to be a useful tool for documenting details under field conditions.
- Although 3D scanning requires more time compared to traditional visual inspection, the process can be optimized by selecting critical details for scanning since it provides substantial advantages over visual inspection. By capturing all visible details at very high accuracy, it reveals information that may not be easily identified during visual inspection.
- The reverse engineering of as-is details plays a vital role in visualizing and comprehending the extent of deterioration. This allows for a more precise calculation of section loss and reduction in bearing area and the identification of damaged strands and reinforcing steel to improve the accuracy of condition assessment and load capacity calculation.

G.6 REFERENCES

1. Ryan, T. W., E. C. E. Lloyd, M. S. Pichura, D. M. Tarasovich, and S. Fitzgerald. *Bridge Inspector's Reference Manual (BIRM)*. Publication No. FHWA-NHI-23-024. Federal Highway Administration, Washington, DC, 2023. https://www.fhwa.dot.gov/bridge/nbis/pubs/nhi23024.pdf.
2. *Manual for Bridge Element Inspection*. American Association of State Highway and Transportation Officials (AASHTO). 2019.
3. Rashidi, M., M. Mohammadi, S. S. Kivi, M. M. Abdolvand, L. Truong-Hong, and B. Samali. A Decade of Modern Bridge Monitoring Using Terrestrial Laser Scanning: Review and Future Directions. *Remote Sensing*, 2020. 12: 3796. doi:10.3390/rs12223796.
4. Wang, Q., and M. K. Kim. Applications of 3D Point Cloud Data in the Construction Industry: A Fifteen-Year Review from 2004 to 2018. *Advances in Engineering Informatics*, 2019. 39: 306–319.
5. Kim, M. K., Q. Wang, and H. Li. Non-contact Sensing Based Geometric Quality Assessment of Buildings and Civil Structures: A Review. *Automation in Construction*, 2019. 100: 163–179.
6. Spencer, B. F., V. Hoskere, and Y. Narazaki. Advances in Computer Vision-Based Civil Infrastructure Inspection and Monitoring. *Engineering*, 2019. 5: 199–222.
7. Czerniawski, T., and F. Leite. Automated Digital Modeling of Existing Buildings: A Review of Visual Object Recognition Methods. *Automation in Construction*, 2020. 113: 103131.
8. Hain, A., A. E. Zaghi, A. Kamali, R. P. Zaffetti, B. Overturf, and F. E. Pereira. Applicability of 3-D Scanning Technology for Section Loss Assessment in Corroded Steel Beams. *Transportation Research Record: Journal of the Transportation*

Research Board, 2019. 2673(3), 271–280. https://doi.org/10.1177/0361198119832887.

9. Wang, R., Y. Wang, S. Devadiga, I. Perkins, Z. Kong, and X. Yue. Structured-light Three-dimensional Scanning for Process Monitoring and Quality Control in Precast Concrete Production. *PCI Journal*, 2021, 66 (6), 17-32. https://doi.org/10.15554/pcij66.6-01.
10. Franceschini, L., B. Belletti, F. Tondolo, and J. Sanchez. Study on the Probability Distribution of Pitting for Naturally Corroded Prestressing Strands Accounting for Surface Defects. *Buildings*, 2022. 12(10):1732. https://doi.org/10.3390/buildings12101732
11. Haleem, A., Javaid, M., Singh, R. P., Rab, S., Suman, R., Kumar, L., and Khan, I. H. (2022). "Exploring the potential of 3D scanning in Industry 4.0: An overview." *International Journal of Cognitive Computing in Engineering*, 3, 161–171.
12. Liu, J., Xu, D., Hyyppa, J., and Liang, Y. (2021). "A survey of applications with combined BIM and 3D laser scanning in the life cycle of buildings." *IEEE Journal of Selected Topics in Applied Earth Observations and Remote Sensing*, 14, 5627–5637.
13. Helle, R. H., and Lemu, H. G. (2021). "A case study on use of 3D scanning for reverse engineering and Quality Control." *Materials Today: Proceedings*, 45, 5255–5262.
14. "Einstar 3D scanner." (n.d.). einstar, <https://www.einstar.com/products/einstar-3d-scanner?variant=43551575507118> (Jul. 30, 2023).
15. Olsen, M. J., Kuester, F., Chang, B. J., and Hutchinson, T. C. (2010). "Terrestrial Laser scanning-based structural damage assessment." *Journal of Computing in Civil Engineering*, 24(3), 264–272.
16. "Topodrone Lidar hi-res." (n.d.). *Drone Mapping Tools*, <https://www.dronemappingtools.com/products/topodrone-lidar-100-lite> (Jul. 30, 2023).
17. Dassault Systèmes. (2022). CATIA V5 [Computer Software]. Version 5-6 Release2022.

If you require assistance accessing this information or require it in an alternative format, contact the Michigan Department of Transportation's (MDOT) Americans with Disabilities Act (ADA) coordinator at Michigan.gov/MDOT-ADA.